Assessing the Influence of Different Structural Features on Multivalent Thermodynamics and Kinetics of Precision Glycomacromolecules

Inaugural-Dissertation
to obtain the academic degree
Doctor rerum naturalium (Dr. rer. nat.)

submitted to the Department of Biology, Chemistry and Pharmacy
of Freie Universität Berlin

by
Sinaida Igde
From Leninabad, Tadshikistan

Berlin, Düsseldorf, October 2016

The work presented in this thesis was accomplished in a period between January 2013 and October 2016 in the Department of Biomolecular Systems at the Max Planck Institute of Colloids and Interfaces, Freie Universität Berlin, Institute of Chemistry and Biochemistry and Institute for Organic Chemistry and Macromolecular Chemistry, Heinrich-Heine-Universität Düsseldorf under supervision of Prof. Dr. Laura Hartmann.

1st Reviewer: Prof. Dr. Laura Hartmann
2nd Reviewer: Prof. Dr. Christoph A. Schalley

Date of defense: 14.11.2016

"I'd like to share a revelation that I've had during my time here. It came to me when I tried to classify your species and I realized that you're not actually mammals. Every mammal on this planet instinctively develops a natural equilibrium with the surrounding environment but you humans do not. You move to an area and you multiply and multiply until every natural resource is consumed and the only way you can survive is to spread to another area. There is another organism on this planet that follows the same pattern. Do you know what it is? A virus. Human beings are a disease, a cancer of this planet. You're a plague and we are the cure."

Agent Smith (Character), from "The Matrix" (Film, 1999)

"Große Zahlen liefern ein statistisch gesehen genaues Ergebnis, von dem man nicht weiß, auf wen es zutrifft. Kleine Zahlen liefern ein statistisch gesehen unbrauchbares Ergebnis, von dem man aber besser weiß, auf wen es zutrifft. Schwer zu entscheiden, welche dieser Arten von Unwissen die nutzlosere ist."

Beck-Bornholdt/ Dubben 2003, Seite 34

Dedicated to my husband and my son, Süleyman Hasan Igde and Nael Elyas Igde

To my precious parents, Tatjana and Matthäus Lel

October, 2016

Table of Contents

List of Abbreviations

Abbreviation	Definition
AA(s)	amino acid(s)
calcd	calculated
CRD	carbohydrate recognition domain
CuCAAC	copper(I)-catalyzed azide-alkyne cycloaddition
D	day(s)
DB	double bond
DP	deprotection
EEC	enthalpy-entropy compensation
e.g.	*exempli gratia*; for example
equiv	equivalent(s)
et al.	*et alteri*; and others
FV	functional valency
H	hour(s)
L	ligand
P	protein
SAC(s)	structure-activity correlation(s)
SAR(s)	structure-activity relationship(s)
SFC(s)	structure-function correlation(s)
SPC(s)	structure-property correlation(s)
RIP(s)	relative inhibitory potency(-ies)
RT	room temperature
T	temperature
UV	ultraviolet
Via	by; through; per

Chemicals	Trivial Name and IUPAC
αMan	α-D-mannopyranoside
βGal	β-D-galactopyranoside
Ac_2O	acetic anhydride
AcOH	acetic acid
ADS	allyloxycarbonyl diamine succinic acid
Ala	alanine
Alloc	allyloxycarbonyl
ASGPR	asialoglycoprotein receptor
BDS	tert-butyloxycarbonyl diamine succinic acid
Boc	tert-butyloxycarbonyl
Con A	*Concanavalin A*
DCM	dichloromethane
DCE	1,2-dichloroethane
DMF	*N,N'*-dimethylformamide
DMSO	dimethyl sulfoxide
DMSO-d_6	deuterated dimethyl sulfoxide (subscript indicates number of deuterons)
E. cristagalli	*Erythrina* cristagalli

EDA	ethylene diamine
EDS	ethylene dioxy diamine succinic acid
Fim H	bacterial adhesin, type 1 fimbrial adhesin
Fmoc	fluorenylmethyloxycarbonyl
Glc	D-glucose
HATU	O-(7-azabenzotriazol-1-yl)-N,N,N',N'-tetramethyluronium hexafluorophosphat
HBTU	O-(benzotriazol-1-yl)-N,N,N',N'-tetramethyluronium hexafluorophosphate
HDO	water peak in heavy water (*Nuclear Magnetic Resonance Spectroscopy*)
HOBT	N-hydroxybenzotriazole
*iv*Dde	1-(4,4-dimethyl-2,6-dioxocyclohex-1-ylidene)isovaleryl
LBB	lectin binding buffer
Lys	lysine
MeαMan	methyl α-D-mannopyranoside
MeCN	acetonitrile
Neu$_5$Ac	N-acetylneuraminic acid
N,N'DMBA	1,3-dimethylbarbituric acid
PEG	poly(ethylene glycol)
Phe	phenylalanine
PS	polystyrene
PyBOP	benzotriazol-1-yl-oxytripyrrolidinophosphonium hexafluorophosphate
RAM	Rink Amide
SDS	small diamine succinic acid
SLe^x	sialylated Lewis X
TDS	triple bond diamine succinic acid
TFA	trifluoroacetic acid
THF	tetrahydrofurane
TMSBr	bromotrimethylsilane
TMSCl	chlorotrimethylsilane
TMSOTf	trimethylsilyl triflate
Trt/-Cl	trityl(-chloride)
TSA	thiosalicyclic acid
WGA	*Wheat Germ Agglutinin*

Methods	Definition
^{1}H	hydrogen (atomic mass = 1 atomic mass units)
^{13}C	carbon-13 (atomic mass = 13 atomic mass units)
^{15}N	nitrogen-15 (atomic mass = 15 atomic mass units)
1 D	one dimension(al)
2 D	two dimension(al)
COSY	*Correlation Spectroscopy*
HRMS ESI	*High Resolution Mass Spectrometry Electrospray Ionization*
MS ESI	*Electrospray Ionization Mass Spectrometry*
RP-HPLC	*Reverse Phase High-Performance Liquid Chromatography*
HSQC	*Heteronuclear Single-Quantum Coherence Spectroscopy*
ITC	*Isothermal Titration Calorimetry*
kinITC	*kinetic Isothermal Titration Calorimetry*

MALDI-TOF	*Matrix Assisted Laser Desorption Ionization Time of Flight Mass Spectrometry*
MS	*Mass Spectrometry*
MS/MS	tandem *Mass Spectrometry* (multiple steps of mass spectrometry selection)
NMR	*Nuclear Magnetic Resonance Spectroscopy*
SPOS	*Solid Phase Organic Synthesis*
SPPoS	*Solid Phase Polymer Synthesis*
SPPS	*Solid Phase Peptide Synthesis*
SPR	*Surface Plasmon Resonance*
TLC	*Thin Layer Chromatography*

Units and symbols	Definition
°C	degree Celsius (centigrade)
%	percent
µL	microliter(s)
µM (µmol/L)	micromolar (micromol(s) per liter)
cm^{-1}	per centimeter(s)
(k)Da	(*kilo*)dalton (1000 dalton)
G	gram(s)
g/ mol	gram per mol(s)
(M)Hz	(*mega*)hertz
I [%]	relative intensity (mass spectrometry)
J/J_{CH}/J_{NH}/$^{1,2,3}J$	coupling constant/carbon-hydrogen coupling/nitrogen-hydrogen coupling/ scalar coupling over one, two, three bond(s)
(k)J	(*kilo*)joule(s)
K	kelvin
K^{-1}	per kelvin
M (mol/L)	molarity (mol(s) per liter)
Mg	milligram(s)
min	minute(s)
mL	milliliter(s)
mol	mol(s)
mol^{-1}	per mol(s)
mM (µmol/L)	millimolar (millimol(s) per liter)
mmol	millimol(s)
mmol/g	millimol(s) per gram
Nm	nanometer
nM (nmol/L)	nanomolar (nanomol(s) per liter)
mol %	mol(s) percent
m/z	mass-to-charge ratio
ppm	parts per million
R_h	hydrodynamic radius (radii)
rpm	rotation(s) per minute
S	second(s)
s^{-1}	per second(s)
T	time
T_R	retention time (RP-HPLC)
V_h	hydrodynamic volume(s)

vol %   volume percent

Summary

This thesis describes the synthesis of a series of precision glycomacromolecules and a study of their multivalent binding thermodynamics and kinetics in the interaction with model lectin Con A. Previous studies performed with glycopolymers, which present an important class of glycomimetics, have revealed that affinities and selectivities of glycopolymer-protein interactions depend on the arrangement of carbohydrate ligands presented on the polymer scaffold, as well as the scaffold's composition and architecture. However, the thermodynamic and kinetic origin of such differences in protein binding in dependence of the polymer scaffold, have not been studied in much detail so far. One reason is the challenges associated with the synthesis of classical glycopolymers, which usually do not allow for a modular and straightforward exchange of certain structural motifs within the polymer scaffold. One approach to overcome this challenge – the one that is described in this thesis – is to design representative glycopolymer model systems, with exact control over their structural properties, as it has been shown with the recently introduced solid phase polymer synthesis (SPPoS) of so-called precision glycomacromolecules. Therefore, the here presented work was particularly interested in the structural features required for these model systems to lead to differences in the binding thermodynamics and kinetics in the association between the glycomacromolecules and the protein.

The backbone of the glycomacromolecules was built up by different building blocks previously introduced for SPPoS. Their use allowed for the conjugation of different αMan derivatives as well as the alternation of the spacing in terms of a varied ligand density along with the chemical composition of the scaffold. Specifically, different αMan linkage on the oligomer backbone was ascertained, varying from a small ethyl triazole linker, over a longer thiol-ether triazole linker to a hydrophobic benzyl triazole linker. Additionally, a different backbone composition by the exchange of different spacer building blocks was achieved. Further, using SPPoS not only linear glycomacromolecules were synthesized but also cyclic glycomacromolecules were obtained. Evaluation of the different cyclization strategies on solid support revealed a two-step method to be best suited for the synthesis of cyclic precision glycomacromolecules, where first a protecting group is removed from the linear precursor before macrocyclization through the formation of an intramolecular amide bond. Further, a potential new tandem reaction to obtain cyclic oligo(amido amines) as scaffold for later glycoconjugation and synthesis of macrocyclic cationic oligo(amido amines) was evaluated, but showed unselective formation of *N*-substituted imides rather than the synthesis of monocyclic rings.

The synthesis of the here reported linear and cyclic glycomacromolecules and the modular exchange of their structural features allowed a systematic elucidation of the influence of (*i*) the ligand density and the spacer length and its chemical composition, (*ii*) the chemical composition of the linker and its length, (*iii*) the number of carbohydrate ligands, (*iv*) the size of the backbone, (*v*) the change in the overall architecture from linear to cyclic and (*vi*) the valency of the multivalent glycomacromolecules, on their multivalent binding. Furthermore, the valency of the protein, either

predominantly dimer or tetramer Con A, was varied by controlling the pH. The impact on the multivalent binding mechanism was evaluated by measuring their binding energetics and kinetics, such as the binding enthalpy ΔH, entropy $-T\Delta S$, binding free energy ΔG, heat capacity ΔC_p, the on- and off-rate constants (k_{on} and k_{off} values) and the transition state of the binding process using Isothermal Titration Calorimetry (ITC) and the recently introduced kinetic ITC (kinITC).

Different correlations between changing the scaffold of the glycomacromolecules and the resulting thermodynamic and kinetic contributions were observed, that might also relate to similar findings for other glycopolymer systems and help to further improve the design of glycopolymers as glycomimetics. In short, values in ΔG were very similar for all glycomacromolecules with the same valency, suggesting ΔG to be insensitive to changes in ligand density and spacer composition. No clear trend regarding the enthalpic and entropic contributions was found for glycomacromolecules varying in their spacing. Further, an architectural change from linear to cyclic glycomacromolecules resulted in similar ΔG values. The enthalpic and entropic values of glycomacromolecules and their binding to dimer and tetramer Con A pinpoint to a sterical hinderance with tetramer Con A that is missing with dimer Con A. Another representative trend was found for glycomacromolecules with different αMan linkers. Insertion of the different αMan linkers has led to a steady increase in the binding affinity in the order short ethyl triazole linker < thiol-ether triazole linker < benzyl triazole linker with dimer Con A and tetramer Con A for mono- to trivalent compounds, and thiol-ether triazole linker < short ethyl triazole linker < benzyl triazole linker for penta- to decavalent compounds and tetramer Con A. The presented study suggests that this is not an effect of the additional ligand-receptor contacts, which have led to higher binding affinities, but is rather due to secondary effects from the linker's chemical composition. From the kinetic studies, it was found that the binding of glycomacromolecules with dimer Con A seems to follow a rebinding mechanism, as it has been proposed by Hunter and Anderson and Weber *et al.*. Here fast k_{on} and k_{off} rates indicate the population of partially bound states as long as the glycomacromolecules and the protein associate. In contrast, the binding of glycomacromolecules to tetramer Con A is indicative of the binding and sliding mechanism, as proposed by Brewer *et al.*. Here, exponentially accelerated k_{on} values and k_{off} values, which stayed reduced or even further decreased, are representative for this binding mode. Regarding the αMan density and the αMan linkers, the same trend was found in the kinetic rate constants as has been found in their binding thermodynamics: While the on- and off-rate were rather insensitive to a changing αMan density and oligomer architecture, the αMan linkers showed a clear difference in the values of the association and dissociation rate constants.

Analysis of the transition state revealed again a similar trend as observed for the previous values: An increasing valency has led to a lower activation free energy $\Delta G_{on}^{\ddagger}$, whereas molecules with the same valency but different ligand density or architecture essentially exhibit the same activation free energy $\Delta G_{on}^{\ddagger}$. Regarding the different linkers presented on the glycomacromolecules, evaluation of the transition state has shown that glycomacromolecules with a benzyl triazole

linkage obtain the lowest activation energy barrier $\Delta G_{on}^{\ddagger}$, followed by the thiol-ether triazole and the ethyl triazole linked glycomacromolecules for the association process. The reverse is true for the dissociation transition state $\Delta G_{off}^{\ddagger}$.

Overall, in this thesis a systematic study of the binding energetics and kinetics of multivalent precision glycomacromolecules binding to dimer and tetramer Con A has been reported by using thermodynamic and kinetic ITC. Changes in the binding energetics and kinetics have been related to their varying scaffold properties. Thus, this study further promotes a deeper insight into the multivalent binding of precision glycomacromolecules and thereby their role as model systems for fundamental studies on multivalency as well as their potential use in biotechnological and biomedical applications.

Zusammenfassung

Die vorliegende Arbeit beschäftigte sich mit der Synthese einer Serie von Präzisionsglykomakromolekülen und der Analyse der Thermodynamik and Kinetik der multivalenten Wechselwirkungen mit dem Modellektin Con A. Vorhergehende Studien mit Glykopolymeren als eine wichtige Klasse der Glykomimetika haben gezeigt, dass Bindungsaffinitäten und -selektivitäten der Glykopolymer-Protein Wechselwirkungen von der Anordnung der Kohlenhydrat-Liganden auf dem Polymer-Grundgerüst, sowie von der Grundgerüstzusammensetzung und -architektur abhängen. Allerdings wurde der thermodynamische und kinetische Ursprung solcher Unterschiede in der Bindung zum Protein in Abhängigkeit vom Polymer-Grundgerüst bislang nicht detailliert untersucht. Eine der Gründe dafür sind die Herausforderungen der Synthese klassischer Glykopolymere, die bislang noch keinen modularen und direkten Austausch bestimmter struktureller Motive im Polymergerüst ermöglichen. Ein Ansatz, um diese Herausforderung zu überwinden und der in dieser Arbeit beschrieben wird, ist die Verwendung repräsentativer Glykopolymer Modelsysteme mit exakter Kontrolle über die strukturellen Eigenschaften. Mit Hilfe der kürzlich eingeführten Festphasenpolymersynthese können solche sogenannten Präzisionsglykomakromoleküle erzeugt werden. Die vorliegende Arbeit interessierte sich daher insbesondere für die strukturellen Eigenschaften der Präzisionsglykomakromoleküle, die potenziell zu Unterschieden in der Bindungsthermodynamik und -kinetik bei der Assoziation zwischen den Glykomakromolekülen und dem Modellektin Con A führen.

Das Gerüst der Glykomakromoleküle wurde hierzu aus verschiedenen Bausteinen zusammengesetzt, die zuvor für die Festphasenpolymersynthese etabliert wurden. Ihre Verwendung erlaubte die Konjugation unterschiedlicher αMan Derivate, sowie die gezielte Variation der Ligandendichte und der chemischen Zusammensetzung des Gerüsts. Auf diese Weise wurden zum einen unterschiedliche αMan Linker zum Rückgrat eingeführt – von einem kurzen Ethyl Triazol Linker, über einen längeren Thiol-Ether Triazol Linker zu einem hydrophoben Benzol Triazol Linker. Zum anderen wurden unterschiedliche Rückgrat Zusammensetzung durch den Austausch verschiedener Spacer Bausteine realisiert. Durch die Nutzung der Festphasenpolymersynthese war es weiterhin möglich nicht nur lineare Glykomakromoleküle zu synthetisieren, sondern auch zyklische Glykomakromoleküle zu erhalten. Eine Evaluierung unterschiedlicher Zyklisierungsstrategien auf der Festphase haben ergeben, dass eine Zwei-Schritt-Methode für die Synthese zyklischer Präzisionsglykomakromoleküle am besten geeignet ist. Zunächst wird hierzu die Schutzgruppe am linearen Precursor entfernt und darauf folgend die Makrozyklisierung unter Bildung einer intramolekularen Amid Bindung durchgeführt. In diesem Zusammenhang wurde auch eine potenziell neue Tandem Reaktion für die Synthese zyklischer Oligo(amido amine) als Rückgrat für eine spätere Glyko-Konjugation beziehungsweise (bzw.) die Synthese von zyklischen kationischen Oligo(amido aminen) untersucht. Diese zeigte jedoch eine unselektive N-substituierte Imid-Bildung anstatt der Synthese von monozyklischen Ringen.

Die erfolgreiche Synthese der in dieser Arbeit gezeigten linearen und zyklischen Glykomakromoleküle, sowie der modulare Austausch ihrer strukturellen Merkmale erlaubten dann die systematische Untersuchung des Einflusses folgender struktureller Eigenschaften auf die multivalente Bindung zum Protein: (*i*) Die Ligandendichte and Spacer-Länge, sowie ihre chemische Zusammensetzung, (*ii*) die chemische Zusammensetzung der Linker und ihrer Länge, (*iii*) die Anzahl der Kohlenhydrat-Liganden, (*iv*) die Größe des Grundgerüsts, (*v*) die Veränderung der gesamten Polymer-Architektur von linear zu zyklisch und (*vi*) die Valenz der Glykomakromoleküle. Weiterhin wurde die Valenz des Proteins durch die Kontrolle des pH Wertes variiert, wobei entweder überwiegend das Con A Dimer oder Tetramer vorhanden sind. Die Auswirkung der oben genannten Strukturvariationen der Glykomimetika, sowie die Valenz des Proteins auf deren multivalenten Bindung, wurden durch Messung der Bindungsenergien und -kinetik, wie zum Beispiel der Bindungsenthalpie ΔH, -entropie $-T\Delta S$, der Freien Bindungsenergie ΔG, der Wärmekapazität ΔC_p, der Assoziations- und Dissoziations-Geschwindigkeitskonstanten (k_{on} und k_{off}) und dem Übergangszustand der Bindungsprozesse untersucht. Diese thermodynamischen und kinetischen Größen wurden mit Hilfe der Isothermalen Titrationskalorimetrie (ITC) und der erst kürzlich eingeführten kinetischen ITC (kinITC) ermittelt.

Unterschiedliche Korrelationen zwischen den Strukturvariationen der Glykomakromoleküle und den resultierenden thermodynamischen und kinetischen Beiträgen wurden gefunden. Diese Beiträge können potenziell auch auf andere Glykopolymere übertragen werden und dabei helfen, neue und verbesserte Glykopolymere als Glykomimetika zu entwickeln. Zusammenfassend konnte die vorliegende Studie zeigen, dass die Werte in ΔG sehr ähnlich sind für alle Glykomakromoleküle mit derselben Valenz, während ΔG unempfindlich gegenüber den Veränderungen in der Ligandendichte und Spacer-Zusammensetzung ist. Kein klarer Trend wurde in Bezug auf die enthalpischen und entropischen Beiträge gefunden für Glykomakromoleküle, die sich in ihrer Ligandendichte unterscheiden. Weiterhin führte die Architekturveränderung von linearen zu zyklischen Glykomakromolekülen zu keiner Änderung der Werte für ΔG. Die enthalpischen und entropischen Beiträge der Bindung von Glykomakromolekülen am Con A Dimer und Tetramer deuten auf eine sterische Hinderung bei Bindung an das Con A Tetramer hin, die bei dem Con A Dimer nicht gefunden wurde. Ein anderer repräsentativer Trend wurde für Glykomakromoleküle gefunden, die sich in ihren αMan Linkern unterscheiden. Die Einführung unterschiedlicher αMan Linker hat zu einer stetig steigenden Bindungsaffinität geführt, in der Reihenfolge Ethyl Triazol Linker < Thiol-Ether Triazol Linker < Benzol Triazol Linker bei Bindung an das Con A Dimer, sowie dem Con A Tetramer für mono- bis trivalente Verbindungen, und Thiol-Ether Triazol Linker < Ethyl Triazol Linker < Benzyl Triazole Linker für penta- bis decavalente Verbindungen und ihrer Bindung an das Con A Tetramer. Die hier präsentierte Studie deutet an, dass dieser Effekt nicht das Ergebnis zusätzlicher Liganden-Rezeptor-Kontakte ist, die zu einer höheren Bindungsaffinität geführt haben, sondern eher das Resultat sekundärer Effekte ist, die durch die Variation in der chemischen Zusammensetzung der Linker zustande gekommen sind. Die kinetischen Studien haben gezeigt, dass die Bindung von Glykomakromolekülen an das Con A

Dimer dem *rebinding* Mechanismus zu folgen scheint, so wie dieser von Hunter und Anderson, sowie Weber *et al.* vorgeschlagen wurde. In einem solchen Mechanismus deuten die k_{on} and k_{off} Geschwindigkeitskonstanten auf die Population von partiell gebundenen Bindungszuständen hin, solange die Glykomakromoleküle und das Protein sich in der Assoziationsphase befinden. Im Gegensatz dazu deuten die kinetischen Daten für die Glykomakromoleküle, die an das Con A Tetramer binden, eher auf den *binding and sliding* Mechanismus hin, so wie er von Brewer *et al.* vorgeschlagen wurde. Für diesen Bindungsmodus sind exponentiell beschleunigte k_{on} Werte, sowie reduzierte oder sogar weiter verringte k_{off} Werte repräsentativ. Bezüglich der αMan Linkern wurde derselbe Trend in den Geschwindigkeitskonstanten gefunden, der bereits in den thermodynamischen Daten beobachtet wurde: Während die k_{on} and k_{off} Werte eher unempfindlich gegenüber einer sich veränderten αMan Dichte sind, wurden klare Unterschiede für die unterschiedlichen αMan Linker in den Assoziations- und Dissoziations- Geschwindigkeitskonstanten gefunden.

Die Analyse der Übergangszustände zeigte erneut einen ähnlichen Trend wie bei den vorangegangenen Messreihen: Eine steigende Valenz der Glykomakromoleküle führt zu einer stetigen Verminderung der Freien Aktivierungsenregie $\Delta G_{on}^{\ddagger}$, wohingegen Moleküle derselben Valenz aber einer unterschiedlichen Ligandendichte oder Architektur im Wesentlichen die gleiche Freie Aktivierungsenergie $\Delta G_{on}^{\ddagger}$ aufweisen. Für die unterschiedlichen Linker Typen wurde die niedrigste Freie Aktivierungsenergie für die Benzol Triazol Linker gefunden, gefolgt vom Thiol-Ether Triazol Linker und dem Ethyl Triazol Linker mit der höchsten freien Aktivierungsenergie. Dies bezieht sich auf den gesamten Assoziationsprozess, wobei die umgekehrte Reihung für den Dissoziations-Übergangszustand $\Delta G_{off}^{\ddagger}$ gilt.

Insgesamt präsentiert diese Arbeit somit eine systematische Studie der Bingungsenergien und -kinetik multivalenter Präzisionsglykomakromoleküle und ihrer Bindung an das Con A Dimer und Tetramer, die mit Hilfe der thermodynamischen und kinetischen ITC ermittelt wurden. Veränderungen der Bindungsenergien und -kinetik wurden direkt in Bezug zu den kontrolliert variierten Strukturen der Glykomakromoleküle gesetzt. Diese Studie trägt somit zu einem vertieften Verständnis multivalenter Bindungsprozesse von Präzisionsglykomakromolekülen bei und zeigt ihr Potenzial als Modelsysteme für Grundlagenstudien der Multivalenz, sowie ihre mögliche Anwendung in der Biotechnologie und Biomedizin.

1. General Introduction

1.1. Glycomimetic structures

The following chapter will give a short introduction into the role of carbohydrates and glycomimetics in biology and medicine, explain the general concept of designing glycomimetic structures and highlight the role of glycopolymers as an important class of glycomimetics.

1.1.1. Natural glycoconjugates in biology and medicine

Carbohydrates present an important class among the natural building blocks of biopolymers. Their role[1-4] in nature and biology is as diverse as their structures and functions[1-3]. Similarly to their biopolymer analogues, such as the oligo/polypeptides and the oligonucleotides, carbohydrates are built up from single building blocks, the monosaccharides, to form higher molecular weight structures, the oligo- and polysaccharides.[4-5] Compared, however, to the other two biological macromolecules, carbohydrates differ in terms of isomerism (stereo- and constitutional isomers) of a single carbohydrate building blocks as well as in their position of the branching between individual carbohydrate building blocks in oligo/polysaccharides.[4-8] Those two properties clearly differentiate the carbohydrates from the other two classes of biopolymers, as they allow to create highly branched oligo-/polysaccharides with an immense alternation of linkage points, also due to their large number of constitutional and stereo-isomers (anomers).[4-6, 8] Along with their first discovery by Emil Fisher in the 19th century, the function of carbohydrates has at first been thought to be limited to nutrition, energy storage and supply and the ability to form cell wall of plants, such as their distribution in Chitin.[9] Around the mid of the 20th century it has been recognized that carbohydrates are not only limited to energy storage and supply, but they are also involved in many other important biological processes[1-3]. For example, the differentiation of the different blood types is due to different oligosaccharide antigens, which alter in their functional end groups.[9] Other very important biological processes involving carbohydrates are the immune function, fertilization as well as infectious deceases.[1, 4] To date it is well-known that in one of the first processes during an infection, it is the carbohydrate mediated recognition of pathogens, such as bacteria, viruses and fungi that triggers the infection cycle.[1, 4] The biological relevance of carbohydrates lies here in their ability to function as ligands and initiate the mentioned biological responses and processes (Figure 1).[1-4]
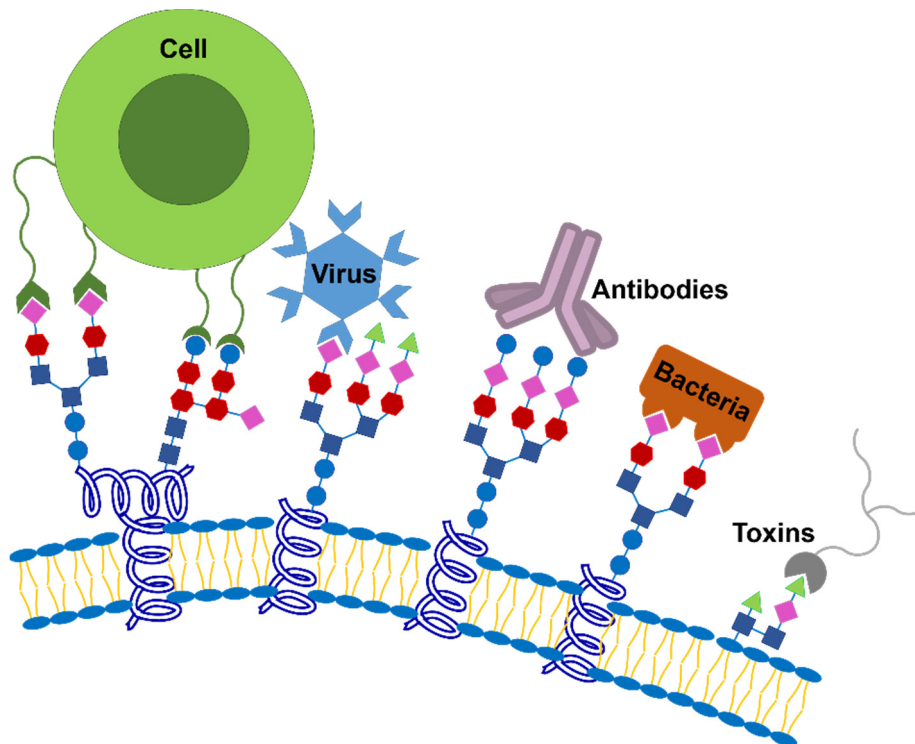
Figure 1. Interactions of cells, pathogens and antibodies through multivalent carbohydrate ligand-receptor interactions.[10]

Pathogens are recognized by the so-called glycocalix.[3-4] The glycocalix[4] is understood as a large number of different heterogeneously arranged carbohydrate structures, which are linked to the outside of an animal or plant cell membrane *via* lipids or proteins (Figure 1).[4, 9] Through the glycocalix, the cell surface serves as a recognition domain for pathogens or other cells or more specifically carbohydrate recognizing receptors on the surface of the cells.[1, 4]

Important examples of carbohydrate recognizing proteins are the lectins and selectins (Figure 2). Lectins are as ubiquitous as the cell-membrane covering carbohydrates[9] and able to very specifically recognize carbohydrates.[6, 11] They are able to selectively encode the information in the complex carbohydrates, which is due to the alternating branching and linkage points as well as the stereochemistry (anomers) and functional group distribution of carbohydrates (site-specific substitution).[1, 4, 7-9] This means that for every lectin, there are specific carbohydrates, which are only recognized by this particular protein.[1, 6, 11] Although the biological functions of lectins and heterogenic glycan arrays on the outer cell-membrane are diverse[8], according to Sharon[1], lectins can be restricted to five main classes with respect to the carbohydrate epitope that they have highest binding affinity to.[1, 6, 8] These include the following carbohydrate epitopes, which are specific for different lectin classes: (*i*) Galactose (Gal) and *N*-acetylgalactosamine, (*ii*) fucose, (*iii*) *N*-acetylneuraminic acid, (*iv*) *N*-acetylglucosamine and (*v*) mannose (αMan).[1, 6]
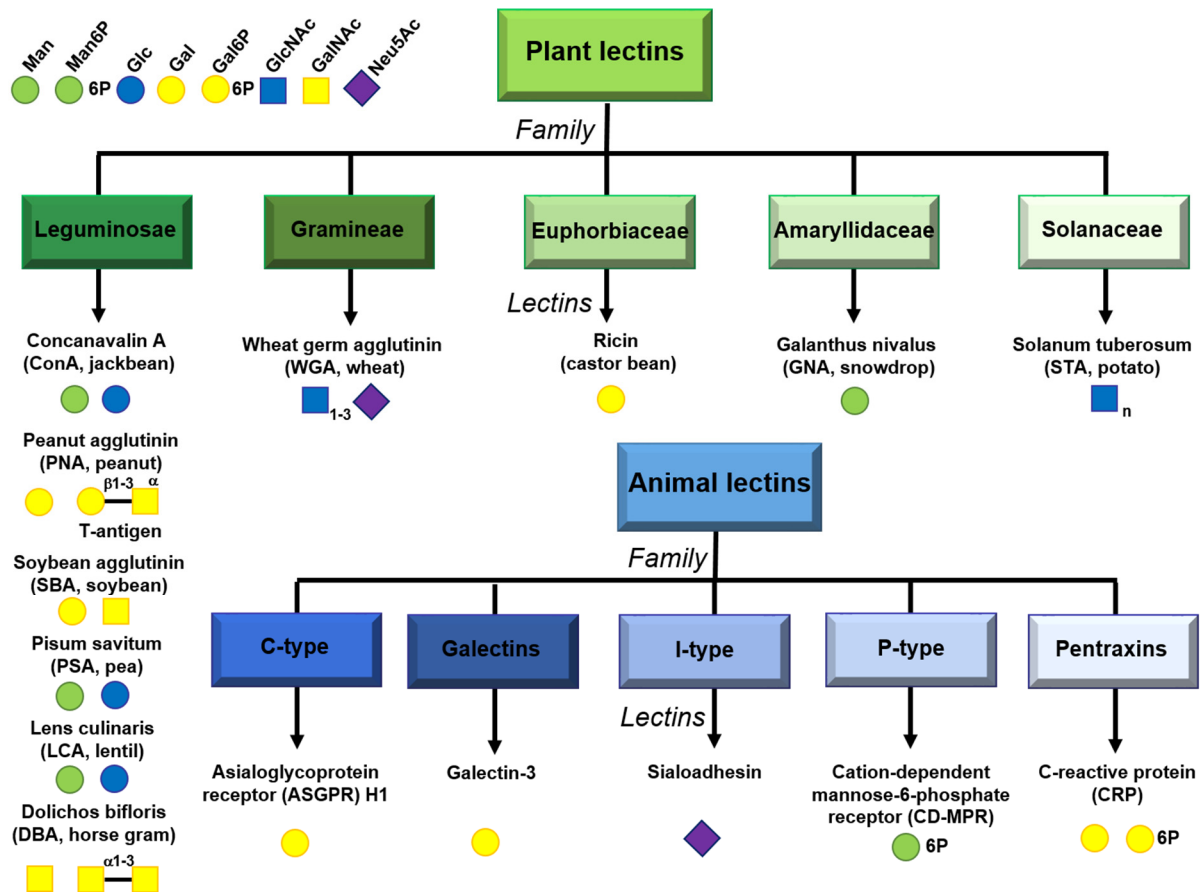
Figure 2. Common plant and animal lectins and their carbohydrate attractants according to Sharon[1].

Besides this specificity of lectins for carbohydrate epitopes, a very characteristic property of the carbohydrate ligand-lectin receptor binding is that their individual interactions are relatively weak.[11-13] Their equilibrium constants are typically in the millimolar[5, 14] and higher micromolar range (10^3 to 10^6 M^{-1}).[5, 11-13] Compared to the interactions between an antibody and antigen[15-16], which obtain equilibrium constants in the micro- and picomolar range (10^4 to 10^{11} M^{-1})[16-17], the carbohydrate protein interactions are weak and in contrast to them not characterized by a "tight" binding.[11-13, 18-19] Today, it is well recognized that nature overcomes the individual weak interactions by combining multiple copies of single carbohydrate ligands, which then bind to clustered proteins presenting several carbohydrate recognition domains (CRD).[5, 11-13, 17] The combination of the single carbohydrate binding epitopes on one oligosaccharide scaffold leads then to collective interactions between one oligosaccharide and its recognizing lectin.[5, 11-13, 17] These collective interactions[11, 14, 20-23] can now compensate for the weak interaction of one single carbohydrate ligand or one single CRD.[5, 11-13, 17] In general, the binding of an oligosaccharide, which presents multiple copies of carbohydrate binding epitopes/ligands to a protein that may have one or multiple carbohydrate binding sites, is known as the "glycoside cluster effect"[11-13, 24-25]. This glycoside cluster effect presents a special form of multivalency[11, 20-23, 26], where the interactions between an $n-$ valent ligand and an $m-$ valent receptor are described (with $n \neq m$ and

$n, m > 1$).[26] Owing to these collective interactions, it is believed that nature is not only able to create a comparably stronger binding event, but also to remain modular and flexible, since single ligands are able to un- and rebind during such processes, resulting in dynamic processes that act far from thermodynamic equilibrium.[11-13, 18-19]

An important example of multivalent binding between the carbohydrates and lectins is the microbial adhesion of the influenza virus to a living cell.[14] The adhesion is initiated through interaction of the trimeric influenza virus hemagglutinin with *N*-acetylneuraminic acid ligands on a host-cell (Figure 3).[4, 14] The collective interactions of multiple sialic acid residues on the host cell and hemagglutinin molecules, mediate the adhesion process and the endocytosis of the virus into the cell interior.[14, 17] Interference with this interaction have been shown for monovalent sialic acid.[4-5] Since the interaction of a monovalent sialic acid with the hemagglutinin are weak, high concentrations of the carbohydrate in the millimolar range have been required.[4-5] In contrast, a multivalent scaffold, which presents several sialic acid residues (e.g. compare Whitesides *et al.*[27-28], sialic acid presenting poly(acrylamide)) was able to even more effectively bind to the virus and thereby to inhibit the interaction between the hemagglutinin and *N*-acetylneuraminic acid.[4-5] This approach of interfering with the adhesion process is called anti-adhesion therapy and presents an important example for the potential use of carbohydrates in medicine.[4] Since multivalent carbohydrates are able to increase the overall binding affinity, lower concentrations of the multivalent scaffold have been required to inhibit the adhesion of the virus to the cell. The binding affinity can thus be modulated by the collective interactions of individual carbohydrate ligands and their presentation on a scaffold. Therefore, understanding the multivalent carbohydrate-lectin interactions remains one main focus in many research fields, as it allows to design even more potent inhibitors, which might interfere with the adhesion of pathogens.[4, 17]
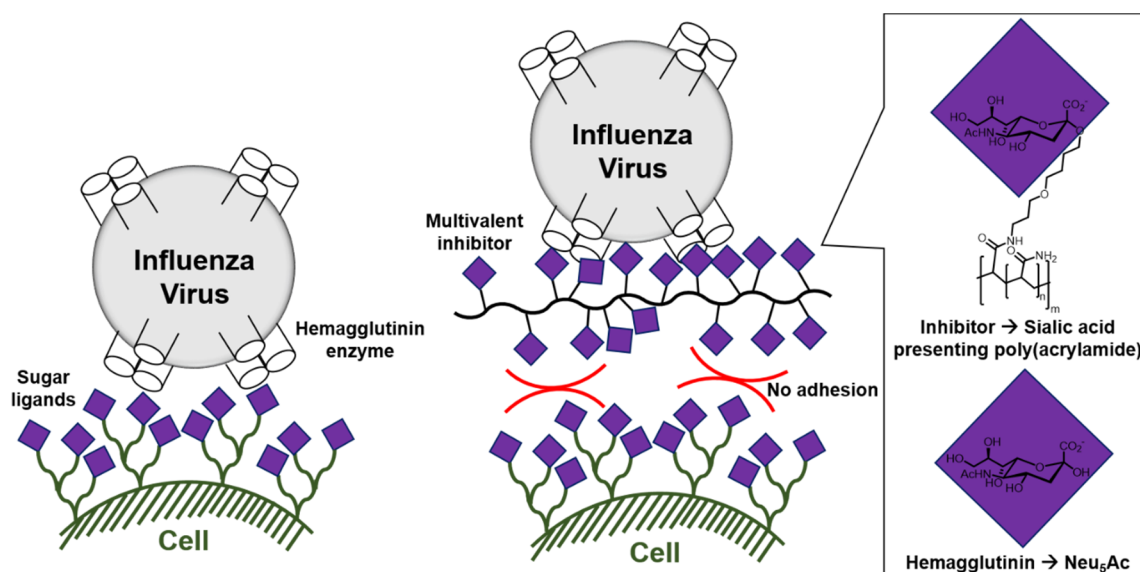
Figure 3. Biological relevance of carbohydrate-protein interactions: Adhesion of pathogens such as the influenza virus to sialic acid according to Whitesides *et al.*[28].

Since it has been suggested that such multivalent interactions are found regularly in biological systems[2-3, 11-12, 20-22], a lot of work has been done for the synthesis of multivalent carbohydrate ligands[29-30] and oligosaccharide mimics. A range of different glycomimetic structures, backbones and architectures have been synthesized to allow for the interference of such carbohydrate-protein interactions as well as to facilitate the understanding of the underlying basic principle of the multivalent effect[5, 25-26].[4-5, 24, 31-40] The use of multivalent glycomimetics substantially reduced the concentration of the glycoligand required to inhibit an adhesion process.[4, 6, 17] This has been demonstrated with a large variety of multivalent glycomimetics e.g. small glycoclusters[29, 34, 41-42], dendritic polymers[5, 43-48] and polymers based on different backbones and architectures, as will be presented in the next subchapter.

1.1.2. Glycomimetic structures – Basic concepts

Despite the scope and importance of natural carbohydrates and their receptors in biology[2-3, 11-12], mechanistic insights[5-6, 33-35, 49-53] into the structure and activity relationships (SAR) of carbohydrate-protein interactions have been hampered by (*i*) the difficult and complex nature of such interactions as well as (*ii*) the heterogeneous and complex structures of natural glycoconjugates. The ubiquitous importance of multivalent interactions in nature have facilitated the development and synthesis of artificial model systems[4-5, 24, 31-40], with whose help the mechanism of carbohydrate-lectin interactions can be characterized. The binding of complex carbohydrates (e.g. oligosaccharides) to proteins primarily takes place between the terminal carbohydrate binding epitopes and the carbohydrate recognition domains of multimeric or clustered lectins.[5-6, 11, 25] It has therefore been suggested[42, 54-55] that the oligosaccharide backbone acts passively during the whole binding process, so that the oligosaccharide scaffold can be replaced by an artificial backbone. Following this concept, researchers have started to use synthetic and artificial scaffolds on which the terminal carbohydrate binding epitopes are presented (Figure 4).[5-6]
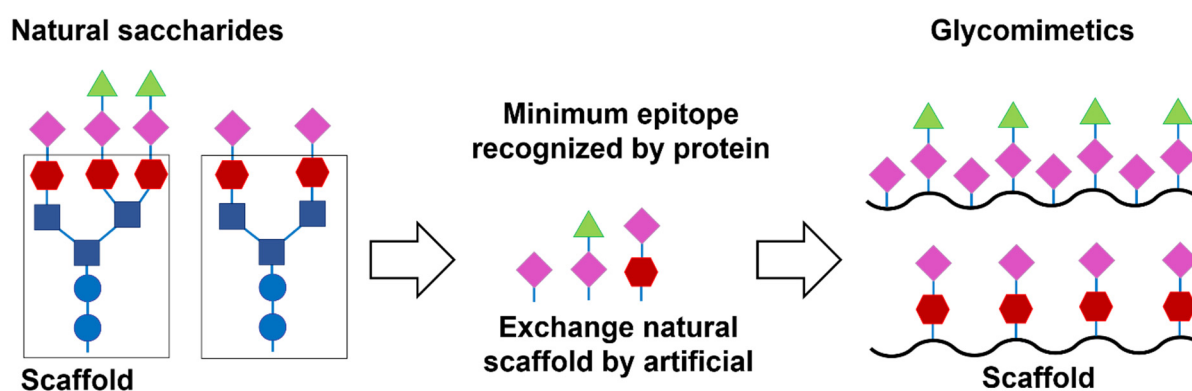
Figure 4. Basic principle of glycomimetics. Glycomimetics are considered as oligosaccharide mimetics with a different scaffold and the presentation of the minimum carbohydrate binding epitopes along the scaffold.

General aspect of glycomimetics

Irrespective of their chemical composition or structural diversity, all glycomimetic ligands have in common an artificial scaffold or backbone, which is presenting multiple copies of carbohydrates.[4-5, 24, 31-40] Their binding to lectins has been extensively studied and a great variety of different scaffolds has been applied for the conjugation and multivalent presentation of carbohydrate ligands.[4-5, 24, 31-40] Common aspects that are taking into consideration for the synthesis of glycomimetics are: (*i*) The ligand density[20-21, 42, 56-63], which may be defined by the spacing between presented carbohydrate ligands, (*ii*) the linker between the carbohydrate ligand and the scaffold connecting both[52, 64], (*iii*) the number of carbohydrate ligands[24, 40, 44, 65-66], (*iv*) the overall size of the glycomimetic structure[5, 33], (*v*) the position of carbohydrate ligands along the backbone[46, 67-70], (*vi*) the type of carbohydrate ligand[6, 42] and (*vii*) the same or a combination of different carbohydrate types (homo- *versus* hetero-multivalency)[42, 55, 71-72]. The variation of these structural features thereby allows to address structure-activity correlations (SACs) of glycomimetic-lectin binding. For this reason and depending on their application, today there is a great number of structurally diverse glycomimetics available. The variety of these different scaffolds has contributed to the nowadays prevalent understanding of the glycoside cluster effect.

The variety in scaffolds of glycomimetics – A few examples

In general, glycomimetic model systems can be subdivided according to their different scaffolds (Figure 5).[4-5, 24, 31-40] These scaffolds range from lower molecular weight compounds[34, 37, 42] over half spherical[5] and spherical ones[41, 45-48, 73] to linear or random-coiled[31-33, 55, 74-77] as well as to glycomimetic compounds, which are presented as biolayers[5, 78] or obtain defined structures, e.g. specific conformations. Such glycomimetics may e.g. include small glyco-clusters[29, 37, 42], -calix[n]arenes[5], -cyclodextrins[5], -dendrimers[41, 45-48, 73], -dendrons[5], -peptides[5, 36, 79-80] and many more. Especially small glyco-clusters have been important for understanding structural aspects necessary for the binding to a multimeric protein receptor. Small glyco-clusters are typically lower molecular weight compounds with well-defined structures that can be synthesized with relative ease. Due to their ease in preparation, large glycomimetic libraries with different structural features can readily be synthesized. Typically, such well-defined lower molecular weight glycomimetics are characterized by a large range of different synthetic scaffolds.[5] The large number of compounds with structural alternations are typically screened for a particular protein, resulting in structure-activity relationships (SARs) as a result of different binding affinities. Many groups have followed this approach, e.g. Lee *et al.*.[5, 11, 81-82] They have prepared over 100 glyco-clusters in search for the highest affinity inhibitor for the hepatic asialoglycoprotein receptor (ASGPR). This approach to study carbohydrate-protein interactions facilitates the comparison and influence of the different glycomimetic scaffolds and is based on the empirical design of glycomimetics.[5]
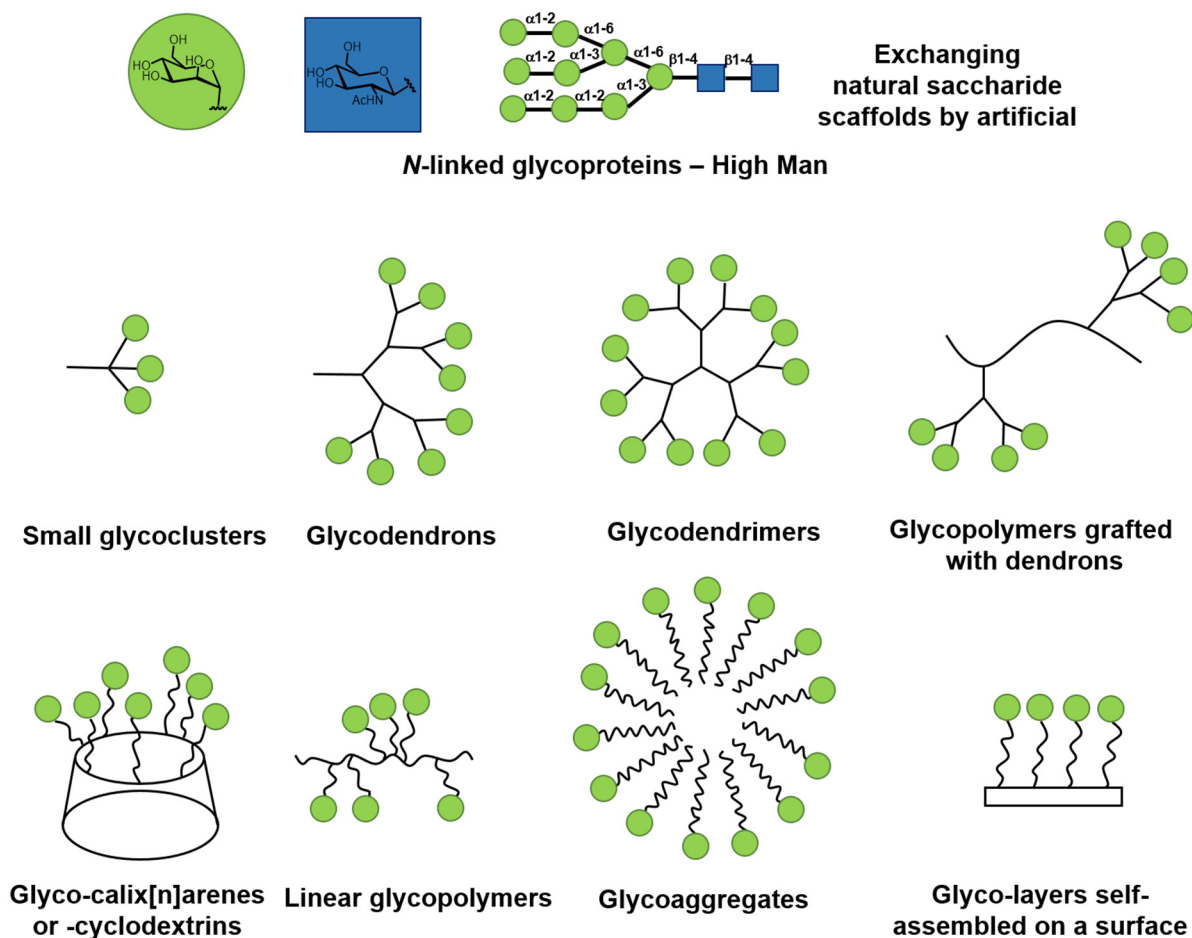
Figure 5. Examples of different glycomimetic structures according to Lindhorst[4].

Other examples of lower molecular weight glycomimetics include different scaffolds that have been studied with the sialylated Lewis X (SLe^x) and its derivatives to inhibit the binding to E-selectin.[5] In this case the design of glycomimetic ligands was based on a rational design. It means that the design of the glycomimetics have been based on structural information of the protein. Into this category falls a range of glycomimetics, which have been synthesized to inhibit bacterial toxins.[5, 83-84] The bacterial toxins belong to the so-called AB₅ family of which the most famous are the shiga-toxin, the shiga-like toxin and the pertussis toxins. Such toxins are characterized on the very symmetric arrangement of the identical carbohydrate binding pockets or subunits.[5] These symmetric subunits are disposed around a core in star-like manner. Bundle's famous STARFISH[84] showed a remarkable enhancement in binding affinity with very flexible linkers between the D-glucose (Glc) scaffold and the presented five repeating gangliosides.[5, 84] Despite the remarkable enhancement in binding, crystallographic data have shown that the STARFISH binds to two toxins rather than to one[5, 84], thus favoring intermolecular binding or a clustering process, which will be discussed in detail the next subchapter.[5]

Another important example of glycomimetic architectures are the higher molecular weight glycomimetics, which are characterized to be spherical in their scaffold and carbohydrate

presentation.[5] Dendrimers and dendrons somehow lie in the middle between the low molecular weight glycomimetics and their high molecular weight analogues, the glycopolymers.[5] Their synthesis is known to be relatively flexible, thereby making it easy to adjust the size and shape as well as its valency.[5] Famous binding studies with glycodendrimers and -dendrons have been performed by Roy *et al.*.[5, 46, 67] In their study with dendrons, which presented *N*-acetylglycosamine ligands for the binding to the Wheat Germ Agglutinin (WGA) protein, they were able to show that enhancement in binding was very much dependent on the valency.[5] While in the former study a successful increase in binding affinity owing to the valency has been shown, the same scaffold decorated with *N*-acetyllactosamine performed significantly worse when the binding to the lectin *E. cristagalli* was studied.[5] Although no detailed conclusion could be drawn so far, many authors hypothesize and argue that a poor enhancement in binding may be due to (*i*) an not optimal ligand spacing[5, 81, 85] or backbone geometry[5, 81, 85] of the presented carbohydrates and (*ii*) the fact that larger scaffolds – which include dendrimers and dendrons – may somehow prevent binding of carbohydrates to the protein for steric reasons[17, 86-89].[5]

Glycopolymers and precision glycopolymers

An important class of higher molecular weight glycomimetics are the glycopolymers[31-33, 55, 74-77]. Glycopolymers can be used to build up high molecular weight and polyvalent structures with a range of different architectures (ranging from linear, branched and star-shaped).[32, 55, 90-91] Typically, artificial backbones are used here, which specifically depend on the polymerization strategy[55, 75, 90-92] used for the synthesis of a particular glycopolymer. Those backbones are either modified with carbohydrates during or after the polymerization resulting in a polyvalent and higher molecular weight macromolecules. Compared to the other classes of glycomimetics, the advantage of glycopolymers lies in their size.[5] Their size is typically in the range of other lectins or even bigger.[5] Compared to other glycomimetics, their size then allows them to associate with the target protein in different ways[17, 86-89] (different possible ways to bind to the protein; see next chapter), thereby either facilitating or diminishing the binding to it[42, 54-55], resulting in higher or lower binding affinities. Depending on the application of glycopolymers, both can be beneficial for the binding process. As the polyvalent nature of glycopolymers makes them highly multivalent glycomimetics, usually a great increase in affinity is observed.[5-6, 42] Their intrinsically disperse nature, however, often hampers a more detailed understanding of their multivalent binding.[6, 32, 90]

Nevertheless, glycopolymers have been successfully used as oligosaccharide mimetics in a great number biological applications[4, 86-89, 92] as well as structure-activity binding studies[33, 74-77, 86-87]. An important example towards the development of potential drugs is the sialic acid presenting poly(acrylamide) influenza hemagglutinin inhibitor as introduced by Whitesides *et al.*[27-28, 86-89] (Figure 3). Other examples include the glycopolymers presented by Haddleton *et al.*[55, 59, 91] (poly(*N*-glycosyl 1,2,3-triazole)), which were used for the interactions with lectins, that play important roles in controlling the immune responses.[55] Important structure-activity studies performed on glycopolymers[5] were reported by Kiessling *et al.*[20-21, 24, 33, 39-40, 56] and Davis *et al.*[93]. The former

group has investigated the impact of different glycopolymer architectures on the resulting binding to lectins. In the latter case, thermodynamic results have revealed that poly(methacrylate) glycopolymers are readily able to cross-link when they were interacting with lectins.[93]

To overcome the limitation of disperse glycopolymers and obtain glycopolymers, which are sequence-defined and even monodisperse, recently so-called precision glycomacromolecules have been introduced by Hartmann *et al.*[94-105]. The group of Hartmann presented a new strategy for the synthesis of precision glycomacromolecules[100-105] based on the Solid Phase Polymer Synthesis (SPPoS)[94-96, 98-103, 105], which will be explained in more details in Chapter 1.3. In contrast to classical glycopolymers, the use of precision glycomacromolecules allows to perform precise SACs based on their chemical composition and architecture.

1.2. Multivalent binding of glycomimetics

The "glycoside cluster effect"[11-13, 24-25] as introduced by Lee *et al.*[11] is one example for the multivalent effect[26] and in general describes an affinity enhancement as a result of collective ligands or interactions between one or several mono- or multimeric protein receptors and a multivalent ligand.[11-13, 24-26] Here, either mono- or multiple carbohydrate ligands can be presented on a glycomimetic scaffolds that then either bind to a multi- or monomeric protein receptor or both.[11-13, 24-26]

Many multivalent binding interactions between glycomimetics and proteins have been shown to be able to create "stronger" binding events as compared to their monovalent reference.[4, 11-13, 24-26] The acceleration in binding affinity has been reported to be due to different so-called multivalent binding modes[6, 18-19, 106-110]. Those binding modes may either participate individually or simultaneously and are believed to be based on the structural features[5-6, 20-21, 55-72] of the glycomimetics and the proteins. As a result, the different binding modes, which are described below, are believed to be specific and sometimes even limited to a certain glycomimetic class.[5]

The following examples will therefore highlight the multivalent binding modes in a general context and describe the basic mechanistic assumptions, which were concluded from a whole different range of glycomimetic structures. Where necessary, explicit examples of glycomimetic structures will be highlighted, supporting the particular multivalent binding mode.

Basic mechanistic assumptions: Definitions of intra- and intermolecular binding and statistical rebinding

The design and synthesis of glycomimetics and especially glycopolymers and the study of their interactions with proteins have led to some basic mechanistic assumptions[20-21, 54-59, 110-113]. The most prevalent ones can be classified into two types of possible binding modes: (*i*) The intramolecular binding of a multivalent ligand to a protein as referring to Whitesides *et al.*[5, 17, 26] and (*ii*) the intermolecular association as referring to Brewer *et al.*[19, 34, 53, 114], Homans *et al.* [115], Toone *et al.*[25,

[37-38, 116] and Ercolani[50] and Schiaffino[50], where a multivalent ligand can accompany several protein molecules, thereby resulting in an aggregative and cross-linking process (Figure 6). (*iii*) Another important example of the multivalent binding mode is the statistical rebinding[18, 106, 110-112, 117], which is further associated with an intermolecular binding process.

(*i*) An *intra*molecular binding process is characterized by the fact that ligands attached to a multivalent scaffold are able to span the binding pockets of one protein.[5, 17, 26] Such complexes may be interpreted as a 1:1 binding, where one n-valent ligand binds to one m-valent receptor.[26] (*ii*) Conversely, an *inter*molecular binding takes place when individual ligands of a multivalent scaffold bind to more than one multimeric protein molecules or vice versa.[6, 49-50, 80, 118] Here, an $n-$ valent ligand might bind to an $m-$ valent receptor through a 1:2 or 2:1 complex (Figure 6).[6, 49-50, 80, 118] Both the intra- and intermolecular processes can be quantified by the thermodynamic state functions.[17, 49, 119-123] (*iii*) The statistical rebinding effect[18, 106, 110-112, 117] is often assumed to participate most likely in intermolecular binding processes. Here, the individual ligands, which are presented on a multivalent scaffold, are able to un- and rebind through micro-equilibria. Literature further differentiates between the a) binding and rebinding mechanism[110], where individual ligands successively associate and dissociate from the binding pocket of one protein and the b) bind-and-jump mechanism[18, 117], where the multivalent ligand is allowed to perform a random walk through the cross-linked proteins.[106]

These three processes can even be connected to each other by their binding equilibria[50]. In their theoretical calculations, Ercolani[50] and Schiaffino[50] as well as Hunter[107-108] and Anderson[108] have shown that the occurrence between an intra- or intermolecular process heavily depends on the concentration of the multivalent scaffold used (and not primarily on its structure).
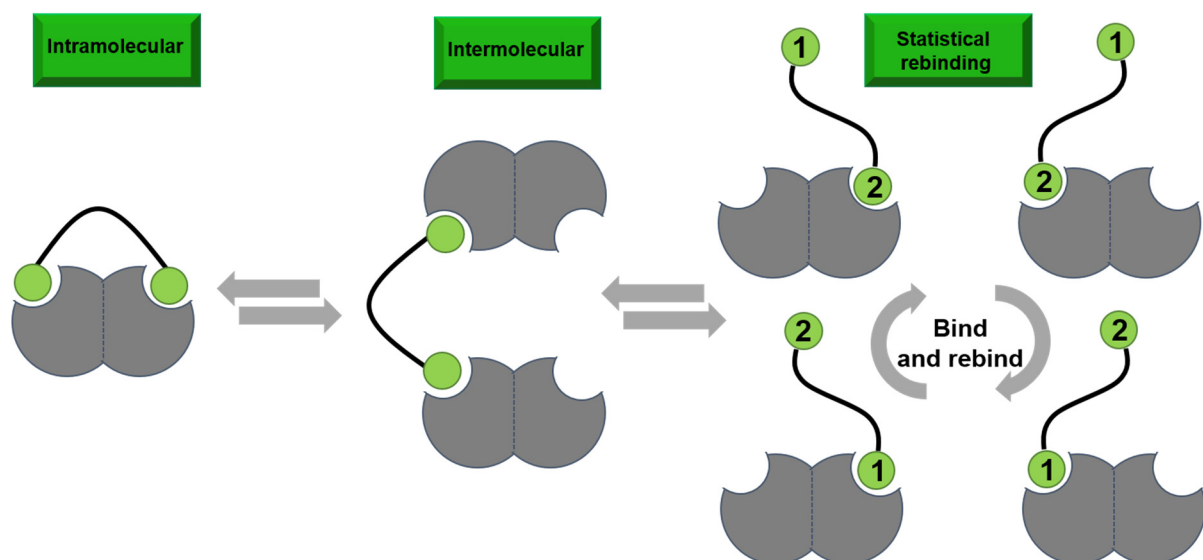
Figure 6. Potential multivalent binding modes of a divalent ligand to a divalent receptor undergoing intra- or intermolecular binding as well as statistical rebinding.

Further, Hunter[107-108] and Anderson[108] have demonstrated that an intermolecular binding process might be accompanied by so-called partially bound states. In this case, either a protein binding pocket or a ligand on the multivalent scaffold may be free, so that micro-equilibria can be estimated[110], where some of the ligands are able to un- and rebind again[110] (Figure 6).

Examples for the intra- *versus* the intermolecular binding

The above intramolecular binding mechanism has been described in detail by Whitesides *et al.*[17], and is based on their experimental results of glycopolymers binding to protein receptors. This mechanism points out that the affinity enhancement, which is observed with such an intramolecular process (a chelate), is a pure entropic correction of the binding free energy.[17, 26, 50] The affinity gain is often termed in this case as the binding "avidity"[17, 124] – a biological term, which has previously been used for antibodies.[17, 124] The binding avidity is here often believed to be significantly higher as compared to its monovalent binding affinity.[17, 26] Associated with this chelate binding mechanism and the significant gain in binding avidity is the sensitivity of spacers[17, 26] between carbohydrate ligands. Often associated with this mechanism is the so-called perfect fit[17, 26], meaning that spacers are designed such that they are able to bridge e.g. two protein binding pockets perfectly.[5-6] These hypotheses have led to the assumption that the spacer connecting the carbohydrate ligands should be "stiff"[6, 40, 73, 84], which mostly should account for the entropic loss during binding.[6, 17, 26] To date, it is still believed that the stiffer the linker, the more probable is the intramolecular binding and the more flexible the linker, the less probable a chelate will form.[6, 17, 26] However, recent studies by Homans *et al.*[115] on the spacer influence as well as theoretical models by Ercolani[50] and Schiaffino[50] show that the binding mechanism resulting in a chelate might be less sensitive for such spacer alternations and more a concentration dependent process.[50]

Although literature shows few examples[6, 40, 73, 125], where binding resulted in a chelate, this binding mode remains the exception rather than the rule.[6, 50] This observation is further supported in recent experimental results by Homans *et al.*[115] and Whitesides *et al.*[111]. The former have found that a favorable entropy can also occur when gain in binding affinity is not significantly higher as compared to a monovalent species.[6, 115] Their experimental results thus made them hypothesize that the role of entropy in an intramolecular binding processes might not be as dramatic as initially suggested. Further, based on their experimental result, as also supported by Brewer *et al.*[19, 34, 53, 114], they even suggest that the role of a chelate binding is not as relevant in biological processes[50] since the chelate effect represents rather a "tight" binding process.[106] However, natural binding processes are rather characterized by a high flexibility of the binding modes.[106] Only due to their several micro-equilibria[110] they are able to maintain a "binding and sliding" (statistical rebinding)[106] of a multivalent ligand. Recent experimental results by Whitesides *et al.*[111] further support this hypothesis. They were able to show that a change in ΔG and the equilibrium binding constants is rather insensitive to changes in the spacer length as well as its chemical composition.[111] Flexible spacers behaved the same way as stiff spacers.[111]

Glycopolymers and their binding modes

Important model systems for which the above binding modes and energetics have been observed are glycopolymers. Typically, glycopolymers are measured on the valency corrected basis[5-6, 80] in inhibition or competition/inhibition experiments and report on activity enhancements most often by IC_{50} values.[6] Interestingly, for glycopolymers it was shown that flexible polymers are as potent as rigid polymers or even better.[6, 126] A few groups have also hypothesized that the mechanism of polymer binding to a surface coated with lectins might go through several binding modes (as described above). It was reported that for such glycopolymer materials the intramolecular binding process may be accompanied by the statistical rebinding event. These observations are also supported by recent results of Brewer *et al.*[106], where the binding of biopolymers prompted them to believe a statistical rebinding event to be operative in terms of a binding and sliding mechanism (a walk through the cross-linked proteins in solution).[106] Often, when lower Relative Inhibitory Potencies (RIPs) and thus lower activities are observed with high molecular weight and high ligand density polymers, or when the comparison of two polymers with different structural features leads to the same RIP values, then steric hindrance is believed to be operative, or the so-called steric shielding effect[5, 12, 17, 86-89].

Precision glycopolymers and their binding modes

Aiming at the decrease of the complexity of the multivalent interactions between glycopolymers and lectins, Hartmann *et al.* introduced so-called precision glycomacromolecules[100-105]. These macromolecules belong to the family of precision polymers[105, 127-128] and are characterized by their monodispersity and sequence-controlled carbohydrate presentation as well as their high synthetic flexibility.[100-105] Their well-defined structure[100-105] makes it now easier to conclude on a structure-property correlation (SPC). To study the influence of different structural features to the model lectin Con A, a range of homo- and hetero-multivalent glycomacromolecules were synthetized *via* the SPPoS (see next chapter).[100-105] Overall, homo-multivalent glycomacromolecules presenting αMan ligands, were found to have an increased RIP with increasing number of αMan ligands.[105] Further, a non-linear correlation between the valency and the RIP was observed for these systems.[105] It was further hypothesized that there seems to be rather an optimum number of carbohydrate ligands resulting in different RIPs, so that binding might take place through a statistical rebinding as well as through sterical shielding.[100-105] Interestingly, it was found that monovalent αMan presenting glycomacromolecules showed an increase in the RIPs as compared to methyl α-mannose (MeαMan).[105] Based on these experimental observations, it was hypothesized that an increase in the RIPs could be a result of secondary effects[42, 54-55] as well as sterical effects[5, 12, 17, 86-89].[105]

1.2.1. General aspects on energetic features of multivalent carbohydrate-lectin interactions

Different binding assays quantifying multivalent binding

There are several methods how to measure and quantify the multivalent binding.[6, 26] Assays such as the hemagglutination and competition/inhibition assays as well as different spectroscopically methods and surface plasmon resonance (SPR) are commonly used to determine the equilibrium binding constant K that gives information on the binding free energy ΔG.[6, 26] Such assays are utilized to determine the binding strength based on the structural features of the multivalent glycomimetics.[6, 26] It is important to consider that the binding assays might significantly differ in their experimental set-up[26] and thus also result in different multivalent complex formation[6, 26, 38, 90], thereby possibly over- or underestimating certain binding contributions.[38]

Microcalorimetry allows for the determination of binding energetics

One important method to determine the binding energetics is microcalorimetry, such as the *Isothermal Titration Calorimetry* (ITC).[26, 129] ITC does not only allow for direct measurement of the binding enthalpy ΔH and calculation of the equilibrium constant K, the binding free energy ΔG and the binding entropy ΔS, but also for the temperature dependent measurement of the binding enthalpy and thus for calculation of the heat capacity ΔC_p.[18, 109, 116, 129-134]

$$\Delta G = -RT \cdot \ln K_a = RT \cdot \ln K_d = \Delta H - T\Delta S \tag{1}$$

Here, ΔG, ΔH and ΔS refer to relative changes in binding free enthalpy/energy, binding enthalpy and entropy, respectively. K_a represents the macroscopic association equilibrium constant and K_d the macroscopic dissociation equilibrium constant.[129] ITC experiments are typically performed in solution.[129] The challenge with using this method, which allows to quantify the interactions, is in preventing the aggregation of the protein during the binding processes and finding the right fit.[129-130, 135] Only when the "right" fit is found for the measured data, these quantities will be representative for the whole binding process.[129-130]

A typical ITC experimental set-up works as follows.[129] The multivalent ligand is placed in the syringe, while the protein is then placed inside the sample cell of an ITC instrument. The instrument contains two cells, the sample and the reference cell, which are shielded by an adiabatic heat jacket. The adiabatic heat jacket allows then to measure differences in the heat between the sample cell and the reference cell in the micro-Joule (μJ) region, which is either released or absorbed when the ligand is continuously added in given time intervals to the sample cell. The addition of constant volumes of the ligand through the syringe into the cell is associated either with the release of heat or consumption, since the most binding process in terms of ligand and receptor interactions are associated with heat changes, as soon as the ligand and the protein associate. The difference in the heat signal and thus in temperature of the sample cell from that of the reference

cell is then recognized by the instrument, and the electrical signal/power required to adjust the sample cell back to the temperature of the reference cell, is then the true measured signal and called the heat flow or heat power signal. The different heat flow signal following every addition of the ligand are then integrated, giving direct access to the measured heat and so to the binding enthalpy.[129-130]

The above described experiment is called the direct titration experiment[130]. However, a reverse situation is also applicable, where the protein is titrated to the ligand, which is then called reverse titration[114] and has been especially used to verify the binding stoichiometries n of multivalent ligands by Brewer *et al.*[114],[129] However, in this case typically large amounts of the protein are required, which most often lead to aggregation problems during the titration experiments, which is one of the known limitations of the micro-calorimetry.[130] Further, another challenge is to use the fitting procedure, which besides the binding enthalpy ΔH then determines the equilibrium constant (K_a or K_d) and the binding stoichiometry n.[129-130] As pointed out by Brewer *et al.*[49], especially for multivalent systems[18-19, 34, 49, 106], it is essential to use the "right" fitting model as only then representative quantities are obtained.[129] In a first case, this has to do the experimenter himself. Here, most experimenter typically try to "valency correct" the data and fit the binding isotherms to a binding model. However, the involvement of the valency in the binding process is something that needs to be determined experimentally.[49, 129] Thus, if the binding isotherm shows a sigmoidal curve with small deviations from that, then already from its shape it can be concluded if the binding process is e.g. a cooperative one or not[53],[129] Therefore, it might be the right choice to at first use the model of *one sets of independent binding sites*. This model will allow to determine the binding stoichiometry n of the multivalent binding process. Only thereafter[49], the binding stoichiometry n can be further verified, if necessary, in a reverse titration experiment, which not only allows to confirm the binding stoichiometries but also gives access into the micro-equilibria, which quantify the binding of individual carbohydrate ligands, one after another (compare Brewer *et al.*[19, 34, 53, 114]).

<u>Typical energetic behavior of carbohydrate-protein interactions</u>

With respect to the enthalpy and entropy, the following energetic picture is most often observed for carbohydrate-protein interactions[6]: The binding enthalpy is more negative than the binding free energy, whereas the entropy is most often compensating for the binding enthalpy with values always being negative, which indicates an unfavorable entropic contribution.[6, 34, 53, 114] This very pronounced and typical enthalpy-entropy compensation[107, 130, 136-139] (EEC) behavior is very characteristic for interactions that participate in water media.[6] The most common interpretation approaches assuming there is a true physical origin of EEC[130] for this observation are (*i*) the loss of conformational degrees of freedom upon binding[6, 107, 130] and (*ii*) solvent reorganization events[6, 130]. As earlier pointed out by Hunter *et al.*[107], EEC hypotheses rely on the following aspects: Where there is structural tightening and thus gain in the binding strength in terms of e.g. hydrogen bonding, then the system loses favorable entropy in terms of degrees of freedom and increasing

complex organization. Conversely, when there is less structural tightening due to structural features of the ligand that do not allow to maximize the hydrogen bonding, then there is more freedom for the ligand to move in space and a lower extent of complex organization. Consequently, there is diminution of the binding enthalpy, whereas the binding entropy gets more favorable (exhibiting less negative values).[107]

From all of these studies it appears, that there seems to be some rational behind the multivalent binding mechanism. Both, the inter- and intramolecular one, were so far concluded from experimental observations of glycomimetics. Nevertheless, the role of the structure of the multivalent ligand and the protein and their resulting energetics[18-19, 34-35, 52, 106] still remains somewhat unclear to conclude on the overall binding mechanism.[6] The current research rather pinpoints to the fact, that the multivalent mechanism[6, 18-19, 50, 106-110] is highly system dependent: A different multivalent glyco-structure and a different protein will potentially yield different binding modes.[6]

1.3. Solid phase polymer synthesis of precision polymers

One of the upmost goals in recent years in polymer chemistry is the synthesis of polymers with well-defined backbones, architectures, monomer sequences, chain-length as well as the control over the structural behavior in water media. Although glycopolymers are considered as the structural mimics of oligosaccharide in terms of their branching points and architectures, their size as well as their collective presentation of carbohydrate ligands, glycopolymers significantly differ from the natural oligosaccharides in one additional aspect: natural oligosaccharides are monodisperse. In contrast, classical polymers usually have a molecular weight distribution. To be able to more closely mimic the natural functions of oligosaccharides, it is thus of great interest to gain absolute control over the molecular weight distribution, selective positioning of branching points and carbohydrate ligands along the backbone as well as the control over the overall polymer architecture.[32, 90]

To further promote the understanding of glycopolymer-receptor interactions and the underlying multivalent binding mechanisms, alternative synthetic procedures have recently been introduced by Hartmann *et al.*[94-105], which allow for a highly modular and monodisperse synthesis of well-defined glycomimetic macromolecules[100-105]. With the assembly of tailor-made functional building blocks, full control is given over the monomer sequence, the chain-length, the backbone composition and the polymer architecture.[94-105] The chemically defined structure as well as the sequence-control along the backbone of such precision macromolecules then allow for direct SPCs and additional insights into their multivalent binding modes, as it has been shown for a first series of precision glycomacromolecules by Ponader *et al.*[100, 103-105]. The general principle of the SPPoS and a few synthetic examples of precision glycomacromolecules introduced by Ponader *et al.* will be shortly highlighted in the next section.

1.3.1. <u>General principle</u>

Solid supported synthesis initially introduced by the pioneering work of Merrifield[140] for the synthesis of peptides (SPPS) currently includes a huge variety of techniques and procedures[141], ranging from the synthesis of large and small peptides[79, 142-148], carbohydrates[149-151], oligonucleotides[152-153], oligosaccharides[149-151, 154-155], glycopeptides[156] as well as the synthesis of artificial biomimetic scaffolds[94-103, 105, 157]. In contrast to the solution synthesis of such biopolymers, the solid phase synthesis is associated with a more rapid synthesis, since time consuming multiple step synthetic procedures including multiple isolation and purifications cycles are circumvented.[158] Here, typically the purification is only performed after the complete oligomer has been prepared and the reagents during the assembly of the oligomers are simply removed by filtration.[141]

Today, the solid supported synthesis can be found in almost every area of synthetic chemistry, allowing also for the synthesis of natural[149-152, 156-157] or biomimetic oligomers[95-99, 105, 157]. One important example is the solid phase synthesis of precision macromolecules, as introduced by Hartmann *et al.*[94-103, 105]. Here, different structures are prepared ranging from linear[94-98], cationic and asymmetrically branched oligo(amido amines)[99] to ß^{3r3}-peptidomimetics[127] and precision glycomacromolecules[100-102, 105]. Compared to the SPPS, this so-called Solid Phase Polymer Synthesis[127-128] (SPPoS) is also based on the repetitive covalent addition of building blocks to an appropriate chosen solid support (Figure 7). The difference between the SPPS and the SPPoS lies in their building blocks.[127] Instead of using natural amino acids (AAs), the preparation of precision polymers[105, 127-128] relies on tailor-made functional building blocks, which are inspired from the classical polymer chemistry. The similarity lies in the use of advanced protection/deprotection, coupling and cleavage protocols known from the SPPS. Thus, the novelty of the SPPoS[127-128] comes from the design of functional building blocks, their assembly and easy exchange on solid phase, allowing to control the positioning, spacing, density and the backbone architecture itself.[127]

The basic principle of the SPPoS is illustrated in Figure 7. For the repetitive addition of the appropriate building block, first the corresponding solid support (polymer beads) presenting appropriate linkers is chosen according to the protecting groups' startegy used.[127] As will be seen in the next subchapter, the by Hartmann *et al.* introduced SPPoS[94-103, 105] of precision polymers[94-99, 105, 127] so far uses the Fmoc coupling strategy[141]. This means that the base labile Fmoc protecting group is used as a temporary protection, following the addition of every building blocks sequence until the oligomer is built up.[141] The linker and the resin used here is then in most cases an orthogonal and acid cleavable resin. Most often, the trityl (Trt) or the Rink Amide (RAM) linkers are used, while the resin itself presents a copolymer of polyethylene glycol (PEG) grafted on polystyrene (PS). These so-called Tentagel supports are important, since the swelling behavior of the resin also significantly influences the final yield.[141] This is due to the fact, that the reaction does not only take place on the linkers' functional groups on solid support, which are presented outside the polymer beads.[141] Since the reaction also proceeds inside the cross-linked matrix, the

resin has to have a good swelling behavior in common solvents used for the SPPoS.[158] The final oligomer is then obtained after repetitive building block addition and deprotection. The addition of each building block to the solid support depends on the linker chemistry, which is chosen according to the protecting group chemistry (orthogonality).[141] Through their functional groups, the building blocks are then coupled to the solid support linker. As it also will be seen in the next subchapter, the functional groups of the building blocks carry a terminal carboxylic acid unit, thus allowing for their condensation to primary amines, which are then presented after each deprotection cycle on solid support.[127] Hence, the oligomers are built up from the *C* to the *N* termini.[127] The chemical composition of the final oligomer mainly depends on the sequence of building blocks, which were used during synthesis.[127] The final oligomer is then simply obtained by cleavage of the covalent bond at the position of the solid support linker.[127]
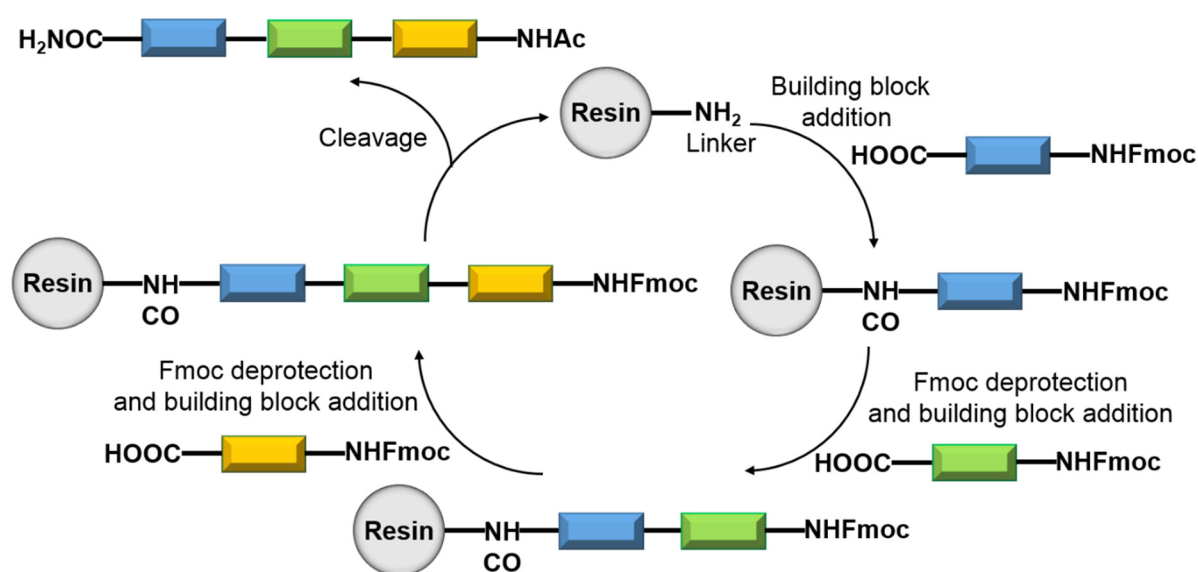
Figure 7. Basic principle of the SPPoS.

Overall, depending also on the backbone structure and properties, molecular weights of about 5000 to 10000 dalton (Da) with up to 20 repeating units can be produced.[127] If bigger polymers are required, then methods to join two macromolecular fragments could be used e.g. based on native chemical ligation methods[159].

1.3.2. Building blocks

A range of different building blocks suitable for SPPoS have been designed by Ponader and Wojcik *et al.*[99-103, 105]. The building blocks can be subdivided into (*i*) functional and (*ii*) spacer building blocks.[127] The functional building blocks allow for the conjugation of biologically active ligands and tags *via* different chemical methods, such as the copper(I)-catalyzed azide-alkyne cycloaddition (CuCAAC) and thiol-ene or thiol-yne chemistry (Figure 8).[99-101, 103, 105, 127] Other functional building blocks are further equipped with orthogonal protecting groups, thereby allowing

to maintain their biological properties as well as their easy synthesis after deprotection.[99, 127] This way the polymer architecture can be readily changed from linear to asymmetrically branched.[99, 127] Further, polycations as well as amphipathic and amphiphilic molecules can be synthesized by alternating protecting group building blocks, e.g. with hydrophobic building blocks.[127]
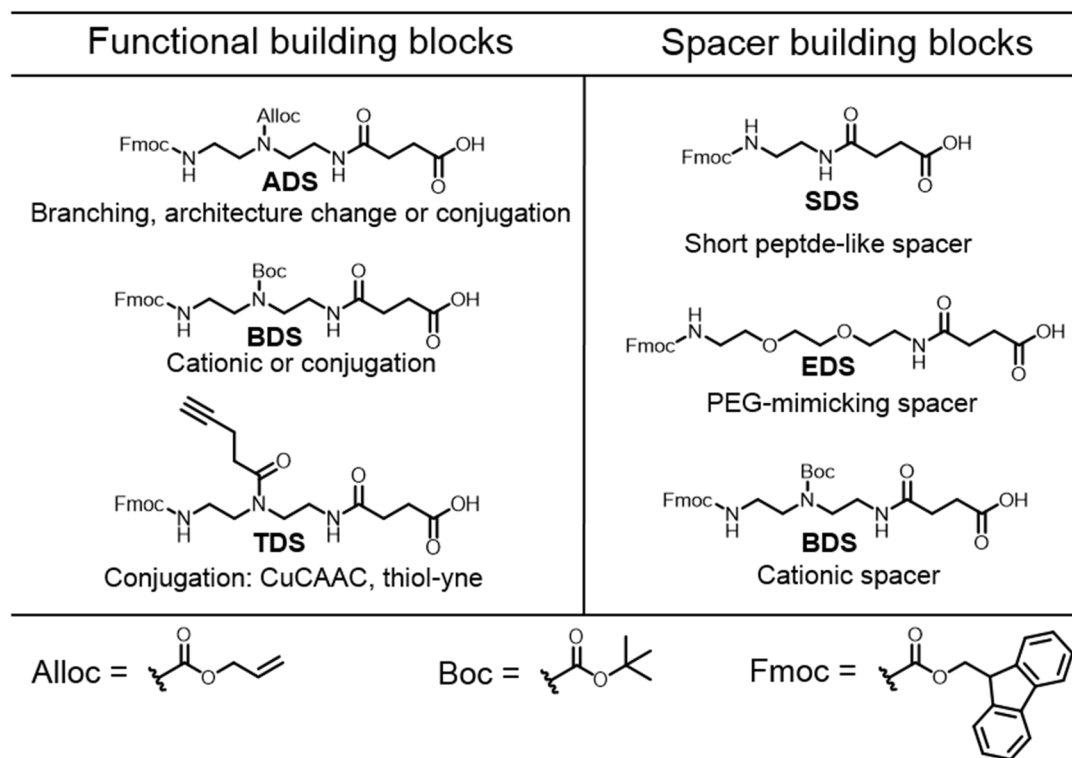
Figure 8. Examples of functional and spacer building blocks used in SPPoS as introduced by Hartmann *et al.*[94-105].

Chiral building blocks allow for the preparation of so-called peptide-mimetics with improved properties, which can adopt secondary structures in water media.[127] Further, a range of so-called spacer building blocks was designed.[96, 100-101, 105, 127] With these spacer building blocks, it is straightforward to modulate the distance between biological tags or biologically active ligands.[96, 100-101, 105, 127]

Hence, this kit of functional and spacer building blocks allows for the very flexible and modular synthesis of different kinds of precision polymers, where structural motifs such as backbone composition, molecular weight, backbone length, branching points, shape and architecture as well as different biologically active ligands and functions can be easily accessed and exchanged.[127]

1.3.3. First generation precision glycomacromolecules

The different functional and spacer building blocks[100, 103, 105, 127] have been applied for the synthesis of precision glycomacromolecules[100, 103, 105, 127]. For the first generation of precision glycomacromolecules, two kinds of building blocks have been used: (*i*) The functional building block that allowed the conjugation of αMan and β-galactose (βGal) ligands with the CuCAAC and thiol-

ene chemistry (TDS) and (*ii*) the spacer building block EDS that mimics the behavior of PEG repeating units, thereby maintaining the flexibility of the oligomer (Figure 9).[103, 105, 127]
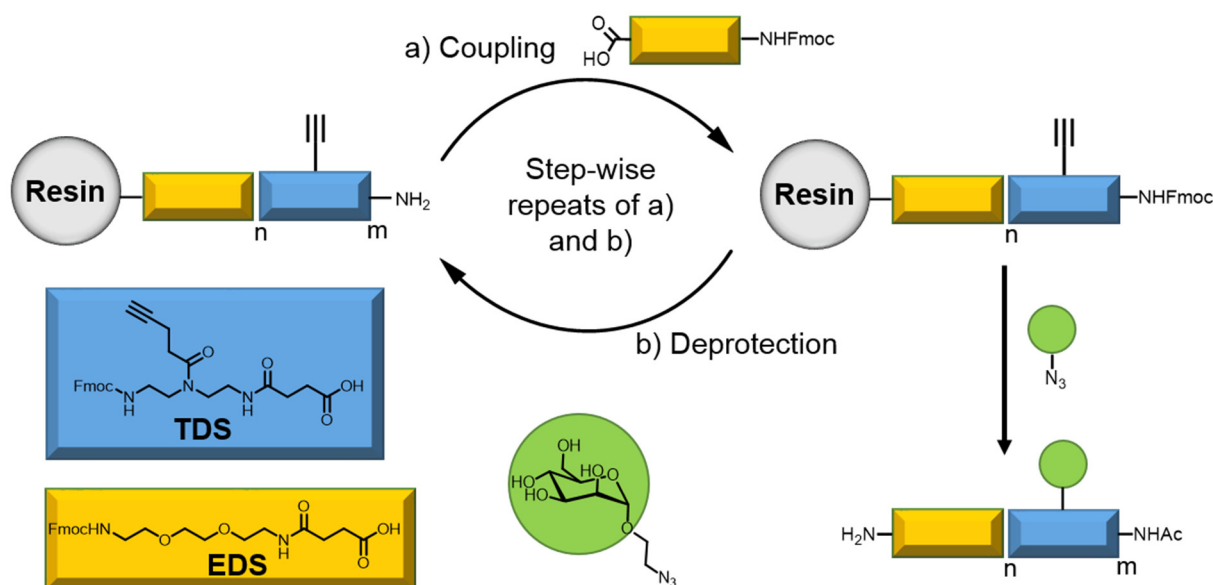
Figure 9. Synthesis of multivalent glycomacromolecules. First, the oligomer backbone is generated, followed by conjugation with carbohydrate ligands using CuCAAC (here shown for αMan ligands).

Using the method as illustrated in Figure 9[105, 127], a first generation of precision glycomacromolecules presenting αMan ligands has been synthesized by Ponader *et al.*[105] and applied to binding studies with the model protein Con A (Figure 10). As mentioned in the previous subchapter, depending on the chemical composition of the final glycomacromolecules, the building blocks TDS[100, 103, 105, 127] and EDS[103, 105, 127] were alternatively assembled on solid support, whereas final on-resin conjugation with αMan azides using CuCAAC allowed to obtain then the final homo-functionalized precision glycomacromolecules[103, 105, 127]. The presented series of the first generation glycomacromolecules differ in terms of their αMan position along the backbone.[105, 127] The backbone length ranged here from penta- to decamers. The pentamers presented the αMan ligands at varied positions along the backbone, whereas in case of the one penta- and decamer, the αMan ligands were placed in close proximity to each other, thereby avoiding a spacing between them and the use of the EDS spacer building block. Thus, the SPPoS synthesis allowed here to vary the αMan position along the backbone as well as the spacing and the valency. This systematic variations in the structural features of precision glycomacromolecules were used so far[105] to study their behavior in their interactions to the model lectin Con A.[105, 127]
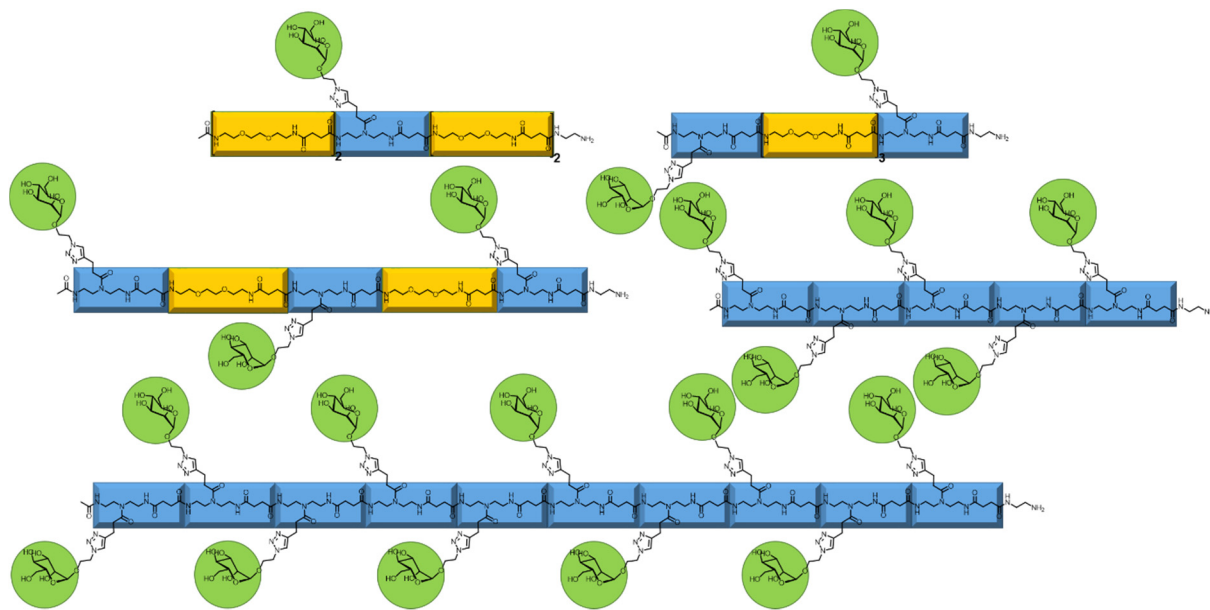
Figure 10. First series of precision glycomacromolecules by Ponader *et al.*[105].

2. Aims and Outline

The "glycoside cluster effect"[11-13, 24-25] as one important example of multivalency[11, 20-23, 26] is characterized as the "enhancement in the activity of multivalent ligand beyond what you would except due to the increase in carbohydrate local concentration (statistical effect) alone"[160]. The large variety of experimental observations of the multivalent effect based on carbohydrate-lectin interactions, have introduced important hypotheses, which describe different binding modes[6, 18-19, 50, 106-110], especially based on the structural features of glycopolymers[12, 42, 56-58, 72, 93]. Today, it is generally presumed that different structural features of glycopolymers directly affect the mechanism of their multivalent binding to a protein.

Recently, the synthesis of so-called precision glycomacromolecules was introduced by Hartmann *et al.*[94-95, 97-102, 105, 127] as one important example of sequence-controlled polymers[90, 127-128, 161]. Precision glycomacromolecules[100, 103-105] are synthesized *via* SPPoS through the sequential coupling of tailor-made building blocks.[96, 99-103, 105, 127] The highly modular assembly of different building blocks allows for control over the monomer sequence, the precise positioning of carbohydrate ligands along the backbone, the spacing as well as the overall chain-length.[94-95, 97-102, 105, 127] With these highly defined glycomacromolecules it should thus be possible to gain deeper insights into the SPC of the multivalent binding of this new class of glycomimetics and glycooligo- and polymers in general.

The motivation of this study is to gain deeper insights into the binding thermodynamics and kinetics of precision glycomacromolecules by controlled variation of several structural features. Indeed, there are only few studies in literature that report on the multivalent binding thermodynamics[19, 25, 49, 72, 93, 109, 115-116] and kinetics[39, 55, 74, 162] of glycopolymers, which also put these quantities into a relation with the chemical structure.

Thus, the main objective of the presented work is to provide basic concepts, which may further help to understand the underlying mechanism of multivalent binding of precision glycomacromolecules as model systems. This study is particularly interested in: (*i*) The impact of ligand density and valency, (*ii*) the effect of the carbohydrate linkage between the αMan ligands and the polymer backbone, (*iii*) potential secondary effects resulting from the polymer backbone as well as (*v*) the contribution of the polymer architecture, varying from linear to cyclic, on the resulting binding energetics and kinetics. To answer these questions a series of linear and cyclic precision glycomacromolecules is designed that allow for such a systematic and comparative study of structure-function correlations (SFCs). Due to their straightforward yet highly variable SPPoS[94-99, 101-102] full control is given over the αMan ligand density, the polymer backbone composition, the polymer architecture as well as the number of αMan ligands attached on the scaffold. The structural features of specifically designed precision glycomacromolecules will be evaluated with the model lectin Con A. To further account for the different protein conformations that might also dramatically impact the binding mechanism, its dimer *and* tetramer conformation will be used in

the binding studies. The binding with the model protein Con A will be studied by applying ITC and the recently introduced *kinetic* ITC (kinITC)[163-165].

Understanding the thermodynamic and kinetic signatures of these model systems and their binding processes, and relating them to their structural features will further help in getting a better understanding of the multivalent effect and potentially promote their application in biomedicine, e.g. as anti-adhesive therapeutics.

3. Results and Discussion

The aim of this thesis was to study the effect of different structural features of glycomimetic precision glycomacromolecules, which may have a substantial influence on the multivalent binding thermodynamics and kinetics. In particular, the objective was to evaluate the effect of the (*i*) spacing between presented carbohydrate ligands on the backbone, (*ii*) the type of linkage between the backbone and the carbohydrate ligand and (*iii*) the change of the overall architecture from linear to cyclic.

The Results and Discussion Part is divided into two parts. The first part, which covers the Chapters 3.1 to 3.3, presents the synthesis of all glycomacromolecules. Here, the synthesis of linear and cyclic precision glycomacromolecules is presented (Chapter 3.1 and 3.2) as well as the evaluation of a cyclization strategy that potentially would allow for a tandem deprotection and macrocyclization, thereby maintaining the synthesis of cyclic oligo(amido amines) (Chapter 3.3).
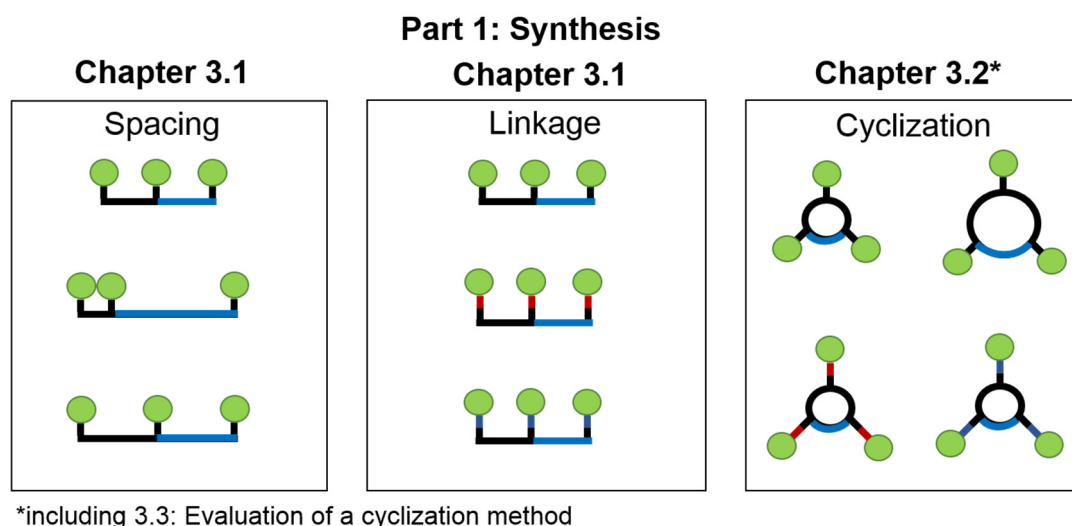
Figure 11. Outline of the Results and Discussion section. Part 1: Synthesis of Precision Glycomacromolecules.

In the second part of this thesis, the chapters 3.4 to 3.6 present the thermodynamic and kinetic studies of precision glycomacromolecules synthesized in chapters 3.1 and 3.2. In Chapter 3.4 first the experimental design of thermodynamic ITC experiments is presented and further covers the use of kinITC as a method for the determination of the multivalent binding kinetics. Here, key considerations for the thermodynamic and kinetic experimental design will be highlighted. The thermodynamic and kinetic data are then discussed according to the structural features of the synthesized precision glycomacromolecules, starting with thermodynamic and kinetic evaluation of the αMan density and different αMan linkers (Chapter 3.5), followed then by Chapter 3.6 presenting the evaluation of the overall oligomer architecture – cyclic *versus* linear glycomacromolecules.

3. Part 1: Synthesis of Precision Glycomacromolecules

3.1. Synthesis of precision glycomacromolecules varying in the spacing along the backbone as well as the linker from the backbone to the carbohydrate

In order to systematically assess the influence of structural features of glycomacromolecules on the multivalent binding mechanism, a series of precision glycomacromolecules was prepared as highly defined model systems following well-established SPPoS protocols[99-101, 105]. These protocols are extended towards the synthesis of glycomacromolecules with up to 14 building blocks and 10 carbohydrate ligands. Precision glycomacromolecules either carry ethylene dioxy spacer units within the oligomer backbone (the so-called EDS[100, 103, 105] building block (see Chapter 1.3.2) or shorter SDS spacer building block (see Chapter 1.3.2)). Further, αMan ligands were introduced at well-defined positions within the oligomer segment by using previously established functionalization protocols[105], where the alkyne side chains of the TDS[100, 103, 105] building blocks are functionalized with carbohydrate azides using CuCAAC coupling. The combination of the functional (TDS) and the spacer building blocks (EDS and SDS) allows for the control over the spacer units as well as spacer composition and thus the ligand density as well as the structural valency and molecular weight. The linkage between the αMan ligands and the backbone can be varied by applying differently functionalized αMan ligands. This was done by using the ethylene functionalized αMan azide and the two functionalized αMan azides carrying the longer propyl thiol-ether ethylene group and the benzyl ethylene group (Scheme 1, red and blue αMan ligands, arbitrarily highlighted as "S" (for thiol) and "B" (for benzyl), respectively).[1] Thus, precision glycomacromolecules were synthesized not only altering in their spacer units and valency but also with three different types of αMan linkers.

---

[1] *O*-propyl-3-thio-*S*-ethyl-5-azido-α-D-mannopyranoside ("S") and *O-p*-benzyl-*p*-ethyl-2-azido-α-D-mannopyranoside ("B") have been provided by Anne Müller (Christian-Albrechts-Universität Kiel, group of Prof. Dr. Thisbe K. Lindhorst).
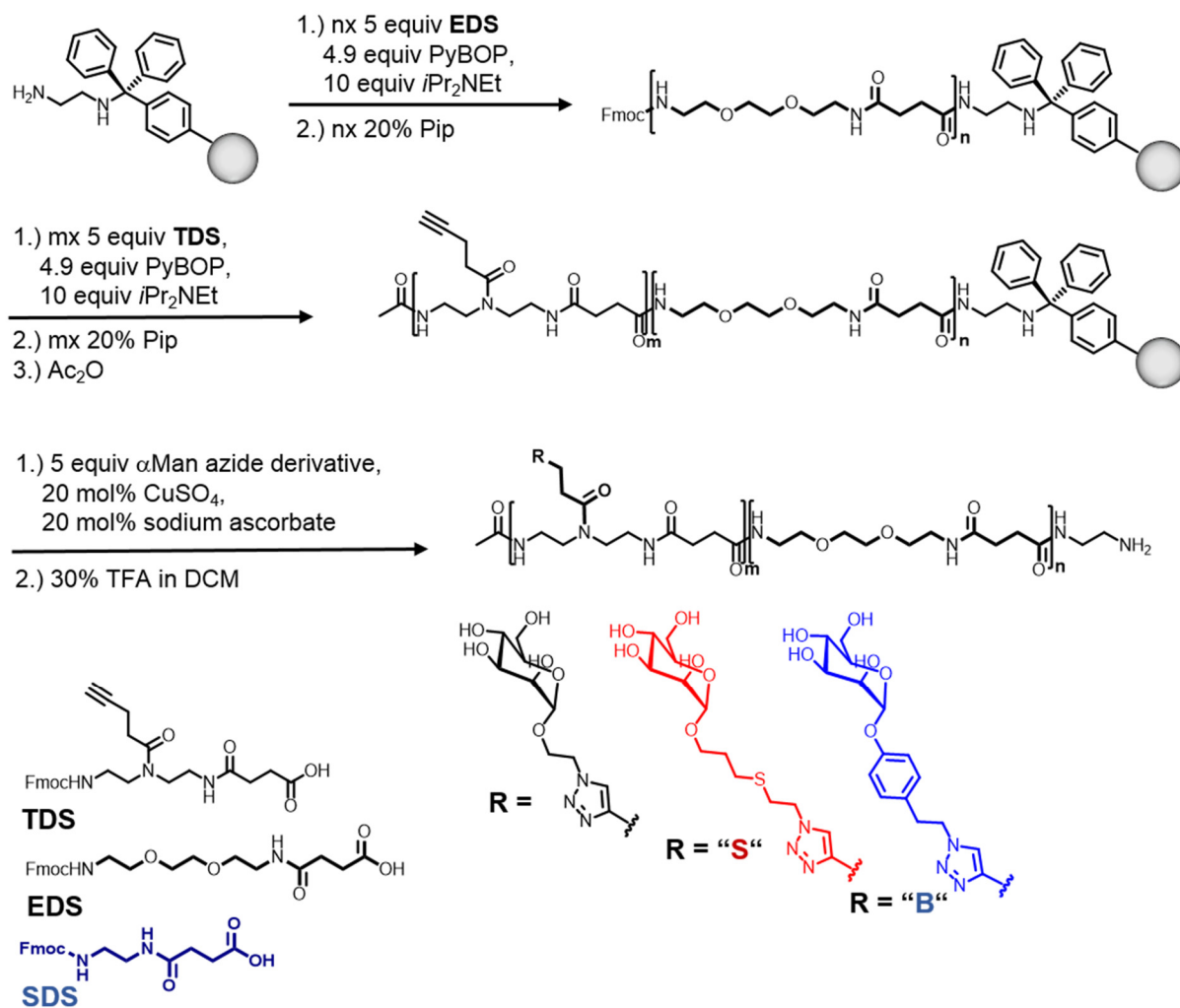
Scheme 1. SPPoS of linear glycomacromolecules with different spacing and αMan linkage.

As solid support, the ethylene diamine (EDA) functionalized Trt Tentagel resin was used due to its good coupling properties that allowed the synthesis of longer oligomer structures (up to 14 repeating units), while maintaining good coupling efficiency.

The different linear glycomacromolecules were synthesized as is shortly described in the following (Scheme 1). The corresponding building blocks were added to the growing oligo(amido amine) chain on solid support by their step-wise addition, using repetitive coupling and Fmoc deprotection. The Fmoc deprotection and coupling procedures were routinely performed following general Fmoc coupling protocols, as were optimized by Ponader *et al.*[100, 103, 105] and Wojcik *et al.*[99, 101-102]. However here, instead of using uronium based coupling reagents such as *O*-(7-azabenzotriazol-1-yl)-*N,N,N',N'*-tetramethyluronium hexafluorophosphate (HATU) or *O*-(benzotriazol-1-yl)-*N,N,N',N'*-tetramethyluronium hexafluorophosphate (HBTU), the phosphonium based coupling reagent (benzotriazol-1-yloxy)tripyrrolidino phosphonium hexafluorophosphate (PyBOP) was used and the excess of equivalents (equiv) of the coupling reagent, building blocks and Hünig's base (*i*Pr₂NEt) were reduced from ~10 and 20 equiv to 4.9 and 10 equiv, respectively.

Larger building block and coupling reagents' excess was not required to drive the coupling process to completion. PyBOP was further used because it is not prone to the guanidinium side-product formation, as it was the case with the uranium based reagents[166], so that the overall yield of the oligomer could be raised. Further, in some of the synthetic procedures, acetylation was performed after each coupling cycle to erase for potential unreacted side-chains resulting in shorter oligomer by-products. If these side-products were still of a few building block repeating units (one to three), then these were simply removed by precipitation from the desired products, since the former still remained in solution. Upon complete formation of the linear oligo(amido amine), the final *N*-terminal capping was performed with acetic anhydride prior to the conjugation with the different αMan building blocks (Scheme 2). Precision glycomacromolecules were then obtained following the CuCAAC for the αMan azide derivatives to the solid supported oligo(amido amine) following the procedure by Ponader *et al.*[105]. The linear precision glycomacromolecules varying in their spacing and αMan linkage were then finally obtained after acidic cleavage from the resin.

Man(3)-5SDS (**1SDS**)

Man(4)-7SDS (**1aSDS**)

Man(1,3,5)-5SDS (**2SDS**)

Man(1,4,7)-7SDS (**2aSDS**)

Man(3)**R**-5 (**1,1S,1B**)

Man(1,5)**R**-5 (**2,2S,2B**)

Man(4)**R**-8 (**1a,1aS,1aB**)

Man(1,6)**R**-6 (**2a,2aS,2aB**)

Man(all)**R**-3 (**3,3S,3B**)

Man(1,9)**R**-9 (**2b,2bS,2bB**)

Man(1,3,5)**R**-5 (**3a,3aS,3aB**)

Man(1,6,7)**R**-7 (**3b,3bS,3bB**)

Man(1,4,7)**R**-8 (**3c,3cS,3cB**)
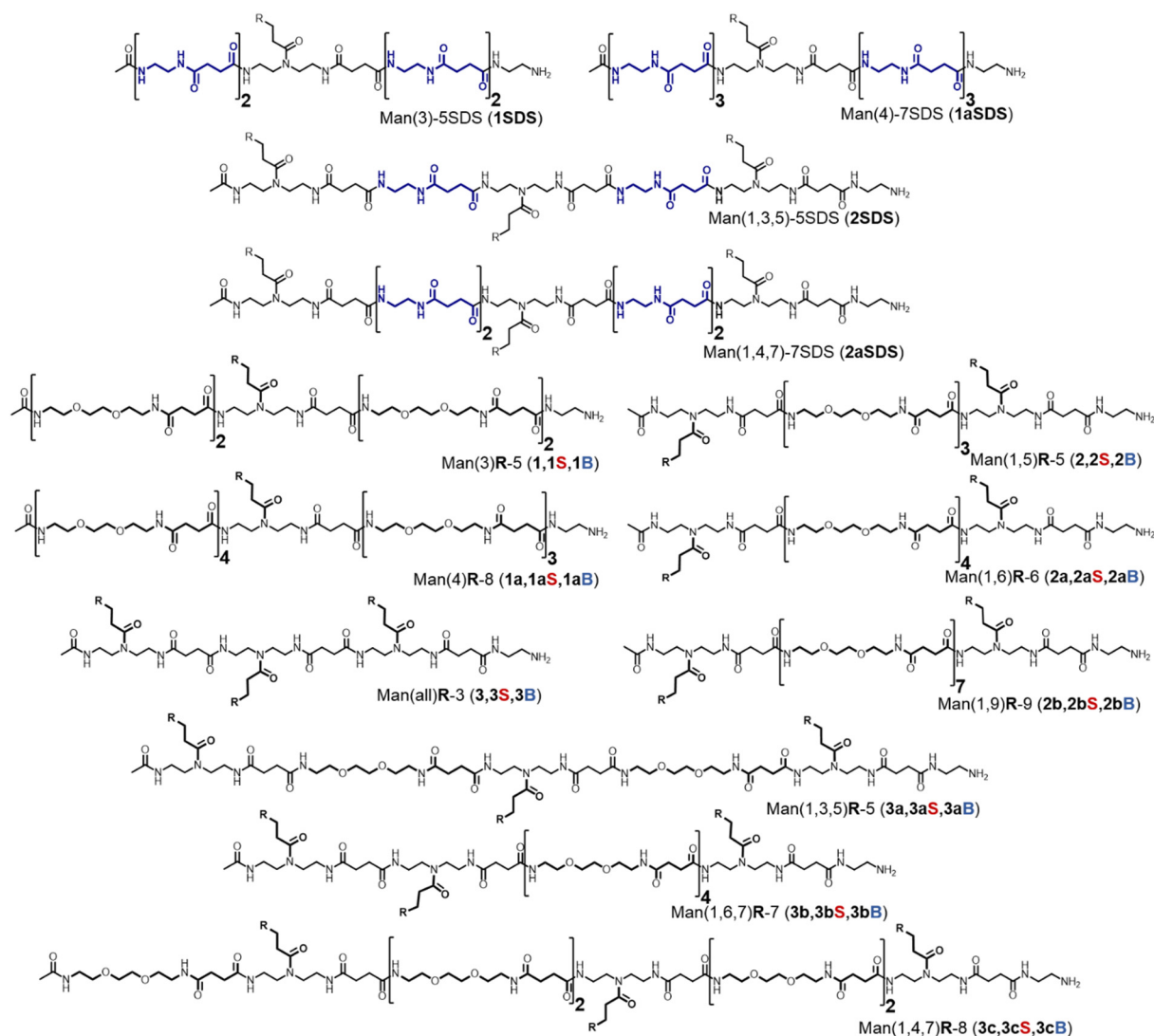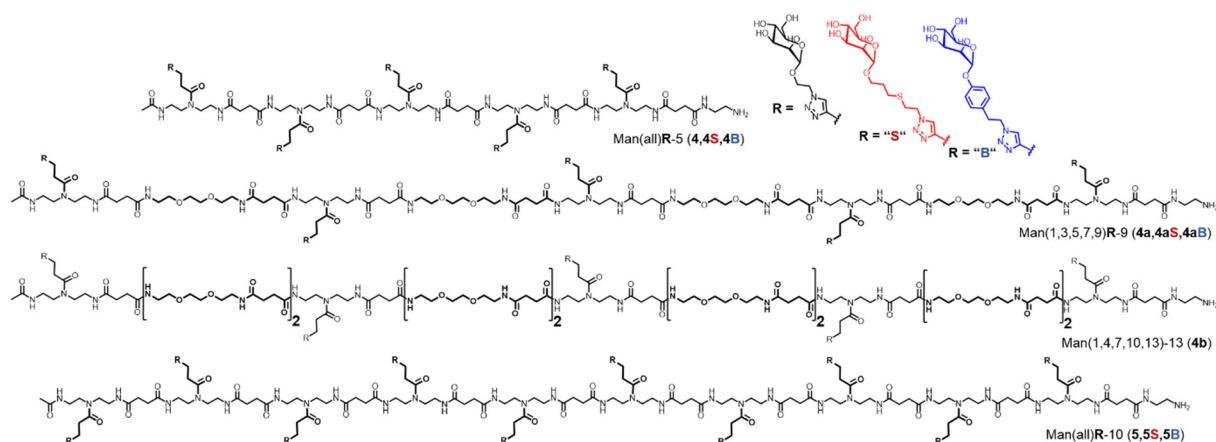
Figure 12. Overview of linear precision glycomacromolecules with different spacing[2] and αMan linkers.

Overall, 37 precision glycomacromolecules were synthesized (Figure 12). These 37 precision glycomacromolecules can be subdivided into three groups. Each of the three groups contains the same backbone composition in terms of spacing and valency, but differs in the αMan linkage. As mentioned above, the different type of αMan linkers are subdivided into a short ethyl triazole linker, a longer thiol-ether triazole linker (highlighted by "S") and a hydrophobic benzyl triazole linker (highlighted by "B"). The nomenclature given for precision glycomacromolecules specifies the type of the binding epitope (here all α-D-mannopyranoside = αMan), their position on the oligomer backbone in parentheses and the final number defining the overall backbone length (e.g. 5 = pentamer). The "R" thereby highlights the type of linkage, where e.g. Man(all)-3 (3) presents the short ethyl triazole linker, whereas Man(all)S-3 (3S) and Man(all)B-3 (3B) correspond to the same backbone composition in terms of spacing and ligand density, but differ in their type of linkage, such as the thiol-ether triazole and the benzyl triazole linkage, respectively. The difference between the EDS and SDS building block spacing is highlighted in the final term "SDS" in the nomenclature. For example, Man(3)-5 (1) corresponds to EDS spacing, whereas Man(3)-5SDS (1SDS) highlights a SDS spacing. All of the above linear glycomacromolecules either differ in terms of their (*i*) ligand density and spacing, (*ii*) their valency or (*iii*) αMan linkage and backbone length and thus in all of the structural parameters that are important for the later evaluation of their impact on the multivalent binding processes.

The purity and chemical composition of the structures was confirmed by RP-HPLC, MALDI-TOF and NMR analysis (see Experimental Part). All of the shown structures were purified by semi-preparative RP-HPLC to maintain a high purity (> 90 % − 96 %), which is an important

---

[2]Compounds 1SDS, 1aSDS, 2SDS and 2aSDS have been synthesized and characterized (NMR, RP-HPLC and MALDI-TOF) by Hendrik Wöhlk (Heinrich-Heine-Universität Düsseldorf, group of Prof. Dr. Laura Hartmann, Master Thesis, April 2015). In this thesis, the above mentioned compounds have been re-synthesized, and their characterization data (NMR, RP-HPLC and MALDI-TOF) reported and discussed in this thesis corresponds to the re-synthesized compounds and characterization data as re-assessed by the author of this thesis.

requirement for the evaluation of the effect of their structural features on the resulting binding energetics and kinetics. Representative RP-HPLC chromatograms and MALDI-TOF spectra are shown for the purified compounds 3c, 4a, 4b and 4a, 4aS, 4aB, which vary in their spacing and αMan linkage, respectively (Figure 13 and 14).
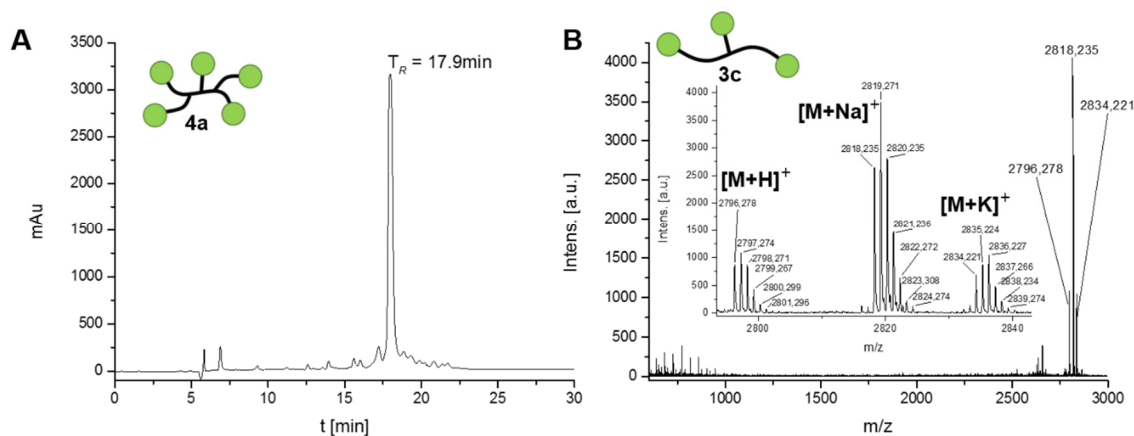
Figure 13. A representative RP-HPLC chromatogram and a MALDI-TOF spectrum of the linear glycomacromolecules 3c (Man(1,4,7)-8): A: Crude RP-HPLC of 4a (Man(1,3,5,7,9)-9); (5 % → 95 % MeCN in 30 min; purity ~70 %). B: MALDI-TOF spectrum of purified 3c (Man(1,4,7)-8).

Figure 13, A shows a representative crude RP-HPLC chromatogram of the pentavalent compound 4a. The compound was directly obtained after cleavage from solid support. As can be seen, compound 4a obtained a reduced purity of about ~70 %, which is a direct consequence of the longer chains and thus additional multiple reactions steps that are necessary with such longer building block sequences. Typically, with every reaction step (deprotection and coupling) the overall yield of the oligomer is reduced by ~1 % − 5 %. Purification by semi-preparative RP-HPLC yields the glycomacromolecules in high purity, which can be seen from Figure 14, A. The RP-HPLC chromatograms are shown here for compounds with different spacers and linkers after purification, which yield the glycomacromolecules in high purities. Figure 14, A also shows the impact of different spacers (left) and linkers (right) on the retention time (T_R). Its evolution during a RP-HPLC method can indirectly pinpoint to the hydrophobicity/hydrophilicity of a macromolecule and thus represent different spacer and linker properties.

The glycomacromolecules presented in Figure 14, A (left) obtain the same αMan linker composition (short ethyl triazole linker), but differ in the number of EDS building blocks and thus in terms of the spacer length between the presented αMan ligands and the overall backbone. For the trivalent ligand 3c, it is seen that it has longer retention times (T_R = 14.8 min) as compared to the pentavalent ligand 4a (T_R = 13.9 min). The more hydrophobic nature of 3c is here not only due to the higher number of EDS spacer building blocks as compared to 4a, but a clear result of the lower number in αMan ligands (compare three (3c) *versus* five (4a)). The additional αMan ligands in 4a compensate for the spacer building blocks and the backbone length, as they increase the hydrophilicity of the whole molecule as compared to 3c. This is further confirmed in the pentavalent

structure 4b, which contains additional numbers of EDS spacer building blocks that overall yields then a higher hydrophobicity of the molecule as compared to 3c (T_R = 17.9 min), which is due to the additional spacers and the overall backbone length (compare eight (3c) to thirteen building blocks (4b)). Figure 13, B and Figure 14, B additionally show the MALDI-TOF spectra of the compounds 3c, 4a and 4b, which obtain the expected mass-to-charge ratios and further confirm the synthesis of monodisperse (monoisotopic mass) glycomacromolecules.

From Figure 14, A (right) it is further seen that the hydrophobicity is not only sensitive to a different building block spacing, but also to a different αMan linkage. The glycomacromolecules 4a, 4aS and 4aB obtain the same spacer composition and length in terms of the oligo(amido amine) backbone. They, however, do differ in their αMan linkage, whereas the number of the αMan ligands is the same. The different αMan linkers either consist of the short ethyl triazole linker, the longer thiol-ether triazole linker ("S") and the benzyl triazole linker ("B"). From the RP-HPLC chromatograms the impact of the different αMan linkers can easily be followed.
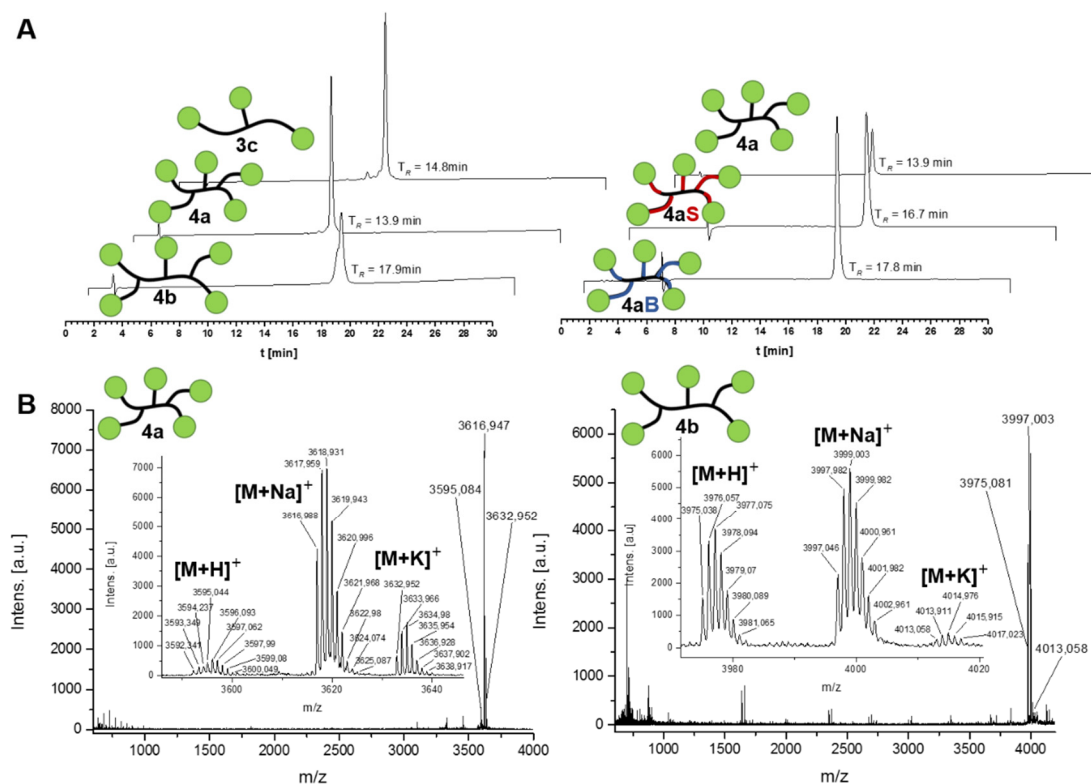
Figure 14. Representative RP-HPLC chromatograms and MALDI-TOF spectra of linear precision glycomacromolecules. A: Left (different EDS spacing): 3c (Man(1,4,7)-8), 4a (Man(1,3,5,7,9)-9) and 4b (Man(1,4,7,10,13)-13); (5 % → 30 % MeCN in 30 min). Right (different αMan linkage): RP-HPLC of 4a (Man(1,3,5,7,9)-9), 4aS (Man(1,3,5,7,9)S-9) and 4aB (Man(1,3,5,7,9)B-9); (5 % → 30 % MeCN in 30 min). B: MALDI-TOF spectra of 4a (Man(1,3,5,7,9)-9) and 4b (Man(1,4,7,10,13)-13).

The shortest linker – the ethyl triazole linker – has the shortest retention time ($T_R = 13.9$ min), followed by the thiol-ether triazole linker ($T_R = 16.7$ min) and the benzyl triazole linker with the longest retention time ($T_R = 17.8$ min). Thus, following these linkers, it is seen that the hydrophobicity increases in the following order ethyl triazole linker < thiol-ether triazole linker < benzyl triazole linker.

Exemplary NMR spectra that allowed to additionally confirm the structural composition in terms of the spacing and the αMan linkage are shown for the compounds 3, 3b and 3c and 3, 3S and 3B (Figure 15 and 16).
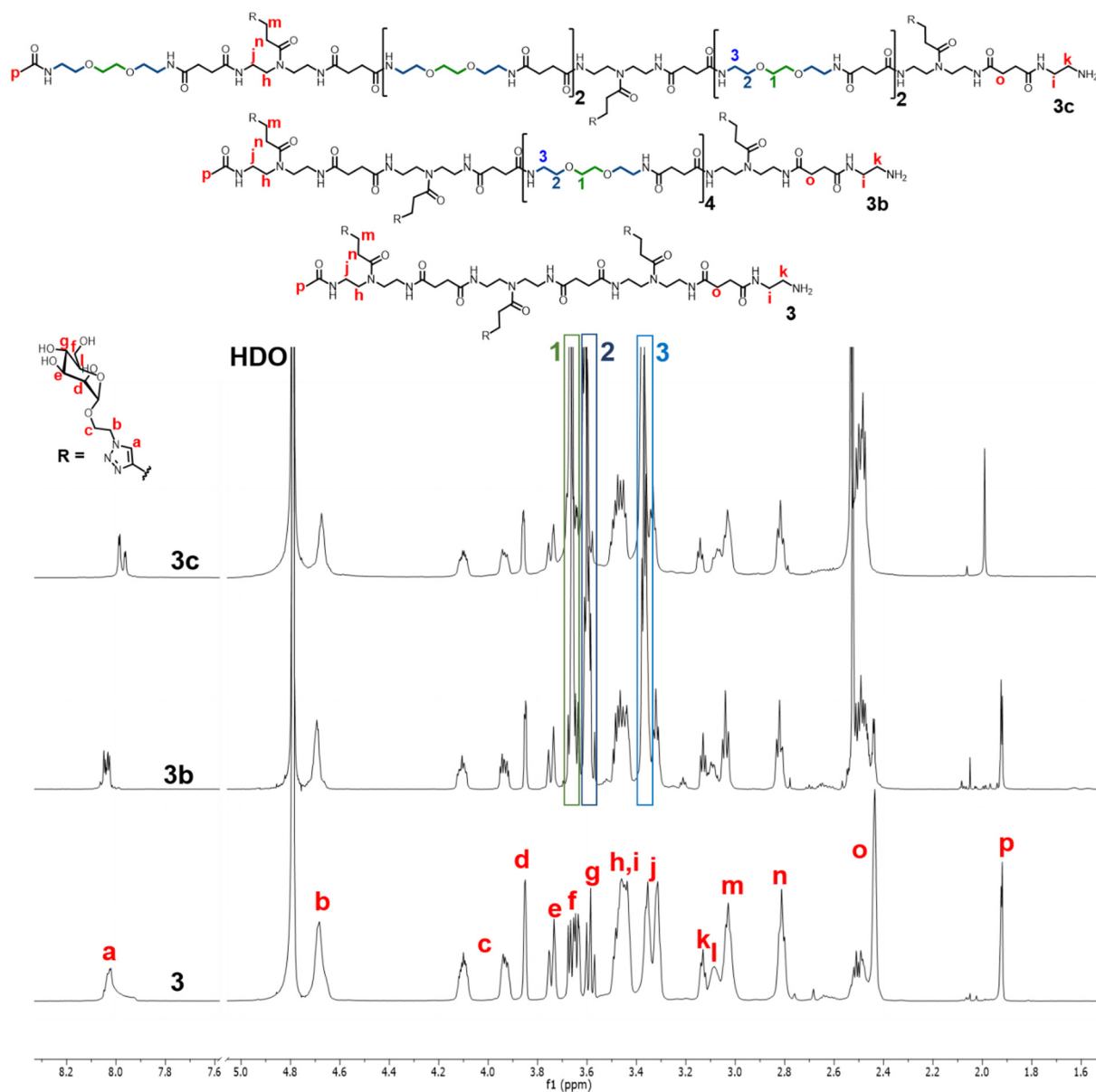
Figure 15. ¹H NMR spectra of compounds 3 (Man(all)-3), 3b (Man(1,6,7)-7) and 3c (Man(1,4,7)-8). The different EDS spacing and their evolution in the ¹H NMR is compared.

Allocation of the protons representative for the spacing and αMan linkers was performed with 2D NMR methods (see Supporting Appendix). The two representative NMR spectra will be shortly

discussed regarding the most important structural aspects representative for the different spacing and linkage.

To visualize the difference between the number of EDS spacers, ^{1}H NMR spectra of the trivalent compounds 3, 3b and 3c are compared. Here, 3 does not contain any EDS spacer building blocks, so that the backbone only consists of three αMan conjugated TDS building blocks. For compounds 3b and 3c, the number of EDS spacer building blocks increases from four to five, where 3b is asymmetrically spaced by collective four EDS building blocks, and 3c is symmetrically spaced by two building blocks between two of the αMan ligand and an additional EDS building block at the N terminus.

As can be seen by comparing the spectra of 3 with the spectra of 3b and 3c, the protons of the EDS building block 1, 2, 3 (between 3.2 and 3.8 ppm) readily appear in the NMR spectra and overlap the backbone protons j (by protons 3) and the αMan protons g and f (by protons 1 and 2). Thus, the EDS spacing can be reasoned for the glycomacromolecules by appearance of these protons in the NMR spectra. It is further important to outline, that although the number of EDS spacers can be assumed from their intensity and thus applying the proton integration, these protons do not tell their exact position along the backbone. The exact spacer building block position may be analyzed in future by applying tandem MS/MS techniques. It is further noteworthy to outline, that the acetyl protons p (at the highest field) in compounds 3 and 3b show a splitting from one singlet (compare 3c) into two singlets. This splitting was observed, when the triazole group was in near proximity to the acetyl protons p (compare 3 and 3b). If however, another building block separated the acetyl protons p and the triazole group (compare 3c, in this case an EDS building block), then the splitting disappeared, so that the two singlets once again fell into one singlet with the same proton intensity. The two singlets were confirmed by ^{1}H/^{13}C HSQC NMR spectra (see Supporting Appendix), where the protons p showed individual $^1J_{CH}$ coupling to two separate carbon signals, thereby excluding the possibility of (pseudo-)doublets. Using a temperature dependent 1D ^{1}H NMR experiment (see Supporting Appendix), it was further confirmed that the splitting into the two singlets (compare 3 and 3b) was due to a mixture of rotational isomers (rotamers), caused by the triazole ring near the acetyl protons p. The α-anomeric protons cannot be seen in the above spectra, as they are hidden behind the HDO solvent signal (around 4.8 ppm, see ^{1}H/^{13}C HSQC NMR in the Supporting Appendix).

To further differentiate the αMan linkers, the ^{1}H NMR spectra of compounds 3, 3S and 3B were compared. All compounds have the same backbone composition and only differ in their αMan linkers. To further simplify the assignment of the linker protons, glycomacromolecules are used for the discussion that do not contain EDS spacing (that would overlap with other proton signals).
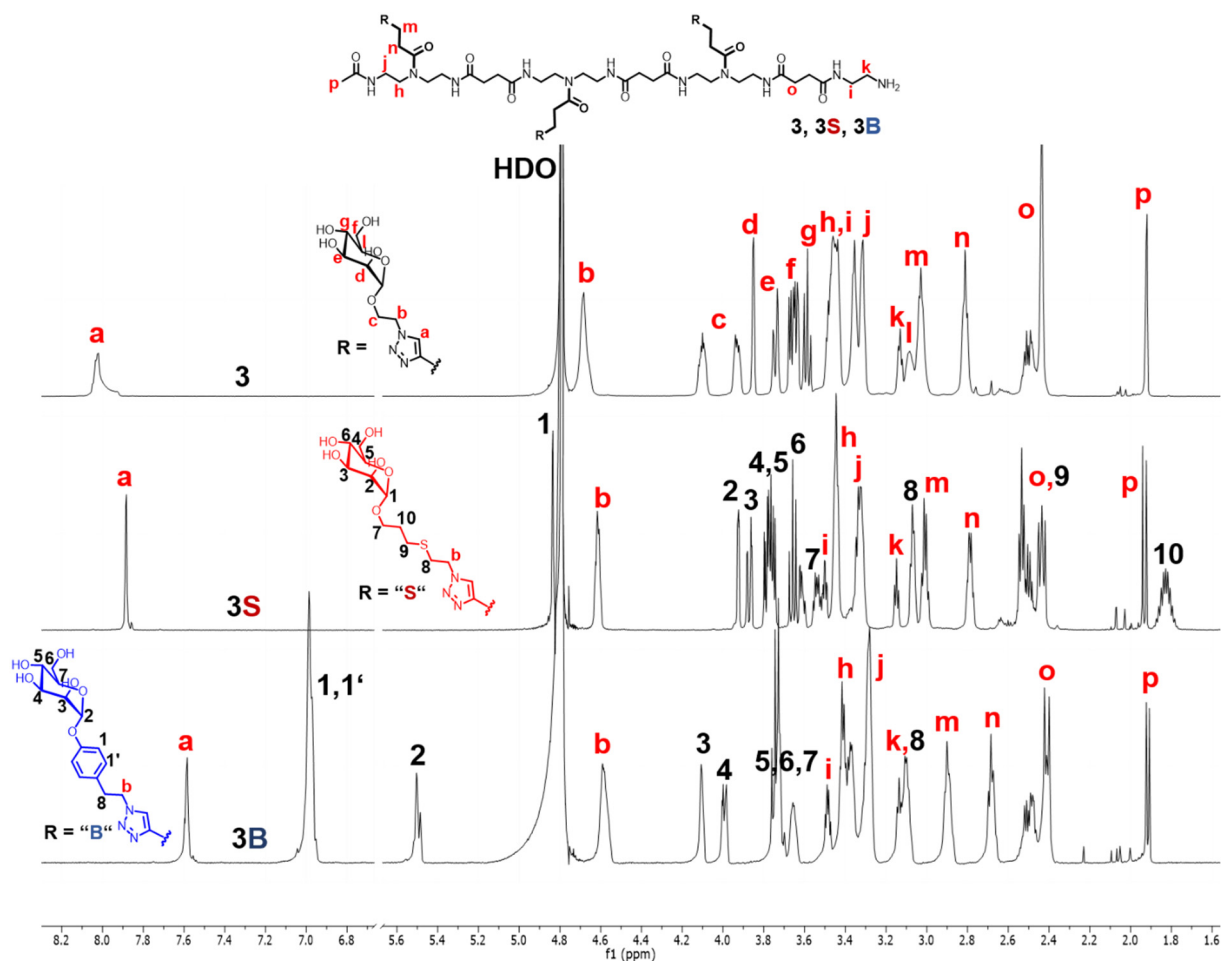
Figure 16. ¹H NMR spectra of 3 (Man(all)-3), 3S (Man(all)S-3) and 3B (Man(all)B-3). The different αMan linkers and their evolution in the ¹H NMR is compared.

Comparing the different linkers, it can readily be seen that the backbone protons (highlighted in red) remain in the same range, although their chemical shifts and splitting changes slightly, thereby also indicating the changing chemical surrounding with the different linkers. It is noteworthy to mention that the methine protons a (of the triazole ring) significantly shift to high field (from around 8 to around 7.5 ppm) in the order short ethyl triazole linker < thiol-ether triazole linker < benzyl triazole linker. The opposite is true for the α-anomeric protons 1 (thiol-ether triazole linker) and 2 (benzyl triazole linker; α-anomeric protons of the ethyl triazole linkers are hidden behind the HDO signal), which have shifted to low field from around 4.8 to 5.5 ppm in the order triazole linker > thiol-ether triazole linker > benzyl triazole linker. The thiol-ether triazole linker protons can be readily assigned, since the chemical shifts of the αMan protons changes significantly (compare protons 2, 3, 4, 5, 6). The same is true for compound 3B (compare protons 3, 4, 5, 6, 7). A more obvious confirmation of the different linkers give the propyl-thiol bridged group protons for 3S (protons 7, 8, 9, 10) and the benzyl ethylene bridged protons of 3B (protons 1, 1' and 8). For compound 3S, the protons 8 and 10 are more easily allocated, because protons 7 and 9 are overlapped by the backbone protons i and o (succinic acid bridges), respectively. To further differentiate for the benzyl triazole linker, one needs to take a look at the protons 1, 1' and 8. The

ethylene proton 8 appears here in the same range as the protons 8 of the thiol-ether triazole linkers. Further, the presence of protons 1 and 1' in the aromatic region then finally confirms benzyl group of the benzyl triazole linked αMan ligands.

Altogether, the combination of the RP-HPLC, MS and NMR spectra allowed to confirm the chemical composition of the glycomacromolecules in terms of the different spacing and αMan linkers as well as their monodispersity.

3.2. Synthesis of cyclic precision glycomacromolecules varying in the spacing along the backbone as well as the linker from the backbone to the carbohydrate

The previous subchapter highlighted the synthesis of linear and sequence-controlled glycomacromolecules. Besides the investigation of the impact of a varying spacer, ligand density and αMan linkage on the resulting multivalent binding mode, one of the main objectives of this thesis was to evaluate the potential influence of a cyclic *versus* linear architecture on the resulting multivalent binding mechanism. In previous studies it has been shown that a change in the polymer architecture might result in different multivalent binding modes, initiated e.g. through a change in their size and a potentially different behavior of the architectures in solution.[24-25, 32-33, 90, 106] To address the role of a changing oligomer architecture on the multivalent binding process, cyclic precision glycomacromolecules were synthesized. Besides the overall control of the chemical structure, an important advantage of the solid phase assembly of functional building blocks is the straightforward control and variation of the architecture itself, as has been shown in the synthesis of asymmetrically branched polycations and peptide-mimetics.[99, 127] One of the objectives of this thesis was therefore to further extent the concept of SPPoS and give access to cyclic precision glycomacromolecules using alternating cyclization methods.

3.2. Part 1: Evaluation of the reaction conditions required for macrocyclization

Currently, there are two major strategies used for the synthesis of cyclic oligomers or polymers. On the one hand, macrocyclization of polymers[167-169] with higher molecular weights is typically performed in solution. On the other hand, cyclic oligomers of lower molecular weight, typically up to 10 kDa, can be synthesized on solid support[144, 148, 170-171]. From classical polymer chemistry and solid phase peptide chemistry it is well-known that macrocyclization reactions are challenging[148, 167]. They are often associated with low yields, since not only monomer macrocyclization can occur, but also formation of e.g. cyclic dimers and trimers as well as linear oligomers.[172] When performed in solution, high dilution conditions are required.[167] Additional challenges for macrocyclization in solution arise from the ability of the macromolecules to freely diffuse, again promoting undesired cyclic and linear oligomerization. The free diffusion of macromolecules can be overcome by applying

the solid phase synthesis and taking advantage of the resin loading. It has been reported that low resin loadings, equal to and smaller than 0.23 mmol/g are well suited for macrocyclizations of peptides.[173-174] The covalent linkage of macromolecules to the solid support as well as the low loading of the resin, create pseudo-dilution conditions[173-174] and circumvent the problem of free diffusion.

Another challenge associated with the solid phase synthesis is the use of the appropriate linker and protecting group chemistry. Although literature presents many advanced methods for the on-resin macrocyclization of peptides[148, 171, 175-176], the synthesis of cyclic glycomacromolecules has to be rather simple in order to fulfill the requirements of a modular approach, as was defined earlier by Hartmann *et al.* for the synthesis of precision macromolecules.[94-99] Therefore, the synthesis of cyclic glycooligomers should only involve a limited number of reaction steps and be compatible with the previously established building blocks, coupling as well as functionalization strategies. Resins, such as the oxime resin used for traceless cyclization upon cleavage[177-178] could not be applied here, since they involve cleavage upon a nucleophilic attack, thus not being compatible with Fmoc peptide chemistry. A variety of resins for cyclization with advanced linker chemistry were designed in the Solid Phase Organic Synthesis (SPOS). For example, cyclative cleavage can be achieved by the use of designed linkers[146, 179] compatible with the Fmoc chemistry, taking advantage of the electrophilically cleavable resins such as the RAM or the Wang resin. However, these strategies are highly advanced and would require additional synthesis and reaction conditions set-up. As an alternative strategy, the macrocyclization of peptides has been shown to progress upon cleavage from the RAM resin[145], by a side-chain-to-tail cyclization, where the *C* terminal thiol group of a cysteine (Cys) side-chain led to an *intra*molecular Michael addition on the *N* terminal maleimide tail of linear peptides[145]. Compounds containing maleimides are however easily hydrolyzed and have been shown to induce cytotoxicity[180-181], which would interfere with the application of cyclic glycomacromolecules in future biomedical and biotechnological applications.
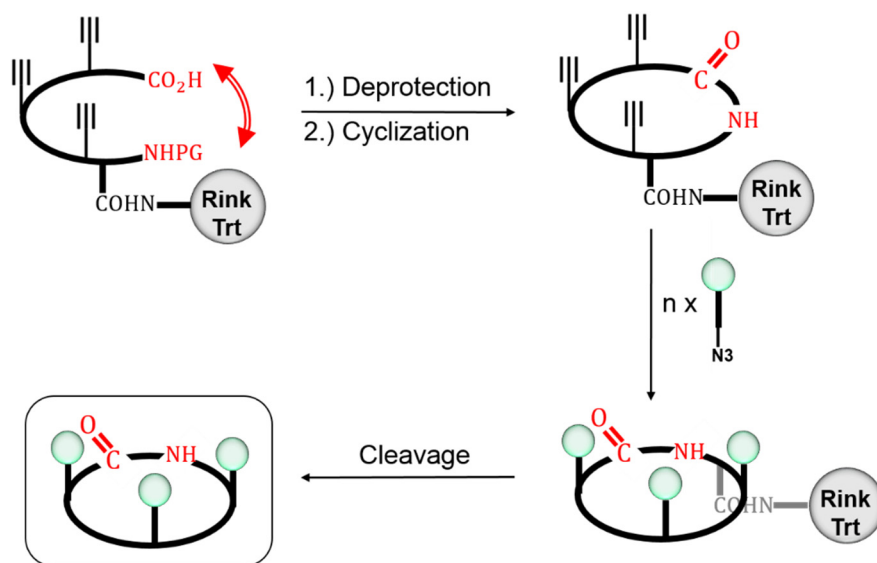
Figure 17. The general concept on solid phase for the synthesis cyclic glycomacromolecules.

Among all of the available methods for macrocyclization, it was therefore intended to find a cyclization strategy, which allows for a relative straightforward excess to cyclic glycomacromolecules on solid support, thereby circumventing advanced synthetic routes and functionalization protocols. Therefore, solid phase linkers and protecting group strategies should be used, which are compatible with the previously introduced Fmoc building block strategy (Figure 9 in General Introduction).

Further, the RAM[158] and the Trt[158] resins are commonly used in the synthesis of peptides and precision macromolecules[99-103, 105, 182]. As mentioned previously, both resins are cleavable by acidolysis[158], thus following the Fmoc strategy, which is compatible with the final electrophilic cleavage. The on-resin side-chain-to-tail macrocyclization of precision glycomacromolecules *via* the formation of an amide (Figure 17) requires therefore the use of an orthogonal protecting group strategy. To yield the monocyclic species, the *C* terminal Lys amine needs to be protected with different orthogonal groups, so that their prior removal has to be performed before the intramolecular condensation of the released amine with the *N* terminal activated carboxylic acid ester (Figure 18). This method is based on general on-resin macrocyclization methods, which already have been described for the synthesis of cyclic peptides[142, 148, 171, 183]. Examples of orthogonal protecting groups used for the cyclization include 1-(4,4-dimethyl-2,6-dioxocyclohex-1-ylidene)isovaleryl (*iv*Dde)[184], allyloxycarbonyl (Alloc)[184-190] and tert-butyloxycarbonyl (Boc)[184]. The former can e.g. be cleaved by hydrozynolysis[184], whereas the second is removed by standard Tsuji-Trost conditions[186-187] and the last can be simply cleaved under acidic conditions[184].

For the evaluation of the macrocyclization process, which includes the deprotection of an orthogonal protecting group first, before the activation of the carboxylic residue in the presence of the free amine, all of the three protecting groups were tested. Evaluation of only two of the protecting groups will be highlighted in the following: the Alloc and Boc protecting group (Figure 18).

Figure 18 exemplarily highlights the synthetic route, which was used for the synthesis of cyclic precision glycomacromolecules and the synthetic steps that were evaluated. Before the macrocyclization, each of the linear precursors were prepared with PyBOP/*i*Pr$_2$NEt activation on-resin. While the main chain was simply built up by repetitive building block addition and Fmoc deprotection (following protocols as described in the previous subchapter), the macrocyclization was achieved using a *C* terminal lysine (Lys) AA that contains a protected amine, while the *N* terminus was equipped with a carboxylic acid residue following simple addition of succinic acid in the presence of *i*Pr$_2$NEt.
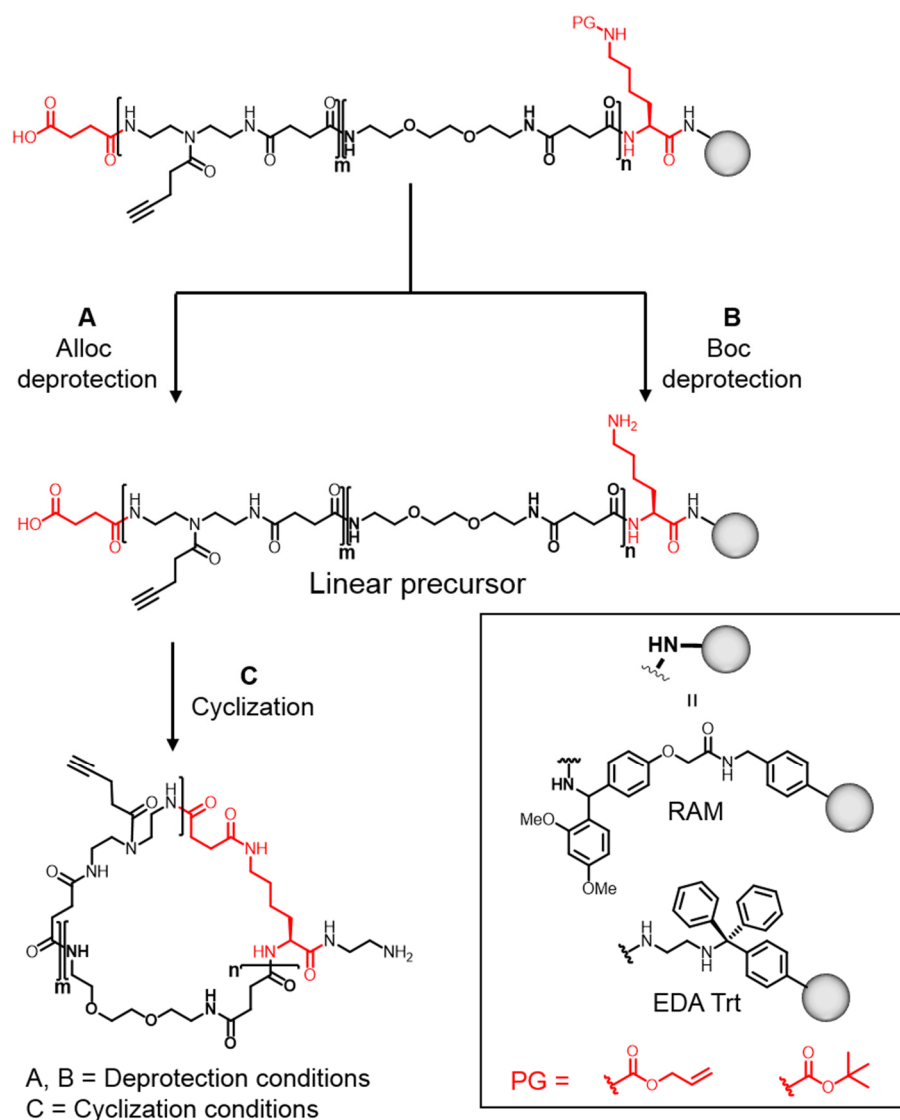
Figure 18. Evaluation of the on-resin side-chain-to-tail macrocyclization process, following different side-chain deprotection techniques (A and B) and cyclization conditions (C), which were tested on different resins.

3.2.1. Synthesis of linear precursors – using Alloc protecting groups

Prior to a backbone macrocyclization, different deprotection methods for Alloc were evaluated The removal of Alloc[184-185, 188-190] is a sensitive method and a challenge, associated with by-products and incomplete deprotection if not handled properly. Many methods for Alloc removal[184-185, 188-189, 191-197] have been developed that primarily vary in the type of the scavenger[191-197] used to trap the released allylic species during reaction. Depending on these, removal can be performed in different solvents and under either slightly acidic[190, 192, 194, 198], nearly neutral[142, 191] or basic conditions[197]. Incomplete reaction/deprotection often results from the oxidation of the palladium catalyst.[142] Here, a proper handling of the argon atmosphere as well as the preparation of a fresh solution is crucial for a successful reaction.[142] Using standard Alloc deprotection protocols[184-185, 188-189, 191-196], it was previously shown that removing the Alloc protecting group under slightly acidic

conditions[192] was the most useful and reliable protocol for the synthesis of asymmetrically branched oligo(amido amines)[99]. The use of the palladium(0) catalyst under nearly neutral conditions[142, 192] has been reported to not always yield good results[99].
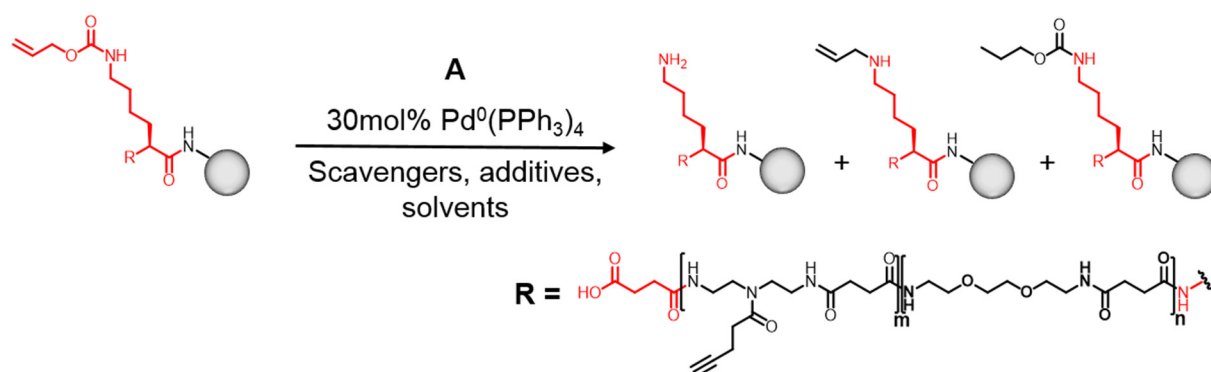
Table 1. Different Alloc deprotection conditions (re-)evaluated in this thesis (critical step before macrocyclization).

Scavenger	Conditions	Time[a]	By-products/Completeness[b]
10 equiv *N,N*-DMBA	30 mol % $Pd^0(PPh_3)_4$ THF;DCM;DMF AcOH or Ac_2O (acidic)	30 − 60 Double DP	*N*-allylation Almost complete Reduction of DB
10 equiv TSA	30 mol % $Pd^0(PPh_3)_4$ THF;DCM;DMF AcOH or Ac_2O (acidic)	30 − 60 Double DP	*N*-allylation Almost complete
10 equiv morpholine	30 mol % $Pd^0(PPh_3)_4$ THF;DCM;DMF; (basic)	30 − 90 Triple DP	*N*-allylation Incomplete Reduction of DB Other by-products[c]
10 equiv Ph_3SiH	30 mol % $Pd^0(PPh_3)_4$ THF;DCM;DMF; (neutral)	30 − 90 Triple DP	*N*-allylation Incomplete Reduction of DB Other by-products[c]

[a] Reaction time is given in min; [b] Deprotection (DP) completeness = completeness of Alloc deprotection; [c] Other by-products correspond to contaminants after reaction, which could not be identified; (tetrahydrofurane (THF), dichloromethane (DCM), *N,N*-dimethylformamide (DMF), AcOH (acetic acid), Ac_2O (acetic anhydride), double bond (DB), tetrakis(triphenylphosphine)palladium(0) ($Pd^0(PPh_3)_4$))

Although the *N*-allylic side-products can be reduced to some extent using different scavengers[191-197], its appearance during reaction cannot be avoided completely, since the *N*-allylation not only participates through the competition of the free amine and the nucleophilic allylic scavenger, but also by the direct intramolecular decarboxylation reaction of the carbamato-π-allylic intermediate.[192] Examples of scavengers that were used here to reduce the amount of the *N*-allylic species include the 1,3-dimethylbarbituric acid (*N,N*-DMBA)[190, 192, 198] and the thiosalicyclic acid (TSA)[192, 199] as well as morpholine[197] and phenylsilane (Ph_3SiH)[142, 191, 195]. The former two scavengers represent Alloc deprotection performed under acidic conditions, whereas the latter two correspond to basic and neutral deprotection conditions, respectively.[192] When acidic conditions with *N,N*-DMBA or TSA were applied, the overall reaction mixture was further acidified

with small amounts of acetic anhydride[196] or acidic acid. However, in the former case, amine trans-acylation by-products[196] can occur, so that acidic acid instead of acetic anhydride was used to further acidify the reaction mixture.

After having tested all of the different deprotection procedures, for the investigated oligomers it turned out that the acidic procedures for removal of Alloc worked best (Table 1). Conditions applied with Ph₃SiH resulted in significant high amount of unidentified by-products. Although the TSA and *N,N'*-DMBA performed both equally good, the reaction resulted in incomplete deprotection with concomitant *N*-allylation that could not be avoided in this process. Therefore, an alternative method for the side-chain deprotection was used, which would allow for a clean removal of the protecting group. It was to be expected that the intramolecular macrocyclization process will result in intermolecular oligomerization by-products as is known from literature[148, 171]. Therefore, the prior steps before the macrocyclization should proceed as clean as possible, including all the building block coupling steps and the most critical deprotection of the side-chain prior to cyclization.

3.2.2. <u>Synthesis of linear precursors – using Boc protecting groups</u>

With respect to the acid cleavable Boc protecting group, various protocols allowing for its selective removal on electrophilically cleavable resins have been reported[200-208]. In order to allow for deprotection prior to cyclization, different protocols from literature were tested on shorter and longer model oligo(amido amines), consisting of five and eight building blocks with varying sequences of TDS and EDS (Table 2). The use of an acid labile protecting group with an acid cleavable resin is not without a risk.[201] As for the macrocyclic synthesis an acid cleavable resin is used, application of acidic conditions to cleave the Boc protecting group might result in partial loss of the linear oligomers attached to the acid labile RAM or EDA Trt linker. The selective removal of Boc with a reduced concomitant loss of the oligomer from the resin has been reported by applying e.g. mixtures of chlorotrimethylsilane (TMSCl)/phenol[203, 209], trimethylsilyl triflate and bromotrimethylsilane (TMSOTF/Br) in the presence of amine bases[200], dilute mineral acids[201, 207-208] such as sulfuric acid (H₂SO₄,conc)[201, 208] and hydrochloric acid (HClaq)[207] in organic solvents, as well as the use of metal chlorides such as tin(IV)chloride[202] and aluminium chloride[206].[201]

To again find a method allowing for a selective side-chain deprotection – the critical step prior to cyclization – some of the mentioned Boc deprotection protocols known from SPPS were applied to the SPPoS of the linear oligo(amido amine) precursors. Here, again both different acid cleavable resins were tested, the RAM and the EDA Trt Tentagel resins.

The use of 1 M TMSCl/3 M phenol[203, 209] showed good compatibility when macromolecules were synthesized on the Rink Amide (RAM) linker (Table 2). However, its use typically required longer reaction times (about 1 1/2 to 2 h) and two to three deprotections cycles (double or triple deprotection). When this protocol was applied to the EDA modified Trt resin, then results obtained for the deprotection as compared to the RAM were inconsistent and further accompanied by unknown by-products. However, the EDA Trt resin is an absolute requirement for the synthesis of

cyclic glycomacromolecules that maintains a free *C* terminal amine after cleavage from the solid support. The free amine allows then for functionalization with a fluorescent label, e.g. for structure-activity evaluations in fluorescence correlation studies. Another approach to selectively cleave the Boc group on acid cleavable resins, is to utilize lower trifluoroacetic acid (TFA) concentrations[201], whereas TFA is usually applied for the cleavage of the whole oligomer from the resin. Small aliquots of TFA were used here (Table 2) and the effect of different solvents was also studied (such as DCM, 1,2-dichloroethane (DCE), dioxane, DMF and THF). According to well-established cleavage procedures[141], DMF should normally be avoided on-resin and washed off before the cleavage of the oligomer with TFA. This is due to the fact that remaining aliquots of basic DMF are known to interfere with acidic TFA cleavages. However, in this case this side effect was even wanted, as it reduces the acidity of TFA and makes the deprotection mixture even milder.
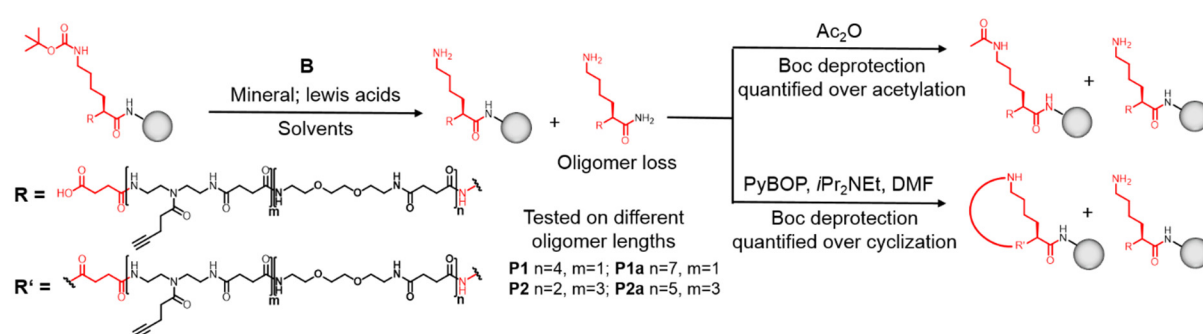
Table 2. Different Boc deprotection conditions evaluated in this thesis.

Conditions	Time[a]	By-products/Completeness	Oligomer loss
1 M TMSCl/3 M phenol	90 – 120[c]	Worked for RAM Failed for EDA Trt → Other by-products[b]	~40 % ~70 % − 80 %
2 % − 20 % TFA in DCM; DCE; dioxane; DMF; THF	30 − 120	Incomplete deprotection Oligomer loss in both resins	Almost complete
30 % H_2SO_{4conc} in dioxane, 0°C − 4°C to RT	2 x 20	Ok for RAM Protocol inconsistent Failed for EDA Trt → Other by-products[b]	~40 % − 60 % Almost complete, but unreliable Other by-products[b]
4 M HCl_{aq} in dioxane, 0°C − 4°C to RT	2 x 20 – 3 x 20	Good for both resins Protocol inconsistent with both resins→ Strongly T dependent	~20 % − 40 % for EDA Trt ~6 % − 10 % for RAM

[a] Reaction time is given in min; [b] Other by-products correspond to contaminants after reaction, which could not be identified; [c] A fresh reagent cocktail was prepared either every 5 − 10 or 30 − 60 min; (room temperature (RT)), temperature (T))

The alternating TFA quantities in different solvents, however again revealed incomplete Boc deprotection accompanied by a significant oligomer loss. This result was independent of the resin used, with both the RAM and the EDA Trt resin experiencing a significant oligomer loss. The

observations are further consistent with previous reports for the Boc deprotection on acid cleavable resins.[201]

Since all the above attempts failed to yield Boc deprotection on electrophilically cleavable resins, in a further attempt it was decided to use concentrated sulphuric acid ($H_2SO_{4/conc}$)[201, 208] and hydrochloric acid (HCl_{aq})[201, 207] diluted with dioxane, as has also been reported previously[201] (Table 2). When a fresh solution of diluted $H_2SO_{4/conc}$ (30 %) and HCl_{aq} (4 M) was applied to the corresponding resin, then a significant exotherm was observed, which was effectively controlled by cooling with a simple ice-bath[201]. The 30 % $H_2SO_{4/conc}$/dioxane performed well on the RAM resin, resulting in complete Boc deprotection after treatment of the solid support twice with a fresh solution for 20 min. Again, complete Boc deprotection was accompanied by an unavoidable loss of the oligomer from the solid support of about 40 % − 60 %. Although this procedure performed adequate regarding a complete Boc removal, it however failed to achieve reproducible results with the EDA Trt resin.

For this reason, the alternative mineral acid method with 4 M HCl_{aq} in dioxane was tested (Table 2). In this case, treatment of both resins revealed primarily the deprotection of Boc. The loss of the oligomer for the RAM was ~10 %, while the loss for the EDA Trt resin was ~20 % − 40 %. Since removal of the Boc protecting group cannot be controlled by deprotection and micro-cleavage, because the final cleavage results in complete removal of Boc, the Boc deprotection had to be quantified either by the subsequent cyclization or simple acetylation with acetic anhydride (Table 2). The absence of the former linear precursor thereby indicated a complete Boc removal. Therefore, in case of the subsequent cyclization process, by-products correspond not only to the Boc removal, but also to by-products resulting from the cyclization process. However, in case of the acetylation process very little by-product formation was observed, indicating that most of the side-product species was formed as a result of the macrocyclization reaction (which will be discussed in the next subchapter). Here, the RAM performed best and the loss of the oligomer from the resin was effectively controlled by cooling of the suspension. These observations are consistent with previous reports of Worley *et al.*[201], who found that cooling may significantly lower the amount of product loss. For the RAM, it was found that cooling with a simple ice-bath for 10 min and slow equilibration to RT only yielded a loss of ~6 % − 10 %, with an overall reaction time of 1 h. Here, the resin was treated three times with a fresh solution for ~20 min. Since the EDA Trt resin is significantly more sensitive to acidolysis, the overall reaction time was reduced to 40 min, where the resin was treated twice with a fresh reagent solution accompanied by controlled cooling. The results obtained for the EDA Trt resin were not always consistent. Most of the time, the procedure yielded a complete Boc removal, whereas other times deprotection was incomplete, resulting in a mixture consisting of the cyclic products and the linear precursor (~10 % − 20 %). The loss of the oligomer was also inconsistent. Although most of the time the cooling was relatively effective, the loss of the oligomer ranged between 20 % − 30 %.

In conclusion, the HCl$_{aq}$/dioxane method was established to be most suitable to obtain the targeted deprotected linear oligo(amido amine) precursors for subsequent cyclization. Compared to other acidic procedures, it yielded most of the times a complete Boc deprotection accompanied by a relatively low loss of the oligomer.

3.2. Part 2: Cyclization of linear precursors

After having established the reaction conditions required to yield a free side-chain amine, synthesis of the monocyclic compounds was performed. The cyclization progress was monitored by RP-HPLC as well as the Kaiser test. RP-HPLC monitoring and the ninhydrine test indicated that the cyclization progress was complete within 1 h. This side-chain-to-tail macrocyclization by activation with PyBOP of the carboxylic acid moiety (in this case an *N*-terminal succinic acid residue), is a well-known and established method from the solid phase synthesis of peptides (SPPS).[148, 171, 183] Applying this strategy for the synthesis of cyclic oligo(amido amines) in this study, however showed formation of oligo- and polymerization side-products as well as dehydration to nitriles.
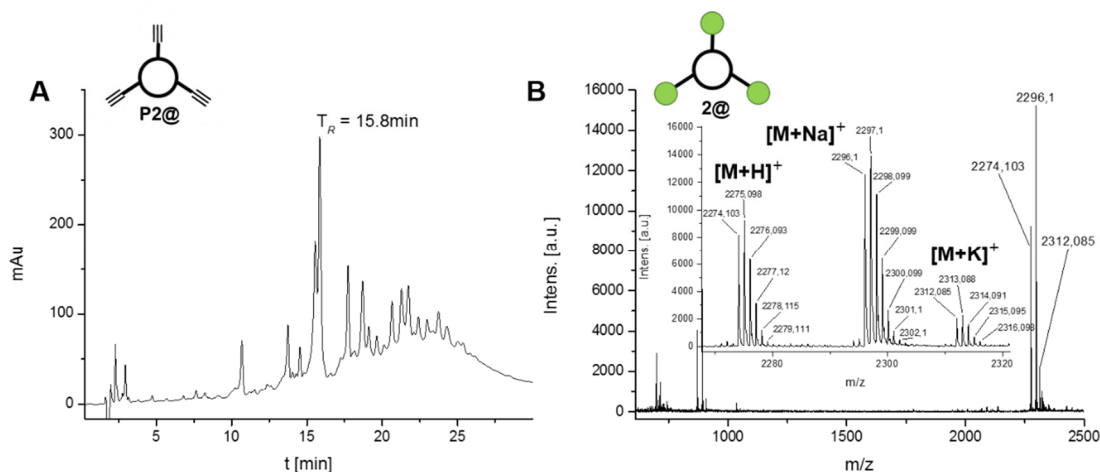
Figure 19. A: Representative crude RP-HPLC chromatogram (direct after on-resin cyclization; purity > 53 %; 5 % → 30 % MeCN in 30 min) and B: Pure MALDI-TOF spectra of the cyclic precision glycomacromolecule 2@ (Man(1,3,5)@5) after αMan conjugation and purification.

For the studied oligo(amido amines) (Table 3, cyclic compounds P1@, P1a@, P2@ and P2a@), reaction with PyBOP and *i*Pr$_2$NEt yielded e.g. the monocyclic product P2@ in a yield of ~53 % (compare Figure 19, A), whereas oligo- and polymerization side-products and nitrile formation[210-212] contributed to the overall yield of ~47 % (Table 3).

In order to improve the cyclization procedure, the effect of different activation strategies was then studied (Table 3). As previously reported for the solid phase synthesis of cyclic peptides[171-172], the use of PyBOP in the presence of equimolar amount of additives such as *N*-hydroxybenzotriazole (HOBT) results primarily in the formation of a monocyclic species with only little cyclic dimer and

trimer by-products[172], by applying also the same low resin loading[148, 171-174] as was used in this study (about 0.23 mmol/g). However, it also has been extensively reported that the cyclization process is sensitive to many changes in a cyclization protocol[148, 167-169, 171], where the macrocyclization e.g. of peptides also strongly depends of the peptide sequence as well as the length.[148, 171] Indeed, although in this study the macrocyclization was not sequence dependent, it was observed that shorter chain-lengths (five repeating units, P1@ and P2@; Table 3) led to higher yield of the monocyclic product (~50 %), whereas longer chains (eight repeating units, P1a@ and P2a@, Table 3) where accompanied with a significantly higher amount of intermolecular oligomerization by-products and thus a significantly reduced yield of the monocyclic species (15 % − 30 %).
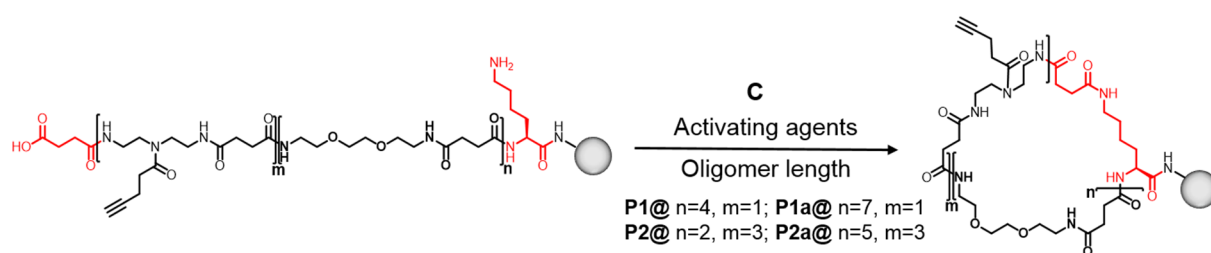
Table 3. Different coupling conditions used for the macrocyclization.

Activating agents[a]	Time[b]	Monocyclic species[c]	By-products[d]
1:1 4.9 equiv PyBOP/HOBT	60	P1@, P2@ (5 BBs[e]) ~50	~50
		P1a@, P2a@ (8 BBs) ~15 − 30	~70 − 85
4.9 equiv PyBOP	60	P1@, P2@ (5 BBs) ~50	~50
		P1a@, P2a@ (8 BBs) ~15 − 30	~70 − 85
1:1 4.9 equiv HATU/HOBT	40	P1@, P2@ (5 BBs) ~15	~85
		P1a@, P2a@ (8 BBs) ~5 − 10	~90 − 95
4.9 equiv HATU	40	P1@, P2@ (5 BBs) ~15	~85
		P1a@, P2a@ (8 BBs) ~5 − 10	~90 − 95
1:1 4.9 equiv HBTU/HOBT	40	P1@, P2@ (5 BBs) ~13	~87
		P1a@, P2a@ (8 BBs) ~5 − 10	~90 − 95
4.9 equiv HBTU	40	P1@, P2@ (5 BBs) ~12	~88
		P1a@, P2a@ (8 BBs) ~5 − 10	~90 − 95

[a] Coupling was performed always in the presence of the same amount of iPr$_2$NEt (10 equiv); [b] Reaction time is reported in min; [c] Formation of the desired monocyclic species is reported in % and was determined from the UV signals using RP-HPLC; [d] By-products correspond to linear and cyclic oligomerization by-products as well as to by-products associated with the coupling reagents (e.g. guanidinium, nitrile formation) and unidentified by-products; [e] BBs means building blocks, which correspond to the repeating units

Further, in this study it was found that the use of PyBOP was the best choice to yield a desired monocyclic oligo(amido amine), also due to its lack of the guanidinium side-product formation[166], which participates in the presence of a free amine with uronium based coupling reagents[166], such as HATU or HBTU. The additional use of the additive HOBT did not lead to a significant improvement.

With the previous use of the uronium based coupling reagents such as HATU and HBTU, the monocyclic species were also obtained, however, in significantly reduced yield of about 10 − 15 %

(Table 3). Other unidentified side-products occurred in addition to the monocyclic species as well as the oligo- and polymerization by-products. Further, addition of HOBT did not lead to any improvement in this case either. Through RP-HPLC monitoring it was observed that the macrocyclization was completed within a reaction time of about 40 min, while the use of PyBOP required 1 h for the cyclization to complete. This indicates that – as is also known from literature[166, 213-214] – uronium based coupling reagents such as HATU and HBTU are significantly faster in their reaction kinetics and more reactive as compared to PyBOP. However, in this case reactivity comes at the cost of selectivity. While PyBOP yields the monocyclic structure in higher quantity, reaction with HATU and HBTU results in larger quantity of by-products.
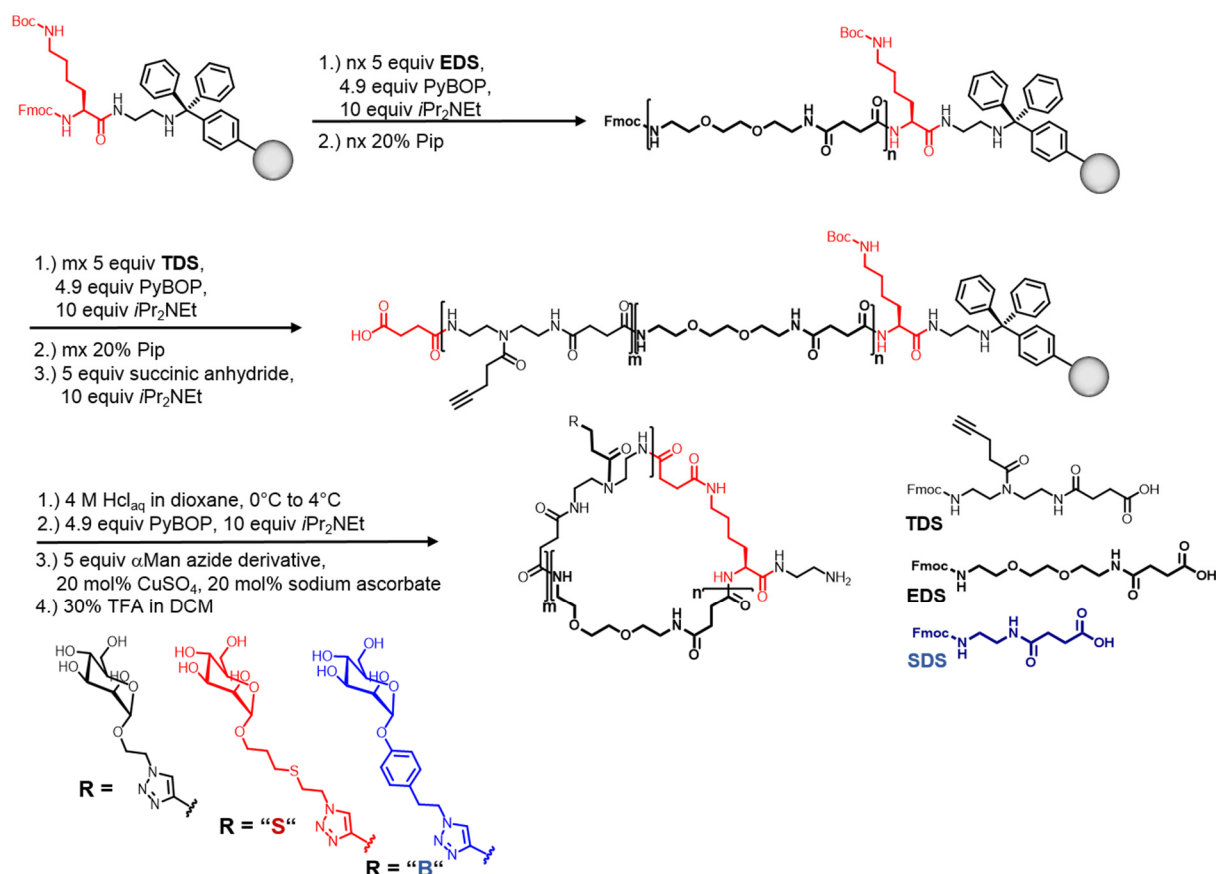
Scheme 2. SPPoS of cyclic precision glycomacromolecules with different spacing and αMan linkage following the Boc side-chain deprotection and cyclization strategy, using PyBOP activation.

In conclusion, the side-chain-to-tail macrocyclization can be readily obtained by activation with PyBOP (Table 3, Scheme 2). The highest isolated yield observed with these macrocyclization processes was about 27 % (the isolated yield ranged between 3 % − 27 %, Figure 20). The desired monocyclic species were isolated and purified by semi-preparative RP-HPLC, after conjugation with the different αMan derivatives using CuCAAC as described in the previous subchapter. The cyclic mixtures on solid support were therefore directly conjugated with the αMan azides on-resin, without prior purification of its cyclic oligo(amido amine) precursors (P1@, P1a@, P2@ and P2a@). It turned out that the direct conjugation of the cyclic mixtures on-resin resulted in less isolated

product loss, whereas isolation of the oligo(amido amine), followed by conjugation of the αMan azides required two purification steps, resulting then in significant loss of the isolated cyclic products. The desired monocyclic species were characterized by NMR, MALDI-TOF and RP-HPLC analysis (see Experimental Part), while oligo- and polymerization by-products were characterized by MALDI-TOF analysis. The desired cyclic glycomacromolecules were obtained in high purity of > 88 % − 95 %.
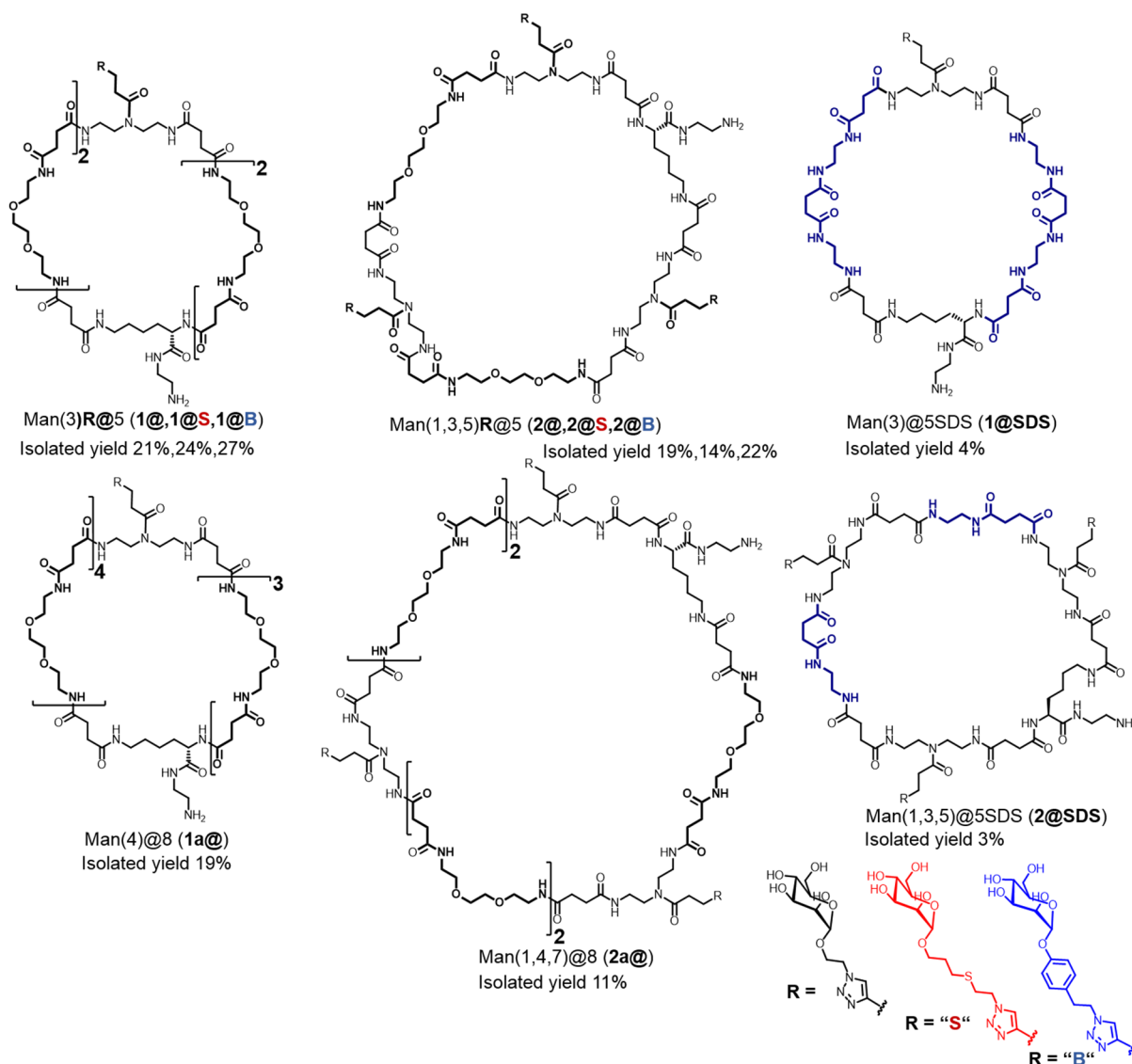
Figure 20. Overview cyclic glycomacromolecules with different spacing and αMan linkers obtained *via* Boc side-chain deprotection and cyclization.[3]

---

[3] 1@SDS and 2@SDS were synthesized and characterized (NMR, RP-HPLC and MALDI-TOF) by Andreas Ludwig (Heinrich-Heine-Universität Düsseldorf, group of Prof. Dr. Laura Hartmann, Bachelor Thesis, October 2015). In this thesis, the characterization data of the above mentioned compounds (NMR) has been re-assessed by the author of this thesis.

Altogether, using the above synthetic procedures, 10 cyclic precision glycomacromolecules were synthesized (Figure 20). These glycomacromolecules differ in their spacing and thus their ligand density and ring-size, as well as in their αMan linkage.

Figure 21 highlights the RP-HPLC chromatograms of cyclic glycomacromolecules, which differ in their spacing (Figure 21, A left) and αMan linkage (Figure 21, A right). Three exemplary MALDI-TOF spectra of compounds 2@, 2@S and 2@B with a varied αMan linkage further confirm the monodispersity of these cyclic glycomacromolecules (Figure 19, B and Figure 21, B). From both RP-HPLC spectra (Figure 21), it can readily be seen that the retention time (T_R) increases with the spacing (from 2@SDS over 2@ to 2a@), thereby making the overall cyclic backbone more hydrophobic (Figure 21, A left). The same holds for glycomacromolecules, which possess the same cyclic backbone but a different αMan linkage (Figure 21, A right). Here, T_R increases with the length and the hydrophobicity of the αMan linkers, in the order 2@ < 2@S < 2@B.
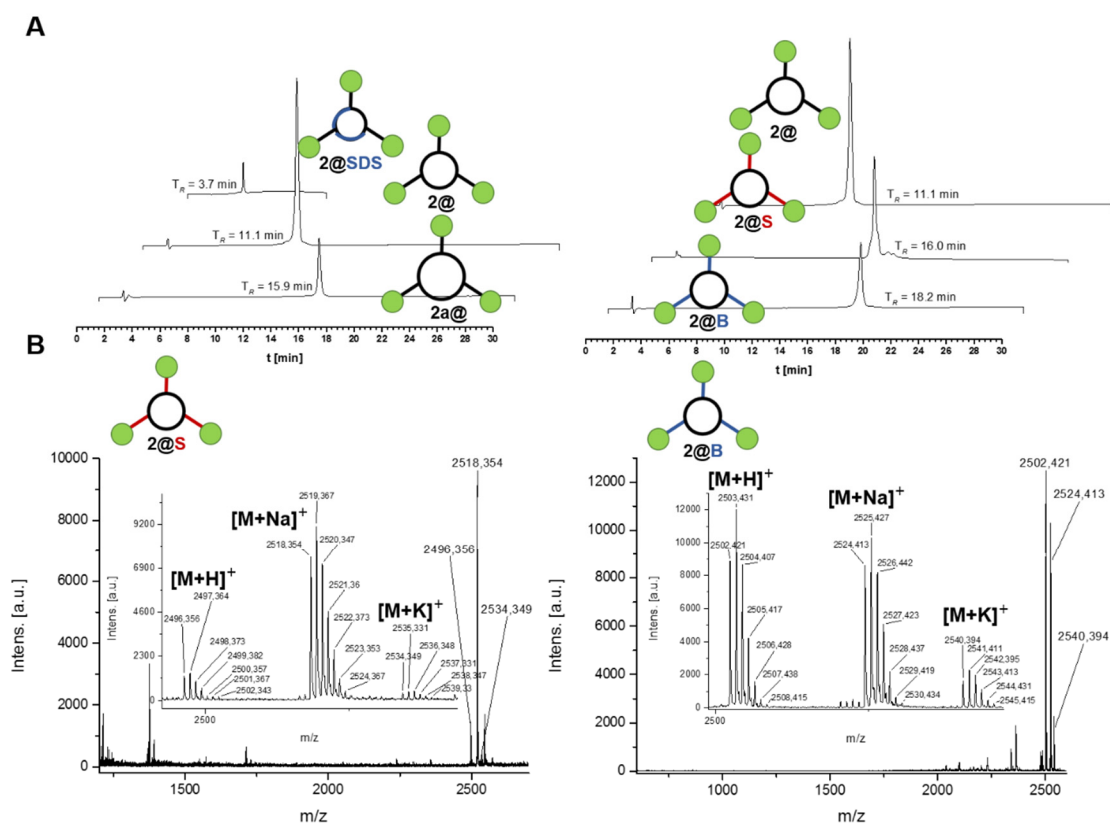
Figure 21. Representative RP-HPLC pure chromatograms (A) and MALDI-TOF spectra (B) of cyclic precision glycomacromolecules with different spacers and linkers. A: Left (different spacer): 2@SDS (Man(1,3,5)@5SDS) (5 % → 95 % MeCN in 10 min), 2@ (Man(1,3,5)@5) and 2a@ (Man(1,4,7)@8) (5 % → 30 % MeCN in 30 min). Right (different linkers): 2@ (Man(1,3,5)@5), 2@S (Man(1,3,5)S@5) and 2@B (Man(1,3,5)B@5) (5 % → 30 % MeCN in 30 min). B: Representative pure MALDI-TOF spectra of 2@S (Man(1,3,5)S@5) and 2@B (Man(1,3,5)B@5).
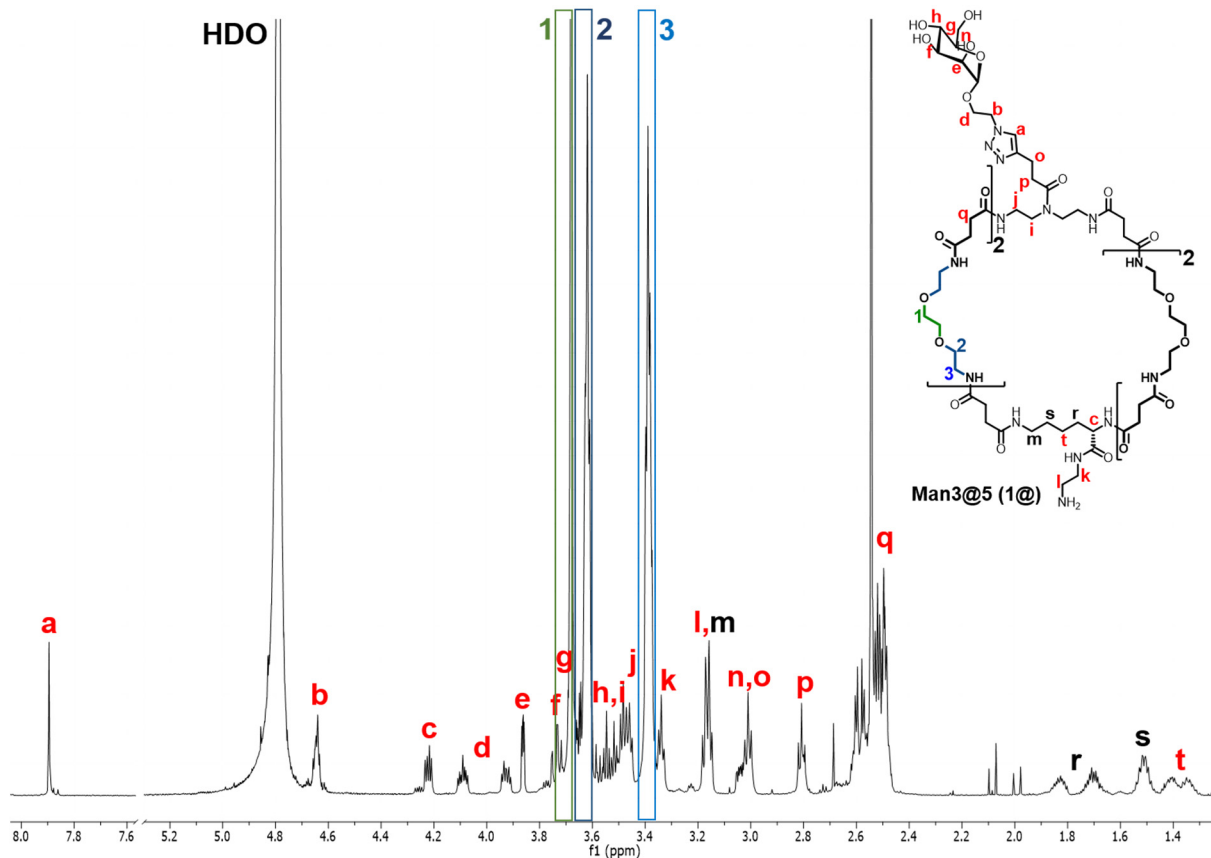
Figure 22. Elucidation of the cyclic structure through its Lys side-chain protons (highlighted black). ^{1}H NMR spectrum of 1@ (Man(3)@5).

Figure 22 exemplary shows the ^{1}H NMR spectrum of the cyclic glycomacromolecule 1@. Elucidation of its cyclic backbone was possible by observing the change in the Lys side-chain CH$_2$ protons m, r and s. The chemical shift of these protons is directly affected, because of their position next to the new formed intramolecular amide bond. The CH$_2$ group protons m (directly next to the new formed amide) shifted from ~3 to ~3.2 ppm after cyclization, whereas the CH$_2$ group protons s shifted from low to high field, by about ~0.2 ppm (from ~1.7 to ~1.5 ppm), giving a clearer splitting of the protons r.

3.3. The use of silylating agents in on-resin cyclization of oligo(amido amines)

The previous subchapter showed that the synthesis of cyclic architectures is realized by a two-step strategy, where a protecting group has to be removed prior to a macrocyclization (in this case a side-chain-to-tail macrocyclization). In general, conventional methods for the synthesis of macrocycles on solid support rely on the use of such two-step strategies[142-143, 148, 171-172, 183]. Therefore, it would be advantageous to evaluate and find reaction conditions, which would allow a "one-pot" synthesis of cyclic architectures, thereby minimizing the overall reactions steps and potential challenges, such as low yields and side-product formation. To address this synthetic challenge, oligo(amido amine) model compounds were used. For the synthesis of such cyclic precision oligomers the aim was to find a tandem reaction, which would allow for the removal of a protecting group and macrocyclization in one step on solid support (Figure 23). Following the concept described in the previous subchapter, it was decided to again build on the side-chain-to-tail cyclization strategy and use Boc as the protecting group in the *C* terminal Lys side-chain. The model sequences consist of ADS building block repeating units[99]. The ADS building block[99] is another functional building block, as previously introduced by Wojcik *et al.*[99], containing a side-chain Alloc protecting group. Here, the Alloc protecting group was expected to be orthogonal to the removal of Fmoc as well as to the tandem macrocyclization protocol. Cleavage of the Alloc protecting groups would generate free secondary amines that could be used for the synthesis of cyclic polycations or for further functionalization with carbohydrate ligands.

To realize such a tandem cyclization reaction, silylating agents in the presence of an amine base were evaluated. The use of silylating agents in peptide chemistry[200, 203-205, 209, 215-216] is known. Selective Boc deprotection was performed using silylating compounds, such as TMSCl[203, 209], silicon tetrachloride (SiCl$_4$)[205] and iodotrichlorosilane (ISiCl$_3$)[204] on acid cleavable resins. Silylating agents in the presence of a base, such as tetrachlorosilane (SiCl$_4$) and pyridine, have been used for the synthesis of aromatic and aliphatic amides as well as for amide coupling of a dipeptide by Wong[215]. Wong proposed that the silylating agent SiCl$_4$ *in situ* activates the carboxylic acid in the presence of amines, leading readily to the formation of amides. He also tested the synthesis of a dipeptide sequence with these activating agents and saw that the benzyloxy protecting group, present in one of the AAs, was not stable to SiCl$_4$/pyridine and has led to deprotection, which caused peptide polymerization. These conditions of using silylating agents either in presence of phenol or a base were later applied by Burgess *et al.*[216] and Cavelier *et al.*[200] for the deprotection of the acid sensitive protecting group Boc on the solid support. The latter group showed that Boc removal of protected AA side-chains could be directly performed on an electrophilically cleavable resin (Wang resin), thereby showing that Boc can also be used as a temporary protecting group. They also mentioned that this strategy could be applied on acid sensitive resins using Fmoc chemistry, where both Fmoc and Boc can be used as temporary protecting groups, allowing for the application of a step-wise on-resin synthesis of cyclic peptides or the introduction of other AAs into the side-chains. Recently, silylating compounds have been used for a mild synthesis of amides and peptides through

a silatropic switch using *S*-silyl thiol esters that spontaneously tautomerize to *O*-silylthionoesters, which upon reaction with alkylammonium bases yield amides.[217]
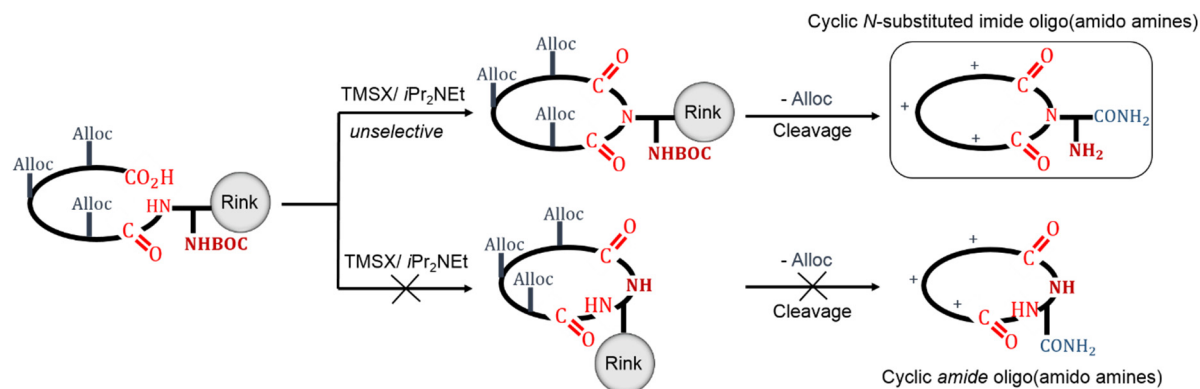
Figure 23. Evaluation of reaction conditions for cyclic/cationic oligo(amido amines) points towards unselective synthesis of cyclic *N*-substituted imides.

Therefore, as referring to the above mentioned considerations and observations that silylating agents[200, 203-205, 209, 215-216] can be used for both, the acid sensitive Boc deprotection[200, 203-205, 209, 216] as well as the potential activation of carboxylic acids[215, 217], the aim was to test for an on-resin tandem cyclization strategy, allowing for an *in situ* removal of Boc and activation of an *N*-terminal carboxylic acid to yield an *intra*molecular macrocyclization. For such a tandem Boc deprotection and on-resin macrocyclization different silyl derivatives were used, such as TMSOTf and TMSBr in the presence of *i*Pr₂NEt. Macrocyclization should thus proceed from the *N*- to the *C*-terminus *via intra*molecular reaction of an *N*-terminal carboxylic acid group with a *C*-terminal Boc protected amine side-chain. Both reagent conditions, TMSOTf/*i*Pr₂NEt and TMSBr/*i*Pr₂NEt, were evaluated for their ability to yield backbone macrocyclization. Cyclic oligo(amido amines) with different ring-sizes (from 22- to 66-membered) were targeted, altering in the number of secondary amine groups within the backbone (from one to five) corresponding to the assembled ADS building block sequences. In addition, the evaluated macrocyclization protocol was compared to a conventional two-step method for on-resin macrocyclization, where the Boc protecting group was cleaved with TMSCl/phenol prior to macrocyclization using PyBOP.

3.3.1. Use of silylating agents for one-pot on-resin cyclization

To evaluate the reaction conditions required to yield a macrocyclization in a side-chain-to-tail manner, it was decided to use the RAM linker, which is compatible with the Fmoc protecting group chemistry. Commercially available Tentagel RAM solid support was used with a loading of 0.23 mmol/g, which allows to create pseudo-dilution conditions[173-174] and thus was expected to prevent or diminish linear and cyclic oligomerization. As already mentioned, the oligo(amido amine) model sequences consisted of ADS building block repeating units, with the orthogonal Alloc group in the side-chain. To be able to systematically test the reaction conditions that would allow for both, the *in situ* Boc protecting group cleavage and cyclization, ring formation of model compound 6 to form the corresponding cyclic compound 6a (22-membered) was evaluated (Scheme 3). In order for the side-chain-to-tail cyclization to occur, the resin was first preloaded with lysine (Lys N^{α}-Fmoc and N^{ε}-Boc protected), introducing an N^{ε}-Boc-protected primary amine in the side-chain that will later on allow for cyclization upon amide formation with a terminal carboxylic group. The linear precursor defining the overall size of the ring as well as the monomer sequence is built up by step-wise addition of ADS building blocks, using standard Fmoc coupling chemistry (Scheme 3). In order to allow for the side-chain-to-tail cyclization with the primary amine side-chain of the Lys residue, the *N*-terminus was transferred into a carboxyl group in the last step of the precursor synthesis. Here, succinic anhydride was coupled to the *N*-terminal amine group after Fmoc cleavage. The ring formation was then tested using a reagent cocktail consisting of either TMSOTf/*i*Pr₂NEt or TMSBr/*i*Pr₂NEt in DCM. The reaction was monitored by cleaving small aliquots from the resin upon treatment with the standard cleavage cocktail for the RAM linker (Figure 24) and performing RP-HPLC analysis. Following the reaction in intervals of 5 min, for an overall reaction time of 30 min, an increasing signal for the formation of the macrocycle 6a and decreasing signal for the linear precursor 6 (Figure 24) was observed. This one-step protocol was then further compared to a conventional two-step method for solid phase macrocyclizations, using TMSCl/phenol[203-205, 209] for prior Boc deprotection, followed by activation with PyBOP for subsequent cyclization. The Boc deprotection using TMSCl/phenol was allowed to proceed for 5 min before quenching and activation with PyBOP, expected to yield the macrocyclization. The monitored reaction time with respect to TMSCl/phenol and PyBOP treatment therefore corresponds to the progress of the Boc removal.
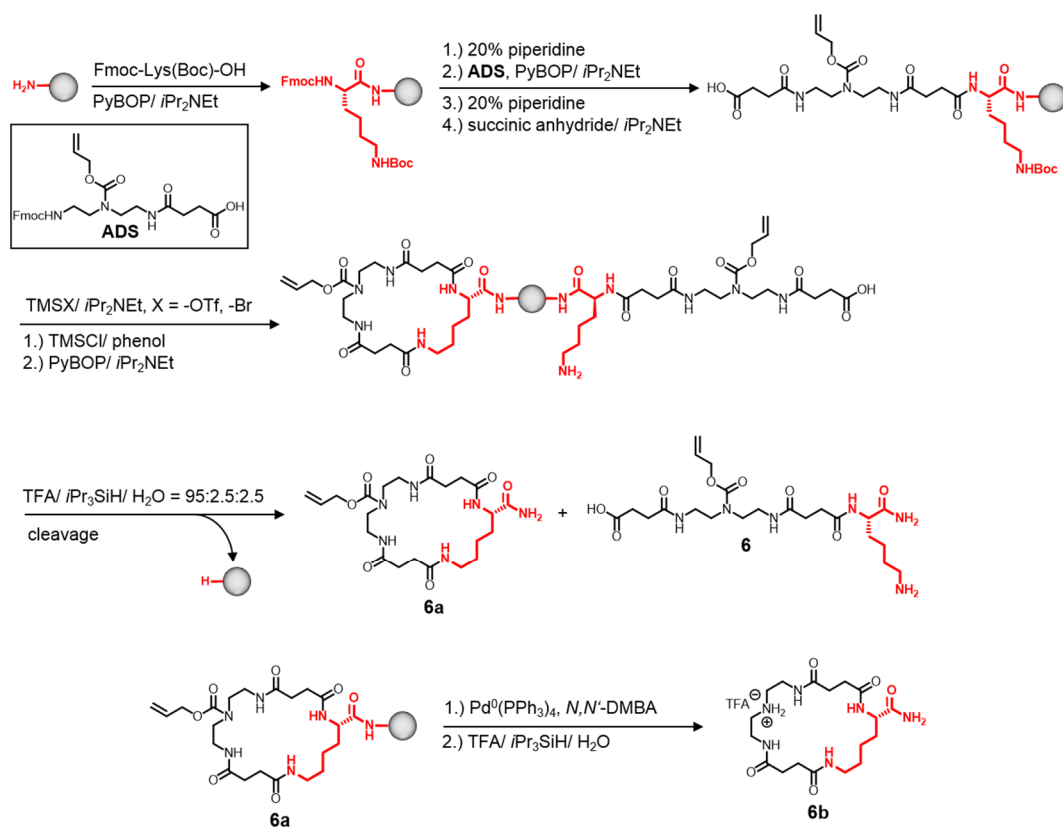
Scheme 3. Targeted one-step synthesis of a 22-membered ring 6a and its cationic derivative 6b. Investigation of the on-resin cyclization using silylating reagents.
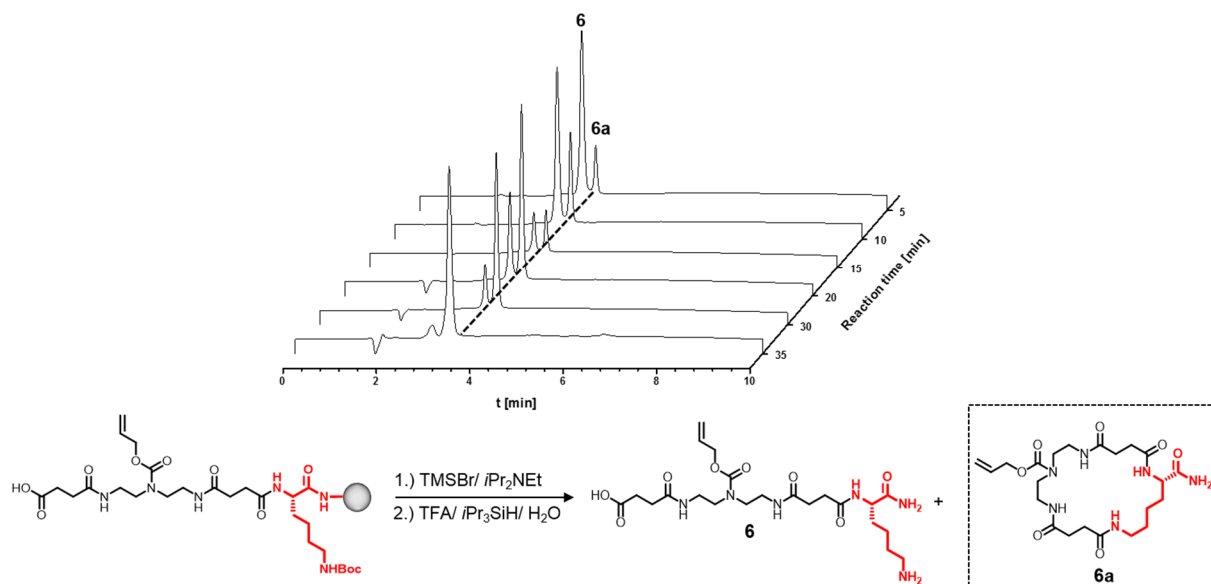
Figure 24. Representative RP-HPLC chromatograms for the targeted cyclization progress (shown for the reaction with TMSBr/*i*Pr₂NEt in DCM), which was monitored after every 5 min.

After the complete reaction as observed by RP-HPLC (Figure 24), the Alloc protecting group was removed by standard Tsuji-Trost conditions[186-187] using tetrakis(triphenylphosphine)palladium(0) ((Pd^0(PPh$_3$)$_4$) in the presence of the allylic scavenger *N,N*'-DMBA, potentially yielding the 22-membered ring 6b with a precisely positioned secondary amine after cleavage from the solid support (Scheme 3). Interestingly, PEG impurities were found in the NMR and MALDI-TOF spectra of the crude material 6a after direct cleavage from solid support (see Supporting Appendix). It is well documented that Tentagel resins are not always stable to the harsh cleavage conditions by using TFA.[218] Treatment of Tentagel resins with TFA sometimes results in the cleavage of PEG3000. To confirm that the loss of PEG (through the ether bonds grafted on PS) was not a result of the cyclization progress and therefore the use of silylating Lewis acids, the linear precursor 6 was cleaved from the solid support. Analysis by NMR and MALDI-TOF (see Supporting Appendix) confirmed that the PEG miscleavage was due to irreversible removal of the oligomer from solid support and not a result of the reaction conditions applied for macrocyclization.

In addition to the above tested reaction conditions on the monocyclic compound 6a, macrocycles differing in ring-size and monomer repeating units were targeted, to systematically access the effect of the backbone length on the macrocyclization efficiency (the only difference being the number of ADS repeating units). For this reason, linear oligomers 6 − 10 varying from one to five ADS repeating units were synthesized, which would potentially result in medium- (33- and 44-membered) to large-sized rings (55- and 66-membered). It is well-known that an increasing chain-length can lead to *inter*molecular reaction and formation of linear and bicyclic by-products[172]. Such oligomerizations can be suppressed to some extent by using low resin loadings[173-174], as already mentioned. In addition, longer chain-lengths can lead to aggregation of the macromolecules on solid support, e.g. by forming a hydrogen network.[219] Such aggregation effects have been reported to affect the coupling and macrocyclization efficiency, as they limit accessibility of the reactive sites.[219] However, recent results of Pei *et al.*[171] studying peptide macrocyclizations on the RAM indicate that longer chain-lengths of ≥ 6 AA sequences are less prone to cyclic and linear oligomerization, whereas small-sized peptide rings (≤ 5 AA sequences) have a higher tendency to bicyclic and tricyclic oligomerization. Further, it has to be mentioned that the functional building blocks used such as ADS correspond to the chain-length of about two AA building blocks, leading to longer sequences coupled with each repeating unit to the solid support. Thus, the overall longer backbone as compared to AAs was expected to be less prone to ring strain, caused by smaller linear sequences (e.g. 6a). In addition, in contrast to conventional AAs the ADS building block used in this study does not obtain sterically demanding moieties, but rather allows free rotation along the single bonds (except for the amide bonds). In the previous chapter, where the synthesis of cyclic glycomacromolecules was discussed based on a conventional two-step procedure, a rather reverse tendency was found for intermolecular oligomerization side-reactions: While shorter chain-lengths of five repeating units have led to less oligomerization by-products, longer chains of eight building blocks were even more prone to cyclic oligomerization. As the functional model building block used

here is very similar to the building blocks used for the synthesis of cyclic glycomacromolecules, the same trend was also expected in this case.
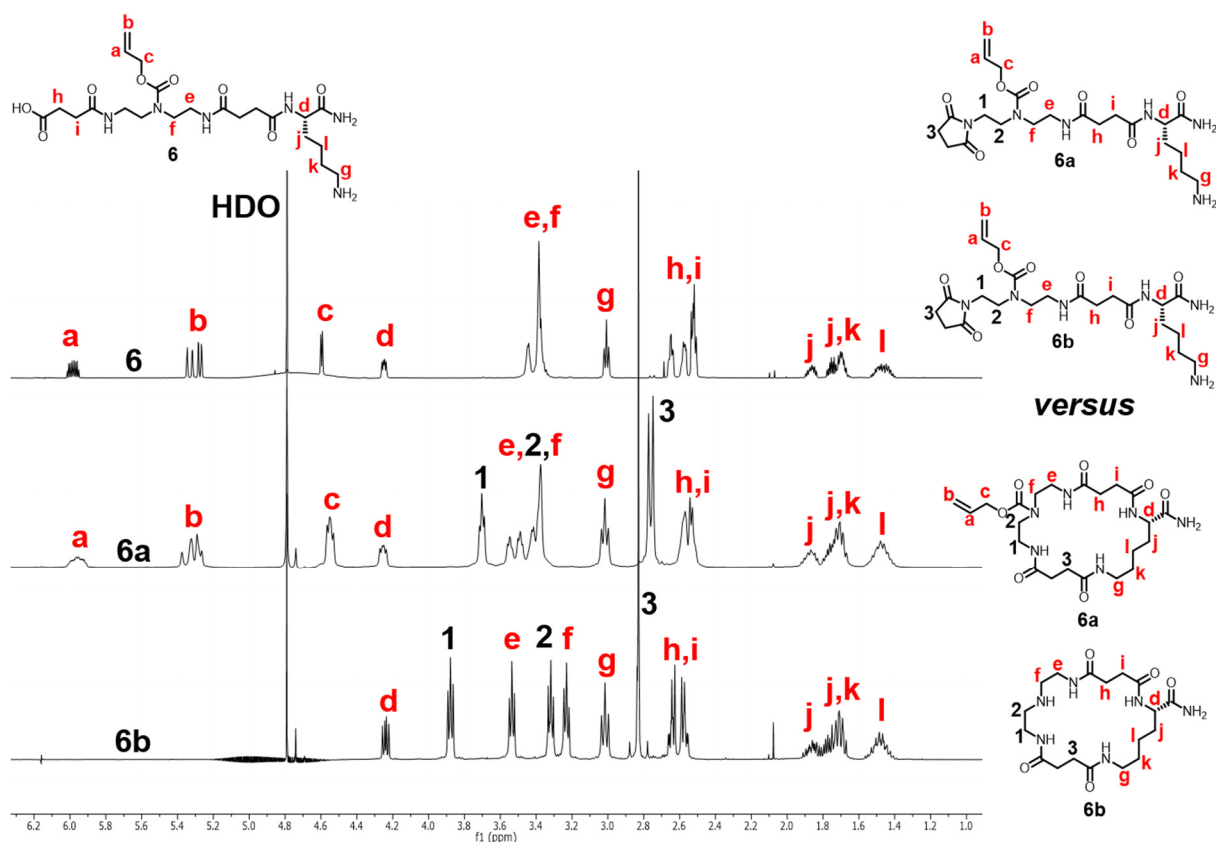
Figure 25. Stacked ^{1}H NMR (D$_2$O) spectra of compounds 6, 6a and 6b, allowing to observe the evolution of the protons after the individual reactions. Proton signals do not correspond to amide macrocycles, but rather to the formation of imides.

NMR analysis was applied to confirm the synthesis of the differently sized cyclic derivatives 6a − 10a and its cations 6b – 10b. Interestingly, analysis by NMR and MALDI-TOF showed the absence of linear and cyclic oligomerization products that were previously observed for the macrocyclization of cyclic glycomacromolecules with the two-step procedure. Analysis by MALDI-TOF and HRMS ESI (see Experimental Part) showed a loss of −18 m/z after complete reaction. In a first approximation this indicates the loss of water, thus being representative for a dehydration reaction and thus the desired amide formation and ring closure reaction. However, a dehydration reaction must not necessarily refer to the formation of an intramolecular amide bond (along with a macrocyclization), but could also occur due to other reaction pathways. Analysis by NMR of the compounds 6a − 10a and 6b – 10b, which were compared to their linear counterparts 6 – 10, indeed supported the hypothesis that it was not the cyclization process, which has led to the loss of water (Figure 25 − 27), but rather to the formation of unexpected imide products.

To evaluate the NMR data and get information on the product formation, the different oligo(amido amines) were first recorded in heavy water to erase for the amide protons. In the 1D NMR spectra of the derivatives 6a − 10a and 6b – 10b (Figure 25 − 27), usually after such a

side-chain-to-tail amide cyclization, one would expect for the Lys CH$_2$ side-chain protons (g, k in Figure 25 and highlighted red in Figure 26 and 27) to change in their chemically shift, as was shown in the previous subchapter in the synthesis of cyclic glycomacromolecules. Due to the deshielding effect created by the new intramolecular amide bond as well as the neighboring shielding effect of g towards the protons k, one would expect the same downfield shift for the CH$_2$ protons (g in Figure 25 and highlighted red in Figure 26 and 27) and a highfield shift of the protons k (k in Figure 25 and highlighted red in Figure 26 and 27) in the cyclic oligo(amido amines) obtained from the one-pot procedure.
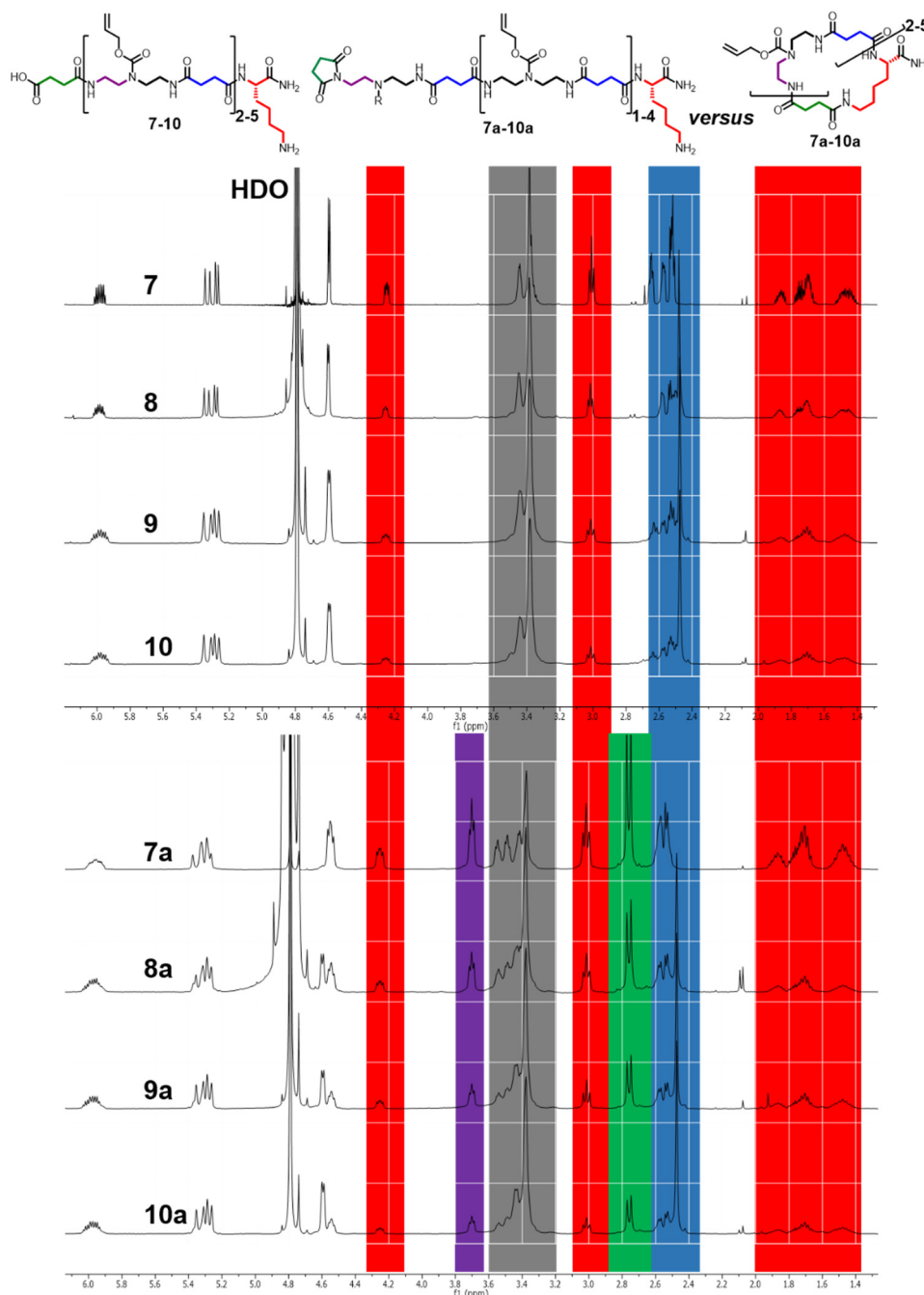
Figure 26. Stacked ^{1}H NMR (D$_2$O) spectra of linear compounds 7 − 10 and their derivatives 7a − 10a, allowing to observe the evolution of the protons with an increasing chain-length/ring-size. Proton signals do not correspond to amide macrocycles, but rather to the formation of imides.

However, the NMR spectra in Figure 25 − 27 show a significant downfield shift of the succinic acid CH_2 protons 3 from ~2.6 to 2.8 ppm (3 in Figure 25, highlighted green in Figure 26 and 27), with the integral being four in each of the spectra. The proton intensity of this signal is always the same for each of the compounds 7a − 10a and 7b – 10b and irrespective of the chain-length.
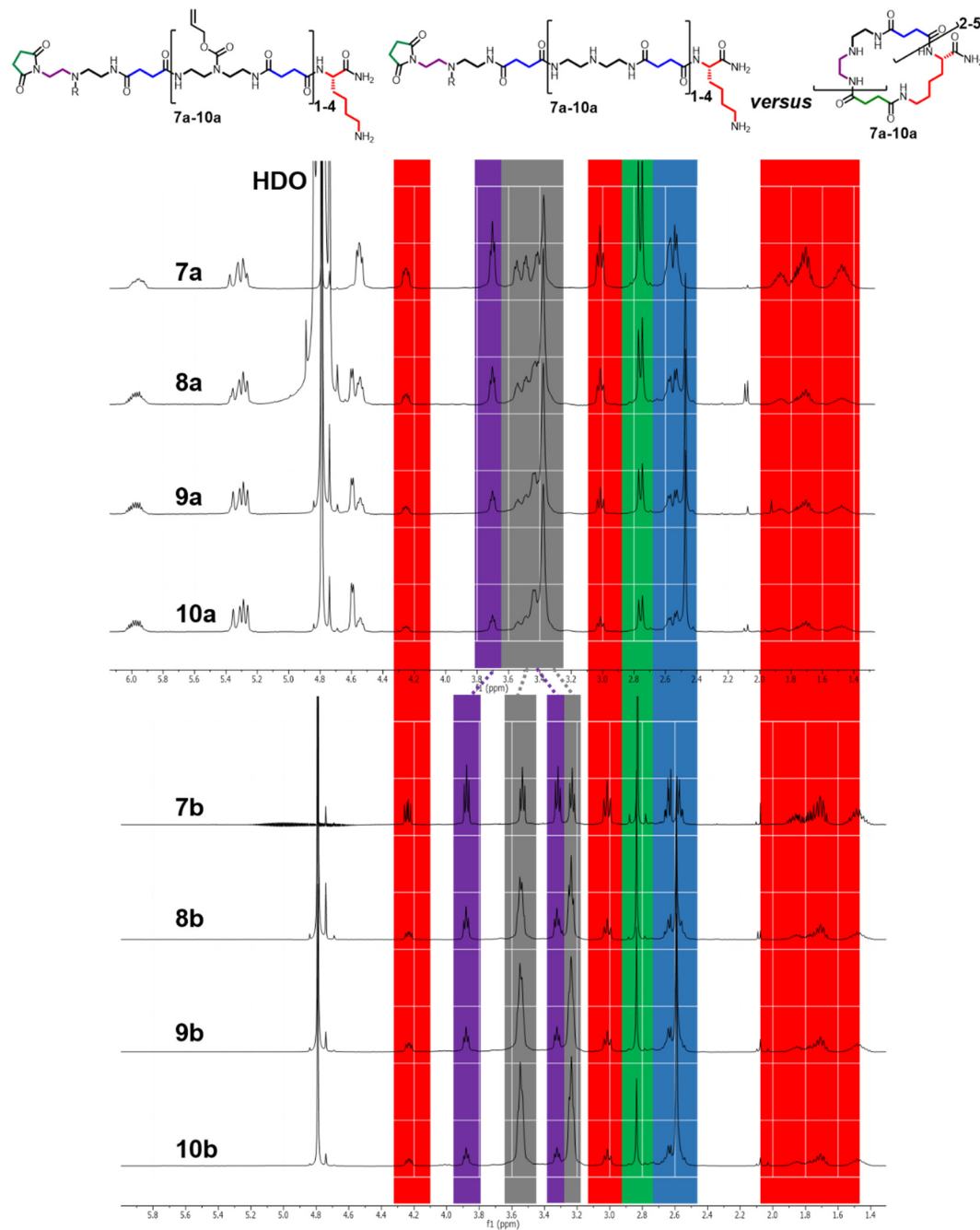
Figure 27. Stacked ¹H NMR (D₂O) spectra of compounds 7a – 10a and their derivatives 7b – 10b, allowing to observe the evolution of the protons with an increasing chain-length/ring-size and Alloc deprotection. Proton signals do not correspond to amide macrocycles, but rather to the formation of imides.

Further, another significant downfield shift was observed for the CH_2 group protons of the diamine groups 1, 2 (protons 1, 2 in Figure 25, highlighted purple in Figure 26 and 27), whereas all

of the Lys side-chain protons remained unchanged after reaction (especially protons g, k in Figure 25, highlighted red in Figure 26 and 27). In compounds 7a − 10a protons 1 were shifted from ~3.4 to 3.7 ppm, whereas their cationic species 7b – 10b even showed a more dramatic downfield shift from ~3.6 to 3.9 ppm and ~3.2 to 3.3 ppm for the protons 1 and 2, respectively (highlighted purple in Figure 26 and 27). Although the ^{1}H NMR spectra in Figure 27 confirmed complete Alloc removal, interestingly all the CH_2 group protons of the two diamine groups (Figure 25, protons 1, e, 2, f) between 3.9 and 3.2 ppm are chemically unequal for the model compound 6, 6a and 6b (Figure 25). The same chemical dissimilarity of the protons 1, e, 2, f was also observed for compounds 7a − 10a and 7b – 10b (Figure 26 and 27, signals are highlighted purple and grey). In addition, there appeared now a sharp singlet with an integral of four, which corresponds to the succinic acid CH_2 protons 3 in Figure 25 (highlighted green in Figure 26 and 27). Inspection of all of the NMR spectra of the compounds 7 − 10, 7a − 10a and 7b − 10b showed, that it was always the same protons that experienced a downfield shift (highlighted green and purple), while the other backbone protons and most importantly the Lys protons remained in the same region, only changing their relative proton intensity due to an increasing number of ADS repeating units. Although analysis by HRMS ESI showed a loss of water and potentially confirmed the amide formation, which typically occurs as one example of a dehydration reaction, the ^{1}H NMR spectra does not correspond to the targeted amide macrocycles. Inspection of the NMR spectra (Figure25 − 27) shows a downfield shift of the CH_2 group succinic acid and diamine protons, that rather indicate the formation of an imide bond.

Indeed, the acid or base catalyzed formation of cyclic imides[220-222], in particular the cyclic aspartimide formation[220-222], is a well-documented side-reaction in the SPPS and known to be AA sequence specific.[220-222] Sequences containing Ala and Gly show larger tendency to undergo undesired reaction with their amide bonds.[220-221] Such reaction therefore requires a somehow "activated" amide bond and an unprotected AA residue, such as a carboxylic acid, e.g. aspartic acid. It has been reported that excess of bases such as NEt$_3$ or iPr$_2$NEt and long reaction times in DCM can lead to cyclic imide formation in 24 h with up to 5 % yield.[220] In addition, it is well-known that the use of silyl compounds can lead to partial activation of the peptide amine, so that e.g. unwanted *N*-methylation takes place upon the peptide bond, which has been recently shown to be important in the synthesis of *N*-methylated cyclic peptides[143]. So in this case, it therefore seems that both has combined, since an excess of both an amine base and silylating agents, iPr$_2$NEt and TMSBr/OTf, were used with 40 and 30 equiv in DCM, respectively. For this reason and after inspection of the above NMR spectra, it seems to be reasonable to assume that instead of the targeted amide macrocycles, *N*-substituted imides have formed.
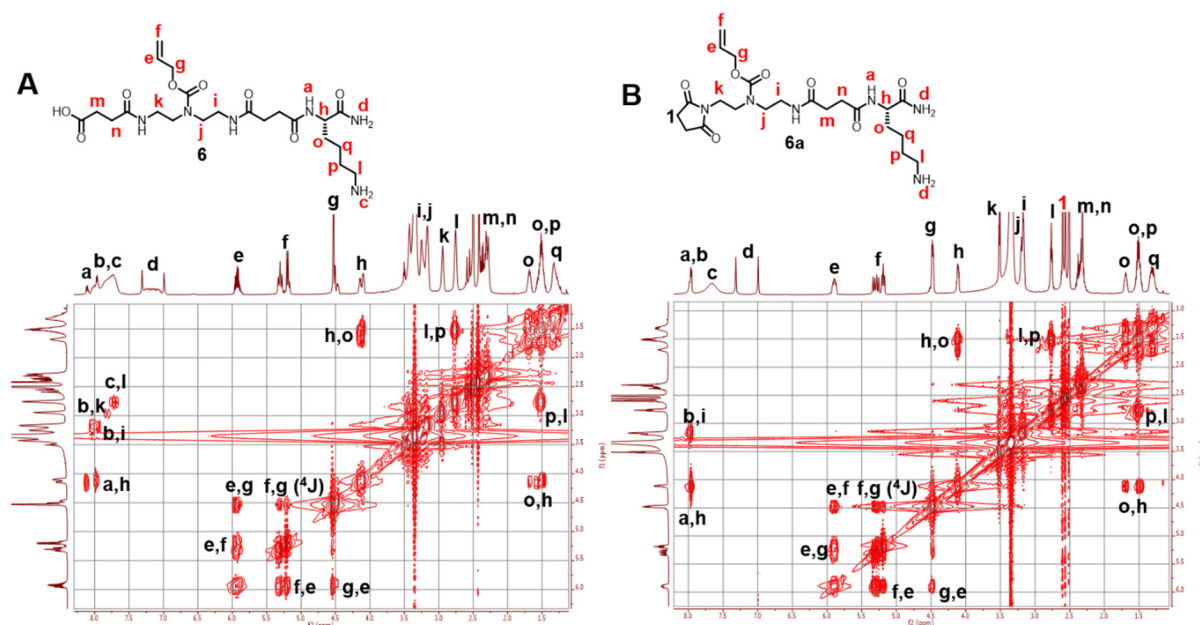
Figure 28. 2D ¹H/¹H COSY NMR spectra (DMSO−d_6) of the linear precursor **6** and its cyclic *N*-substituted imide derivative **6a**. The right NMR spectrum indicates an unselective five-membered imide formation instead of a 22-membered amide macrocycle.

To get a more detailed picture into the products of the above described reaction, a 2D ¹H/¹H COSY NMR analysis of the compounds **6** and **6a** was performed, this time in deuterated dimethyl sulfoxide (DMSO−d_6) (Figure 28). Visualisation of the amine and amide protons would also help now to decide on the amide or imide cyclization progress. Inspection of the COSY spectra A confirmed the linear precursor, showing the different amide and amine protons a, b, c, which exhibit cross-coupling peaks to their neighboring protons h, k, i and l. Comparing now their potential cyclic derivative **6a** to its precursor **6** reveals that: (*i*) The amine proton c as well as the other Lys side-chain protons remain unchanged (o, p, q, l, h), whereas (*ii*) the cross-coupling of the amide proton b to the CH$_2$ group k disappears. These two observations pinpoint to an unselective formation of an *N*-substituted imide bond, as it is shown in the COSY spectra B of compound **6a** (Figure 28). Further, the *N*-substituted imide formation would further explain the significant downfield shift of the diamine CH$_2$ protons k from ~3.0 to 3.4 ppm, as well as that of the singlet 1, shifted from ~2.4 to 2.6 ppm (previously being chemically equal with n, m). This signal further corresponds to the chemically equivalent CH$_2$ groups of the five membered imide, showing an integral of four.

In contrast to targeted intramolecular amide macrocycles, analysis by NMR instead points at an unselective formation of *N*-substituted cyclic imides. To confirm this hypothesis, in the next subchapter the reaction process will again be re-evaluated on model peptides, which may further help to identify the imide bond and support the current hypothesis.

3.3.2.Investigation of imide formation during one-pot cyclization using model peptides

In order to test the hypothesis of imide formation, model tri- and tetrapeptides were synthesized (11 and 12[4]). The same silylating agent protocols previously used for the oligo(amido amines) were applied on the two peptides. The tripeptide lysine-alanine-phenylalanine (Lys-Ala-Phe) and the tetrapeptide lysine-alanine-phenylalanine-phenylalanine (Lys-Ala-Phe-Phe) were used, as they present model sequences for cyclic peptides, which are usually difficult to synthesize[148, 171]. Such difficulties arise on the one hand from the length of the sequence, where small-sized peptides with ≤ 5 AA sequences are considered to be more challenging during cyclization[148, 171]. On the other hand, peptide sequences containing basic AAs, such as Lys, and apolar as well as sterically demanding AAs, such as Ala and Phe are known to be difficult to cyclize also due to the all-L conformation of the peptide backbone[148, 171]. Further, the Lys and Ala peptide sequences as well as the *N* terminal succinic acid were used, since they are known to be sensitive to the formation of cyclic imides (*via* activation of their amide bonds and reaction with the unprotected succinic acid residue). All previously tested reaction conditions were applied to the tri- and tetrapeptide linear precursor 11 and 12 (Scheme 4) and the reaction was monitored by RP-HPLC (not shown).
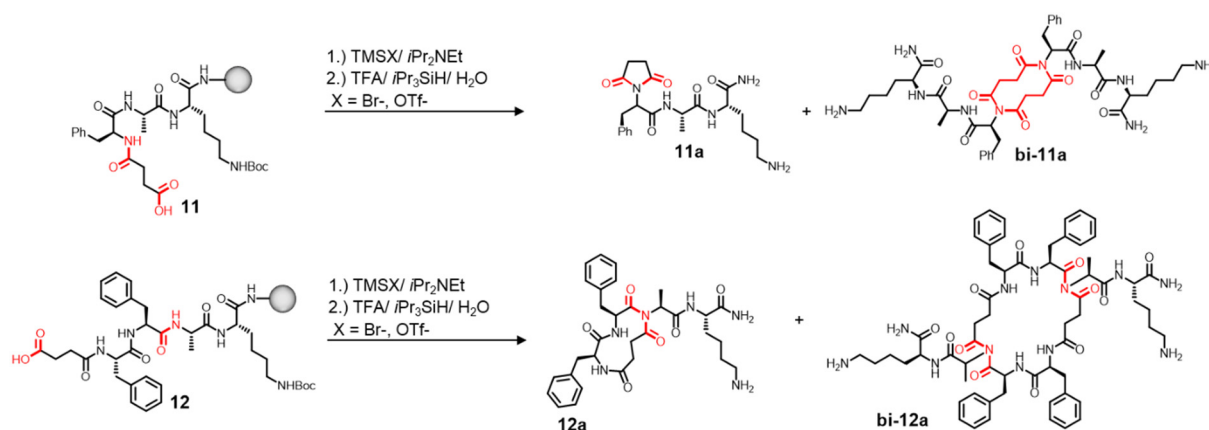
Scheme 4. Synthesis of the tri- and tetrapeptides 11a, bi-11a and 12a and bi-12a confirmed the *N*-substituted imide formation to be sequence independent and thus always resulting from the acceleration by a base and silylating agents.[5]

Treatment of the peptide-loaded RAM resin with TMSOTf and TMSBr in the presence of *i*Pr₂NEt, as well as treatment with TMSCl/phenol for the Boc deprotection and subsequent coupling

---

[4]Linear tetrapeptide 12 has been synthesized and characterized (NMR, RP-HPLC and MALDI-TOF) by Genesha Olgar (Heinrich-Heine-Universität Düsseldorf, group of Prof. Dr. Laura Hartmann, Bachelor Thesis, November 2015). In this thesis, the characterization data of the mentioned linear tetrapeptide have been re-assessed by the author of this thesis. Analysis and evaluation of the in this thesis presented 2D ¹H/¹H COSY NMR and 2D ¹H/¹⁵N HSQC NMR spectra of the mentioned linear tetrapeptide has exclusively been performed by the author of this thesis and has not been presented previously.

[5]Mono- and bi-cyclic tetrapeptides 12a and bi-12a have been synthesized and characterized (NMR, RP-HPLC and MALDI-TOF) by Genesha Olgar (Heinrich-Heine-Universität Düsseldorf, group of Prof. Dr. Laura Hartmann, Bachelor Thesis, November 2015). In this thesis, the characterization data of the mentioned cyclic tetrapeptides have been re-assessed by the author of this thesis. Analysis and evaluation of the in this thesis presented 2D ¹H/¹H COSY NMR and 2D ¹H/¹⁵N HSQC NMR spectra of the mentioned cyclic tetrapeptides has exclusively been performed by the author of this thesis and has not been presented previously.

with PyBOP, resulted in conversion of 11, 12 to 11a, bi-11a and 12a, bi-12a after 2 h 40 min, respectively (Scheme 4). Applying different 2D NMR methods for the analysis of their structural composition confirmed the formation of *N*-substituted imides, thereby also showing that the reaction is sequence-independent and always a result of the applied silylating agents in the presence of an amine base.

To be able to elucidate the imide moiety, 2D NMR spectra of the linear precursor 12 and its cyclic imide derivatives 12a and bi-12a were compared after the applied reactions (Figure 29 and 30). Full assignment of the proton resonances of compound 12 was accomplished by using ^{1}H/^{1}H COSY NMR (Figure 29, A). Allocation of each the peptide monomers of 12 was possible due to the cross-coupling peaks of their amide protons (compare a, b, c, d) to their protons at the chiral center (compare j, g, i, h), as well as the coupling of the latter to their diastereotopic protons (s, k, p, l), respectively. A hint towards the formation of cyclic *N*-substituted imides is then given in the COSY spectrum of 12a (Figure 29, B) by the missing amide proton signal a and the significant downfield shift of its neighbor at the chiral center j by ~0.3 ppm, as well as its sole coupling to the methyl protons s – also confirmed by the pronounced quartet of j. Noteworthy is also the downfield shift of the succinic acid protons o, n from ~2.4 to 2.5 ppm. Further, the presence of the free amine protons e after reaction, identified by their cross-coupling to the CH$_2$ group m of the Lys residue, clearly shows the absence of a macrocyclic species.
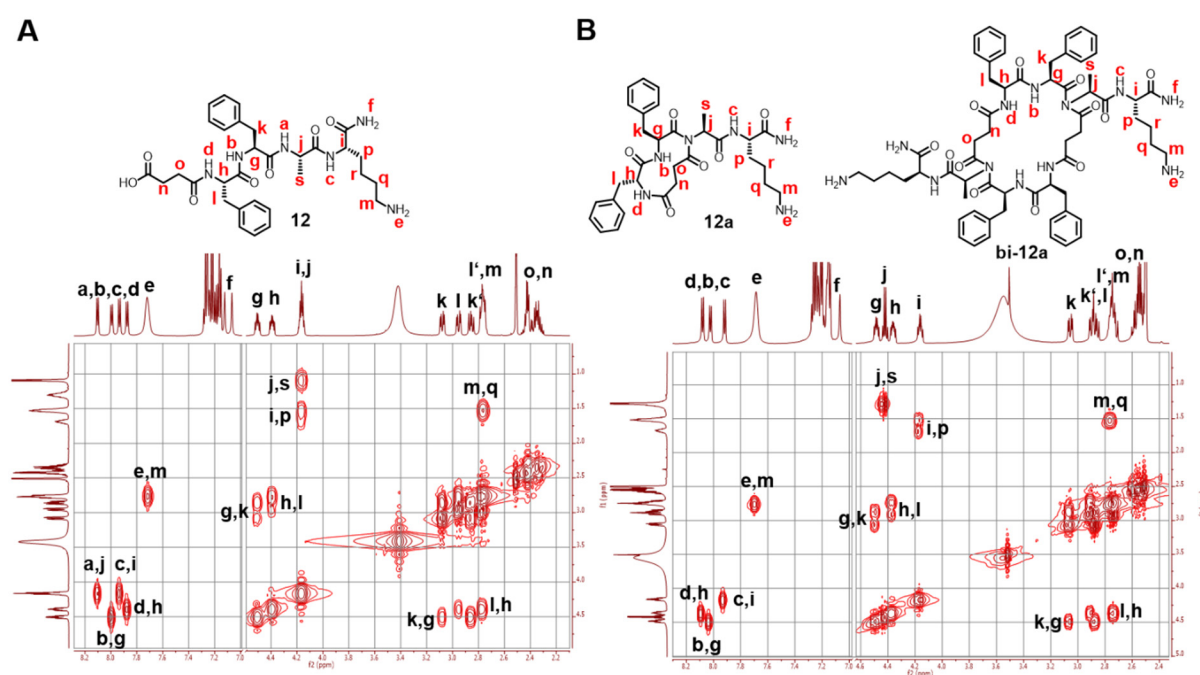
Figure 29. 2D ^{1}H/^{1}H COSY NMR spectra (DMSO−d_6) of the linear tetrapeptide 12 (A) and its mono- and bicyclic imide derivatives 12a and bi-12a (B). The COSY spectra of 12a and bi-12a confirms that reaction took preferentially place at the Ala amide bond, as shown by the protons cross-coupling assignment. This confirms the lack of the reaction selectivity as well as the Ala amide to be more prone to imide formation as previously reported[221].

58
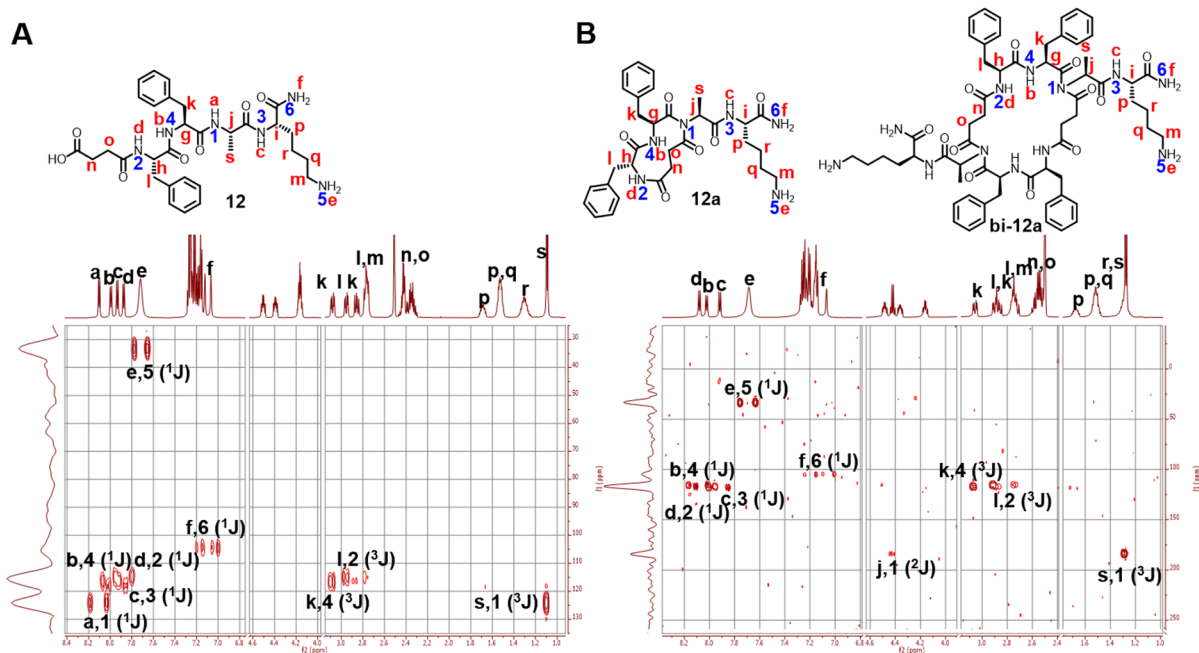
Figure 30. 2D ^{1}H/^{15}N HSQC spectra (DMSO–d_6) of linear precursor 12 (A) and its mono- and bicyclic derivatives 12 and bi-12a (B). HSQC spectra obtain residuals of $^2J_{NH}$ and $^3J_{NH}$ coupling, which made it possible to confirm the *N*-substituted imide bond (s, 1).

The *N*-substituted imide bond was further affirmed by ^{1}H/^{15}N HSQC NMR (Figure 30). The HSQC spectra showed that the amide and amine protons were correctly assigned in the COSY NMR of 12 and 12a. Further, the HSQC spectra also confirmed the structural composition of 12 and 12a as well as the imide moiety by residual signals, resulting from $^2J_{HN}$ (i, 2 and k, 4) and $^3J_{HN}$ (s, 1) coupling. Along with the residuals in the HSQC spectra of 12 and 12a, the significant downfield shift of proton 1, from ~120 ppm (12) to ~200 ppm (12a), additionally approved the five-membered *N*-substituted cyclic imide bond, as this region is a known imide bond region in ^{15}N NMR. In addition, MeOH hydrolysis was performed with the *N*-substituted imides 12a and bi-12a (Figure 31), which revealed the corresponding methyl esters 12-ME and bi-12-ME (or their constitutional isomers). Hydrolysis with pure MeOH was slow and has only led to small amount of the methyl esters. This is in agreement with previous reports for the hydrolysis of aspartimides in peptide sequences.[222] However as reported previously, when catalytic amounts of *i*Pr$_2$NEt (2 %, v/v) were added[222], the methyl hydrolysis was complete within 45 min, thereby confirming the cyclic imide bond.

Silylating agents in the presence of bases have earlier been used by Wong[215] for the synthesis of amides. For the mechanism he proposed that the silylating agent SiCl$_4$ *in situ* activates the carboxylic acid in the presence of alkylammonium and aromatic amine bases, such as triethylamine (NEt$_3$) and pyridine. Thus, he concluded that SiCl$_4$/pyridine can be used to activate the carboxylic acid, which would eliminate the need of using additional coupling reagents, e.g. for peptides or activated acyl chlorides required for polycondensations. On the mechanism he reported that the

initial step involves decomposition of the SiCl₄·pyridine complex, which was concluded from the desolvation of the SiCl₄·Pyr precipitate.
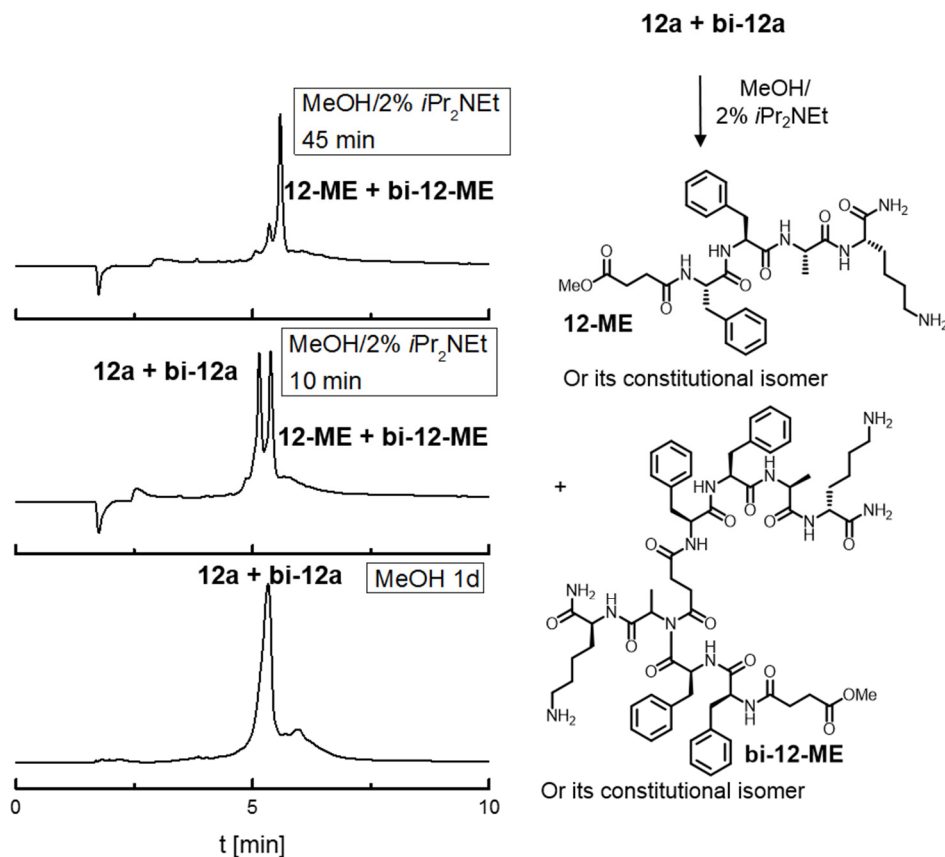
Figure 31. Progress of the MeOH hydrolysis of 12a and bi-12a to its methyl esters 12-ME and bi-12-ME (or its constitutional isomers) to confirm the cyclic imides, and representative RP-HPLC chromatograms, showing the reaction progress (5 % → 95 % MeCN in 10 min).

In fact, the same was observed when TMSBr/iPr₂NEt was used as reagent. When these reagents were mixed together in DCM, a white precipitate occurred in an exothermic reaction indicating TMSBr·iPr₂NEt complex formation. Upon addition of this reagent to the solid support, the precipitate was re-dissolved. Further, Wong[215] proposed that the reaction can take place *via* addition and elimination of the *in situ* formed aminosilanes and acyloxysilanes. Thus, the mechanism can go through a nucleophilic attack of the amine (or aminosilane) on the activated acyloxysilane. The leaving group would then be an oxytrimethylsilane and thus the driving force for this reactions, is the formation of stable Si-O bonds.[215] Further Cavelier *et al.*[200] proposed that interactions of the base and the silylating agent with the *in situ* released primary amine and the carboxylic group may contribute to bring the both chain-ends to closer proximity.

The results of this study do not yet give mechanistic insights into the reaction pathway and so far do not allow further comparison to previous studies. However, the results lead to a number of first important information on the use of silylating agents in macrocyclization of oligo(amido amines): (*i*) The use of silylating agents in the presence of an amine base did not lead to an one-

step tandem macrocyclization, but instead point towards the unselective formation of *N*-substituted cyclic imides. (*ii*) Interestingly, the use of the traditional method, where the silyl reagent TMSCl/phenol is used first to remove the Boc group, followed by activation and coupling with PyBOP/*i*Pr$_2$NEt did not lead to an amide macrocycle. Instead, again *N*-substituted cyclic imides were formed as the main product with the amide macrocycle being the by-product of the reaction with ~5 % yield. (*iii*) Further, such unselective imide formation only took place in the presence of the trialkylammonium base *i*Pr$_2$NEt. No imide cyclization was observed by applying the different TMSX reagents without the addition of the base. (*iv*) The counter-ion seems to have a pivotal role during macrocyclization. TMSCl in the presence of *i*Pr$_2$NEt was also tested. However, no macrocyclization occurred here.

3. Part 2: Thermodynamic and Kinetic Parameters of Precision Glycomacromolecules Binding to Con A

The previous part of the Results and Discussion presented the synthesis of linear and cyclic precision glycomacromolecules. These glycomacromolecules vary in important structural motifs, which have been previously shown in literature to affect the multivalent binding (such as valency[24, 33, 40, 44, 65-67], ligand density[33, 56, 60-63] and carbohydrate presentation in terms of multivalent architectures[33, 46, 67-69]). In this second part of the Results and Discussion, the multivalent binding of the synthesized linear and cyclic precision glycomacromolecules to the model protein Con A was investigated using ITC and kinITC, giving access to thermodynamic and kinetic parameters of ligand-receptor complex formation and will be discussed in the following.

At first (Chapter 3.4), the kinITC method as well as the experimental design of ITC experiments will be presented. The experimental design and quality of the data will be shortly highlighted in this context, as they are important to support and understand the following discussion of the thermodynamic and kinetic data.

The following chapters (Chapter 3.5 and Chapter 3.6) will then discuss the influence of different structural motifs of precision glycomacromolecules on the resulting binding thermodynamics and kinetics. The discussion is subdivided into two parts. In the first part the influence of ligand density (αMan spacing) and different αMan linkers on the binding thermodynamics and kinetics is described (Chapter 3.5). The second part then covers the influence of the overall oligomer architecture – linear *versus* cyclic – on the multivalent binding thermodynamics and kinetics (Chapter 3.6).

3.4. kinITC: Basic concepts

Recently, the so-called kinITC[163-165] was introduced, giving the opportunity to derive both, thermodynamic and kinetic information from an ITC experiment. In this chapter, shortly the use of kinITC for the performed binding studies will be explained. Furthermore, a brief outline of the experimental design of the ITC experiments will be given as well as important information on the data quality of the ITC derived thermodynamic and kinetic parameters. For further details on the method, a comprehensive overview of kinITC is described by Dumas *et al.*[163], Butcher *et al.*[164] and Yonetani *et al.*[165].

3.4.1. Experimental design of thermodynamic and kinetic ITC

Thermodynamic ITC

For thermodynamic and kinetic characterization of the influence regarding the different structural motifs of precision glycomacromolecules in their binding to Con A, ITC was used. ITC allows for the characterization of the binding thermodynamics as well as the binding kinetics, whereas the different predominant Con A conformations (dimer *versus* tetramer) were maintained by altering the buffer composition and the pH (a pH of 5.2 was used for the Con A dimer[34, 114, 131, 223], whereas a neutral pH 7.4 was used for the Con A tetramer[131, 223]; for further information see Experimental Part). Thermodynamic data were extracted from the obtained binding isotherms, where a non-linear fitting procedure (in this case *one sets of independent binding sites*) allowed to determine the binding enthalpy ΔH, the stoichiometry n and the equilibrium binding constant K (either K_a or K_d). These quantities allowed then for further calculation of the binding free energy ΔG and the binding entropy $-T\Delta S$, according to the Gibbs-Helmholtz equation (1) (see General Introduction, Chapter 1.2.1).

To eliminate any unspecific enthalpic contributions (heat of dilution, ligand dilution), control experiments were performed by titration of the glycomacromolecule ligand into the corresponding buffer solution. The obtained data of ligand dilution were subtracted from data points obtained for ligand-protein titration experiments. The ITC experiments were further designed according to the Wiseman's $c-$values. This critical parameter presents a unitless constant, which is of significant importance in the determination of the binding isotherm's shape (a sigmoidal shape is normally mandatory)[224]:

$$c = n_b \cdot K_a \cdot c_{P,0} = \frac{n_b \cdot c_{P,0}}{K_d} \qquad (2)$$

Here n_b represents the protein's binding sites per monomer and thus the stoichiometry, K_a and K_d the equilibrium association and dissociation constant, and $c_{P,0}$ the total concentration of the protein. Typically, it is recommended to perform measurements inside the traditional range between $1 < c < 1000$, to allow for a sigmoidal shape of the binding isotherm with representative resolved values for n, K_d, ΔH and $-T\Delta S$.[224] For ITC experiments especially with lower affinity ligands, which is the case for monosaccharides (and monovalent glycomacromolecules) with a dissociation equilibrium constant K_d typically in the mM range, the fulfilment of the prescribed $c-$values is problematic, since very high protein concentrations are required (typically above 120 μM) in order to compensate for the low binding constants. Brewer *et al.*[49, 225] reported on the use of a 483 μM Con A solution, when its interactions were studied with a 20 mM methyl α-D-mannopyranoside (MeαMan) solution.[49, 225] The use of such high protein concentrations in ITC experiments is however challenging, since precipitation of the protein occurs here during experiments, which is one of the well-known limitations[130, 135] of the ITC. To somewhat overcome this challenge, in a series of ITC experiments with low affinity ligands (typically lacking sigmoidal-

shaped binding curves) Turnbull[226] has found, that dissociation equilibrium binding constants K_d and other thermodynamic parameters, n, ΔH and $-T\Delta S$, can still be obtained accurately. Here, the $c-$ values may lie outside the traditional range, with a lower limit of $c < 1$. As long as the ligand and protein concentrations are however determined accurately and care is taken with respect to the binding isotherms in terms of good signal-to-noise ratios (good resolved binding curves), then still well resolved thermodynamic quantities can be obtained.[226] The same precipitation problem also applies to high affinity ligands (e.g. multivalent glycomacromolecules with binding constants in the lower nM range). But in this case it is the high affinity of the ligand, which most often leads to precipitation of the likely cross-linked protein. Conversely to lower affinity ligands, lower protein concentrations are required for higher affinity ligands according to the $c-$ value. Thus, for the lower and upper limits of the $c-$ values, representative for low and high affinity ligands, it is essentially the instrumental limitations[130, 135], which most likely lead to under- or overestimation of the measured and determined thermodynamic quantities.

Estimation of error sources in thermodynamic parameters

Following the above context, important concerns have been raised in literature[130, 135] regarding the quality of the determined thermodynamic values using ITC. It is very important to outline that ITC measurements and the thermodynamic parameters directly determined from them, have instrumental and analytical limitations.[130, 135] Such limitations include systematic error sources performed during experimental design[135] as well as the magnitude of errors determined in the thermodynamic parameters[130]. Such systematic error sources arise from: (*i*) Poorly defined ligand and protein concentrations, (*ii*) baseline drifts during the experiments and (*iii*) the experimental design regarding the $c-$ values and the concomitant fitting procedure (instrumental limitations), which is then more or less able to produce representative parameters depending on the $c-$ values and the ligand concentration.

As stated above, one of the main source of errors lies the estimations of the concentrations. An error in the ligand concentration directly translates into errors in K_d and ΔH values, while errors in estimating the protein concentration directly affect the binding stoichiometry n.[130, 135]

Another limitation comes from the ITC instrument itself, where good resolved parameters are normally only obtained following the recommended traditional range of the $c-$ values.[130, 135] Omitting this traditional range can lead to large errors in the fitted values, such as in the binding enthalpy ΔH and $-T\Delta S$ (which is then further calculated), the equilibrium constant K_d and the binding stoichiometry n .[130, 135] In the present study, the $c-$ values ranged between $\sim 0.7 < c < 16670$ (with the lower limit for some of the monovalent glycomacromolecules and with the upper limit representative for one of the decavalent glycomacromolecules binding to tetramer Con A; also see the according tables in the following chapters, which list the $c-$ values and the Experimental Part). Most of the ligands were inside this traditional range, however, especially the mono- and decavalent ligands exceeded the lower and upper limits of the recommended $c-$ values

range. As already mentioned above, Turnbull[226] has found that thermodynamic parameters can still be well resolved outside the traditional limits, as long as the binding isotherms obtain well-defined curvatures (e.g. Langmuir like), the signal-to-noise ratios of their heat flow signals are low and attention is paid to adjust the ligand and protein concentrations.[226] Due to the unresolved curve fitting as a result of the $c-$ values, the fitting error for the equilibrium constant K_d, ΔH and $-T\Delta S$ will be higher as compared to values that lie inside the traditional range.[130] Since the error in $-T\Delta S$ is computed as $-T\Delta S = \Delta G - \Delta H$, the error of ΔH dominates in $-T\Delta S$, also because of the small relation between K_d and ΔH.[130, 135] Although for values in ΔH and $-T\Delta S$, determined for $c-$ values outside the traditional range, the error is likely to range between ± 15 % and ± 20 %, the binding constant K_d obtains errors of about ± 10 %.[130, 135] Because of the logarithmic dependence of the ΔG on the binding constant, the error in ΔG is rather small.[130, 135] Thus, compared to the ΔH and $-T\Delta S$ values, errors in the ΔG values are sufficiently small. Therefore, regarding measurements performed outside the traditional range, it can be concluded that ΔG values are sufficiently resolved, while ΔH and $-T\Delta S$ have to be considered as estimates, taking into account larger deviations.

To further avoid an underestimation of errors, an error propagation was performed, which includes possible random error sources in the final parameter estimates (see Experimental Part). The error propagation simply computes these three possible error sources ((*i*), (*ii*) and (*iii*)) into the final thermodynamic values. In this study, either repeated measurements have been performed (over $2-5$ experiments) or one measurement to describe the thermodynamic parameters for a specific ligand and Con A conformation. a) If n series of measurements have been performed, then at first, a standard deviation of the values was estimated. As the experiments were, however, performed from the same ligand and protein stock solution, uncertainties arising from estimating the ligand and protein stock concentrations were additionally considered in the error analysis (see Experimental Part). Thus, after the estimation of the standard deviation for n series of measurements, the final reported error in each of the following thermodynamic data (n, K_d, ΔH, $-T\Delta S$ and ΔG) was determined only after adding the error in the ligand and protein concentration and the baseline drift as well as the error resulting from exceeding the traditional c – value limits (for compounds outside the traditional c – value range). b) The same procedure was also used for the error estimation in thermodynamic quantities, which have been determined from *one* measurement. However here, the mentioned uncertainties were not added to a standard deviation, but to the error resulting from the fit (see Experimental Part). Under each of the presented data sets in the following chapters, it is therefore highlighted, whether (*i*) *one* or n series of measurements have been performed, and (*ii*) the range of the c – values is reported.

<u>Kinetic ITC</u>

Determination of the binding kinetics was then performed from the binding isotherms obtained in the same ITC experiment. Since reversible physical binding interactions are associated with heat changes[165], in general the kinITC – as one example of the thermal analysis allowing for

determination of the binding kinetics– was recently introduced by Yonetani *et al*.[165], Butcher *et al*.[164] and Dumas *et al*.[163]. In an ITC experiment, the heat flow signal carries kinetic information, since the signal is a time profile initiated by the injection of a reactant.[227] Thus, the release (or absorption) of heat Q using thermal analysis takes place upon concentration changes of all reactants involved in the process and kinetics can be measured with the (in case of this study) released heat, in terms of the perturbation from equilibria (relaxation kinetics).[165, 227] In the here presented ITC experiments, the glycomacromolecule ligands present in the syringe were titrated in successive injections at defined volumes and regular time intervals (typically with injection numbers $i = 1, ...,30$, depending on the titrant/ligand volume) into the sample cell, filled with Con A.[163-165] During the experiment, the heat Q for each injection number i is measured as a function of time. The time-dependent thermal power $P(t)$ important for the determination of the rate constant is given by[165, 227]:

$$P(t) = \frac{dQ}{dt}. \tag{3}$$

In such ITC experiments, each successive injection of the glycomacromolecule ligand from the syringe into the sample cell presents a perturbation of the equilibrium, with the heat being released.[163-165] For determination of the individual association rate constants k_{on}, each heat profiles was examined independently to determine the binding kinetics from the relaxation time period[164] (the injection period of a reactant is not included in kinetic analysis[163-165]). For determination of the rate constants, in general, the following expression was considered that presents the reversible bimolecular binding interaction of the glycomacromolecule ligands (L) with the protein Con A (P):

$$L + P \underset{k_{off}}{\overset{k_{on}}{\rightleftarrows}} LP \tag{4}$$

In the presented study, only binding interactions with a negative molar enthalpy occurred. With every injection of L, the equilibrium (before *ith* addition of L) was thus perturbed within the titration experiment and the system under study underwent complex formation L·P, associated with heat release and concentration changes of L, P and L·P until a new equilibrium was established (after *ith* addition of L).[163-165] The system in the cell then either consisted of only P (only at the beginning of the experiment, before the first injection of L) or of the three species involved in the binding interactions, with free L, P and bound L·P.[163-165] For determination of the binding kinetics, the relaxation time period of each heat signal was followed, thereby excluding the titration time period. The following equation was considered for determination of the binding kinetics, which gives information on the amount of heat associated with converting n moles of a ligand into complex[164-165, 227]:

$$P(t) = \frac{dQ}{dt} = -\Delta H V_0 c'_{LP}(t), \qquad\qquad (5)$$

where c_{LP} is the molar concentration of the complex and c' is its time derivative, which depends on the injection number i and thus the volume and concentration of titrated L. $P(t)$ is the time-dependent thermal power, ΔH is the molar enthalpy (the heat produced during or at ith injection) and V_0 the starting volume of the solution in the sample cell, respectively.[163-165] Here, in general the thermal power $P(t)$ is proportional to the rate of the reversible binding reaction and the heat Q produced is proportional to the amount/concentration that interacts in a calorimeter cell.[163-165, 227]

Before extracting kinetic parameters following each (ith) injection and thus each heat flow signal in an ITC experiment, the raw ITC thermal power function $P(t)$ was corrected for the instrument response time k_{ITC} and baseline substration was performed (Figure 32). The importance to correct the raw data for the instrumental response time k_{ITC} has been described in detail by Dumas *et al.*[163], Butcher *et al.*[164] and Yonetani *et al.*[165].
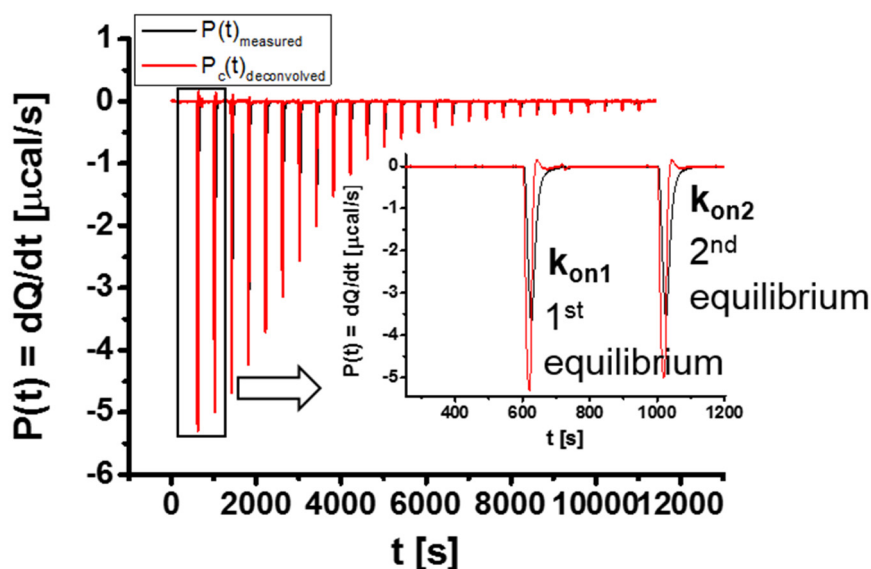
Figure 32. A representative titration experiment, where each injection of a ligand (L) corresponds to a heat flow signal (excluding the injection period), from which the relaxation kinetics may be determined. Black: Raw heat power traces before deconvolution. Red: Deconvolved raw heat power trace after accounting for the instrumental rate constant k_{ITC}.

In ITC experiments, a correction has to be done for the thermal inertia of the calorimeter instrument (the instrument response function)[163-165, 227], since the binding kinetics are investigated on the basis of thermally induced equilibrium distortions/transitions, thus following equilibria of relaxation kinetics.[165, 227] The relaxation kinetics have typically to be longer (ca. 10 s) than the instrument response time k_{ITC}.[163-165] Therefore, the obtained ITC experimental data, that is the thermal power signals $P(t) = \frac{dQ}{dt}$ following ith injection, was corrected for the instrumental dynamic response, where any remaining deconvolved heat flow signal was then a result of the relaxation

kinetics of the systems under study.[164] The deconvolution/correction of the raw power function was performed by numerical integration using Tian's equation (6)[163-164, 227]:

$$P(t)_c = \frac{1}{k_{ITC}} \frac{dP(t)}{dt} + P(t) \qquad (6)$$

Here, Pc corresponds to the *corrected* thermal power and k_{ITC} is the instrumental time constant.[163-164, 227] The instrumental time constant required to correct the raw power function was determined as is described in the Experimental Part and by Yonetani *et al.*[165], Butcher *et al.*[164] and Dumas *et al.*[163].

After deconvolution, the kinetic analysis was now accomplished using a least-squares minimization procedure. This least squares non-linear curve fitting procedure was written by Dr. Susanna Röblitz and Dr. Marcus Weber (Konrad-Zuse-Institut für Informationstechnik, Berlin) and is based on the fitting procedure as described by Butcher *et al.*[164] (see Supporting Appendix).[6] This allowed the numerical determination of the individual k_{on} values (for every heat period following every injection). Individual k_{on} values were then summarized into one weighted average k_{on} value, following the procedure of Butcher *et al.*[164]. The k_{on} value was weighted averaged over the uncertainties resulting from random error sources[164] (see Experimental Part). The backward rate constant k_{off} was then calculated using the relationship with the equilibrium constant and k_{on} ($K_d = k_{off}/k_{on}$).[164]

Errors in the on- and off-rate constants were estimated, following the error propagation as described by Butcher *et al.*[164] (for a brief explanation, see Experimental Part). Those errors correspond to true uncertainties in the given ITC measurements. Errors such as in the protein concentration and the baseline drift were also computed in the data, whereas the error in the ligand concentration is already included in the error of the K_d value, which is further computed in the error of k_{on} and k_{off} values.

---

[6]The least squares non-linear curve fitting procedure for kinITC has been written by Dr. Susanna Röblitz and Dr. Marcus Weber (Konrad-Zuse-Institut für Informationstechnik, Berlin; see also Supporting Appendix). Every measurement (including experimental design), determination, calculation and evaluation of the rate constants including their uncertainties has been performed by the author of this thesis. The kinITC least squares minimization procedure, required for the determination, calculation and evaluation of the measured ITC data (binding isotherms), has been provided by Dr. Susanna Röblitz and Dr. Marcus Weber. They have written the MATLAB scripts, which then allowed the calculation/determination of the rate constants. These written MATLAB scripts have been applied for the calculation/determination of the kinetic constants by the author of this thesis.

3.5. Influence of ligand density and linker composition on multivalent thermodynamics and (rebinding) kinetics

The use of glycopolymers[31-33, 55, 74-77] binding to carbohydrate-recognizing proteins as model systems to elucidate the multivalent effect, has led to important mechanistic insights that are prevalent in our nowadays understanding of the so-called multivalent binding modes[6, 18-19, 50, 106-110]. The SPCs for glycopolymer-receptor complex formation brought up a couple of generalized hypotheses on how certain structural features of the polymer influence the multivalent binding: (*i*) The ligand density of glycopolymers may influence the resulting binding energetics and thereby alter the overall binding affinity[12, 20-21, 42, 56-59]; (*ii*) secondary effects, which result from the influence of the polymer backbone upon binding may passively contribute to the overall binding process[42, 54-55], thereby enhancing or minimizing the overall binding affinity; and (*iii*) where there are multiple and collective interactions of several carbohydrate ligands, there is a prevalent statistical rebinding effect[18, 107, 110-113], which results from the close proximity of adjacent carbohydrate ligands. Here, the close proximity of carbohydrate ligands to the binding pockets of the protein may be directly coupled to the carbohydrate ligand density that may have a substantial influence on their rebinding.

So far, most of these mechanistic insights rely on studies that have been performed with disperse glycopolymers. One drawback, when studying the energetic and kinetic features of the multivalent effect with such highly advanced glycopolymers, is that their inherent structural complexity makes it difficult to correlate their binding properties with their structural features. Although much attention has been paid to study the (re-)binding kinetics of glycopolymers[76, 162, 228], so far a systematic study of this effects has not been reported.

The following chapter describes the application of the previously synthesized precision glycomacromolecules as model systems to study the influence of a series of their structural features, on the resulting protein receptor binding. Con A was used as a model lectin, both as a predominantly bi- and tetravalent receptor. In particular, the focus of this study was to elucidate: (*i*) The impact of the ligand density and linker composition, (*ii*) the influence of a polymer backbone composition, (*iii*) as well as the effect of the valency and molecular weight on the resulting binding energetics and kinetics. For this purpose, the binding of precision glycomacromolecules to Con A was studied as previously described by using ITC and the recently introduced kinITC[163-165].

3.5.1. Underlying ligand design

The main objective of this work was to provide basic concepts, which may help to understand the underlying mechanisms of multivalent binding[6, 18-19, 50, 106-110] of precision glycomacromolecules. In particular, this study aimed at the elucidation of the influence of the ligand density, valency and potential secondary effects, resulting from the oligomer backbone on the binding thermodynamics and kinetics. Therefore, a first series of linear precision glycomacromolecules with varying

structural features were prepared as highly defined model systems, as has been described in Chapter 3.1 (Figure 33). These 36 glycomacromolecules (Figure 33) differ in their ligand density, αMan linkage and valency. All of these glycomacromolecules (1 – 5, 1S – 5S and 1B – 5B) present αMan derivatives at well-defined positions along the oligomer backbone. Glycomacromolecules 1 − 1a/1S − 1aS/1B − 1aB, 2 − 2b/2S − 2aS/2B − 2bB, 3 − 3c/3S − 3aS/3B − 3aB and 4 − 4b/4S − 4aS/4B − 4aB obtain the same structural valency, ranging from n = 1 − 5, respectively. Differences in αMan density are obtained by varying the number and positions of EDS building block spacing units. These 36 glycomacromolecules can be further subdivided into three series of 12 glycomacromolecules. These three series differ in their αMan linkage pattern.
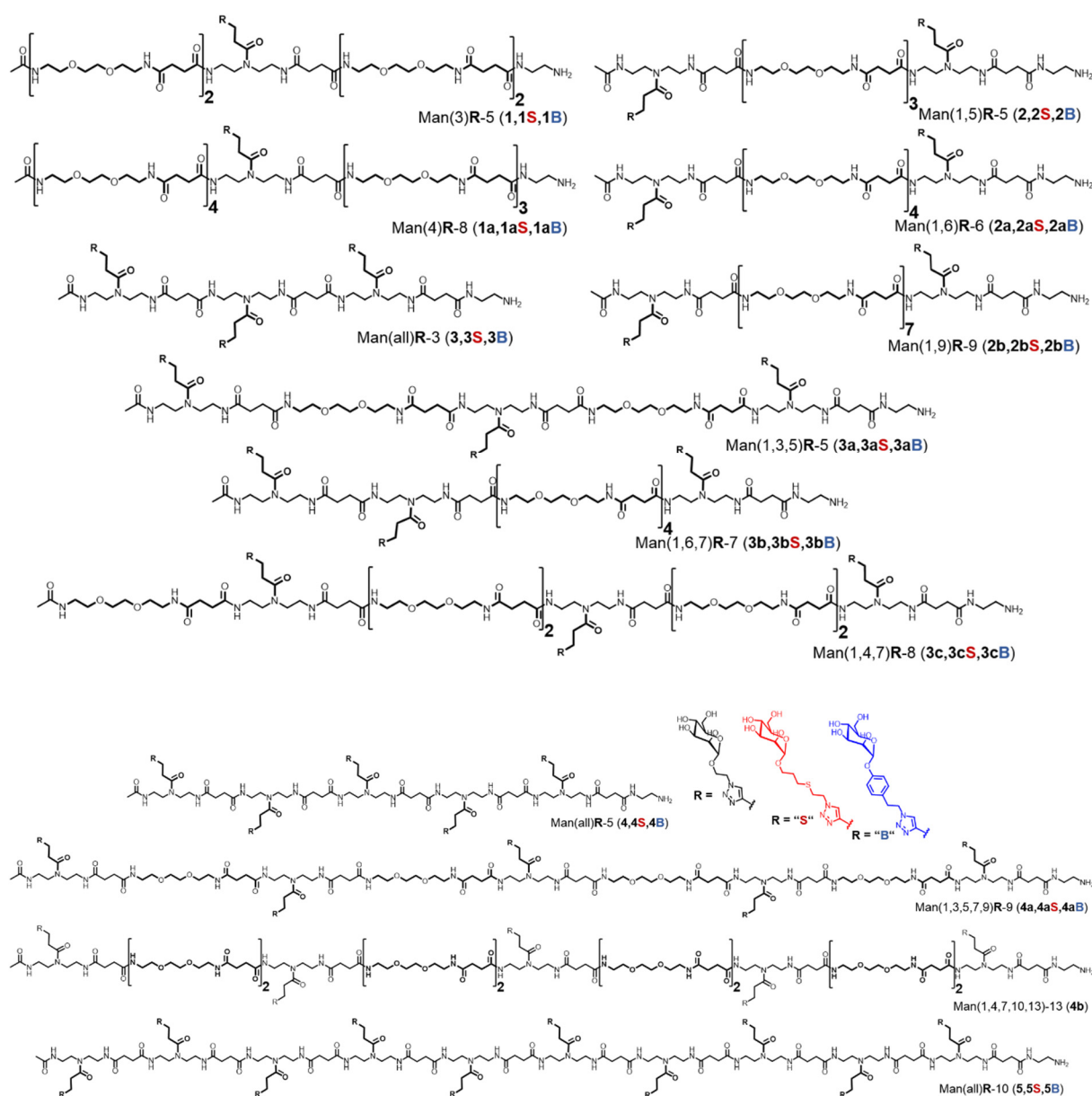
Figure 33. Structures of a first series of precision glycomacromolecules varying in the valency, ligand density as well as αMan linkage, applied for ITC experiments.

The three different linker types consist of (*i*) the short ethyl triazole linker, (*ii*) the longer thiol-ether triazole linker (highlighted as "S" in the nomenclature) and (*iii*) the benzyl triazole linker (highlighted as "B" in the nomenclature). The first one applies to the common αMan linker type that was used in previous binding studies by Ponader *et al.*[100, 103, 105]. In contrast, the longer thiol-ether triazole linker should account for possible differences in the length between the anomeric center and the oligomer backbone. The benzyl triazole linker was further used to increase the hydrophobicity at the anomeric center. With these so-called secondary binding motifs, additional enhancement in binding affinity can be modulated, where the chemical composition of the linker triggers additional binding forces in terms of e.g. hydrogen bonding or favorable solvation reorganization. In case of the benzyl triazole linker, previous studies by Lindhorst *et al.*[229-230] have shown that further enhancement in binding affinity can be indeed achieved with such secondary and hydrophobic binding motifs, directly attached to the anomeric carbon. They have demonstrated that this linker is able to account for additional secondary effects, resulting from its chemical composition[230]. It was presumed that in case of the benzyl triazole linker, it is the interactions between the benzyl ring and other hydrophobic moieties of the protein receptor (Fim H[4] in the studies from the Lindhorst *et al.*[230]) that triggers an accelerating binding affinity.[230] Similarly, it has been further reported that Con A contains hydrophobic binding cavities near its binding pockets[6, 231]. It was therefore expected that the length and the hydrophobicity of these αMan linkers would also affect the binding affinity of glycomacromolecules to Con A. The multiple presentation of these secondary binding motifs should further lead to an acceleration of the binding energetics and kinetics, whereas the systematic change of the above mentioned structural features in turn permits then the correlation with their thermodynamic and kinetic signatures.

Since there is inconsistency in literature regarding the terminology of "valency", in the following discussion this term will refer either to the "structural" or "functional valency" (as previously introduced by Brewer *et al.*[34, 49, 53, 106, 114]). Those two valency terms are differentiated here, because the former refers to the actual valency of the molecule, while the latter indicates the number of αMan ligands that "actively" participate in the binding process and that need to be determined experimentally (compare Brewer *et al.*[34, 49, 53, 106, 114].). Further, in this study "carbohydrate/αMan ligand density" is defined in terms of introduced "spacing units" between the presented αMan ligands on the oligomer scaffold (irrespective of its chemical composition and length). The use of the term ligand density is more appropriate in describing the binding behavior of the here presented glycomacromolecules. From previous measurements, it was seen that such glycomacromolecules are highly flexible and rather behave as random coils in buffered solutions[103], so that the changes in the spacing are rather expressed as the changes in the αMan ligand density of the solubilized and non-rigid constructs.

3.5.2. Influence of the ligand density on thermodynamics

Thermodynamic data were obtained from the non-linear fitting procedure (*one sets of independent binding sites*), which allowed to quantify the binding stoichiometry n, the dissociation equilibrium constant K_d, and the binding enthalpy ΔH, whereas the functional valency (FV), the binding free energy ΔG and the binding entropy $-T\Delta S$ were then computed from these parameters using $FV = 1/n$ and the Gibbs-Helmholtz equation (1) (see General Introduction, Chapter 1.2.1), respectively. The interactions of the individual glycomacromolecules, which varied in their ligand density, were characterized with two Con A conformations (predominantly dimer and tetramer Con A), which were maintained by different buffer compositions (see Experimental Part and table captions).[34, 114, 131, 223] The obtained thermodynamic quantities of the linear glycomacromolecules varying in their αMan density are summarized in Table 4 and 5. Table 4 shows the data of glycomacromolecules binding to the Con A dimer, whereas Table 5 reports data of the glycomacromolecules binding to the Con A tetramer. For determination of the binding thermodynamics to dimer Con A, 31 of the 36 glycomacromolecules were measured.

In general, the presented thermodynamic data in this study will discuss trends rather than focusing on specific values obtained for single glycomacromolecules. According to this, the following discussion is only restricted to values that follow a general trend, within the series of measured thermodynamic values. Quantities for a given measurement that lie outside such a general trend, will not be discussed in detail. These values lying outside the general trend may be due to one of the mentioned limitations[130, 135] in the ITC instrument, its fitting procedures[130] and the experimental design[130, 135] as outlined in Chapter 3.4.1 (even if the highest possible error was calculated and considered for them), and should be evaluated by additional methods, e.g. other binding assays, before drawing any detailed conclusions. In general, binding free energy ΔG values are considered robust and present rather precise values than estimates (due to the reasons mentioned in Chapter 3.4.1 and by Chodera *et al.*[130] – their dependence on K_d is a logarithmic one). In contrast, enthalpic ΔH and entropic $-T\Delta S$ values should in general be rather considered as estimates, which follow a general trend.

Table 4. ITC derived thermodynamic binding energetics of glycomacromolecules with different linkers binding to dimer Con A (measured at 298.15 K).

Ligand	$\overline{FV}$[a]	$\overline{\Delta G}$[b]	$\overline{K_d}$[c]	$\overline{\Delta H}$[b]	$\overline{-T\Delta S}$[b]	$\overline{c}$[d]
Monovalent (ethyl triazole linker)						
Man(3)-5 (1)	0.7 ± 0.3	-20.3 ± 0.7	278 ± 82	-29 ± 6	$+9 \pm 6$	~1*
Man(4)-8 (1a)	0.9 ± 0.2	-19.7 ± 0.6	361 ± 91	-29 ± 6	$+9 \pm 6$	~1*
Monovalent (thiol-ether triazole linker)						
Man(3)S-5[1] (1S)	0.8 ± 0.1	-23.6 ± 0.2	75 ± 5	-20 ± 1	-4 ± 1	~3
Man(4)S-8[1] (1aS)	1.1 ± 0.1	-23.6 ± 0.1	72 ± 4	-27 ± 2	$+4 \pm 2$	~3
Divalent (ethyl triazole linker)						
Man(1,5)-5 (2)	1.4 ± 0.5	-20.4 ± 0.5	266 ± 58	-51 ± 15	$+31 \pm 15$	~1*
Man(1,6)-6 (2a)	1.7 ± 0.3	-22.0 ± 0.2	141 ± 2	-44 ± 3	$+22 \pm 3$	~2
Man(1,9)-9 (2b)	2.3 ± 0.7	-21.9 ± 0.2	145 ± 10	-57 ± 14	$+35 \pm 14$	~2
Divalent (thiol-ether triazole linker)						
Man(1,5)S-5[1] (2S)	1.8 ± 0.2	-25.8 ± 0.1	30 ± 2	-46 ± 3	$+20 \pm 3$	~7
Man(1,6)S-6[1] (2aS)	1.8 ± 0.2	-26.0 ± 0.1	28 ± 1	-45 ± 3	$+19 \pm 3$	~7
Man(1,9)S-9[1] (2bS)	1.8 ± 0.2	-25.6 ± 0.1	33 ± 1	-45 ± 3	$+20 \pm 3$	~6
Divalent (benzyl triazole linker)						
Man(1,6)B-6[1] (2aB)	2.6 ± 0.3	-29.1 ± 0.1	8.0 ± 0.4	-62 ± 4	$+33 \pm 4$	~27
Man(1,9)B-9[1] (2bB)	1.4 ± 0.2	-26.8 ± 0.1	21 ± 1	-35 ± 2	$+8 \pm 2$	~11
Trivalent (ethyl triazole linker)						
Man(all)-3 (3)	2.6 ± 0.4	-23.3 ± 0.2	85 ± 7	-64 ± 7	$+41 \pm 7$	~3
Man(1,3,5)-5 (3a)	2.1 ± 0.3	-23.3 ± 0.2	82 ± 5	-54 ± 6	$+31 \pm 6$	~2

Man(1,6,7)-7 (**3b**)	3.4 ± 0.4	-23.2 ± 0.2	87 ± 6	-95 ± 6	$+72 \pm 6$	~2
Man(1,4,7)-8 (**3c**)	2.3 ± 0.4	-22.7 ± 0.5	107 ± 20	-63 ± 9	$+40 \pm 9$	~2
Trivalent (thiol-ether triazole linker)						
Man(all)S-3[1] (**3S**)	2.3 ± 0.3	-28.2 ± 0.1	11.5 ± 0.6	-63 ± 4	$+35 \pm 4$	~18
Man(1,3,5)S-5[1] (**3aS**)	1.6 ± 0.2	-26.8 ± 0.1	20 ± 1	-38 ± 3	$+11 \pm 3$	~10
Man(1,6,7)S-7[1] (**3bS**)	2.4 ± 0.3	-27.4 ± 0.1	16.0 ± 0.7	-65 ± 4	$+37 \pm 4$	~11
Man(1,4,7)S-8[1] (**3cS**)	2.6 ± 0.4	-27.2 ± 0.4	17 ± 3	-63 ± 7	$+35 \pm 7$	~12
Trivalent (benzyl triazole linker)						
Man(all)B-3 (**3B**)	2.2 ± 0.3	-29.9 ± 0.3	5.7 ± 0.6	-59 ± 4	$+29 \pm 4$	~42
Man(1,3,5)B-5 (**3aB**)	2.6 ± 0.4	-30.6 ± 0.2	4.3 ± 0.4	-68 ± 7	$+37 \pm 7$	~55
Man(1,6,7)B-7 (**3bB**)	2.7 ± 0.3	-29.4 ± 0.2	7.2 ± 0.5	-73 ± 5	$+43 \pm 5$	~31
Man(1,4,7)B-8 (**3cB**)	2.3 ± 0.3	-29.4 ± 0.2	7.0 ± 0.5	-60 ± 4	$+29 \pm 4$	~31
Pentavalent (ethyl triazole linker)						
Man(all)-5 (**4**)	3.2 ± 0.5	-26.5 ± 0.4	23 ± 3	-64 ± 8	$+37 \pm 8$	~10
Man(1,3,5,7,9)-9 (**4a**)	3.2 ± 0.4	-25.9 ± 0.4	29 ± 4	-77 ± 6	$+51 \pm 6$	~10
Man(1,4,7,10,13)-13 (**4b**)	5.0 ± 0.8	-26.0 ± 0.2	28 ± 2	-128 ± 15	$+102 \pm 15$	~9
Pentavalent (thiol-ether triazole linker)						
Man(all)S-5[1] (**4S**)	2.6 ± 0.3	-29.2 ± 0.1	7.8 ± 0.4	-62 ± 4	$+32 \pm 4$	~8
Pentavalent (benzyl triazole linker)						
Man(all)B-5 (**4B**)	6.7 ± 0.8	-37.5 ± 0.2	0.27 ± 0.02	-112 ± 7	$+74 \pm 7$	~903
Man(1,3,5,7,9)B-9 (**4aB**)	3.0 ± 0.6	-35.7 ± 0.4	0.6 ± 0.1	-46 ± 4	$+11 \pm 4$	~414
Decavalent (ethyl triazole linker)						
Man(all)-10 (**5**)	5.7 ± 0.7	-29.1 ± 0.5	8 ± 2	-106 ± 10	$+77 \pm 10$	~26

	Decavalent (benzyl triazole linker)					
Man(all)B-10 (**5B**)	7 ± 2	-40.9 ± 0.6	0.07 ± 0.02	-59 ± 14	$+18 \pm 14$	$\sim 1511^*$

[a] $\overline{FV}$ is defined as $\overline{FV} = \frac{1}{n}$ and was experimentally determined from the binding stoichiometry n. [b] Gibbs free binding energy $\overline{\Delta G}$, enthalpy $\overline{\Delta H}$ and entropy $-\overline{T\Delta S}$ are reported in kJ mol⁻¹. [c] Dissociation equilibrium constant $\overline{K_d}$ is reported in μM. Errors in $\overline{FV}$, $\overline{\Delta G}$, $\overline{\Delta H}$, $-\overline{T\Delta S}$ and $\overline{K_d}$ refer to the error propagation as described in the Experimental Part. [d] $\overline{c}$ − values refer to the quality of the fit and the corresponding error propagation in the Experimental Part. "*" marks ITC measurements, whose $\overline{c}$ − values are outside the traditional range (as described in Chapter 3.4.1). All thermodynamic quantities refer to best mean values, expect for measurements, which were performed one time (those are highlighted with "¹"). Measurements were performed in acetate buffer pH 5.20 ± 0.02 at 298.15 K, with Con A obtaining its dimer conformation[34, 114, 131, 223].

Table 5. ITC derived thermodynamic binding energetics of glycomacromolecules with different linkers binding to tetramer Con A (measured at 298.15 K).

Ligand	$\overline{FV}$[a]	$\overline{\Delta G}$[b]	$\overline{K_d}$[c]	$\overline{\Delta H}$[b]	$-\overline{T\Delta S}$[b]	$\overline{c}$[d]
MeαMan[e]	1.0	-22	132	-29	$+6$	−
Monovalent (ethyl triazole linker)						
Man(3)-5 (1)	0.8 ± 0.1	-20.9 ± 0.2	221 ± 16	-27 ± 2	$+6 \pm 2$	~ 2
Man(4)-8 (1a)	0.7 ± 0.1	-21.6 ± 0.2	163 ± 14	-19 ± 1	-3 ± 1	~ 2
Monovalent (thiol-ether triazole linker)						
Man(3)S-5¹ (1S)	0.6 ± 0.1	-23.0 ± 0.3	94 ± 13	-13 ± 2	-10 ± 2	~ 4
Man(4)S-8¹ (1aS)	0.8 ± 0.1	-23.0 ± 0.3	94 ± 11	-13 ± 2	-10 ± 2	~ 3
Monovalent (benzyl triazole linker)						
Man(3)B-5¹ (1B)	0.9 ± 0.1	-25.7 ± 0.2	32 ± 3	-23 ± 2	-3 ± 2	~ 11
Man(4)B-8¹ (1aB)	0.9 ± 0.1	-25.5 ± 0.2	34 ± 1	-26 ± 2	$+1 \pm 2$	~ 9
Divalent (ethyl triazole linker)						
Man(1,5)-5¹ (2)	1.2 ± 0.2	-25.0 ± 0.3	43 ± 4	-29 ± 2	$+4 \pm 2$	~ 7
Man(1,6)-6¹ (2a)	1.1 ± 0.1	-24.3 ± 0.2	56 ± 5	-29 ± 2	$+4 \pm 2$	~ 6

Man(1,9)-9[1] (2b)	1.4 ± 0.2	-24.9 ± 0.2	43 ± 4	-35 ± 3	$+10 \pm 3$	~7
Divalent (thiol-ether triazole linker)						
Man(1,5)S-5 (2S)	1.4 ± 0.2	-26.4 ± 0.2	22 ± 2	-41 ± 4	$+15 \pm 4$	~17
Man(1,6)S-6 (2aS)	1.4 ± 0.2	-26.0 ± 0.2	28 ± 2	-44 ± 3	$+18 \pm 3$	~13
Man(1,9)S-9 (2bS)	1.4 ± 0.1	-25.4 ± 0.2	36 ± 3	-39 ± 3	$+13 \pm 3$	~9
Divalent (benzyl triazole linker)						
Man(1,5)B-5[1] (2B)	1.9 ± 0.2	-29.4 ± 0.2	7.1 ± 0.5	-54 ± 7	$+25 \pm 7$	~43
Man(1,6)B-6[1] (2aB)	1.9 ± 0.2	-29.8 ± 0.2	6.1 ± 0.5	-47 ± 6	$+17 \pm 6$	~50
Man(1,9)B-9[1] (2bB)	2.2 ± 0.3	-29.5 ± 0.2	6.9 ± 0.5	-53 ± 6	$+23 \pm 6$	~38
Trivalent (ethyl triazole linker)						
Man(all)-3[1] (3)	1.6 ± 0.2	-28.6 ± 0.4	10 ± 2	-31 ± 3	$+2 \pm 3$	~32
Man(1,3,5)-5 (3a)	2.6 ± 0.3	-32.0 ± 0.3	2.5 ± 0.3	-57 ± 5	$+25 \pm 5$	~151
Man(1,6,7)-7[1] (3b)	1.7 ± 0.2	-29.0 ± 0.3	8 ± 1	-30 ± 2	$+1 \pm 2$	~37
Man(1,4,7)-8 (3c)	2.3 ± 0.3	-30.6 ± 0.3	4.5 ± 0.5	-50 ± 3	$+19 \pm 3$	~88
Trivalent (thiol-ether triazole linker)						
Man(all)S-3 (3S)	2.3 ± 0.3	-33.4 ± 0.2	1.4 ± 0.1	-53 ± 4	$+20 \pm 4$	~238
Man(1,3,5)S-5[1] (3aS)	1.5 ± 0.1	-31.3 ± 0.6	3.3 ± 0.9	-34 ± 3	$+3 \pm 3$	~116
Man(1,6,7)S-7 (3bS)	2.3 ± 0.3	-33.0 ± 0.3	1.6 ± 0.2	-55 ± 4	$+22 \pm 4$	~220
Man(1,4,7)S-8 (3cS)	1.5 ± 0.2	-31.9 ± 0.2	2.6 ± 0.2	-37 ± 6	$+5 \pm 6$	~142
Trivalent (benzyl triazole linker)						
Man(all)B-3[1] (3B)	2.0 ± 0.5	-39.7 ± 0.7	0.11 ± 0.03	-45 ± 10	$+5 \pm 10$	~2425*
Man(1,3,5)B-5[1] (3aB)	2.5 ± 0.6	-38.9 ± 0.6	0.15 ± 0.04	-70 ± 15	$+31 \pm 15$	~2534*
Man(1,6,7)B-7[1] (3bB)	1.9 ± 0.2	-34.7 ± 0.3	0.8 ± 0.1	-40 ± 3	$+5 \pm 3$	~312
Man(1,4,7)B-8[1] (3cB)	2.0 ± 0.2	-37.3 ± 0.6	0.3 ± 0.1	-53 ± 6	$+16 \pm 6$	~981

	$\overline{FV}$	$\overline{\Delta G}$	$\overline{K_d}$	$\overline{\Delta H}$	$-\overline{T\Delta S}$	$\bar{c}$
Pentavalent (ethyl triazole linker)						
Man(all)-5[1] (4)	5 ± 1	-37.8 ± 0.9	0.2 ± 0.1	-75 ± 18	$+37 \pm 18$	~1112*
Man(1,3,5,7,9)-9[1] (4a)	5 ± 1	-39.6 ± 0.7	0.12 ± 0.04	-124 ± 26	$+84 \pm 26$	~2274*
Man(1,4,7,10,13)-13[1] (4b)	5 ± 1	-38.0 ± 0.7	0.2 ± 0.1	-80 ± 19	$+42 \pm 19$	~1199*
Pentavalent (thiol-ether triazole linker)						
Man(all)S-5 (4S)	2.5 ± 0.3	-32.1 ± 0.3	2.4 ± 0.3	-87 ± 6	$+54 \pm 6$	~145
Man(1,3,5,7,9)S-9 (4aS)	2.6 ± 0.3	-35.5 ± 0.8	0.6 ± 0.2	-73 ± 6	$+37 \pm 6$	~532
Pentavalent (benzyl triazole linker)						
Man(all)B-5 (4B)	5 ± 2	-42 ± 1	0.05 ± 0.02	-102 ± 22	$+60 \pm 22$	~6821*
Man(1,3,5,7,9)B-9 (4aB)	2.1 ± 0.5	-41.6 ± 0.5	0.05 ± 0.01	-50 ± 11	$+8 \pm 11$	~5682*
Decavalent (ethyl triazole linker)						
Man(all)-10 (5)	9 ± 3	-41.9 ± 0.6	0.05 ± 0.01	-194 ± 41	$+152 \pm 41$	~7132*
Decavalent (thiol-ether triazole linker)						
Man(all)S-10 (5S)	5 ± 1	-39 ± 1	0.2 ± 0.1	-124 ± 26	$+85 \pm 26$	~2450*
Decavalent (benzyl triazole linker)						
Man(all)B-10[1] (5B)	6 ± 2	-44 ± 1	0.02 ± 0.01	-155 ± 36	$+110 \pm 36$	~16670*

[a] $\overline{FV}$ is defined as $\overline{FV} = \frac{1}{\bar{n}}$ and was experimentally determined from the binding stoichiometry n. [b] Gibbs free binding energy $\overline{\Delta G}$, enthalpy $\overline{\Delta H}$ and entropy $-\overline{T\Delta S}$ are reported in kJ mol^{-1}. [c] Dissociation equilibrium constant $\overline{K_d}$ is reported in µM. Errors in $\overline{FV}$, $\overline{\Delta G}$, $\overline{\Delta H}$, $-\overline{T\Delta S}$ and $\overline{K_d}$ refer to the error propagation as described in the Experimental Part. [d] $\bar{c}-$ values refer to the quality of the fit and the corresponding error propagation in the Experimental Part. "*" marks ITC measurements, whose $\bar{c}-$ values are outside the traditional range (as described in Chapter 3.4.1). All thermodynamic quantities refer to best mean values, expect for measurements, which were performed one time (those are highlighted with "1"). Measurements were performed in lectin binding buffer (LBB) pH 7.40 ± 0.01 at 298.15 K, with Con A obtaining its dimer-tetramer equilibrium conformation[131, 223]. [e] Data for MeαMan were taken from the review of Brewer *et al.*[49], have originally been described by Toone *et al.*[131] and correspond to ITC measurements with tetramer Con A.

First, the functional valency (FV) of the glycomacromolecules in their binding to both the Con A dimer and tetramer will be discussed, followed then by the discussion of the αMan density and linker influence on the binding enthalpy and entropy along with the FV. These structural features are then also shortly discussed according to the binding with dimer and tetramer Con A. Thereafter, the discussion of the free binding energy is presented, followed then by the influence of these varying structural features on different entropic terms, such as the configuration and solvation entropy, $-T\Delta S_{conf}$ and $-T\Delta S_{solv}$.

3.5.3. Monovalent glycomacromolecules for assessing the role of the oligomer backbone

At first, it was intended to assess the potential role of the oligomer backbone during the binding process. So far, it has been reported that backbones of glycopolymers may contribute to e.g. an unfavorable shielding of the protein's binding site, thereby making it less accessible for the ligand to approach or *vice versa*[17]. Further, it has also been concluded that secondary effects[42], such as the "passive interactions" of a polymer backbone with the protein, may enhance or reduce the binding affinity. Thereby such secondary effects between the polymer backbone and the protein may lead to an overall gain in free energy due to a favorable entropy[93]. To investigate whether the oligomer backbone of the glycomacromolecules potentially exhibits such "secondary" or possible "shielding" effects, a set of two monovalent glycomacromolecules with an overall different length of the oligomer backbone (1 (Man(3)-5) and 1b (Man(4)-8)) was measured in binding to dimer and tetramer Con A, and their binding energetics were compared to those of the monosaccharide MeαMan[49, 131]. As the αMan linker type of compounds 1 and 1b is more similar to MeαMan, only those two compounds will be discussed here, as they are expected to not additionally contribute to the binding through their linker types (as it might be the case for 1S, 1aS and 1B, 1aB, which has been shown by Lindhorst *et al.*[230] for monovalent αMan ligands, employing the thiol-ether and benzyl linkers[230]). The comparison of these two compounds to MeαMan allows to comment only on potential secondary effects, resulting from the oligomer backbone.

Inspection of their binding to tetramer Con A shows that their free energy values equal those of MeαMan, with ΔG (1) ≈ − 21 kJ mol^{-1} and ΔG (1a) ≈ − 22 kJ mol^{-1} (compared to ΔG(MeαMan) ≈ − 22 kJ mol^{-1}). Further, enthalpy and entropy values of 1 (Man(3)-5) binding to tetramer Con A are consistent with the reported values for MeαMan[49, 131], with ΔH ≈ − 27 kJ mol^{-1} and $-T\Delta S$ ≈ + 6 kJ mol^{-1} (compared to ΔH (MeαMan) ≈ − 29 kJ mol^{-1} and $-T\Delta S$ (MeαMan) ≈ + 6 kJ mol^{-1}). However, for the longer glycomacromolecule 1a (Man(4)-8) binding to tetramer Con A, the enthalpic contribution is lowered by about ~8 kJ mol^{-1}, whereas its entropic contributions became favorable with $-T\Delta S$ ≈ − 3 kJ mol^{-1}. Although the energetic contributions of 1a result in the same overall ΔG values, as compared to the other monovalent compounds, the enthalpic and entropic values indicate a potentially different binding behavior. In this case, a secondary effect might result from a steric shielding of the room captivating Con A tetramer due to its additional binding pockets.

3.5.4.<u>Defining the binding process: Functional valency (FV)</u>

Following the first results for the monovalent glycomacromolecules, di- to decavalent glycomacromolecules were measured in ITC. Within a series of glycomacromolecules with the same structural valency, different ligand densities were obtained by variation of the number of EDS spacer units (see Chapter 3.1 and Figure 33) and αMan linkage, applying different αMan building blocks. Thus, these glycomacromolecules are inspired by previous studies on glycopolymers, which have led to the hypotheses that the variation in the ligand density and linker composition of a glycopolymer will alter its resulting binding affinity. Depending on the accessibility of ligands during binding and the linker's chemical composition, a different ligand density and carbohydrate linkage may maximize or minimize the complex formation. Through a systematic variation of the ligand density and αMan linkers for different structural valencies, potential effects on the binding thermodynamics can give new insights into the underlying multivalent binding mechanisms.
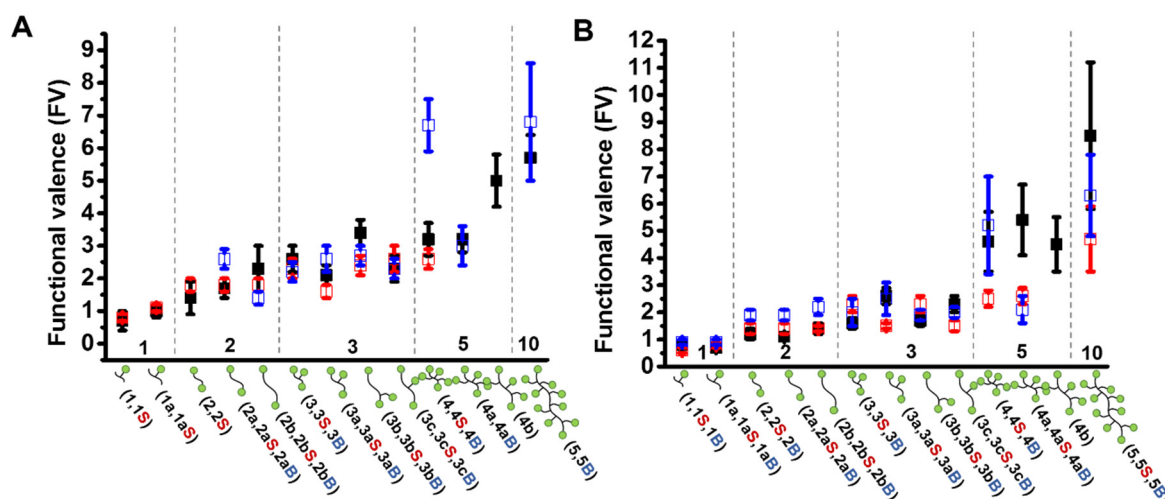
Figure 34. Functional valency (FV) that defines an intermolecular binding process. Irrespective of the Con A composition, glycomacromolecules prefer intermolecular binding of Con A molecules. A: FV ($FV = 1/n$) for the binding of glycomacromolecules to the Con A dimer. B: FV for the interactions of glycomacromolecules with tetramer Con A.

For these reasons, in this study it was first intended to clarify, whether an altering density and αMan linkage would result in different thermodynamic terms. To rationalize results obtained for glycomacromolecules that differ in these structural features, at first the binding process needs to be defined. According to Brewer *et al.*[34, 49, 53, 106, 114] the binding stoichiometry – the n value – is an important parameter that defines the overall binding process. For this reason, it is important to not correct the obtained data for the structural valency and to not fit obtained results to a binding model, before the experimental confirmation of the binding stoichiometry n. According to Brewer *et al.*, the functional valency ($FV = 1/n$) is defined as the mean of the number of carbohydrate ligands binding separate protein molecules. The FV presents the reverse binding stoichiometry and therefore determines the ligand valency during the binding process, which most of the time differs

from the structural valency (not all of the αMan ligands have to actively participate in the binding process). As evident from the FV (Table 4 and 5), multivalent binding proceeds through an *inter*molecular process, where glycomacromolecules prefer binding of individual Con A molecules, irrespective of the Con A conformation[34, 49, 53, 106, 114]. The glycomacromolecules presenting multiple αMan ligands are thereby able to bind with two or more separate Con A molecules, which is indicated by FV > 1 (Figure 34). The results obtained here are consistent with those obtained by Brewer *et al.*[34, 53, 106, 114] who have shown that although the model systems have a certain structural valency, this does not necessarily means that all of the carbohydrate ligands actively participate in the binding process. From Figure 34, A and B, it can further be seen that the FV mainly depends on the number of the αMan ligands attached on the oligomer backbone. Both structural motifs, such as the αMan ligand density and the linkers do not dramatically alter this term. Therefore, the FV increases along with the structural valency, with the decavalent glycomacromolecules (5, 5S, 5B) showing the highest and the divalent compounds (2 − 2b, 2S − 2bS, 2B − 2bB) exhibiting the lowest values in the FV. This trend is observed for both Con A conformations.

For dimer Con A, the FV shows that the glycomacromolecules are able to bind on average one or two Con A dimers for mono- to trivalent systems (1a − 1b, 2a – 2b, 3a – 3c), whereas the higher valent (penta- and decavalent, 4 – 4b, 5) analogues are able to bind on average up to three, five and six Con A molecules, respectively (Figure 34). Values of the FV of glycomacromolecules studied with tetramer Con A are more or less the same for di- to trivalent compounds compared with dimer Con A. This intermolecular binding process and the ability of precision glycomacromolecules to bind several Con A molecules is further in agreement with previous results, where in-solution dual focus fluorescent spectroscopy (dfFCS) and turbidimetry measurements have demonstrated the favorable binding of one or two Con A molecules to di- and trivalent ligands, (2) (Man(1,5)-5) and 3a (Man(1,3,5)-5), respectively.[103] Thus, along with these results, it can be concluded that in a titration experiment such as in ITC, precision glycomacromolecules favor an intermolecular binding to Con A.

To this general trend, there are, however, a few exceptions that show unexpectedly higher FV values (Figure 34). However, as was outlined in Chapter 3.4.1, the error, especially in the protein concentration, might result in unexpected binding stoichiometries n, whereas errors in the ligand concentration will directly impact the binding enthalpy ΔH and the dissociation equilibrium constant K_d, and following the computation, also the binding entropy $-T\Delta S$ (see Chapter 3.4.1).[130] Therefore, the role of these unexpected values, exceeding the general trend, should not be overestimated. Nevertheless, the obtained data shows a clear trend for an increasing FV with an increasing structural valency of both, ligand and receptor.

Along with the number of ligand-receptor interactions, the FV describes the evolution of the energetic terms, the binding enthalpy and entropy. From Brewer *et al.*[35, 49, 53, 106, 114] it is known that the FV is proportional to the binding enthalpy. This means that more ligand-receptor contacts will lead to a more negative binding enthalpy, whereas fewer ligand-receptor interactions result in

the diminution of the binding enthalpy.[35, 49, 53, 106, 114] Ultimately, the FV directly affects the evolution of the binding enthalpy and entropy, as will be discussed in the next subchapter.

3.5.5. The effect of ligand density on the binding enthalpy and entropy

Before discussing the change in the enthalpic and entropic terms along with altering structural features of the glycomacromolecules, basic considerations regarding the FV as well as the evolution of the enthalpy and entropy need to be defined. Those are necessary to understand the binding process and the following discussion. The following discussion will only refer to one of the three series of glycomacromolecules, specifically choosing the short ethylene spacer as an example. But the general trend concluded from these data also refers to the other two series of glycomacromolecules, either carrying the thiol-ether triazole or benzyl triazole linker.

If the influence of a varying αMan density is compared for glycomacromolecules with the same linker (e.g. compare the binding of glycomacromolecules with the small ethyl triazole linker to tetramer Con A), the following general trend can be observed. As defined above, the FV is proportional to the number of ligand-receptor interactions and the binding enthalpy. Following this general statement, it can be concluded that similar values in FV should result in similar binding enthalpy terms. For compounds 2, 2a and 3, 3b as well as 3a, 3c this is indeed the case. Conversely to the binding enthalpy, the entropic term is not proportional to the FV, suggesting that it does not de- or increase along with the FV. Along with a de- or increasing binding enthalpy, the entropy may either become more or less positive (less or more favorable). Nevertheless, the entropic values are linked to the enthalpic term, so that its contribution steadily de- or increases in the order of the enthalpy gain or loss. The described relation between the enthalpy and entropy is true for either of the three series of glycomacromolecules (glycomacromolecules which obtain the same αMan linker). From this relationship between the binding enthalpy and entropy, two situations regarding these terms can therefore be differentiated: a) From the thermodynamic data, it can easily be seen that an enthalpic gain is most often accompanied by a more positive entropic value, resulting in a higher entropy cost (e.g. compare 2b to 2, 2a; 3a, 3c to 3, 3b and 4a to 4). b) Conversely, the reverse situation applies in the same order when there is enthalpic loss (less negative values, due to lower ligand-receptor contacts), which is then accompanied by a relative entropic gain (less positive values).

Considering these two situations, the following conclusion regarding these two energetic terms and the influence of the ligand density can be drawn: (i) For glycomacromolecules that contain the same valency but a different αMan ligand density, similar values in ΔH go along with similar values in $-T\Delta S$ for compounds with similar FV (e.g. compare 2, 2a and 3, 3b as well as 3a, 3c). (ii) Conversely, if there are glycomacromolecules with the same valency but an altering αMan ligand density, which significantly differ in the FV values, then a varying contribution in ΔH and $-T\Delta S$ can be seen (e.g. compare 2b to 2, 2a; 3a, 3c to 3, 3b and 4a to 4).

Although the binding enthalpy decreases (enthalpic gain) with the FV, most often its favorable decrease is accompanied by an entropy loss (e.g. compare 2b to 2, 2a; 3a, 3c to 3, 3b and 4a to 4).

Again, this situation especially applies to glycomacromolecules with the same structural valency but altering αMan density. Within each of the three series of the glycomacromolecules carrying the same linker, it is further seen that a different αMan ligand density either leads to similar or altering FV values along with similar or altering contributions in ΔH and $-T\Delta S$. However, a clear trend regarding a higher or a lower αMan ligand density, just based on their spacer alternations, is not seen from this data. On the one hand, a smaller ligand density might be accompanied by a higher enthalpic (and lower entropic) gain, whereas a higher αMan density rather shows diminution in ΔH and gain in $-T\Delta S$. On the other hand, the exact reverse situation might apply for other compounds. Thus, following this data it can be concluded that the thermodynamic terms change only along with the FV of the glycomacromolecules, where glycomacromolecules with the same structural valency but different αMan ligand density, might either obtain similar or varying enthalpic and entropic contributions. This seems rather to be independent of the αMan ligand density, since there is no clear trend regarding its influence on the enthalpic and entropic terms.

Further, similar values in ΔH and $-T\Delta S$ suggest similar values in the overall binding free energy ΔG, so that from here it can be concluded that alternations in the αMan ligand density do not lead to subtle changes in ΔG. This insensitivity of ΔG to alternations in the αMan ligand density not only applies to similar ΔH and $-T\Delta S$ values. This situation also does apply to different ΔH and $-T\Delta S$ contributions, and thus in cases where each of the both energetic terms is compensating the other. Although, for example, a changing αMan density has led to changes in ΔH (e.g. a lower and more favorable ΔH), the entropy cost in such cases is significantly higher as compared to other compounds of the same structural valency but different αMan density (e.g. compare 2b to 2, 2a; 3a, 3c to 3, 3b and 4a to 4). Alternatively, compounds (e.g. compare 2, 2a and 3, 3b as well as 3a, 3c), which obey an enthalpic diminution (less favorable ΔH) are compensated by an entropic gain (less positive $-T\Delta S$). The two situation again then translate to the following general conclusions. Glycomacromolecules with the same linker and structural valency but varying αMan ligand density, show an overall similar ΔG. For similar values in ΔH and $-T\Delta S$ this situation is straightforward. Although there might be differences in their ΔH and $-T\Delta S$, potentially pointing at a different binding behavior, these changes do not translate to changes in ΔG. Instead and due to the compensatory behavior of either of these two energetic terms, all compounds that contain the same structural valency but a different αMan density, essentially obey the same or similar values in ΔG (e.g. compare 2, 2a, 2b; 3, 3a, 3b, 3c and 4, 4a, 4b). The here described spacer insensitivity and general evolution of the enthalpic and entropic data also holds true for glycomacromolecules, which bind to dimer Con A.
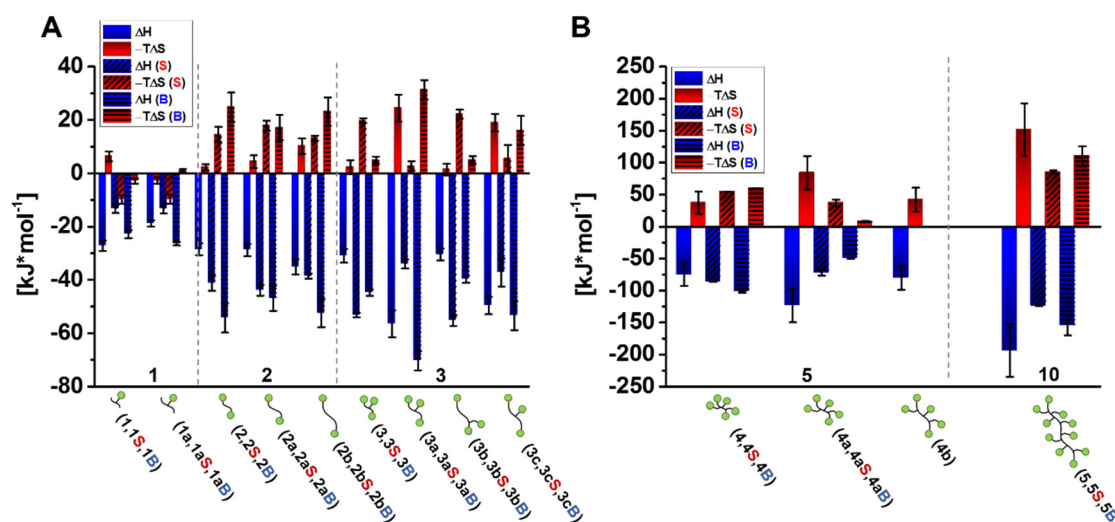
Figure 35. Changes of the binding enthalpy and entropy for glycomacromolecules varying in their αMan linkage in their binding to tetramer Con A. A: mono- to trivalent glycomacromolecules. B: penta- to decavalent glycomacromolecules.

3.5.6. The effect of αMan linkers on the binding enthalpy and entropy

Although the enthalpic and entropic data point to an insensitivity of the binding free energy on the αMan ligand density, a dramatic difference in these terms can be found when comparing molecules with the same structural valency and αMan density, but different αMan linkers. Comparing glycomacromolecules with the thiol-ether triazole and benzyl triazole linker to those with the short ethyl triazole linker, a clear difference in the enthalpic and entropic terms can be seen. While values in FV do not change significantly, their enthalpic and entropic terms clearly differ. Here, the evolution of the enthalpic and entropic terms essentially points to differences in the binding free energy terms of these compounds, since there is reduced compensatory effect of either ΔH or $-T\Delta S$. In their sum, these terms lead to detectable differences in ΔG, since compared to other compounds, one ligand may be favorable by both, the enthalpic and entropic term (Table 4). Furthermore, when glycomacromolecules with the same structural valency and ligand density and thus FV, but different αMan linkers are compared, a dramatic change in ΔH and $-T\Delta S$ is observed that does not result from a difference in FV. If, however, each of the linker types are compared separately (within the three series of glycomacromolecules), the FV steadily increases and thus also ΔH and $-T\Delta S$ within one linker type, as the FV is proportional to the binding enthalpy. Consequently, it can be concluded that the three different αMan linkers exhibit different inherent binding affinities that directly translate into the different binding behavior of the glycomacromolecules. As already outlined in the first section of this subchapter, the different αMan linkers already lead to different binding affinities in the monovalent glycomacromolecules. This observation further supports the linker hypothesis, as for the monovalent species the number of ligand-receptor interactions cannot be in- or decreased, but remains nearly constant. The data of the multivalent glycomacromolecules therefore shows the principle of additivity, where an

optimized affinity is maintained for the monovalent ligands (through the use of secondary effects, such as the hydrophobic benzyl triazole linker) and then multiplied by their multivalent presentation on the oligomer backbone.
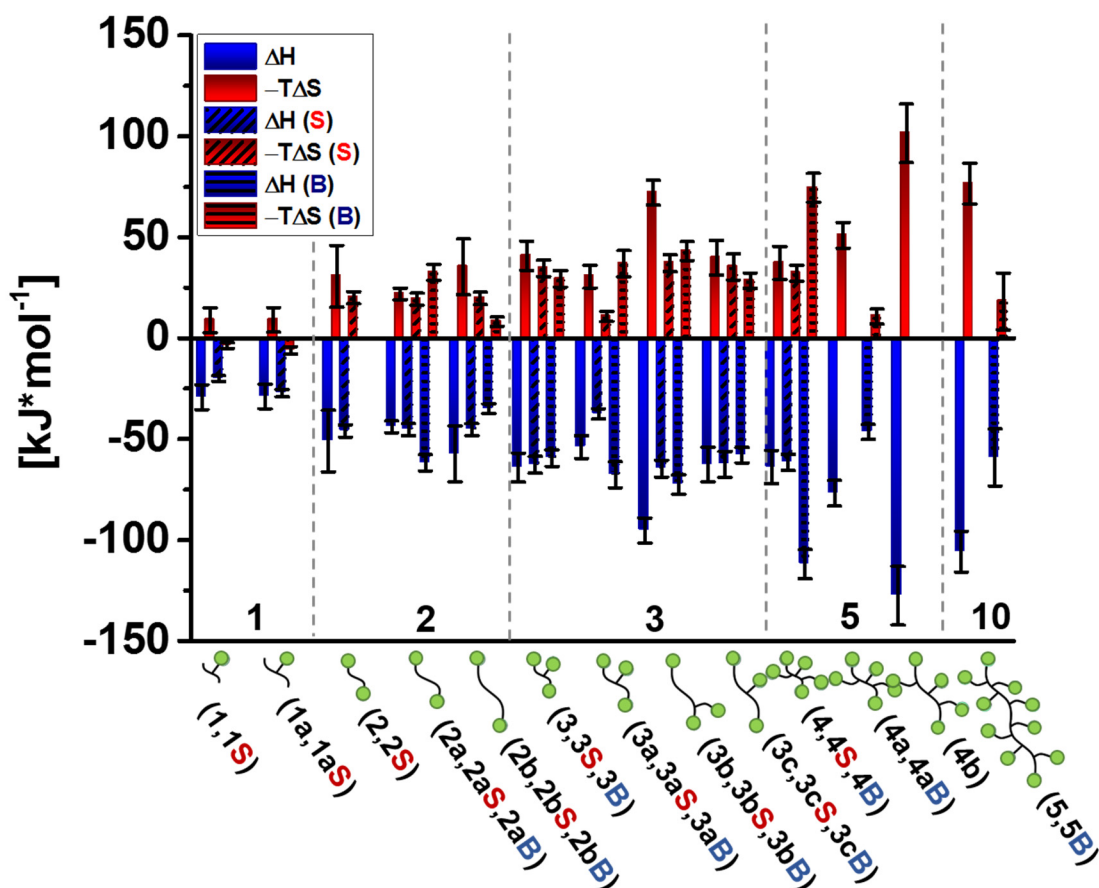
**Figure 36.** Changes of the binding enthalpy and entropy for glycomacromolecules varying in their αMan linkage in their binding to dimer Con A.

This is in agreement with previous studies, where several effects have been reported to affect multivalent interactions of glycopolymers to proteins. Among these effects, one hypothesis assumes that the carbohydrate linker between the anomeric center and the polymer backbone can dramatically influence the multivalent binding processes.[33, 56, 59, 72] The presented results on the αMan linker influence of the glycomacromolecules further support this hypothesis.

In the last chapter, it was shown that within a series of glycomacromolecules with the same linker, enthalpic and entropic terms rather show compensatory effects resulting in the same ΔG. Looking at the glycomacromolecules with the same structural valency and the short ethyl triazole linker, different trends for the enthalpic and entropic contributions depending on the ligand density were observed. Thus, so far, there is no clear indication for the role of spacing of the ligands on the resulting enthalpic and entropic contributions in binding to Con A. Overall, for this series of

glycomacromolecules and their interactions with dimer Con A, it can be concluded that the binding processes are rather enthalpy driven (which is again in agreement with their FV values).

If one takes now a look at the series of glycomacromolecules carrying the thiol-ether triazole linkers and compares them again regarding a changing αMan ligand density, now a clear trend for ΔH and $-T\Delta S$ is found. If the thiol-linked class of glycomacromolecules is compared to the former class with the ethyl triazole linkers, it is seen that the thiol-linked glycomacromolecules are favored either in ΔH or $-T\Delta S$ over the ethyl triazole linker. Again, the above result support the hypothesis that the αMan linkers indeed have large impact on the binding, whereas the αMan ligand density does not. If these glycomacromolecules are compared to the ethylene linked glycomacromolecules in their binding to dimer Con A (Table 4), then it is seen that in this case the thiol-linked compounds are favored in the binding entropy. Thus, in binding to dimer Con A, interestingly, the longer thiol-linked glycomacromolecules do not benefit from additional enthalpic gain. Its length therefore rather seem to be favored by a beneficial entropy and did not lead to increased ligand-receptor contacts.

Compared to the other two series of glycomacromolecules, compounds presenting the αMan benzyl triazole linkers also either show an enhanced enthalpic or entropic term, lacking a clear trend within this series of molecules (Table 4). Overall, the benzyl linked glycomacromolecules show a more favorable enthalpy and entropy terms (depending on the ligand) as compared to the other two series. A clear trend regarding the structural features so far, however, was not found. Thus altogether, the binding free energy follows the order of ethyl triazole linker > thiol-ether triazole linker > benzyl triazole linker, with the benzyl linked glycomacromolecules showing the highest binding affinity.

3.5.7. Comparison between binding to dimer and tetramer Con A

From the determined thermodynamic data of this study, it is seen that not only the linkers affect the binding energetics, but also the structural valency of the Con A receptor. A different binding behavior is observed when glycomacromolecules with the same linker either bind to dimer or tetramer Con A, as they show a significant difference in their binding energetics.

For example, the glycomacromolecules with the small ethyl triazole linker show FV values that are lower for the di- to the trivalent species in their binding to tetramer Con A, as compared to dimer Con A (Table 4, Table 5, Figure 34). These lower values in FV go along with the diminution of the binding enthalpy and a gain in the binding entropy. One possible explanation for the more favorable entropy would be the steric hindrance of the bigger tetramer Con A. The room captivating size of tetramer Con A along with the small size of the glycomacromolecules, may reduce the number of ligand-receptor interactions, thereby decreasing the binding enthalpy. Conversely, for the di- to trivalent ligands (e.g. compare 1, 1a; 2, 2a, 2b and 3, 3a, 3b, 3c) in binding to the smaller dimer Con A, it is seen that these compounds are rather favored in ΔH, which also should correlate with their higher FV values.

The argument regarding a possible steric hindrance resulting from the Con A size can, however, not be used to interpret the thermodynamic data of the higher valent analogues (e.g. compare 4, 4a and 5). In contrast to the results for the lower valent ligands, these species are accompanied by more favorable enthalpy values, suggesting additional ligand-receptor interactions, which are beneficial in binding to tetramer Con A (along with their higher FV). Here, the higher valency of the Con A tetramer along with the higher valencies of the glycomacromolecules (e.g. compare 4, 4a and 5) would indeed result in additional ligand-receptor contacts, thereby outweighing a beneficial binding entropy due to possible steric effects, observed for their lower valent counterparts. These observations for the higher valent analogues binding to the large Con A tetramer are, further in agreement with previous studies by Kiessling *et al.*[12], reporting on the statistical effect[12].

3.5.8. The effect of ligand density on the binding free energy

From the above discussions regarding the FV, binding enthalpy and entropy, it was seen that there are possibly several different effects, which might contribute to differences in the enthalpic and entropic terms. The above observations based on the structural features of the glycomacromolecules binding to Con A, may allow the following hypotheses: (*i*) Different αMan linkers clearly affect the binding of glycomacromolecules to Con A, (*ii*) depending on the size and valency of ligand and/or receptor steric, hindrance might affect receptor binding and (*iii*) a statistical effect might be operative, when the ligands as well as the receptor are of higher valency, which outweighs possible steric hinderance and increases the number of possible ligand-receptor contacts. These observations are also in agreement with previous studies, where several effects have been reported to overlap each other in the binding enthalpy and entropy (especially for multivalent binding processes).[6, 49, 107]

While there is no clear trend for the individual enthalpic and entropic contributions, the binding free energy data shows a pronounced trend for all investigated glycomacromolecules (Figure 37, A and B). Regarding each of the three series of glycomacromolecules with the same valency but a different αMan ligand density, the following conclusion can be drawn. Glycomacromolecules with the same structural valency but an altering αMan ligand density, have very similar ΔG values. Although their enthalpic and entropic terms might differ, these most likely result in an enthalpy-entropy compensation[107, 130, 136-139] (EEC), so that the variations in the spacing, so far, have no influence on the binding free energy (Figure 37, A and B). One possible explanation for this spacer insensitivity of ΔG might be the yet inappropriate length scale of the glycomacromolecules, as compared to the binding sites of the Con A protein. From previous studies by Ponader *et al.*[103], it was seen that such glycomacromolecules are highly flexible in water media, and most likely adopt coiled structures in buffered solutions. Further, recent reports by Nguyen *et al.*[72] have concluded that the binding of large-sized polymers to Con A also leads to an overall intermolecular binding process, although these polymers indeed obey an "appropriate" length and size, as compared to the distance of the protein's binding pockets. Thus, these observations might further support the

hypothesis that the binding free energy is rather insensitive to alternations in the spacing of carbohydrate ligands attached to polymeric scaffolds. Overall, regardless of the spacing of the carbohydrate ligands on the scaffolds for the studied glycomacromolecules, ΔG only decreases with a higher FV. This can be attributed to an increasing number of ligand-receptor interactions, as is evident from the binding stoichiometry (Table 4 and 5) and thus statistically more available binding states.

Although there is no influence of the αMan ligand density on ΔG, which holds true for both Con A conformations (see Figure 37, Table 4 and Table 5), a clear influence of the different αMan linkers can be observed, leading to different ΔG values for each of the three different series. Glycomacromolecules presenting the benzyl triazole linkers show the lowest ΔG values, followed by the thiol-ether triazole and the ethyl triazole linked compounds, which obtain the highest and least favorable ΔG values in each of the three series of glycomacromolecules for binding to dimer Con A (Figure 37, A). The same applies for mono- to trivalent glycomacromolecules for binding to tetramer Con A, while penta- to decavalent compounds follow the order benzyl triazole linker < ethyl triazole linker < thiol-ether triazole linker (Figure 37, B). As was already seen from the above discussion of the binding enthalpy and entropy, the significant gain in ΔG is not due to additional ligand-receptor interactions, as the values in FV are similar for all of the three series of glycomacromolecules. Thus, this behavior rather points to the dependence of ΔG on the αMan linker's chemical composition. This behavior is clearly seen from the ΔG values of the monovalent compounds (1, 1S, 1B and 1a, 1aS, 1aB), where the number of interactions are not minimized nor maximized. Thus, changes in ΔG are due to an already inherent different binding affinity, initiated by the composition of the αMan linkers.

The observed changes in ΔG further correlate with the structural valency of the glycomacromolecules. The higher the structural valency, the lower the ΔG values. These results are again irrespective of the Con A conformation. However, values in ΔG (tetramer Con A) are significantly lower as compared to ΔG (dimer Con A), although values in FV are similar. This result indicates that although the FV might be more or less the same for either the Con A dimer or tetramer, there is a significant favorable contribution in ΔG of the higher valent Con A. Therefore, not only the ligand, but also the protein valency matters. Further, although the valency of the protein does not seem to actively participate in the binding process in terms of additional ligand-receptor contacts, which can be seen from the FV values, the presence of additional binding pockets in tetramer Con A, however, somehow seems to influence the binding process, thereby resulting in higher binding affinities as compared to dimer Con A. As the glycomacromolecules are so far only able to accompany an intermolecular binding to Con A, this observation might be a result of the so-called statistical effect as introduced by Kiessling *et al.*[12], where the close proximity of available binding pockets of Con A enhances the overall binding affinity.
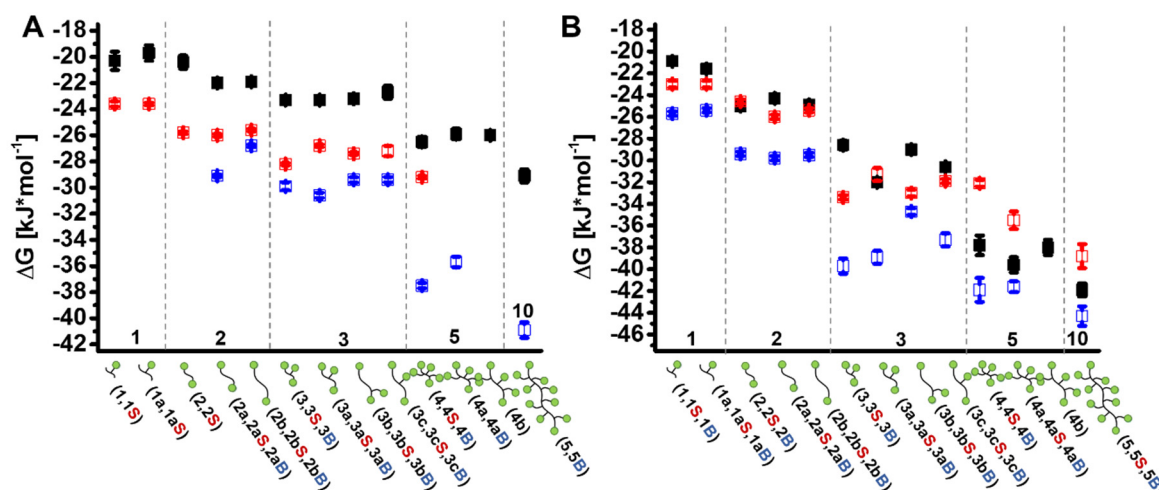
Figure 37. ΔG values derived from ITC measurements for the binding of different glycomacromolecules to dimer Con A (A) and tetramer Con A (B).

Interestingly, the observed decrease in ΔG with increasing valency shows a non-linear correlation with either of the three series of glycomacromolecules. Where at first decrease in ΔG is only moderate for the divalent species, additional contribution of one more carbohydrate ligand significantly lowers ΔG for the trivalent glycomacromolecules. The same holds true also for the pentavalent compounds. In contrast to these results and although the FV is highest and thus ΔG is lowest for decavalent systems, additional gain in ΔG, as compared with the pentavalent ligands, is only moderate (Table 4 and Table 5, Figure 37). This result indicates, that there may be some kind of an "efficient" ligand density along the oligomer backbone. This would potentially mean that for a certain size of a glycomacromolecule, there is only a limited number of Con A proteins that can bind to the presented αMan ligands, without causing a significant steric repulsion of the proteins. If such binding processes are thus limited by the size of the ligand and the protein, there is only an effective number of ligands along with an effective ligand density, allowing the protein to bind to these. Hence, the overall system will be able to captivate only few of the αMan ligands, but additional carbohydrate ligands of the higher valent analogues might further contribute to a decrease in the binding free energy. As a result, the binding here might clearly get more favorable as compared to their lower valent molecules. But the overall gain in ΔG will be only moderate, as the protein binding to the αMan ligands are limited by their size and the size of the glycomacromolecule as well as its αMan density.

3.5.9. The impact of ligand density and αMan linkage on different entropic terms

A strong dependency of the entropic term was previously attributed to the general glycoside cluster effect[6, 25, 38, 93] and is also observed for some of the studied glycomacromolecules. For example, the binding of glycomacromolecules with the short ethyl triazole linker to dimer Con A generally shows an unfavorable contribution in the binding entropy (2 − 2b, 3a − 3c, 5a − 5b).

Previous studies on glycopolymers have shown that upon binding of polyvalent and high density ligands, there was a diminution in the enthalpic term, which has been described to be a thermodynamic signature of an intermolecular aggregative[38, 93], more "endothermic-like" process. It was further suggested, that compounds with a high ligand density seem to exhibit comparatively favorable entropic values as to ligands with a lower ligand density. Indeed, this study showed that for some glycomacromolecules an increasing number of spacing units within the glycomacromolecule can result in higher entropy cost (more positive entropy values) (3 − 3c, 5 − 5b). Thus, in this case, higher ligand densities are relatively favored by the entropy as compared to lower ligand densities. However, summarizing the results for the three series of glycomacromolecules, there is no clear trend that would support the above assumptions. In case of the Con A tetramer, the binding of lower valent seems to be favored by a more favorable entropy. But no clear trend was found here regarding the ligand density along with a more favorable entropy. In contrast, the high density and high valent ligands (e.g. 5, 5S and 5B) even showed a gain in enthalpy, associated with higher entropic costs. Therefore, from this study it is seen that a higher valency as well as αMan density did not lead to favorable entropic values that would result in endothermic-like processes. These results are consistent with latest result on a thermodynamic study reported by Nguyen *et al.*[72], who showed that the entropy was always unfavorable and even increased with the structural valency.

Nevertheless, to further study other potential entropic effects, such as configuration and solvation entropies that might change with the different linkers and may give better insight into the underlying effects of receptor binding, temperature dependent ITC measurements were performed. Chervenak *et al.*[116, 132-134] have previously described studies, where the configuration and translational entropies can be determined. They[132-133] have shown that changes in entropy of solvation and configuration in carbohydrate-lectin interactions can be determined by following a thermodynamic cycle (Born-Haber-Cycle).[6] As the entropy increases with an increasing temperature, the heat capacity of a binding process increases and is assumed to be proportional to the former. Further, a change in entropy with temperature (e.g. from T_1 to T_2) equals the heat flow divided by the temperature, which is related to the heat capacity change of n moles of a ligand (L) and protein (P) to n moles of the L·P complex[6]:

$$\left(\frac{\partial S}{\partial T}\right)_p = \frac{C_p}{T} \tag{7}$$

$$\Delta S = \frac{Q_{rel}}{T} = n \cdot C_p \cdot \frac{\Delta T}{T} \tag{8}$$

Equation (8) can be re-written as:

$$\Delta S = n \cdot C_p \cdot \ln\frac{T_1}{T_2}. \tag{9}$$

Thus, it has been shown[132-133] that a determination of the heat capacity change in combination with the experimental measured values of the overall binding entropy ΔS, can be used to calculate the otherwise inaccessible entropy change of solvation and configuration by applying the thermodynamic cycle.[6] With the help of these different entropic contributions, different entropic effects are now visible. These entropic effects might for instance claim, whether an arrangement of αMan ligands is favorable or if potential water reorganization effects might participate in the binding process. Herein, the entropy change is split into different contributions to the overall binding entropy, and equals the sum of the entropy change of solvation ΔS_{solv}, configuration ΔS_{conf} as well as the translational and rotational entropy change $\Delta S_{trans+rot}$, which has been defined by Kauzmann[232] as one important entropy contribution in a binding process.[6]

$$\Delta S = \Delta S_{solv} + \Delta S_{conf} + \Delta S_{trans+rot} \tag{10}$$

Since the entropy is a state function, the entropy change in configuration ΔS_{conf} can be determined from the overall (measured) entropy change ΔS, and from the relation of the heat capacity (which can be experimentally determined) to the solvation entropy ΔS_{solv}, according to the thermodynamic cycle and the following equation[6]:

$$\Delta S_{solv} = \Delta S_{solv}^* + \Delta C_p \cdot \ln \frac{T}{T^*}. \tag{11}$$

Here, ΔS_{solv}^* accounts for electrostatic contributions and protonation processes, which is assumed to be zero for carbohydrate-lectin interactions, while $T^* = 385.15$ K equals the temperature upon which no solvent changes are assumed.[6] The translation and rotational entropy change $\Delta S_{trans+rot}$ has been suggested by Murphy *et al.*[233] to equal -33.5 J mol^{-1} K^{-1}.[6] Hence, from knowing the measured overall binding entropy ΔS and heat capacity ΔC_p, the solvation entropy ΔS_{solv} can be calculated, while solving for ΔS_{conf} gives the entropy change in configuration.[6]

Following this concept, the solvation entropy was determined first as was previously described by Chervenak *et al.*[116, 132-134]. Determination of the solvation entropy was possible after the heat capacity change ΔC_p has been identified. The heat capacity was calculated by measuring enthalpy changes for a range of different temperatures, which allows for the calculation of the heat capacity according to Kirchhoff's law[133]. For determination of the heat capacity ΔC_p of multivalent ligand binding to Con A, standard ITC titration experiments were performed at 298.15 K, 303.15 K and 308.15 K. Binding enthalpies derived at different temperatures were plotted as ΔH against T (Figure 38, A), where ΔC_p was obtained from the slope of linear regression analysis according to equation (12):

$$\Delta H(T_2) = \Delta H(T_1) + \Delta C_p(T_2 - T_1) \tag{12}$$

From the heat capacity change, the solvation entropy was then calculated (equation (11)) and rearrangement of the entropic equation (10) allowed for determination of the configuration entropy. To account for the FV during the binding process, the translations and rotational entropy contribution, which was assumed to be -33.5 J mol^{-1} K^{-1}[233], was multiplied with the FV, as was determined from the same ITC experiment at 298.15 K. Thus, equation (10) was re-written and applied as:

$$\Delta S = \Delta S_{solv} + \Delta S_{conf} + \Delta S_{trans+rot} \cdot FV \tag{13}$$

The term $\Delta S_{trans+rot} \cdot FV$ thereby only affected the calculation of ΔS_{conf}, whereas ΔS_{solv} was not affected by these changes, but was only sensitive to the changes in ΔC_p. Thus, while the evolution of ΔS_{solv} is only affected by ΔC_p, ΔS_{conf} was dependent on the evolution of the measured overall entropy ΔS, the FV and the solvation entropy ΔS_{solv}. Table 6 shows the evolution of the ITC derived thermodynamic parameters with the three different temperatures (298.15 K, 303.15 K and 308.15 K), required for the calculation of the heat capacity change ΔC_p, the solvation ΔS_{solv} and configuration entropies ΔS_{conf}, such as the FV and the binding enthalpy. Table 7 shows the different entropic contributions determined for the mono- and trivalent species (1, 1S, 1B and 3a, 3aS, 3aB) in their binding to the Con A tetramer, determined from the thermodynamic enthalpy, heat capacity and FV values.

For the configuration and solvation entropy (Figure 38, B), it was found that the short ethyl triazole linker seems to be favored in configuration entropy. This effect becomes even more pronounced as the valency increases (from mono- to trivalent). In that case, the solvation entropy is not favorable in binding to tetramer Con A. In contrast to these results, the thiol-ether triazole linker is rather favored in the solvation entropy and not the configuration one. This is, however, only true for the monovalent species, as for the trivalent compound the order seems to have changed into the opposite, thus favoring the configuration entropy. Conversely, the monovalent compound containing the benzyl triazole linker is unfavorable in both entropic terms, whereas its trivalent counterpart shows a favorable solvation entropy. The latter result pinpoints at the hydrophobic effect and favorable water reorganizations processes during binding.
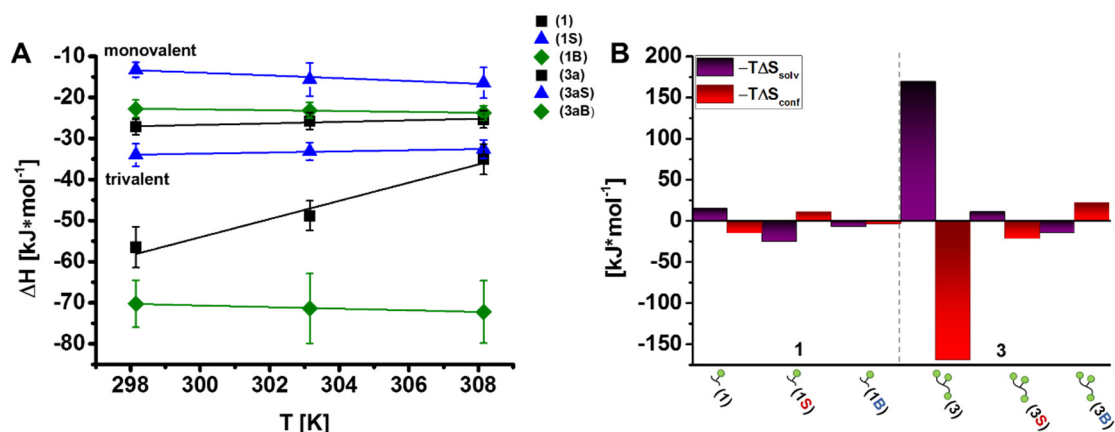
Figure 38. A: Evolution of the binding enthalpy ΔH with temperature allowed the determination of the heat capacity change ΔC_p. **B**: Different entropies ($-T\Delta S_{solv}$, $-T\Delta S_{conf}$) describing the binding process of mono- and trivalent glycomacromolecules to tetramer Con A ($-T\Delta S_{solv}$ was determined from ΔC_p).

These observations indicate that with the different linkers, there is a kind of switch in which the favorable configuration entropy finally results in a favorable solvation entropy, in the order of short ethyl triazole linker < thiol-ether triazole linker < benzyl triazole linker. Thus, the most favorable configuration entropy is found for the small ethyl triazole linker, whereas a significantly favorable solvation entropy is found for the trivalent benzyl triazole linked compounds. In a potential scenario, in case of the ethylene and thiol-ether triazole linker, the favorable αMan ligand arrangement during binding, seems to be accompanied by an unfavorable organization of solvent molecules. For the short linker, this effect is more pronounced as for the longer thiol-ether triazole linker. In contrast to this, for compound 3aB presenting the benzyl triazole linker, the observed value could be attributed to a favorable hydrophobic effect, where organization of water molecules is favorable and counterbalanced by an inappropriate arrangement of the αMan ligands during binding.

Table 6. Evolution of ITC derived thermodynamic parameters with temperature of mono- and trivalent glycomacromolecules with different linkers binding to tetramer Con A. Measurements were performed at different temperatures (298.15 K, 303.15 K, 308.15 K), allowing for determination of the heat capacity change ΔC_p (from evolution ΔH with T according to Kirchhoff's law[133]).

Ligand	$\overline{FV}^{[a]}$	$\overline{\Delta G}^{[b]}$	$\overline{K_d}^{[c]}$	$\overline{\Delta H}^{[b]}$	$-\overline{T\Delta S}^{[b]}$	$\Delta C_p^{[d]}$	$\overline{c}^{[e]}$
Monovalent (ethyl triazole linker)							
Man(3)-5¹ (**1**) 25°C	0.8 ± 0.1	−20.9 ± 0.2	221 ± 13	−27 ± 2	+6 ± 2	+186 ± 38	~2
Man(3)-5¹ (**1**) 30°C	0.7 ± 0.1	−20.7 ± 0.2	267 ± 19	−26 ± 2	+5 ± 2	−	~2
Man(3)-5¹ (**1**) 35°C	0.7 ± 0.1	−20.7 ± 0.2	311 ± 22	−25 ± 2	+5 ± 2	−	~1
Monovalent (thiol-ether triazole linker)							
Man(3)S-5¹ (**1S**) 25°C	0.6 ± 0.1	−23.0 ± 0.3	94 ± 13	−13 ± 2	−10 ± 2	−335 ± 134	~4
Man(3)S-5¹ (**1S**) 30°C	0.32 ± 0.04	−22.2 ± 0.7	147 ± 38	−16 ± 4	−7 ± 4	−	~8
Man(3)S-5¹ (**1S**) 35°C	0.27 ± 0.03	−21.5 ± 0.7	196 ± 51	−17 ± 4	−5 ± 4	−	~6
Monovalent (benzyl triazole linker)							
Man(3)B-5 (**1B**) 25°C	0.9 ± 0.1	−25.7 ± 0.2	32 ± 3	−23 ± 2	−3 ± 2	−99 ± 21	~11
Man(3)B-5 (**1B**) 30°C	0.8 ± 0.1	−25.4 ± 0.2	42 ± 4	−23 ± 2	−2 ± 2	−	~8
Man(3)B-5 (**1B**) 35°C	0.7 ± 0.1	−24.8 ± 0.3	54 ± 5	−24 ± 2	−1 ± 2	−	~6
Trivalent (ethyl triazole linker)							
Man(1,3,5)-5 (**3a**) 25°C	2.6 ± 0.3	−32.0 ± 0.3	2.5 ± 0.3	−57 ± 5	+25 ± 5	+2213 ± 485	~151
Man(1,3,5)-5 (**3a**) 30°C	2.3 ± 0.3	−30.7 ± 0.3	5.1 ± 0.5	−49 ± 4	+18 ± 4	−	~70
Man(1,3,5)-5 (**3a**) 35°C	1.8 ± 0.3	−29.2 ± 0.3	11 ± 3	−35 ± 4	+6 ± 4	−	~34
Trivalent (thiol-ether triazole linker)							
Man(1,3,5)S-5¹ (**3aS**) 25°C	1.5 ± 0.1	−31.3 ± 0.6	3.3 ± 0.9	−34 ± 3	+3 ± 3	+137 ± 27	~116

Man(1,3,5)S-5 (**3aS**) 30°C	1.4 ± 0.2	-31.7 ± 0.6	3.5 ± 0.9	-33 ± 2	$+1 \pm 2$	–	~118
Man(1,3,5)S-5[1] (**3aS**) 35°C	1.5 ± 0.2	-31.1 ± 0.7	5 ± 1	-33 ± 2	$+2 \pm 2$	–	~76
Trivalent (benzyl triazole linker)							
Man(1,3,5)B-5[1] (**3aB**) 25°C	2.5 ± 0.6	-38.9 ± 0.6	0.15 ± 0.04	-70 ± 15	$+31 \pm 15$	-199 ± 47	~2534*
Man(1,3,5)B-5[1] (**3aB**) 30°C	2.5 ± 0.6	-38.9 ± 0.6	0.20 ± 0.05	-71 ± 17	$+33 \pm 17$	–	~2534*
Man(1,3,5)B-5[1] (**3aB**) 35°C	2.6 ± 0.6	-39.7 ± 0.6	0.19 ± 0.05	-72 ± 16	$+33 \pm 16$	–	~2534*

[a] $\overline{FV}$ is defined as $\overline{FV} = \frac{1}{n}$ and was experimentally determined from the binding stoichiometry n. [b] Gibbs free binding energy $\overline{\Delta G}$, enthalpy $\overline{\Delta H}$ and entropy $-T\overline{\Delta S}$ are reported in kJ mol^{-1}. [c] Dissociation equilibrium constant $\overline{K_d}$ is reported in µM. [d] Heat capacity change ΔC_p, determined from evolution of ΔH with temperature (Kirchoff's law[133]), is reported in J K^{-1} mol^{-1}. Errors in $\overline{FV}$, $\overline{\Delta G}$, $\overline{\Delta H}$, $-T\overline{\Delta S}$, $\overline{K_d}$ and ΔC_p refer to the error propagation as described in the Experimental Part. [e] $\bar{c}$ $-$ values refer to the quality of the fit and the corresponding error propagation in the Experimental Part. "*" marks ITC measurements whose $\bar{c}$ $-$ values are outside the traditional range (as described in Chapter 3.4.1). All thermodynamic quantities refer to best mean values, expect for measurements, which were performed one time (those are highlighted with "1"). Measurements were performed in LBB pH 7.40 $\pm$ 0.01 at 298.15 K, 303.15 K and 308.15 K, with Con A obtaining its dimer-tetramer equilibrium conformation[131, 223].

Table 7. Solvation and configuration entropic contributions for mono- and trivalent glycomacromolecules with different linkers binding to tetramer Con A. Solvation and configuration entropic contributions were determined from the heat capacity change ΔC_p, the measured overall entropic contributions $\overline{\Delta S}$ and the rotational and translational entropies times the $\overline{FV}$, $\Delta S_{trans+rot} \cdot \overline{FV}$.

Ligand	$\overline{\Delta S}$[a]	$\Delta S_{trans+rot} \cdot \overline{FV}$[a]	ΔS_{solv}[b]	ΔS_{conf}[b]	$-T\Delta S_{solv}$[c]	$-T\Delta S_{conf}$[c]
Monovalent (ethyl triazole linker)						
Man(3)-5 (**1**)	-21 ± 6	-19	-48	$+52$	$+14$	-16
Monovalent (thiol-ether triazole linker)						
Man(3)S-5 (**1S**)	$+33 \pm 6$	-29	$+86$	-34	-26	$+10$
Monovalent (benzyl triazole linker)						
Man(3)B-5 (**1B**)	$+10 \pm 7$	-28	$+25$	$+14$	-8	-4

Trivalent (ethyl triazole linker)						
Man(1,3,5)-5 (**3a**)	−82 ± 17	−86	−567	+570	+169	−170
Trivalent (thiol-ether triazole linker)						
Man(1,3,5)S-5 (**3aS**)	−9 ± 10	−48	−35	+74	+10	−22
Trivalent (benzyl triazole linker)						
Man(1,3,5)B-5 (**3aB**)	−105 ± 19	−84	+51	−123	−15	+37

[a] Experimentally determined overall binding entropy $\overline{\Delta S}$ is reported for the standard state temperature (298.15 K). The tabulated $\Delta S_{trans+rot}$ was multiplied with the experimentally determined $\overline{FV}$ to account for the multivalent effect (which differs from the structural valency[34]. A different $\overline{FV}$ can also apply to monovalent compounds, see Table 6). According to Murphy *et al.*[233] $\Delta S_{trans+rot}$ equals −33.5 J K⁻¹ mol⁻¹ for monovalent binding. $\Delta S_{trans+rot} \cdot \overline{FV}$ was determined for the standard state temperature (298.15 K). [b] Entropy of solvation ΔS_{solv} was determined from the heat capacity change $\overline{\Delta C_p}$ and the entropy of configuration ΔS_{conf}, from the summation of the measured overall entropic term $\overline{\Delta S}$ (see equation 13). Experimentally determined overall binding entropy $\overline{\Delta S}$ and the entropy of solvation ΔS_{solv} and configuration ΔS_{conf} are reported in J K⁻¹ mol⁻¹. [c] Standard state entropy of solvation $-T\Delta S_{solv}$ and configuration $-T\Delta S_{conf}$ is reported in kJ mol⁻¹, assuming 298.15 K.

3.5.10. Influence of the ligand density and linkage on rebinding kinetics

Much attention has been paid to target and modulate the binding affinity in multivalent glycopolymer systems determined by thermodynamic studies or binding assays, e.g. measuring the inhibitory potential of glycopolymer systems. However, in order to gain a deeper insight into their multivalent binding, it is also important to take a look at the kinetics of ligand-receptor complex formation. The binding affinity is described as a state function and thus depends on the free energy difference between the bound and unbound state. The kinetics of complex formation depend on the height of the (rate-determining) free activation barrier, separating the free und bound states. Since carbohydrate-receptor interactions are weak, especially the so-called rebinding kinetics are believed to play an important role for complex formation and stability. When one of the carbohydrate ligands attached to the polymer binds to the receptor, it will not stay bound, but rather unbind fast in micro-equilibria. Through the close proximity of a high number of carbohydrate ligands on the glycopolymer, there is an increased statistical chance for rebinding. Thus, the statistical rebinding effect[18, 106, 110-112, 117] has been invoked in several studies to be a "long-lasting binding" and to be the kinetic origin of a (relatively) high affinity. An important assumption here is also that the ligand density and the inherent variation of the spacer units as well as the molecular weight, may have a different contribution on the resulting rate constants. Previous studies differentiate between (*i*) the hip-and-hop or bind-and jump mechanism[18, 117] in large aggregates[106] (exhibiting very low k_{off} values, indicative for high avidity binding in biological systems) and (*ii*) the un- and rebinding mechanism[107-108, 110, 112, 234] of single epitopes to the same binding site of a protein, which are excited or actively forced to unbind by a competing ligand[112-113, 234] (k_{off} values are here accelerated, resulting in concentration dependent so-called "effective" off-rates), and (*iii*) the binding and rebinding of different carbohydrate ligands to the same binding pocket of the protein during the association process in the early steps of binding[110]. The observation of how a different valency and ligand density affects the association and dissociation rates, provides an indirect way of identifying those molecular features that impact and pinpoint to the rebinding kinetics.

The following discussion will therefore highlight the results from the kinITC experiments deriving evolution of the binding kinetics of precision glycomacromolecules, binding to predominantly dimer or/and tetramer Con A. Although in literature much attention has been paid to understand the multivalent binding in terms of state functions and binding affinities[19, 25, 49, 72, 93, 109, 115-116], only a few studies report on the multivalent binding kinetics[76, 162, 228], also in terms of the above described rebinding processes. This study was therefore aiming to contribute to a deeper understanding of multivalent binding kinetics, by using the presented set of glycomacromolecules. Based on the structural features of the studied precision glycomacromolecules, the observed trends for the binding kinetics will be discussed.

3.5.11. Evolution of k_{on} and k_{off} values with the ligand density and linkage

Previously, Dumas *et al.*[163], Butcher *et al.*[164] and Yonetani *et al.*[165] have demonstrated that ITC cannot only be used to give thermodynamic information. In addition, binding isotherms from ITC measurements can also provide kinetic parameters (as has been described in Chapter 3.4, further see Experimental Part and Supporting Appendix). *Via* this so-called kinITC method[163-165], it is possible to derive the kinetic association rate constant k_{on} from the binding isotherms, where a non-linear least squares fitting of each of the heat flow signals in one binding isotherm gives individual k_{on} values (see also Experimental Part and Supporting Appendix).[7] These can then be weighted averaged into one single k_{on} value, and the dissociation rate constant k_{off} is then simply obtained, following the relationship between the two rate constants and the equilibrium dissociation constant ($K_d = k_{off}/k_{on}$). Table 8 and 9 show the determined values for the rate constants k_{on} and k_{off} and the equilibrium dissociation constant K_d for glycomacromolecules in binding to dimer (Table 8) and tetramer Con A (Table 9).

Similar to the thermodynamic data derived from the ITC experiments, the presented kinetic data in this study will be discussed looking at trends rather than focusing on precise values of single precision glycomacromolecules. k_{on} and k_{off} values should in general be rather considered as estimates, since they are highly ligand and protein concentration dependent and thus heavily dependent on the accurate experimental design in terms of the ligand and protein concentrations[135]. Further, although the k_{on} values are determined by an independent fitting procedure (see Chapter 3.4, Experimental Part and Supporting Appendix) and therefore only influenced by the ligand and protein concentrations, k_{off} values additionally depend on K_d, which is determined from the fitting procedure, as is used to quantify the binding thermodynamics (slope of the binding curve, *one sets of independent binding sites*). Thus, here k_{off} values are heavily affected also by the shape of the binding isotherm, which is given by the c – values (the fitting procedure as the instrumental limitation). Thus, all of these parameters here should be regarded as estimates, even if the measurements exhibit representative c – values (tolerated c – values lie in the range $1 < c < 1000$[130, 135, 224, 226]). The c – values are highlighted in each table, where they describe the quality of the data in terms of the fitting procedure[130, 135, 224, 226], which is important for k_{off} and K_d values. Data whose c – values lie outside the traditional range are further

---

[7]The least squares non-linear curve fitting procedure for kinITC has been written by Dr. Susanna Röblitz and Dr. Marcus Weber (Konrad-Zuse-Institut für Informationstechnik, Berlin; see also Supporting Appendix). Every measurement (including experimental design), determination, calculation and evaluation of the rate constants including their uncertainties has been performed by the author of this thesis. The kinITC least squares minimization procedure, required for the determination, calculation and evaluation of the measured ITC data (binding isotherms), has been provided by Dr. Susanna Röblitz and Dr. Marcus Weber. They have written the MATLAB scripts, which then allowed the calculation/determination of the rate constants. These written MATLAB scripts have been applied for the calculation/determination of the kinetic constants by the author of this thesis.

highlighted in the corresponding table by "*". In the data it is further highlighted whether *one* or

n series of measurements were performed.

Table 8. Kinetic data of glycomacromolecules with different linkers binding to dimer Con A. Measurements were performed at 298.15 K and correspond to the same measurements used for determination of thermodynamic parameters. The rate constants were obtained using the kinITC method.

Ligand	$\overline{k_{on,g}}$[a]	$\overline{k_{off,g}} \cdot 10^{-3}$[b]	$\overline{K_d}$[c]
Monovalent (ethyl triazole linker)			
Man(3)-5 (**1**)	302 ± 97	84 ± 37*	278 ± 82*
Man(4)-8 (**1a**)	309 ± 89	112 ± 43*	361 ± 91*
Monovalent (thiol-ether triazole linker)			
Man(3)S-5[1] (**1S**)	568 ± 78	42 ± 6	75 ± 5
Man(4)S-8[1] (**1aS**)	591 ± 78	43 ± 6	72 ± 4
Divalent (ethyl triazole linker)			
Man(1,5)-5 (**2**)	158 ± 40	42 ± 14*	266 ± 58*
Man(1,6)-6 (**2a**)	459 ± 64	65 ± 10	141 ± 9
Man(1,9)-9 (**2b**)	452 ± 66	65 ± 11	145 ± 10
Divalent (thiol-ether triazole linker)			
Man(1,5)S-5[1] (**2S**)	2153 ± 284	65 ± 9	30 ± 2
Man(1,6)S-6[1] (**2aS**)	2329 ± 306	66 ± 9	28 ± 1
Man(1,9)S-9[1] (**2bS**)	1818 ± 239	61 ± 8	33 ± 1
Divalent (benzyl triazole linker)			
Man(1,6)B-6[1] (**2aB**)	3513 ± 479	28 ± 4	8.0 ± 0.4
Man(1,9)B-9[1] (**2bB**)	1859 ± 248	38 ± 6	21 ± 1
Trivalent (ethyl triazole linker)			
Man(all)-3 (**3**)	1420 ± 216	120 ± 21	85 ± 7
Man(1,3,5)-5 (**3a**)	1235 ± 172	101 ± 16	82 ± 5
Man(1,6,7)-7 (**3b**)	857 ± 122	75 ± 12	87 ± 6
Man(1,4,7)-8 (**3c**)	760 ± 192	81 ± 26	107 ± 20
Trivalent (thiol-ether triazole linker)			
Man(all)S-3[1] (**3S**)	6054 ± 817	70 ± 9	11.5 ± 0.6
Man(1,3,5)S-5[1] (**3aS**)	4280 ± 579	85 ± 13	20 ± 1
Man(1,6,7)S-7[1] (**3bS**)	4034 ± 524	65 ± 9	16.0 ± 0.7
Man(1,4,7)S-8[1] (**3cS**)	4392 ± 893	74 ± 19	17 ± 3
Trivalent (benzyl triazole linker)			
Man(all)B-3 (**3B**)	6631 ± 1197	38 ± 8	5.7 ± 0.6
Man(1,3,5)B-5 (**3aB**)	8318 ± 1270	36 ± 6	4.3 ± 0.4
Man(1,6,7)B-7 (**3bB**)	7274 ± 888	52 ± 8	7.2 ± 0.5

Man(1,4,7)B-8 (**3cB**)	6970 ± 999	49 ± 8	7.0 ± 0.5
Pentavalent (ethyl triazole linker)			
Man(all)-5 (**4**)	5650 ± 1082	128 ± 31	23 ± 3
Man(1,3,5,7,9)-9 (**4a**)	2924 ± 586	85 ± 21	29 ± 4
Man(1,4,7,10,13)-13 (**4b**)	3095 ± 438	86 ± 13	28 ± 2
Pentavalent (thiol-ether triazole linker)			
Man(all)S-5[1] (**4S**)	10108 ± 1338	79 ± 11	7.8 ± 0.4
Pentavalent (benzyl triazole linker)			
Man(all)-5B (**4B**)	70359 ± 13853	19 ± 4	0.27 ± 0.02
Man(1,3,5,7,9)B-9 (**4aB**)	75059 ± 15406	42 ± 11	0.6 ± 0.1
Decavalent (ethyl triazole linker)			
Man(all)-10 (**5**)	14114 ± 3329	113 ± 35	8 ± 2
Decavalent (benzyl triazole linker)			
Man(all)B-10 (**5B**)	1001093 ± 270158	69 ± 24	0.07 ± 0.02

[a] Mean association rate constant $\overline{k_{on,g}}$ is reported in M^{-1} s^{-1}. [b] Mean dissociation rate constant $\overline{k_{off,g}}$ is reported in s^{-1}. Rate constants were determined by fitting the ITC raw data from every heat flow signal, following the relaxation period for every injection of the ligand L (kinITC method, see Chapter 3.4.1 and Experimental Part). Errors in the rate constants correspond to true uncertainties, following error propagation as described by Butcher *et al.*[164] and in the Experimental Part. [c] Dissociation equilibrium constant $\overline{K_d}$ is reported in µM and was determined from the same ITC experiments used to determine the thermodynamic parameters. Errors in $\overline{K_d}$ refer to the error propagation of thermodynamic parameters as described in the Experimental Part. "*" marks ITC measurements whose $\overline{c}$ − values are outside the traditional range (as described in Chapter 3.4.1). For $\overline{c}$ − values, see Table 4 and 5. All kinetic quantities refer to best weighted average values from *n* series of measurements, expect for measurements, which were performed one time (those are highlighted with "1"). Here, the weighted average rate constants refer to weighted average values of all of the heat flow profiles from one measurement (see also Experimental Part). Measurements were performed in acetate buffer pH 5.20 ± 0.02 at 298.15 K, with Con A obtaining its dimer conformation[34, 114, 131, 223].

Table 9. Kinetic data of glycomacromolecules with different linkers binding to tetramer Con A. Measurements were performed at 298.15 K and correspond to the same measurements used for determination of thermodynamic parameters. The rate constants were obtained using the kinITC method.

Ligand	$\overline{k_{on,g}}$[a]	$\overline{k_{off,g}} \cdot 10^{-3}$[b]	$\overline{K_d}$[c]
Monovalent (ethyl triazole linker)			
Man(3)-5 (**1**)	223 ± 32	49 ± 8	221 ± 16
Man(4)-8 (**1a**)	206 ± 33	34 ± 6	163 ± 14
Monovalent (thiol-ether triazole linker)			
Man(3)S-5[1] (**1S**)	560 ± 95	52 ± 12	94 ± 13
Man(4)S-8[1] (**1aS**)	380 ± 66	36 ± 6	94 ± 11
Monovalent (benzyl triazole linker)			
Man(3)B-5[1] (**1B**)	802 ± 122	26 ± 5	32 ± 3
Man(4)B-8[1] (**1aB**)	695 ± 92	24 ± 4	34 ± 1

Divalent (ethyl triazole linker)			
Man(1,5)-5[1] (**2**)	847 ± 127	36 ± 6	43 ± 4
Man(1,6)-6[1] (**2a**)	799 ± 120	45 ± 8	56 ± 5
Man(1,9)-9[1] (**2b**)	1212 ± 188	52 ± 9	43 ± 4
Divalent (thiol-ether triazole linker)			
Man(1,5)S-5 (**2S**)	1907 ± 295	42 ± 7	22 ± 2
Man(1,6)S-6 (**2aS**)	1504 ± 225	41 ± 7	28 ± 2
Man(1,9)S-9 (**2bS**)	1445 ± 206	52 ± 8	36 ± 3
Divalent (benzyl triazole linker)			
Man(1,5)B-5[1] (**2B**)	5457 ± 788	39 ± 6	7.1 ± 0.5
Man(1,6)B-6[1] (**2aB**)	4918 ± 731	30 ± 5	6.1 ± 0.5
Man(1,9)B-9[1] (**2bB**)	5308 ± 791	37 ± 6	6.9 ± 0.5
Trivalent (ethyl triazole linker)			
Man(all)-3[1] (**3**)	9067 ± 1959	87 ± 24	10 ± 2
Man(1,3,5)-5 (**3a**)	9863 ± 907	24 ± 6	2.5 ± 0.3
Man(1,6,7)-7[1] (**3b**)	6816 ± 1220	57 ± 13	8 ± 1
Man(1,4,7)-8 (**3c**)	8148 ± 1406	36 ± 7	4.5 ± 0.5
Trivalent (thiol-ether triazole linker)			
Man(all)S-3[1] (**3S**)	22372 ± 3296	32 ± 5	1.4 ± 0.1
Man(1,3,5)S-5 (**3aS**)	15435 ± 4512	52 ± 20	3.3 ± 0.9
Man(1,6,7)S-7 (**3bS**)	21280 ± 3838	35 ± 8	1.6 ± 0.2
Man(1,4,7)S-8 (**3cS**)	16471 ± 2289	43 ± 7	2.6 ± 0.2
Trivalent (benzyl triazole linker)			
Man(all)B-3[1] (**3B**)	122107 ± 43663	13 ± 7*	0.11 ± 0.03*
Man(1,3,5)B-5[1] (**3aB**)	109083 ± 31723	17 ± 6*	0.15 ± 0.04*
Man(1,6,7)B-7[1] (**3bB**)	33075 ± 5740	28 ± 6	0.8 ± 0.1
Man(1,4,7)B-8[1] (**3cB**)	71177 ± 18512	21 ± 7	0.3 ± 0.1
Pentavalent (ethyl triazole linker)			
Man(all)-5[1] (**4**)	70099 ± 27773	17 ± 9	0.2 ± 0.1*
Man(1,3,5,7,9)-9[1] (**4a**)	131697 ± 45834	15 ± 7	0.12 ± 0.04*
Man(1,4,7,10,13)-13[1] (**4b**)	78106 ± 24964	17 ± 7	0.2 ± 0.1*
Pentavalent (thiol-ether triazole linker)			
Man(all)S-5 (**4S**)	11160 ± 1954	27 ± 6	2.4 ± 0.3
Man(1,3,5,7,9)S-9 (**4aS**)	27058 ± 10270	17 ± 8	0.6 ± 0.2
Pentavalent (benzyl triazole linker)			
Man(all)-5B (**4B**)	211772 ± 91094	11 ± 7*	0.05 ± 0.02*
Man(1,3,5,7,9)B-9 (**4aB**)	553986 ± 72055	28 ± 9*	0.05 ± 0.01*
Decavalent (ethyl triazole linker)			

Man(all)-10 (**5**)	624181 ± 197756	28 ± 8	$0.05 \pm 0.01^*$
Decavalent (thiol-ether triazole linker)			
Man(all)S-10 (**5S**)	244591 ± 123398	$42 \pm 29^*$	$0.2 \pm 0.1^*$
Decavalent (benzyl triazole linker)			
Man(all)B-10[1] (**5B**)	2602403 ± 893615	$45 \pm 25^*$	$0.02 \pm 0.01^*$

[a] Mean association rate constant $\overline{k_{on,g}}$ is reported in M^{-1} s^{-1}. [b] Mean dissociation rate constant $\overline{k_{off,g}}$ is reported in s^{-1}. Rate constants were determined by fitting the ITC raw data from every heat flow signal, following the relaxation period for every injection of the ligand L (kinITC method, see Chapter 3.4 and Experimental Part). Errors in the rate constants correspond to true uncertainties, following error propagation as described by Butcher *et al.*[164] and in the Experimental Part. [c] Dissociation equilibrium constant $\overline{K_d}$ is reported in μM and was determined from the same ITC experiments used to determine the thermodynamic parameters. Errors in $\overline{K_d}$ refer to the error propagation of thermodynamic parameters as described in the Experimental Part. "*" marks ITC measurements whose $\bar{c}$ − values are outside the traditional range (as described in Chapter 3.4.1). For $\bar{c}$ − values, see Table 4 and 5. The weighted average rate constants refer to weighted average values of all of the heat flow profiles from one measurement (see also Experimental Part). Measurements were performed in LBB pH 7.40 ± 0.01 at 298.15 K, with Con A obtaining its dimer-tetramer equilibrium conformation[131, 223].

First, taking a look at the k_{on} and k_{off} values for glycomacromolecules binding to dimer Con A (Figure 39, A and Figure 40 A), there is a clear increase in k_{on} values with the structural valency. Thus, the decrease in the dissociation equilibrium constant (K_d), indicating higher binding affinities, is a result of higher on-rates as one moves from mono- to decavalent glycomacromolecules. In contrast, k_{off} values show rather a small or almost no increase with the valency. Consistent with the higher binding affinity, as was observed in their thermodynamic signatures, k_{on} values of benzyl triazole carrying compounds are higher, followed then by the longer thiol-ether triazole and the ethyl triazole linker containing glycomacromolecules. The opposite trend is found for the k_{off} values, with the ethyl triazole containing compounds having highest values in k_{off} and the benzyl triazole linked molecules obtaining the lowest values in k_{off}. In contrast to the αMan linkers, which strongly impact the binding kinetics and show a clear trend regarding the on- and off-rates, there is no such clear trend for the αMan density.

Further, as one moves from mono- to decavalent systems, enhancement in binding affinity seems to result from relatively high and fast association and dissociation rates (Figure 39, A and Figure 40, A, Table 8). In a simplified picture of such binding kinetics, the k_{on} value is an intrinsic property of the individual carbohydrate ligands involved in the interaction with the protein. k_{on} is high, when there are individual favorable interactions. k_{off} also heavily depends on the interactions in the bound state. Here, k_{off} is low, when there are strong individual interactions or an effect that stabilizes these[235]. In this case, the system has to overcome a significant energy barrier for unbinding (a process that is unfavorable in terms of enthalpy, but favorable in terms of entropy). If however, k_{off} does not change significantly with an increasing valency, then there can be many weak interactions contributing to binding, as is observed in this study.

The here described behavior in k_{on} and k_{off} values pinpoints at a rebinding event, where due to each of those weak binding interactions of individual αMan ligands, a constant binding, unbinding and rebinding occurs. This finding is in agreement with Hunter[107-108] and Anderson[108] as well as

recent theoretical calculations by Weber *et al.*[110], who have shown that in such intermolecular and weak interactions, there is significant population of partially bound states in the early step of the association (before system reaches thermodynamic equilibrium). Here, the individual interactions may be broken one after the other with relatively small cost in energy.
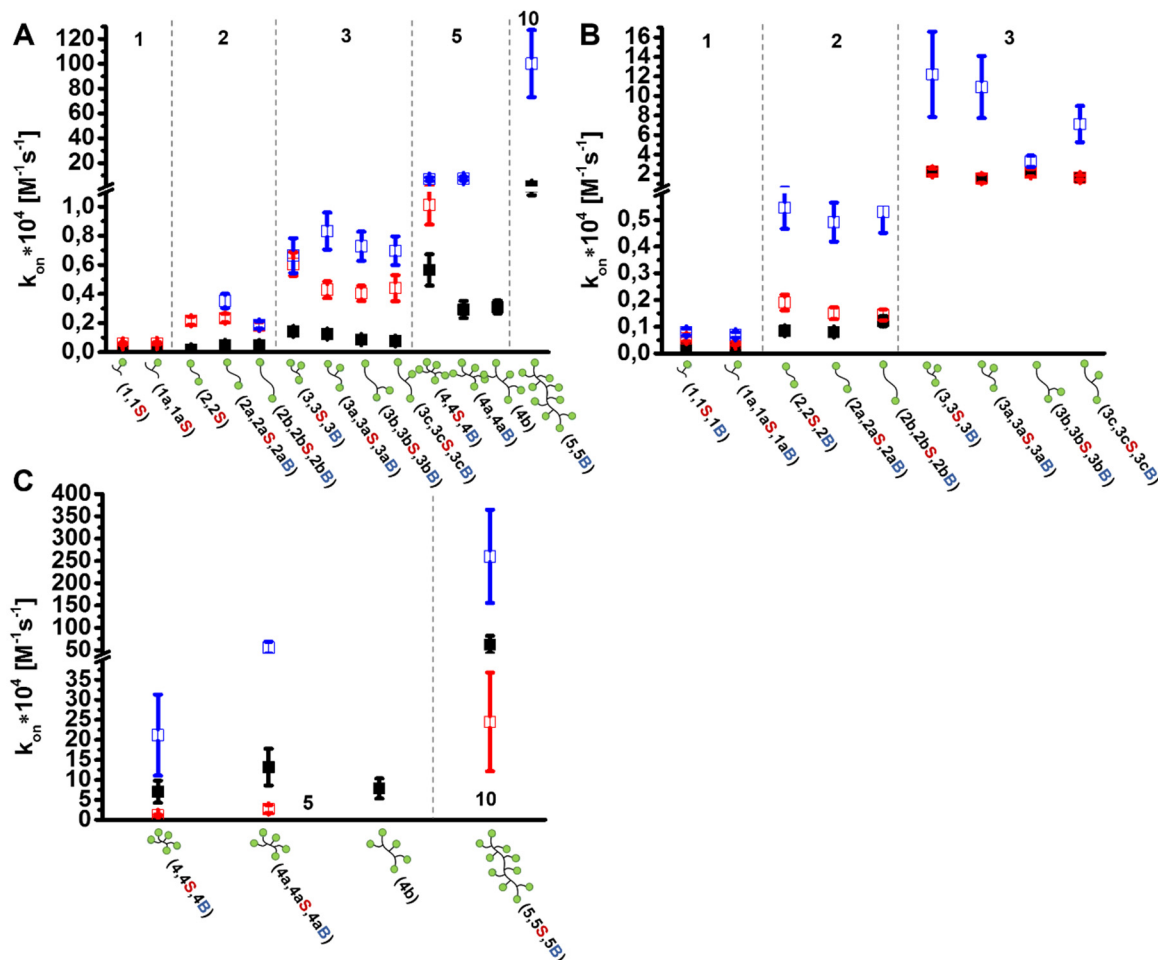
Figure 39. Kinetic association rate constants k_{on} obtained for glycomacromolecules, carrying the different αMan linkers and their binding to dimer (A) and tetramer Con A (B and C).

Although it is generally believed that the association rate constant (k_{on}) would not change significantly in a rebinding event, while the dissociation rate constant (k_{off}) would be slowed if proximity effects occurred, this study shows – in agreement with theoretical calculations of Weber *et al.*[110] – that the on-rate constants increases significantly with the valency, while the off-rate constant would more or less remain in the same range. This behavior of the rate constants is a result of fast dissociation and re-association during the course of an increasing ligand concentration. Because binding at individual binding sites is weak, fluctuations between free and bound states make the interaction accessible to interchanging kinetics, thereby occupying partially bound states. Further, due to the adjacent ligands attached to one scaffold and near the protein's

binding pocket, there is a higher statistical chance that these processes occur as the valency of the molecule increases.

The binding of glycomacromolecules with tetramer Con A (Figure 39 B, C and Figure 40, B) shows a slightly different behavior of the rate constants. In this case, k_{on} values show an exponential dependency on the structural valency. Therefore, from the presented results, glycomacromolecules that bind to tetramer Con A seem to benefit from significantly higher k_{on} values. Overall, it can be assumed that the increase in valency of both, the glycomacromolecules and Con A, lead to a higher probability of a binding event and thus a pronounced increase in the k_{on} values. Further, with respect to the αMan linker, the benzyl triazole linked compounds show highest increase in k_{on} values (a similar trend was observed for glycomacromolecules binding to dimer Con A). Although glycomacromolecules binding to dimer Con A showed clear differences in the k_{on} values for the thiol-ether triazole and the ethyl triazole linker (with the ethyl triazole linker having the lowest increase in the k_{on} values; B >S > ethyl triazole linker), k_{on} values for these compounds binding to tetramer Con A do not exhibit such significant differences. For the thiol-ether triazole and ethyl triazole linked glycomacromolecules binding to tetramer Con A, k_{on} values rather stay in the same range (with slightly elevated k_{on} values for mono- to divalent compounds), whereas for their higher valent analogues (penta- to decavalent) even the reverse situation applies. Here, the k_{on} values for the ethyl triazole linked glycomacromolecules are higher than those of the thiol-ether triazole αMan linkers.

In contrast to the k_{on} values of glycomacromolecules binding to tetramer Con A, the k_{off} values show a slightly different trend in dependence of the αMan linkers (Figure 39 B, C and Figure 40, B). All of the k_{off} values for the thiol-ether triazole and ethyl triazole linked glycomacromolecules are in the same range, with k_{off} (S) $\approx k_{off}$ (ethylene), while the benzyl linked glycomacromolecules again show the lowest dissociation rates (k_{off}(S) $\approx k_{off}$(ethylene) $> k_{off}$(B)), representative for the longest complex life-time. The situation, however, changes for the penta- and decavalent compounds, where k_{off} values of all the glycomacromolecules stay in the same range (k_{off}(S) $\approx k_{off}$(ethylene) $\approx k_{off}$(B)). If the k_{off} values of glycomacromolecules binding to tetramer Con A are compared to those binding to dimer Con A, the following general trend is found. For compounds with the benzyl and thiol-ether triazole linker, k_{off} values stay in the same order of magnitude with those of dimer Con A. In contrast to those, compounds with the short ethyl triazole linker have significantly reduced k_{off} values as compared to those of dimer Con A. As a result, the binding of these ethyl triazole linked glycomacromolecules to tetramer Con A is accompanied by an exponential increase in the on-rates and further also profits from reduced k_{off} values, indicating a longer overall residence time of the complexes. Also, in contrast to glycomacromolecules that bind to dimer Con A, where both of the kinetic rate constants are rather elevated, the binding of the glycomacromolecules to tetramer Con A exhibits exponentially increasing k_{on} values accompanied by k_{off} values, which rather stay in the lower range (ethyl triazole linker) and do not raise with the k_{on} values (benzyl triazole and thiol-ether triazole linker).

Overall, the observed trends in on- and off-rate constants for glycomacromolecules binding to tetramer Con A are a strong indication for the binding and sliding mechanism. In this case, earlier studies[106] have shown that the binding of multivalent compounds is more similar to a random-walk of the compounds through the cross-linked proteins. This binding and sliding mechanism is very representative in binding processes, where cross-linked protein molecules are involved, which is the case for the here presented systems binding to tetramer Con A. The kinetic picture of such processes is characterized by accelerated k_{on} values and either k_{off} values, which stay in the same region (but do not raise) or even reduce with the facilitated k_{on} values. Hence, for the presented glycomacromolecules in binding to tetramer Con A, it can be assumed that this mechanism might be the origin of the observed trends in the kinetic study.
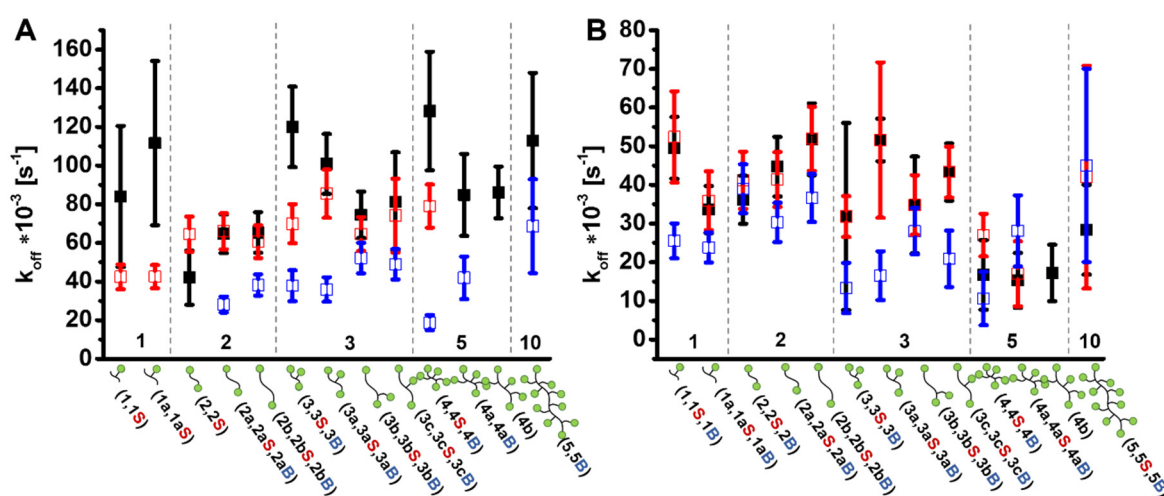

Figure 40. k_{off} values for glycomacromolecules binding to dimer (A) and tetramer Con A (B).

3.5.12. Transition state parameters of exemplary glycomacromolecules with different linkers

As so far the thermodynamic and the kinetic parameters were able to describe the binding processes, in a further attempt to gain a more detailed mechanistic inside, the transition state parameters were evaluated. Since the thermodynamic parameters are state functions, which only describe the difference between the bound and unbound state, and kinetic parameters depict the way between those states, the transition state relates the kinetic with the thermodynamic quantities, which then help to get a more detailed picture of the binding process. To get insight into the transition state quantities, the kinetic rate constants, the on- and off-rates, were ascertained at different temperatures, specifically at 298.15 K, 303.15 K and 308.15 K. Therefore, the isothermal titration of the selected glycomacromolecules to the Con A tetramer was measured at these temperatures. The kinetic rate constants were determined from each of the obtained binding isotherms, measured at different temperatures by using the kinITC method (see Chapter 3.4, Experimental Part and Appendix). The transition state parameters were then obtained using the

Eyring equation (14)[236]. Here, the activation enthalpy was first determined from an Eyring Plot, following the transition state theory[236]. Through the Eyring equation, the kinetic on- and off-rate constants were related to the thermodynamic parameters as follows:

$$k = \frac{k_B T}{h} \exp\left(-\frac{\Delta G^\ddagger}{RT}\right) = \frac{k_B T}{h} \exp\left(-\frac{\Delta H^\ddagger}{RT} + \frac{\Delta S^\ddagger}{R}\right), \tag{14}$$

where $h = 6.626\cdot10^{-34}$ J·s is Planck's constant and $k_B = 1.3806\cdot10^{-23}$ J·K^{-1} is the Boltzmann constant. Here, $\Delta G^\ddagger$ is the activation free energy and thus the energy barrier that must be overcome for the multivalent glycomacromolecule (L) and Con A (P) to associate into a complex or for the complex L·P to readily dissociate. As such, this energy barrier is directly related to the rate of association (k_{on}) and the rate of dissociation (k_{off}), which were determined for each of those three temperatures. The temperature dependence of the rate constants was then used to determine the transition state enthalpy $\Delta H^\ddagger$, following the linear expression of equation (14):

$$\ln\left(\frac{k}{T}\right) = -\frac{\Delta H^\ddagger}{RT} + \frac{\Delta S^\ddagger}{R} + \ln\left(\frac{k_B}{h}\right) = -\frac{\Delta H^\ddagger}{RT} + \frac{\Delta S^\ddagger}{R} + \ln(\alpha). \tag{15}$$

The transition state enthalpy $\Delta H^\ddagger$ was calculated from the slope ($a = -\frac{\Delta H^\ddagger}{R}$) of a plot $\ln\left(\frac{k}{T}\right)$ *versus* the inverse temperature. Further, k represents either $k = k_{on}$ or $k = k_{off}$, which were used to determine the transition state enthalpy for the association and the dissociation process, with $\Delta H^\ddagger = \Delta H^\ddagger_{on}$ and $\Delta H^\ddagger = \Delta H^\ddagger_{off}$, respectively. Although the y-intercept contains the entropy term ($b = \frac{\Delta S^\ddagger}{R} + \ln(\alpha)$) and the pre-exponential term (α) from which the transition state entropy $\Delta S^\ddagger$ can be obtained, calculation of $\Delta S^\ddagger$ was not performed here in this way, because the y-intercept is known to be a large extrapolation of $\Delta S^\ddagger$, which is assumed with a large error in estimating $\Delta S^\ddagger$.[237]

After the calculation of the transition state enthalpies of the on- and off-processes ($\Delta H^\ddagger_{on}$ and $\Delta H^\ddagger_{off}$), the activation free energies, $\Delta G^\ddagger_{on}$ and $\Delta G^\ddagger_{off}$, were directly determined from the Eyring equation (16):

$$\Delta G^\ddagger = RT\left[\ln\left(\frac{k_b T}{h}\right) - \ln(k)\right] \tag{16}$$

The rate constant k again corresponds to either the weighted averaged k_{on} or k_{off} values, which were determined with the kinITC method (as described above) at every temperature. $\Delta G^\ddagger_{on}$ or $\Delta G^\ddagger_{off}$, were calculated from the weighted average values of the k_{on} and k_{off} rate constants that cover the three temperatures, and the error in $\Delta G^\ddagger_{on}$ or $\Delta G^\ddagger_{off}$ is given as the error of the weighted average (for a detailed description, see Experimental Part). The transition state entropy for the on- or off-state, $-T\Delta S^\ddagger_{on}$ or $-T\Delta S^\ddagger_{off}$, was then simply calculated using the Gibbs-Helmholtz equation.

$$T\Delta S^{\ddagger} = \Delta H^{\ddagger} - \Delta G^{\ddagger} \qquad (17)$$

The transition state parameters were determined for representative glycomacromolecules carrying the ethyl triazole, the thiol-ether triazole and the benzyl triazole linkers. To only account for the linker influence on the transition state parameters, the binding of monovalent compounds with the three different linker types to tetramer Con A were measured, and the transition parameters then determined as described above. To further account for the evolution of the multivalent effect, the binding of trivalent compounds to tetramer Con A was measured analogously. The different transition states can simply be separated into the on- and off- transition states and their Gibbs free energy, enthalpy and entropy of activation. These two states describe the way and the energetic height that separates the unbound and the transition state, as well as the transition state and the bound state.

Table 10 shows the evolution of the ITC derived kinetic parameters (weighted average rate constants) with the three different temperatures (298.15 K, 303.15 K and 308.15 K), required for the determination of the transition state enthalpies of the on- and off-processes ($\Delta H^{\ddagger}_{on}$ or $\Delta H^{\ddagger}_{off}$) using the Eyring plot (15) and the activation free energies, $\Delta G^{\ddagger}_{on}$ or $\Delta G^{\ddagger}_{off}$, using the Eyring equation (16). For calculation of the activation free energies $\Delta G^{\ddagger}_{on}$ or $\Delta G^{\ddagger}_{off}$, using the Eyring equation (16), the weighted average k_{on} and k_{off} values were combined to one weighted average k_{on} and k_{off} value (thus weighted over their uncertainties at the given temperature range). The substitution of these values into the Eyring equation (16) allowed then the calculation of $\Delta G^{\ddagger}_{on}$ or $\Delta G^{\ddagger}_{off}$ (see also Experimental Part). Table 11 shows the on- and off- transition state parameters that were determined, using the Eyring equation (16) for the compounds 1, 1S, 1B and 3a, 3aS and 3aB, while Figure 41 presents the Eyring plots of mono- and trivalent glycomacromolecules, which allowed the calculation of the on- and off- activation enthalpies ($\Delta H^{\ddagger}_{on}$ or $\Delta H^{\ddagger}_{off}$).

For the error propagation in $\Delta H^{\ddagger}_{on}$ or $\Delta H^{\ddagger}_{off}$ and $-T\Delta S^{\ddagger}_{on}$ or $-T\Delta S^{\ddagger}_{off}$, the method by Girolami *et al.*[238] was used, that further accounts for the errors in the minimum and maximum rate constants, as well as errors in the minimum and maximum temperatures and present true uncertainties (see Experimental Part.) The errors in $\Delta G^{\ddagger}_{on}$ or $\Delta G^{\ddagger}_{off}$ were calculated from the error of the weighted average rate constants (see Table 10, right columns), which were weighted over the three rate constants evolving with temperature (see Experimental Part).

Table 10. Evolution of ITC derived kinetic rate constants of glycomacromolecules with different linkers measured at different temperatures (298.15 K, 303.15 K, 308.15 K), allowing for determination of activation Gibbs free binding energy $\Delta G^{\ddagger}_{on/off}$, transition state enthalpy $\Delta H^{\ddagger}_{on/off}$ and entropy $-T\Delta S^{\ddagger}_{on/off}$ using the Eyring equation (16) and Eyring plot (15), respectively.

Ligand	$\overline{k_{on,g}}$ [a]	$\overline{k_{off,g}} \cdot 10^{-3}$ [b]	$\overline{k_{on,g,dT}}$ [c]	$\overline{k_{off,g,dT}} \cdot 10^{-3}$ [c]
Monovalent (ethyl triazole linker)				
Man(3)-5 (**1**) 25°C	223 ± 32	49 ± 8	214 ± 18	55 ± 5
Man(3)-5^1 (**1**) 30°C	212 ± 31	57 ± 9	–	–
Man(3)-5^1 (**1**) 35°C	209 ± 30	65 ± 10	–	–
Monovalent (thiol-ether triazole linker)				
Man(3)S-5^1 (**1S**) 25°C	560 ± 102	52 ± 12	197 ± 32	37 ± 7
Man(3)S-5^1 (**1S**) 30°C	240 ± 70	35 ± 14	–	–
Man(3)S-5^1 (**1S**) 35°C	132 ± 39	26 ± 10	–	–
Monovalent (benzyl triazole linker)				
Man(3)B-5^1 (**1B**) 25°C	802 ± 122	26 ± 5	820 ± 73	31 ± 3
Man(3)B-5^1 (**1B**) 30°C	822 ± 124	34 ± 6	–	–
Man(3)B-5^1 (**1B**) 35°C	840 ± 133	45 ± 8	–	–
Trivalent (ethyl triazole linker)				
Man(1,3,5)-5 (**3a**) 25°C	9863 ± 1907	24 ± 6	7296 ± 885	30 ± 4
Man(1,3,5)-5 (**3a**) 30°C	7305 ± 1246	37 ± 7	–	–
Man(1,3,5)-5 (**3a**) 35°C	5308 ± 1671	60 ± 26	–	–
Trivalent (thiol-ether triazole linker)				
Man(1,3,5)S-5^1 (**3aS**) 25°C	15435 ± 4512	52 ± 20	10238 ± 1836	45 ± 10

Man(1,3,5)S-5 (**3aS**) 30°C	12578 ± 3687	44 ± 17	−	−
Man(1,3,5)S-5[1] (**3aS**) 35°C	7780 ± 2398	41 ± 17	−	−
Trivalent (benzyl triazole linker)				
Man(1,3,5)B-5[1] (**3aB**) 25°C	109083 ± 31723	17 ± 6*	67398 ± 11223	13 ± 3*
Man(1,3,5)B-5[1] (**3aB**) 30°C	70522 ± 19069	14 ± 5*	−	−
Man(1,3,5)B-5[1] (**3aB**) 35°C	55480 ± 15438	10 ± 4*	−	−

[a] Mean association rate constant $\overline{k_{on,g}}$ is reported in M⁻¹ s⁻¹. [b] Mean dissociation rate constant $\overline{k_{off,g}}$ is reported in s⁻¹. Rate constants were determined by fitting the ITC raw data from every heat flow signal, following the relaxation period for every injection of the ligand L (kinITC method, see Chapter 3.4 and Experimental Part). Errors in the rate constants correspond to true uncertainties, following error propagation as described by Butcher *et al.*[164] and in the Experimental Part. Rate constants were determined at different temperatures (298.15 K, 303.15 K, 308.15 K), allowing for the calculation of the activation enthalpy $\Delta H^{\ddagger}_{on/off}$ from the Eyring plot. [c] Weighted average $\overline{k_{on,g,dT}}$ and $\overline{k_{off,g,dT}}$ values allowed for the determination of the activation free energy $\Delta G^{\ddagger}_{on/off}$ directly from the Eyring equation (16). Their weighted average values were determined from the $\overline{k_{on,g}}$ and $\overline{k_{off,g}}$ values at different temperatures. Errors in the weighted averaged $\overline{k_{on,g,dT}}$ and $\overline{k_{off,g,dT}}$ values correspond to the error of the weighted average, as described in the Experimental Part. "*" marks ITC measurements whose $\bar{c}$ − values are outside the traditional range (as described in Chapter 3.4.1). All kinetic quantities refer to best weighted average values from *n* series of measurements, expect for measurements, which were performed one time (those are highlighted with "1"). Here, the weighted average rate constants refer to weighted average values of all of the heat flow profiles from one measurement (see also Experimental Part). Measurements were performed in LBB pH 7.40 ± 0.01 at 298.15 K, with Con A obtaining its dimer-tetramer equilibrium conformation[131, 223].

Table 11. Transition state parameters for the on- and the off-transition state. Representative on- and off-rates were determined at 298.15 K, 303.15 K, 308.15 K. The transition state parameters were then determined from the Eyring plot (15) and the Eyring equation (16) as described above (see also Experimental Part).

Ligand	$\Delta G^{\ddagger}_{on}$ [a]	$\Delta H^{\ddagger}_{on}$ [a]	$-T\Delta S^{\ddagger}_{on}$ [a]	$\Delta G^{\ddagger}_{off}$ [b]	$\Delta H^{\ddagger}_{off}$ [b]	$-T\Delta S^{\ddagger}_{off}$ [b]
Monovalent (ethyl triazole linker)						
Man(3)-5 (**1**)	+59.7 ± 0.2	−7 ± 9	+67 ± 9	+80.2 ± 0.2	+19 ± 10	+62 ± 10
Monovalent (thiol-ether triazole linker)						
Man(3)S-5 (**1**)	+59.9 ± 0.4	−115 ± 24	+175 ± 23	+81.2 ± 0.5	−57 ± 21	+139 ± 21

Monovalent (benzyl triazole linker)						
Man(3)B-5 (**1**)	+56.4 ± 0.2	+1 ± 10	+55 ± 10	+81.6 ± 0.3	+41 ± 13	+41.0 ± 13
Trivalent (ethyl triazole linker)						
Man(1,3,5)-5 (**3a**)	+51.0 ± 0.3	−49 ± 15	+100 ± 15	+81.7 ± 0.4	+65 ± 19	+16 ± 18
Trivalent (thiol-ether triazole linker)						
Man(1,3,5)S-5 (**3a**)	+50.1 ± 0.4	−54 ± 21	+104 ± 20	+80.7 ± 0.6	−20 ± 25	+101 ± 24
Trivalent (benzyl triazole linker)						
Man(1,3,5)B-5 (**3a**)	+45.5 ± 0.4	−54 ± 20	+99 ± 19	+83.9 ± 0.5	−38 ± 24	+122 ± 24

[a] Activation Gibbs free binding energy $\Delta G^{\ddagger}_{on/off}$, transition state enthalpy $\Delta H^{\ddagger}_{on/off}$ and entropy $-T\Delta S^{\ddagger}_{on/off}$ are reported in kJ mol⁻¹. Errors in $\Delta G^{\ddagger}_{on/off}$, $\Delta H^{\ddagger}_{on/off}$ and $-T\Delta S^{\ddagger}_{on/off}$ follow error analysis as described in the Experimental Part. Activation Gibbs free binding energy $\Delta G^{\ddagger}_{on/off}$ and transition state entropy $-T\Delta S^{\ddagger}_{on/off}$ are reported for the standard state temperature (298.15 K).
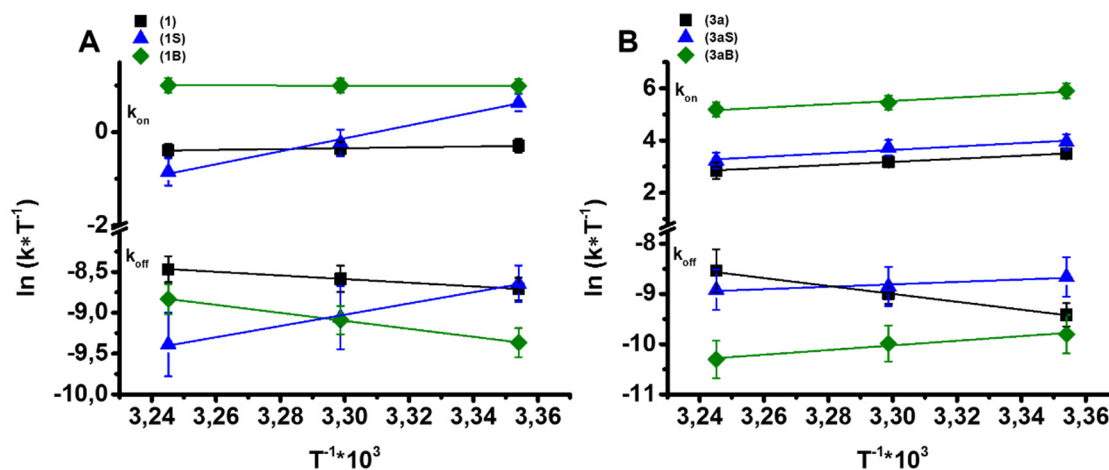
Figure 41. Eyring plots for determination of the activation enthalpy of the mono- (A) and trivalent compounds (B) with different αMan linkers.

The energy level diagrams of the binding processes of mono- and trivalent compounds, associating to tetramer Con A are summarized in Figure 42, A, B and C.

When these monovalent compounds in their binding to tetramer Con A are compared, then it is readily seen that the activation free energy for the on-state lies in the same range for 1 and 1S (Figure 42, A and Table 11). In contrast to those two, the monovalent compound carrying the benzyl triazole linker 1B lowers the energy barrier by about -4 kJ mol^{-1}. This makes the overall association process more favorable for 1B, as compared to 1 and 1S. Although there is a clear difference in the energetic contributions of the on-state between 1, 1S and 1B, the off-transition state (dissociation of the complexes) shows similar activation free energy values. This suggests that the association process more dramatically influences the association energy barriers, as compared to the dissociation processes. Here, the energetic value of the dissociation energy of compound 1 shows that its complex stability with tetramer Con A is only marginally weaker, by about $+1$ to $+2$ kJ mol^{-1}, compared to 1S and 1B, respectively. With respect to the trend of the different αMan linkers, their activation free energy further demonstrate what has already been seen in the last subchapters. The binding of glycomacromolecules carrying benzyl triazole linkers is significantly favored over the binding of compounds carrying the thiol-ether triazole or ethyl triazole linkers.

If one compares now the mono- to the trivalent species 3a, 3aS and 3aB, the impact of an increased binding affinity due to additivity can directly be seen (Figure 42, B, C and Table 11). Regarding the Gibbs activation energy, the energy barrier of the trivalent species is now lowered by about -9 to -10 kJ mol^{-1} for 3a, 3aS and 3aB, respectively. This is most likely due to the additional number of αMan ligands. At the same time, the energy barrier for the unbinding process increases by about $+2$ kJ mol^{-1}, thereby prolonging the complex half-life. The same trend for the activation free energy that was already observed for the monovalent glycomacromolecules, was also found for the trivalent species, where the Gibbs activation energy is lowered in the order 3a > 3aS > 3aB. The difference in the activation barrier between 3aB and the other two ligands 3a

and 3aS, is again more pronounced as just for 3a and 3aS, where the activation free energy is rather similar with −1 kJ mol⁻¹ for the latter, while compound 3aB shows a lower energy barrier of about −4 kJ mol⁻¹.
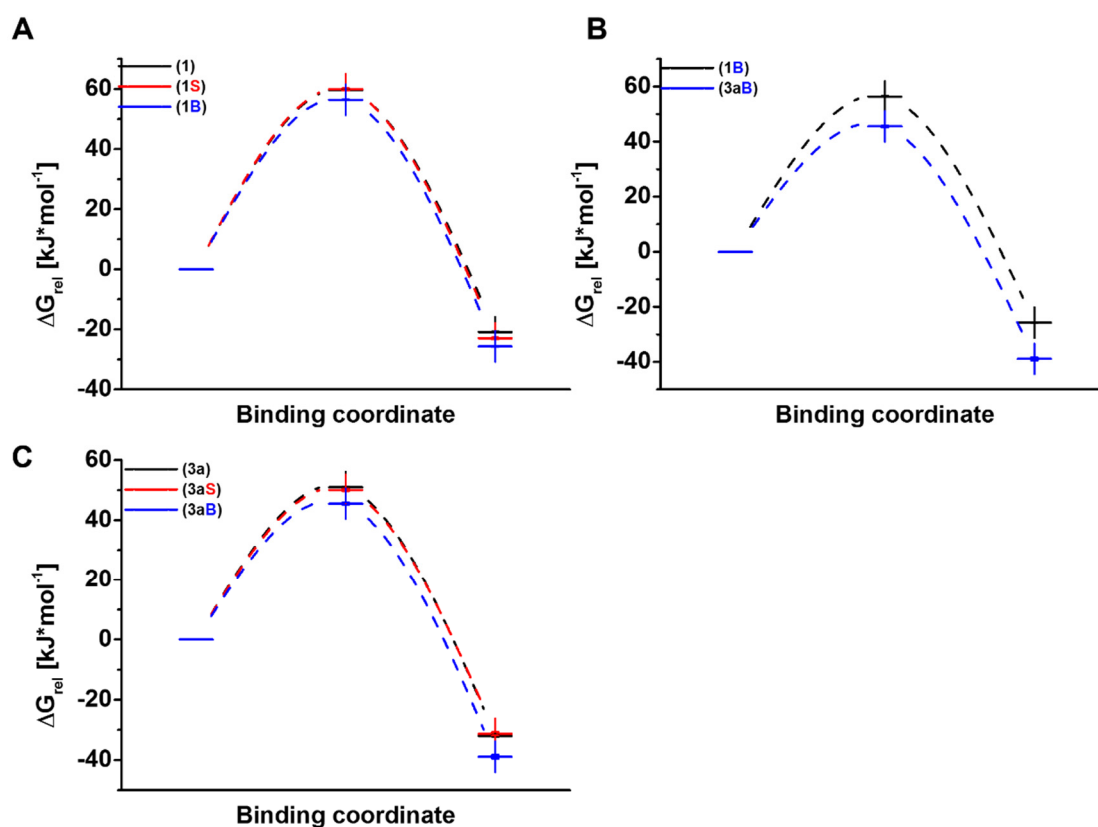

Figure 42. Energy diagrams with respect to the activation free energy $\Delta G^{\ddagger}$ for mono- (A) and trivalent glycomacromolecules (C) with different αMan linkers binding to tetramer Con A, and the comparison of the energetic evolution between the mono- to trivalent species (B).

For compounds 1 and 1B, it can be seen that their activation enthalpy is in the same order of magnitude, where the activation enthalpy is here more favorable for 1 than for 1B. A clear difference in the activation enthalpy is found for 1S as compared to the other two. Thus, 1S shows the lowest favorable activation enthalpy, followed by 1 and 1B (1S < 1 < 1B). Compared to the activation enthalpy, the reverse development in the activation entropy is found for 1, 1S and 1B. Here, 1S shows the highest energy barrier in activation entropy, followed by 1 and with 1B having the lowest entropic barrier (1S > 1 > 1B). Literature suggests[239] that the activation entropy is often positive and unfavorable for the association process (the reverse applies to the activation enthalpy). This is believed to be a result of either (*i*) the loss of degrees of freedom (such as translational and rotational degrees of freedom) or (*ii*) ascribed to water rearrangements, which may be not optimal for the association state (e.g. resulting in rather highly ordered water molecules).[239] Indeed, for all of the three monovalent species, positive activation entropy terms were found, suggesting one of these entropic processes to be responsible for activation entropy barriers.

If the activation enthalpy and entropy of the mono- and trivalent species are now compared, it can be seen that although 1B has a slightly positive activation enthalpy, the trivalent species 3aB, clearly profits from a lower activation enthalpy value (as opposed by a high energy barrier of the activation entropy). This indicates that for 3aB the on-transition state is favorable due to a negative activation enthalpy, possibly due to the formation of favorable interactions. In contrast, the activation entropy is highly unfavorable. From the determination of the entropic terms (see Chapter 3.5.9), it was found that the relatively unfavorable entropy was due to the entropy of configuration, whereas the solvation entropy was favorable for this binding process. Therefore, the origin of the high entropic barrier of 3aB might be due to an improper arrangement of the αMan ligands in the bound state and an unfavorable conformation of the glycomacromolecule that it adopts during binding. Inspection of the activation free energy for trivalent compounds with different linkers binding to tetramer Con A shows that for all of the three species, the activation enthalpies (Table 11) seem to be more or less in the same range for the on-state, where 3a has the highest energy barrier compared to 3aS and 3aB, whose activation enthalpies are in the same range. In all of the three compounds, it is the entropic energy barrier that is the origin for the activation free energy barrier for the on-transition state. Although the enthalpic barriers for the trivalent compounds are in the same range, compound 3aB exhibits a lower activation free energy barrier, of about -4 kJ mol^{-1}. The reason for its lower energy barrier lies in the activation entropy. Although, the entropic barrier is relatively high for all of the three compounds, the activation entropy of 3aB is lower by about -4 kJ·mol^{-1} compared to 3aS, making the interactions of this ligand and Con A more favorable. Compared to 3a, there is no significant lowering in the entropic barrier for 3aB (-1 kJ mol^{-1}). Instead, here it is the lower enthalpic barrier (-5 kJ mol^{-1}) that makes 3aB the best compound in binding to tetramer Con A. Therefore, there is a fine balance between those two energetic terms that lowers the overall activation free energy.

Altogether, for the on- and the off-states, it was seen that the energetic states are highly linker dependent. The influence of the linker, when presented multivalent, was further demonstrated to lower the energy barriers, thereby making an association for the protein and the ligands more probably in terms of binding kinetics. Further, the association energy barriers for mono- and trivalent species once again indicated the lowering of the energy barriers to be most likely a result of additivity.

3.6. Influence of linear and cyclic architectures on multivalent thermodynamics and (rebinding) kinetics

In the last chapter, it was shown that linear precision glycomacromolecules have been used successfully as model compounds to study multivalent binding to the lectin receptor Con A. The results for these linear glycomacromolecules, which varied in their spacer as well as linker, have shown that their binding to dimer and tetramer Con A strongly depends on the linker composition

and valency. In contrast, an altering ligand density did not dramatically alter the binding affinity, e.g. resulting in similar binding free energy values.

For the multivalent binding of glycopolymers to proteins, it has been further reported that a different polymer architecture[24-25, 32-33, 90, 106] may alter the binding affinity, e.g. by differences in the size and hydrodynamic radii as a result of different possible conformations or presentation of the multivalent ligands (compare linear polymers[24, 32-33, 55, 106], dendrimers[24, 33, 38, 47], dendrons[24, 32-33, 47], etc.[24, 32-33]). Other variations in the architecture include star-shaped[32, 75, 90], coil-coiled[32, 90] and cyclic polymers[240-244]. Cyclization of linear architectures has been shown to affect the properties of polymers through different effects[240-241, 243-245]. (*i*) The switch from a linear to a cyclic architecture is motivated by a certain change in the conformation, which leads to a desirable presentation of the carbohydrate ligands, as has been shown for cyclic multivalent glycopeptides binding to Wheat Germ Agglutinin (WGA) by Wittman *et al.*[36, 79]. (*ii*) The cyclic architecture might further dramatically differ from its linear counterpart by other dynamic properties[240, 245-248], which affect their behavior in solution[240-241, 245]. It has been reported[240] that the random-coiled behavior of linear and cyclic polymers differs dramatically.[240-241, 245] For instance, the hydrodynamic mean radius (R_h) as well as the hydrodynamic volume (V_h) are considered to be significantly smaller for cyclic polymers.[240, 245] As their diffusion properties are directly affected by these quantities, it has been hypothesized that the shape and topology of linear and cyclic architectures directly affects their diffusion behavior.[240-241, 245] While the diffusion behavior of linear polymers rather resembles a snake-like motion, cyclic polymers are believed to move in an amoeba-like fashion[246].[240] For both diffusion behaviors of linear and cyclic polymers, the presence or absence of chain ends is critical.[240-241, 245] Thus, a different architecture, in terms of a linear *versus* a cyclic one, is thereby believed to control the polymer properties and thus their behavior in solution[240].

So far, differences in the binding to proteins have been only studied with above mentioned glycopolymer architectures (compare Kiessling *et al.*[24, 33, 56], Haddleton *et al.*[55, 59] and Stenzel *et al.*[75]). From these studies, it was then hypothesized that the changing polymer architecture dramatically alters the binding affinity through the adoption of different multivalent binding modes. Such multivalent binding modes are not only triggered by the structural features of the different architectures, but also by their solution behavior. Although topological differences between linear and cyclic polymers are well-known, so far no systematic study has been reported, which compares the binding properties of linear and cyclic multivalent polymer architectures. One reason that hinders straightforward access to cyclic glycopolymers is their challenging synthesis, e.g. *via* classical polymer synthesis[242-244]. Besides the intrinsic dispersity of the linear precursor, cyclization in terms of an intramolecular, mono-cyclic process is further complicated by additional cyclic and linear oligomerization by-products[242-243].

With respect to these background information, in this thesis it was therefore investigated whether a switch in the architecture, from linear to cyclic, might affect the binding kinetics and possibly the binding affinity of precision glycomacromolecules. In Part 1 of the Results and

Discussion Part (Chapter 3.2), the synthesis of cyclic precision glycomacromolecules was shown to yield monodisperse and mono-cyclic species. The interactions of cyclic precision glycomacromolecules with dimer and tetramer Con A were quantified using ITC and kinITC experiments, as previously shown for the linear glycomacromolecules. The determined thermodynamic and kinetic quantities were then related to their linear analogues. Similarly to the linear constructs, cyclic glycomacromolecules vary in their valency as well as in their ligand spacing and spacer composition. Furthermore, the ring-size was varied by cyclization of linear precursors of different chain-lengths. It was hypothesized that the ring-size is another important parameter that might mediate the binding process to Con A. As the ring-size of the molecules might affect their Brownian motion and thus their diffusion properties as described above, potentially this might affect the binding process in terms of the binding kinetics. Further, the different binding affinities in terms of thermodynamics might possibly be the result of altering random-coiled conformations, not only due to the different architectures, but also due to a different size.

3.6.1. Ligand design of linear and cyclic glycomacromolecules

To reveal the impact of the cyclic architecture, possibly changing the binding behavior to Con A, a series of cyclic glycomacromolecules were compared to their linear counterparts carrying one to three αMan side chains. A series of eight linear and cyclic glycomacromolecules was synthesized by SPPoS as described in Chapter 3.2, Part 2. The linear and cyclic glycomacromolecules were varied in the spacing from one to four spacer building blocks (Figure 43 and 44). In addition, not only the length of the spacers was changed, but also the spacer composition, allowing to further control the length (Figure 43 and 44). For this purpose the shorter SDS spacer building block was used, which further allows to control the backbone length and ring-size (as compared to EDS).

The ring-size was varied from small (5 building blocks consisting of TDS and SDS sequences), to middle (5 building blocks consisting of TDS and EDS sequences) to larger rings (8 building blocks consisting of TDS and EDS sequences) (Figure 44). The designation of trivalent linear glycomacromolecules (Figure 43) was adapted here (from 3a and 3c to 2 and 2a) to match those of their corresponding cyclic derivatives (2@ and 2a@) (Figure 44). Although the same linear trivalent glycomacromolecules are presented in this chapter, as already has been shown in the synthesis and linker dependency chapter (Chapter 3.1 and 3.5), their previous nomenclature is omitted here.
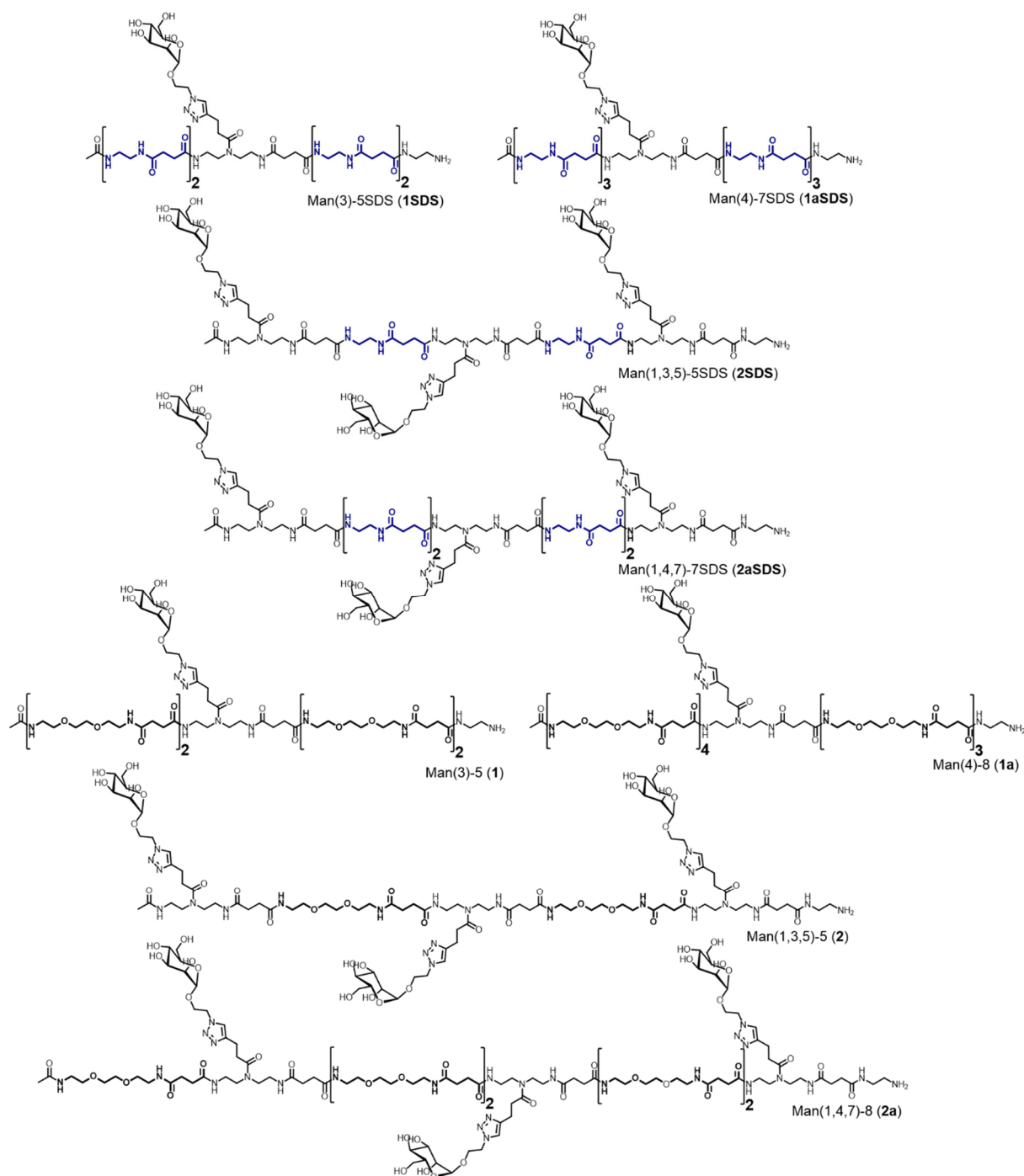
Figure 43. Overview linear glycomacromolecules varying in the backbone and spacer length as well as composition (SDS (highlighted in blue) *versus* EDS (highlighted in bold) spacer building blocks). Glycomacromolecules increase in their spacer length from top to bottom, either for the mono- or trivalent compounds.[8]
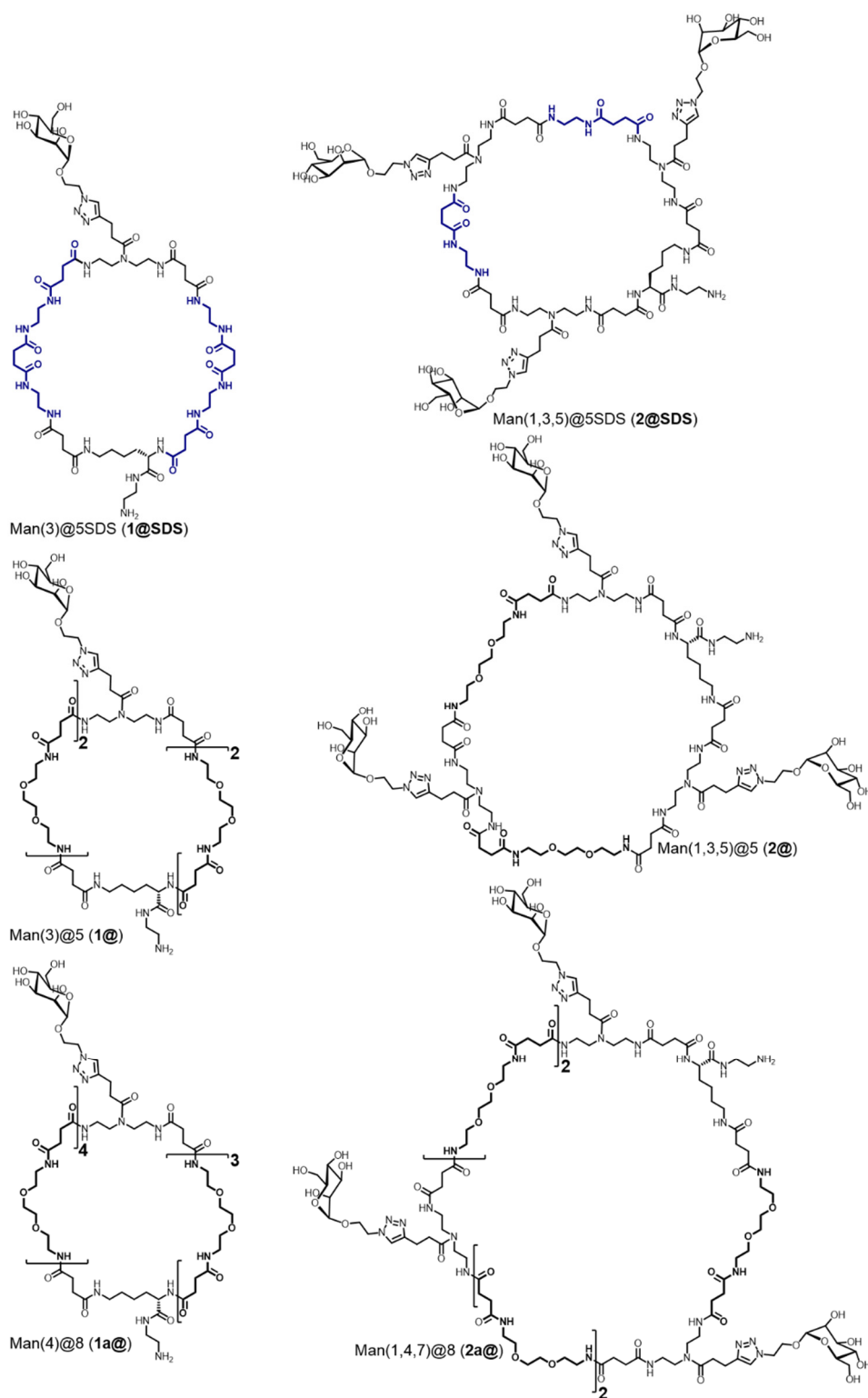
Figure 44. Overview cyclic glycomacromolecules varying in the backbone and spacer length as well as composition (SDS (highlighted blue) *versus* EDS (highlighted bold) spacer building blocks). Glycomacromolecules increase in their ring-size from top to bottom.[9]

---

[9] 1@SDS and 2@SDS were synthesized and characterized (NMR, RP-HPLC and MALDI-TOF) by Andreas Ludwig (Heinrich-Heine-Universität Düsseldorf, group of Prof. Dr. Laura Hartmann, Bachelor Thesis, October 2015). In this thesis, the characterization data of the above mentioned compounds (NMR) has been re-assessed by the author of this thesis.

3.6.2. <u>Influence of the linear and cyclic architectures on the binding thermodynamics</u>

The ITC titration experiments were performed as was described in the previous chapters (see Chapter 3.4), using a normal titration and the *one sets on independent binding sites* model to fit the previously integrated titration/data points. The ITC experiments therefore yielded information on the binding enthalpy ΔH, stoichiometry n and affinity K_d, from which the Gibbs free binding energy ΔG and the binding entropy $-T\Delta S$ were determined according to the Gibbs-Helmholtz equation (1) (see General Introduction, Chapter 1.2.1). Data of the linear and cyclic glycomacromolecules for their binding to dimer and tetramer Con A are shown in Table 12 and Table 13, respectively.

The linear and cyclic monovalent glycomacromolecules were measured[10] and compared, in order to account for the alteration in the architecture as well as the length and the ring-size. Since the thermodynamic values of all monovalent species binding to dimer Con A were similar and independent of the architecture, it was decided that only the monovalent linear species were measured against tetramer Con A. The trivalent linear and cyclic species were compared in the same manner to dimer and tetramer Con A as the monovalent ones.

---

[10]a) ITC measurements of compounds 1SDS, 1aSDS, 2SDS and 2aSDS at 298.15 K have been performed by Hendrik Wöhlk (Heinrich-Heine-Universität Düsseldorf, group of Prof. Dr. Laura Hartmann, Master Thesis, April 2015). In this thesis, the here listed thermodynamic quantities have been re-assessed using the methods and error calculation described in this thesis. Kinetic evaluation of the same binding isotherms has completely and exclusively been performed by the author of this thesis. Their rate constants including their uncertainties are presented in this thesis for the first time. b) ITC measurements of compounds 1@SDS and 2@SDS have been performed by Andreas Ludwig (Heinrich-Heine-Universität Düsseldorf, group of Prof. Dr. Laura Hartmann, Bachelor Thesis, October 2015). In this thesis, the thermodynamic and kinetic quantities previously reported by Andreas Ludwig have been re-assessed using the methods and error calculation described in this thesis.

Table 12. ITC derived thermodynamic binding energetics of linear and cyclic glycomacromolecules with different spacers binding to dimer Con A (measured at 298.15 K).

Ligand	$\overline{FV}$[a]	$\overline{\Delta G}$[b]	$\overline{K_d}$[c]	$\overline{\Delta H}$[b]	$-\overline{T\Delta S}$[b]	$\overline{c}$[d]
Monovalent linear (SDS spacer)						
Man(3)-5SDS (**1SDS**)	0.9 ± 0.1	-23.4 ± 0.2	80 ± 6	-26 ± 2	$+2 \pm 2$	~3
Man(4)-7SDS (**1aSDS**)	0.8 ± 0.1	-22.1 ± 0.3	137 ± 16	-19 ± 1	-3 ± 1	~2
Monovalent linear (EDS spacer)						
Man(3)-5 (**1**)	0.7 ± 0.3	-20.3 ± 0.7	278 ± 82	-29 ± 6	$+9 \pm 6$	~1*
Man(4)-8 (**1a**)	1.0 ± 0.2	-19.7 ± 0.6	361 ± 91	-29 ± 6	$+9 \pm 6$	~1*
Monovalent cyclic (EDS spacer)						
Man(3)@5 (**1@**)	0.9 ± 0.2	-19.4 ± 0.6	395 ± 92	-25 ± 5	$+6 \pm 5$	~0.3*
Man(4)@8 (**1a@**)	1.0 ± 0.2	-20.9 ± 0.5	215 ± 46	-25 ± 5	$+4 \pm 5$	~1*
Trivalent linear (SDS spacer)						
Man(1,3,5)-5SDS (**2SDS**)	1.6 ± 0.4	-23.5 ± 0.5	78 ± 16	-37 ± 11	$+14 \pm 11$	~3
Man(1,4,7)-7SDS (**2aSDS**)	2.1 ± 0.3	-24.5 ± 0.9	52 ± 19	-54 ± 5	$+29 \pm 5$	~4
Trivalent linear (EDS spacer)						
Man(1,3,5)-5 (**2**)	2.1 ± 0.3	-23.3 ± 0.2	82 ± 5	-54 ± 6	$+301 \pm 6$	~2
Man(1,4,7)-8 (**2a**)	2.3 ± 0.4	-22.7 ± 0.5	107 ± 20	-63 ± 9	$+40 \pm 9$	~2
Trivalent cyclic (EDS spacer)						
Man(1,3,5)@5 (**2@**)	3.3 ± 0.4	-23.8 ± 0.2	70 ± 5	-74 ± 8	$+50 \pm 8$	~3
Man(1,4,7)@8 (**2a@**)	2.5 ± 0.3	-24.0 ± 0.3	63 ± 8	-61 ± 4	$+37 \pm 4$	~2

[a] $\overline{FV}$ is defined as $\overline{FV} = \frac{1}{n}$ and was experimentally determined from the binding stoichiometry n. [b] Gibbs free binding energy $\overline{\Delta G}$, enthalpy $\overline{\Delta H}$ and entropy $-\overline{T\Delta S}$ are reported in kJ mol⁻¹. [c] Dissociation equilibrium constant $\overline{K_d}$ is reported in μM. Errors in $\overline{FV}$, $\overline{\Delta G}$, $\overline{\Delta H}$, $-\overline{T\Delta S}$ and $\overline{K_d}$ refer to the error propagation as described in the Experimental Part. [d] $\overline{c}$ − values refer to the quality of the fit and the corresponding error propagation in the Experimental Part. "*" marks ITC measurements whose

$\bar{c}$ − values lie outside the traditional range (as described in Chapter 3.4.1). Thermodynamic quantities determined from these measurements should be considered as estimates. (For details regarding the error propagation of thermodynamic parameters, see Chapter 3.4.1 and Experimental Part). 2 − 3 ITC measurements were performed with linear and cyclic glycomacromolecules containing the EDS spacer (1 − 2a and 1@ − 2a@) and the SDS spacer (1SDS − 2aSDS). Therefore, all thermodynamic quantities refer to best mean values. Measurements were performed in acetate buffer pH 5.20 ± 0.02 at 298.15 K, with Con A obtaining its dimer conformation[84, 114, 131, 223].

Table 13. ITC derived thermodynamic binding energetics of linear and cyclic glycomacromolecules with different spacers binding to tetramer Con A (measured at 298.15 K).

Ligand	$\overline{FV}$[a]	$\overline{\Delta G}$[b]	$\overline{K_d}$[c]	$\overline{\Delta H}$[b]	$-\overline{T\Delta S}$[b]	$\bar{c}$[d]
Monovalent linear (SDS spacer)						
Man(3)-5SDS (1SDS)	0.7 ± 0.1	−22.1 ± 0.4	138 ± 20	−18 ± 2	−4 ± 2	~3
Man(4)-7SDS (1aSDS)	0.7 ± 0.2	−21.9 ± 0.9	150 ± 54	−18 ± 6	−4 ± 6	~2
Monovalent cyclic (SDS spacer)						
Man(3)@5SDS[1] (1@SDS)	1.0 ± 0.4	−21.9 ± 0.6	147 ± 38	−9 ± 5	−13 ± 5	~3
Monovalent linear (EDS spacer)						
Man(3)-5 (1)	0.8 ± 0.1	−20.9 ± 0.2	221 ± 16	−27 ± 2	+6 ± 2	~2
Man(4)-8 (1a)	0.7 ± 0.1	−21.6 ± 0.2	163 ± 14	−19 ± 1	−3 ± 1	~2
Trivalent linear (SDS spacer)						
Man(1,3,5)-5SDS (2SDS)	3.0 ± 0.4	−30.5 ± 0.2	4.6 ± 0.3	−59 ± 7	+28 ± 7	~83
Man(1,4,7)-7SDS (2aSDS)	3.3 ± 0.5	−29.9 ± 0.3	6 ± 1	−92 ± 16	+62 ± 16	~66
Trivalent cyclic (SDS spacer)						
Man(1,3,5)@5SDS[1] (2@SDS)	2.5 ± 0.3	−32.9 ± 0.3	1.7 ± 0.2	−60 ± 4	+27 ± 4	~216
Trivalent linear (EDS spacer)						
Man(1,3,5)-5 (2)	2.6 ± 0.3	−32.0 ± 0.3	2.5 ± 0.3	−57 ± 5	+25 ± 5	~151
Man(1,4,7)-8 (2a)	2.3 ± 0.3	−30.6 ± 0.3	4.5 ± 0.5	−50 ± 3	+19 ± 3	~88

Trivalent cyclic (EDS spacer)						
Man(1,3,5)@5 (**2@**)	2.7 ± 0.4	-32.2 ± 0.2	2.3 ± 0.2	-59 ± 5	$+27 \pm 5$	~164
Man(1,4,7)@8 (**2a@**)	2.5 ± 0.3	-31.1 ± 0.2	3.6 ± 0.3	-59 ± 4	$+28 \pm 4$	~103

[a] $\overline{FV}$ is defined as $\overline{FV} = \frac{1}{n}$ and was experimentally determined from the binding stoichiometry n. [b] Gibbs free binding energy $\overline{\Delta G}$, enthalpy $\overline{\Delta H}$ and entropy $-\overline{T\Delta S}$ are reported in kJ mol^{-1}. [c] Dissociation equilibrium constant $\overline{K_d}$ is reported in µM. Errors in $\overline{FV}$, $\overline{\Delta G}$, $\overline{\Delta H}$, $-\overline{T\Delta S}$ and $\overline{K_d}$ refer to the error propagation as described in the Experimental Part. [d] $\overline{c}-$ values refer to the quality of the fit and the corresponding error propagation in the Experimental Part. All $\overline{c}-$ values lie inside the traditional range. (For details regarding the error propagation of thermodynamic parameters, see Chapter 3.4.1 and Experimental Part). All thermodynamic quantities refer to best mean values, expect for measurements, which were performed one time (those are highlighted with "1"). Measurements were performed in LBB pH 7.40 $\pm$ 0.01 at 298.15 K, with Con A obtaining its dimer-tetramer equilibrium conformation[131, 223]

3.6.3. <u>Enthalpic and entropic contributions for linear and cyclic glycomacromolecules along with the FV and the binding free energy</u>

As can be seen from the thermodynamic data of linear and cyclic glycomacromolecules, the FV for all of the mono- and trivalent species is respectively in the same range (Table 12 and 13, Figure 45, A). Since the FV is proportional to ΔH (see discussion Chapter 3.5.4 and following), enthalpic values increase along with the FV, which is readily seen from Figure 45, A and B. The exception is compound 2@, which shows an unexpected high FV in binding to dimer Con A, exceeding the number of potential binding sites. At this point, it is not clear, whether this is an artefact of the measurement or indeed a feature of this particular glycomacromolecule. Further experiments would be required to elucidate this finding.

The FV values for the cyclic and linear glycomacromolecules in binding to tetramer Con A (Figure 45, A empty squares) are slightly higher as compared to those of dimer Con A (Figure 45, A filled squares), whereas compound 2a@ shows the same FV in binding to both dimer and tetramer Con A (Figure 45, A, filled square is overlapped). For 2@ and 2a, the reverse situation to the former ligands is found, where the ΔH values along with the FV are lower for binding to tetramer Con A, as compared to those of dimer Con A.
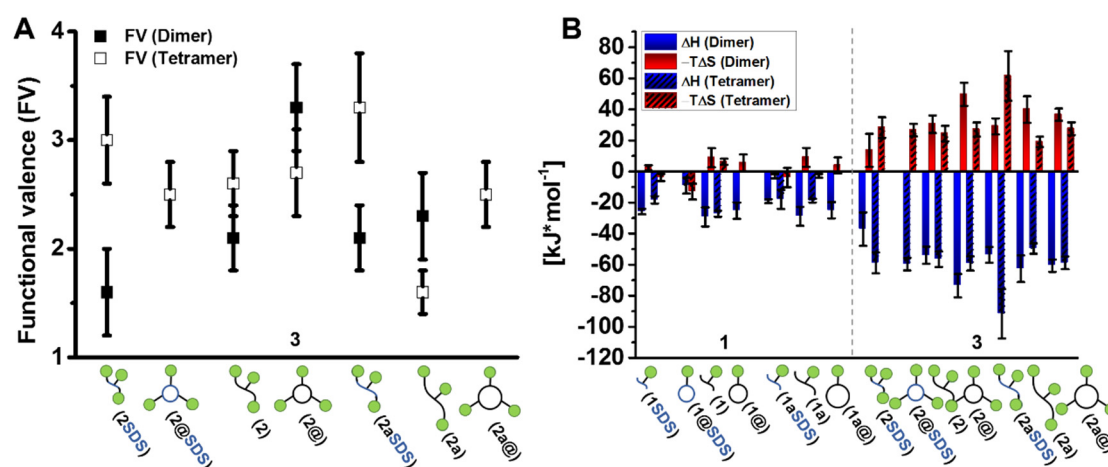
**Figure 45. A:** FV (FV = $1/n$) of trivalent linear and cyclic glycomacromolecules binding to dimer (filled squares) and tetramer Con A (empty squares), describing the evolution of ΔH. **B:** Evolution of ΔH and $-T\Delta S$ of linear and cyclic glycomacromolecules binding to dimer (non-dashed) and tetramer Con A (dashed).

With respect to differences in the (*i*) polymer architecture, (*ii*) the length of linear compounds and the ring-size, as well as (*iii*) the distance between the presented αMan ligands and spacer composition, no clear trend was found regarding the binding enthalpy and entropy. The data on the ΔG values (Figure 46), however, shows the binding processes to be insensitive to changes in (*i*) the oligomer architecture, (*ii*) the distance between the αMan ligands as well as (*iii*) the size of the rings

and the length of the oligomer. For the current study, ΔG is only clearly sensitive to an increasing valency on both, the multivalent ligands and the protein.
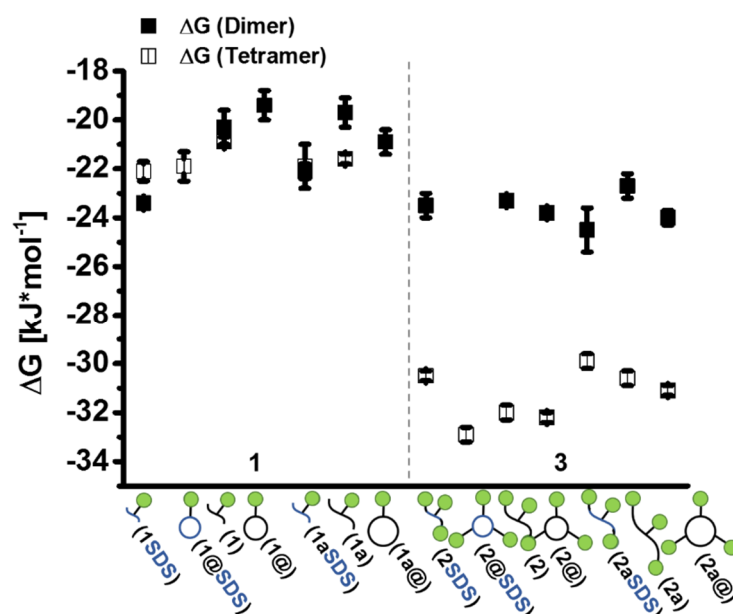

Figure 46. Binding free energy ΔG of linear and cyclic glycomacromolecules binding to dimer Con A (filled squares) and tetramer Con A (empty squares).

Potential reasons for the insensitivity of the binding thermodynamics regarding the change in the oligomer architectures, might be rationalized by the following assumptions. From literature it is known, that a change from a linear to a cyclic architecture might affect the conformation and the behavior in solution[240, 245-248]. A different conformation in solution suggests that the oligomers would obtain different hydrodynamic mean radii R_h. Thus, during the binding process and in a biological water environment, varying hydrodynamic mean radii R_h are believed to manifest themselves in different binding affinities. From the above thermodynamic data, where cyclic and linear glycomacromolecules were compared, it was seen that the binding affinity does not vary with a change in the architecture. This suggests, that the conformational behavior in the water environment of the presented linear glycomacromolecules equals those of the cyclic glycomacromolecules when these bind to Con A. From previous studies by Ponader *et al.*[103], it is further known that linear glycomacromolecules are highly flexible, which behave as random-coiled structures in solution. The thermodynamic results of the presented cyclic glycomacromolecules suggest that their conformational behavior in solution might be very similar to those of their linear counterparts. Further investigations on the characterization of glycomacromolecules in solution, e.g. by light scattering are ongoing.

The presented thermodynamic data rather suggest that the linear and cyclic glycomacromolecules have very distinct multivalent binding modes. A possible explanation for this observation might further be the yet inappropriate length-scale of the linear and cyclic glycomacromolecules (compared to Con A), which so far only allows for intermolecular binding.

However, recent studies by Nguyen *et al.*[72] as well as by Turnbull *et al.*[115] have shown that although glycopolymers[72] and other glycoclusters[115] may obtain the right length-scale to target other binding modes, these compounds still favor intermolecular binding.

3.6.4. <u>Determination of the solvation and configuration entropies for linear and cyclic glycomacromolecules[11]</u>

As was described in one of the previous chapters (Chapter 3.5.9), the solvation $-T\Delta S_{solv}$ and configuration entropies $-T\Delta S_{conf}$ were determined from the summation of the general entropic term $-T\Delta S$. In order to investigate a potential impact of the linear and cyclic architectures of the presented glycomacromolecules on the different entropic contributions, the individual entropic terms for the binding processes to tetramer Con A were determined from ITC measurements (as has been described by Chervenak *et al.*[116, 132-134] and in Chapter 3.5.9).

The results are summarized in Table 15, while Table 14 shows the evolution of the thermodynamic data and most importantly the evolution of the binding enthalpy ΔH and the FV with temperature. The binding enthalpy ΔH allowed the calculation of the heat capacity change ΔC_p, which then further permitted the calculation of the solvation entropy ΔS_{solv}. The configuration entropies ΔS_{conf} were calculated with the known solvation entropy ΔS_{solv} and the overall measured binding entropy ΔS, whereas the FV accounted for the actual translational and rotational penalties $\Delta S_{trans+rot}$ during the binding process (see Chapter 3.5.9).

---

[11]a) ITC measurements of compounds 1SDS, 1aSDS, 2SDS and 2aSDS at 298.15 K have been performed by Hendrik Wöhlk (Heinrich-Heine-Universität Düsseldorf, group of Prof. Dr. Laura Hartmann, Master Thesis, April 2015). In this thesis, the here listed thermodynamic quantities have been re-assessed using the methods and error calculation described in this thesis. Kinetic evaluation of the same binding isotherms has completely and exclusively been performed by the author of this thesis. Their rate constants including their uncertainties are presented in this thesis for the first time. ITC measurements of the compounds 1SDS and 2SDS at 303.15 K and 308.5 K as well as the evaluation, determination and calculation of all of their in this thesis presented thermodynamic quantities have exclusively been performed by the author of this thesis. Kinetic evaluation of the same binding isotherms has exclusively been performed by the author of this thesis. Their rate constants including their uncertainties are presented in this thesis for the first time. b) ITC measurements of compounds 1@SDS and 2@SDS at different temperatures (298.15 K, 303.15 K and 308.15 K) have been performed by Andreas Ludwig (Heinrich-Heine-Universität Düsseldorf, group of Prof. Dr. Laura Hartmann, Bachelor Thesis, October 2015). In this thesis, the thermodynamic and kinetic quantities previously reported by Andreas Ludwig have been re-assessed using the methods and error calculation described in this thesis. Determination and evaluation of the entropic terms $\Delta S_{trans+rot} \cdot FV$ for the above mentioned compounds is reported for the first time in this thesis.

Figure 47. A: Evolution of the binding enthalpy ΔH with temperature allowed the determination of the heat capacity change ΔC_p. **B:** Different entropies ($-T\Delta S_{solv}$, $-T\Delta S_{conf}$) describing the binding process of linear and cyclic glycomacromolecules to tetramer Con A ($-T\Delta S_{solv}$ was determined from ΔC_p).

Table 14. Evolution of ITC derived thermodynamic parameters with temperature of mono- and trivalent linear and cyclic glycomacromolecules with different spacers binding to tetramer Con A. Measurements were performed at different temperatures (298.15 K, 303.15 K, 308.15 K), allowing for determination of the heat capacity change ΔC_p (from evolution of ΔH with T according to Kirchhoff's law[133]).

Ligand	$\overline{FV}$ [a]	$\overline{\Delta G}$ [b]	$\overline{K_d}$ [c]	$\overline{\Delta H}$ [b]	$-\overline{T\Delta S}$ [b]	ΔC_p [d]	$\bar{c}$ [e]
		Monovalent linear (SDS spacer)					
Man(3)-5SDS (**1SDS**) 25°C	0.7 ± 0.1	−22.1 ± 0.4	137 ± 20	−18 ± 2	−4 ± 2	−293 ± 109	~3
Man(3)-5SDS (**1SDS**) 30°C	0.5 ± 0.1	−21.0 ± 0.4	242 ± 43	−20 ± 2	−1 ± 2	−	~2
Man(3)-5SDS (**1SDS**) 35°C	0.7 ± 0.1	−21.5 ± 0.9	238 ± 82	−21 ± 6	−1 ± 6	−	~2
		Monovalent cyclic (SDS spacer)					
Man(3)@5SDS[1] (**1aSDS**) 25°C	1.0 ± 0.4	−21.9 ± 0.6	147 ± 38	−9 ± 5	−13 ± 5	+553 ± 340	~3
Man(3)@5SDS[1] (**1aSDS**) 30°C	1.0 ± 0.3	−21.9 ± 0.7	170 ± 44	−6 ± 2	−16 ± 2	−	~2
		Monovalent linear (EDS spacer)					
Man(3)-5 (**1**) 25°C	0.8 ± 0.1	−20.9 ± 0.2	221 ± 13	−27 ± 2	+6 ± 2	+186 ± 38	~2
Man(3)-5[1] (**1**) 30°C	0.7 ± 0.1	−20.7 ± 0.2	267 ± 19	−26 ± 2	+5 ± 2	−	~2
Man(3)-5[1] (**1**) 35°C	0.7 ± 0.1	−20.7 ± 0.2	311 ± 22	−25 ± 2	+5 ± 2	−	~1
Man(4)-8 (**1a**) 25°C	0.7 ± 0.1	−21.6 ± 0.2	163 ± 14	−19 ± 1	−3 ± 1	+164 ± 35	~2
Man(4)-8 (**1a**) 30°C	0.7 ± 0.1	−21.3 ± 0.2	214 ± 18	−19 ± 2	−3 ± 2	−	~2
Man(4)-8 (**1a**) 35°C	0.6 ± 0.1	−21.1 ± 0.2	267 ± 22	−17 ± 1	−4 ± 1	−	~1
		Trivalent linear (SDS spacer)					
Man(1,3,5)-5SDS (**2SDS**) 25°C	3.0 ± 0.4	−30.5 ± 0.2	4.6 ± 0.3	−59 ± 7	+28 ± 7	+2666 ± 578	~83
Man(1,3,5)-5SDS (**2SDS**) 30°C	2.1 ± 0.3	−30.7 ± 0.7	5 ± 1	−52 ± 4	+22 ± 4	−	~76
Man(1,3,5)-5SDS (**2SDS**) 35°C	1.7 ± 0.2	−30.0 ± 0.2	8 ± 1	−36 ± 2	+6 ± 2	−	~48

	$\overline{FV}$	$\overline{\Delta G}$	$\overline{K_d}$	$\overline{\Delta H}$	$-\overline{T\Delta S}$	ΔC_p	$\bar{c}$
Trivalent cyclic (SDS spacer)							
Man(1,3,5)@5SDS[1] (**2@SDS**) 25°C	2.5 ± 0.3	-32.9 ± 0.3	1.7 ± 0.2	-60 ± 4	$+27 \pm 4$	$+2935 \pm 569$	~216
Man(1,3,5)@5SDS[1] (**2@SDS**) 30°C	2.2 ± 0.3	-32.0 ± 0.4	3.1 ± 0.4	-50 ± 4	$+18 \pm 4$	–	~119
Man(1,3,5)@5SDS[1] (**2@SDS**) 35°C	1.8 ± 0.2	-32.5 ± 0.4	3.1 ± 0.4	-32 ± 2	-1 ± 2	–	~116
Trivalent linear (EDS spacer)							
Man(1,3,5)-5 (**3a**) 25°C	2.6 ± 0.3	-32.0 ± 0.3	2.5 ± 0.3	-57 ± 5	$+25 \pm 5$	$+2213 \pm 485$	~151
Man(1,3,5)-5 (**3a**) 30°C	2.3 ± 0.3	-30.7 ± 0.3	5.1 ± 0.5	-49 ± 4	$+18 \pm 4$	–	~70
Man(1,3,5)-5 (**3a**) 35°C	1.8 ± 0.3	-29.2 ± 0.3	11 ± 3	-35 ± 4	$+6 \pm 4$	–	~34
Man(1,4,7)-8 (**2a**) 25°C	2.3 ± 0.3	-30.6 ± 0.3	4.5 ± 0.5	-50 ± 3	$+19 \pm 3$	$+1297 \pm 293$	~88
Man(1,4,7)-8 (**2a**) 30°C	2.1 ± 0.3	-28.9 ± 0.7	11 ± 3	-46 ± 6	$+17 \pm 6$	–	~38
Man(1,4,7)-8 (**2a**) 35°C	1.6 ± 0.2	-28.1 ± 0.4	17 ± 2	-37 ± 2	$+9 \pm 3$	–	~23
Trivalent cyclic (EDS spacer)							
Man(1,3,5)@5 (**2@**) 25°C	2.7 ± 0.4	-32.2 ± 0.2	2.3 ± 0.2	-59 ± 5	$+27 \pm 5$	$+1806 \pm 356$	~164
Man(1,3,5)@5[1] (**2@**) 30°C	2.5 ± 0.3	-30.3 ± 0.3	6.4 ± 0.6	-55 ± 4	$+25 \pm 4$	–	~63
Man(1,3,5)@5 (**2@**) 35°C	1.9 ± 0.2	-28.7 ± 0.2	13.6 ± 0.9	-42 ± 3	$+14 \pm 3$	–	~27
Man(1,4,7)@8 (**2a@**) 25°C	2.5 ± 0.3	-31.1 ± 0.2	3.6 ± 0.3	-59 ± 4	$+28 \pm 4$	$+1660 \pm 320$	~103
Man(1,4,7)@8 (**2a@**) 30°C	2.2 ± 0.3	-30.0 ± 0.2	6.8 ± 0.4	-50 ± 3	$+20 \pm 3$	–	~54
Man(1,4,7)@8 (**2a@**) 35°C	1.9 ± 0.2	-28.5 ± 0.2	15 ± 1	-42 ± 3	$+14 \pm 3$	–	~26

[a] $\overline{FV}$ is defined as $\overline{FV} = \frac{1}{n}$ and was experimentally determined from the binding stoichiometry n. [b] Gibbs free binding energy $\overline{\Delta G}$, enthalpy $\overline{\Delta H}$ and entropy $-\overline{T\Delta S}$ are reported in kJ mol^{-1}. [c] Dissociation equilibrium constant $\overline{K_d}$ is reported in µM. [d] Heat capacity change ΔC_p, determined from evolution of ΔH with temperature (Kirchoff's law[133]), is reported in J K^{-1} mol^{-1}. Errors in $\overline{FV}$, $\overline{\Delta G}$, $\overline{\Delta H}$, $-\overline{T\Delta S}$, $\overline{K_d}$ and ΔC_p refer to the error propagation as described in the Experimental Part. [e] $\bar{c}$ − values refer to the quality of the fit and the corresponding error propagation in the Experimental Part. All $\bar{c}$ − values are inside the traditional range. (For details regarding the error propagation of thermodynamic parameters, see Chapter 3.4.1 and Experimental Part). All thermodynamic quantities refer to best mean values, expect for measurements, which were performed one time (those are highlighted with "1"). Measurements were performed in LBB pH 7.40 ± 0.01 at 298.15 K, 303.15 K and 308.15 K, with Con A obtaining its dimer-tetramer equilibrium conformation[131, 223].

Table 15. Solvation and configuration entropic contributions for mono- and trivalent linear and cyclic glycomacromolecules with different spacers binding to tetramer Con A. Solvation and configuration entropic contributions were determined from the heat capacity change ΔC_p, the measured overall entropic contributions $\overline{\Delta S}$ and the rotational and translational entropies times the $\overline{FV}$, $\Delta S_{trans+rot} \cdot \overline{FV}$.

Ligand	$\overline{\Delta S}$[a]	$\Delta S_{trans+rot} \cdot \overline{FV}$[a]	ΔS_{solv}[b]	ΔS_{conf}[b]	$-T\Delta S_{solv}$[c]	$-T\Delta S_{conf}$[c]
Monovalent linear (SDS spacer)						
Man(3)-5SDS (**1SDS**)	+13 ± 8	−22	+75	−40	−22	+12
Monovalent cyclic (SDS spacer)						
Man(3)@5SDS (**1aSDS**)	+43 ± 17	−33	−142	+218	+42	−65
Monovalent linear (EDS spacer)						
Man(3)-5 (**1**)	−21 ± 6	−19	−48	+52	+14	−16
Man(4)-8 (**1a**)	+9 ± 4	−25	−42	+76	+13	−23
Trivalent linear (SDS spacer)						
Man(1,3,5)-5SDS (**2SDS**)	−95 ± 23	−100	−683	+688	+204	−205
Trivalent cyclic (SDS spacer)						
Man(1,3,5)@5SDS (**2@SDS**)	−90 ± 14	−84	−752	+746	+224	−223
Trivalent (linear EDS spacer)						
Man(1,3,5)-5 (**2**)	−82 ± 17	−86	−567	+570	+169	−170
Man(1,4,7)-8 (**2a**)	−64 ± 11	−76	−332	+344	+99	−123
Trivalent cyclic (EDS spacer)						
Man(1,3,5)@5 (**2@**)	−90 ± 16	−90	−463	+462	+138	−138
Man(1,4,7)@8 (**2a@**)	−93 ± 14	−84	−425	+416	+127	−124

[a] Experimentally determined overall binding entropy $\overline{\Delta S}$ is reported for the standard state temperature (298.15 K). The tabulated $\Delta S_{trans+rot}$ was multiplied with the experimentally determined $\overline{FV}$ to account for the multivalent effect (which differs from the structural valency[34]; a different $\overline{FV}$ can also apply to monovalent compounds, see

Table 14). According to Murphy *et al.*[233] $\Delta S_{trans+rot}$ equals -33.5 J K^{-1} mol^{-1} for monovalent binding. $\Delta S_{trans+rot} \cdot \overline{FV}$ was determined for the standard state temperature (298.15 K). [b] Entropy of solvation ΔS_{solv} was determined from the heat capacity change $\overline{\Delta C_p}$, and the entropy of configuration ΔS_{conf} from the summation of the measured overall entropic term $\overline{\Delta S}$ (see equation 13). Experimentally determined overall binding entropy $\overline{\Delta S}$ and the entropy of solvation ΔS_{solv} and configuration ΔS_{conf} are reported in J K^{-1} mol^{-1}. [c] Standard state entropy of solvation $-T\Delta S_{solv}$ and configuration $-T\Delta S_{conf}$ are reported in kJ mol^{-1}, assuming 298.15 K.

Figure 47, B shows the solvation and configuration entropic values for the different mono- and trivalent linear and cyclic glycomacromolecules. Comparing the different glycomacromolecules binding to tetramer Con A, it is seen that for all of the linear and cyclic glycomacromolecules the configuration entropy $-T\Delta S_{conf}$ is favorable (negative value), whereas the solvation entropy $-T\Delta S_{solv}$ is unfavorable (positive values). Except for 1SDS, this result is true for all of the glycomacromolecules binding to tetramer Con A. The different entropy contributions vary only in their order of magnitude, but the relationship between those two entropic terms stays the same. Especially the monovalent glycomacromolecules show diminished contributions of the solvation and configuration entropies, which increase for the trivalent linear and cyclic compounds by several orders of magnitude in the either of the directions.

Structures of the same valency but a different architecture show no clear trend regarding the solvation and configuration entropies. Instead the solvation and configuration entropies seem to decrease with an increasing backbone length and ring-size (Figure 47, B from left to right) for trivalent linear and cyclic glycomacromolecules. Compared to the trivalent cyclic and linear structures with the SDS spacer building block, the EDS containing trivalent molecules further have diminished entropic terms, suggesting that $-T\Delta S_{solv}$ becomes more favorable and $-T\Delta S_{conf}$ less favorable with an increasing backbone length and ring-size. The only exception here is the trivalent cyclic ligand 2a@ with the largest ring-size, whose entropic values are in the same range as compared to those of the smaller trivalent ring 2@.

The origin of the observed values for the monovalent species lies in the heat capacity change of the binding processes. A heat capacity change, which accounts for all of the here presented ligands, is believed to be either a result of the change of the protein's conformation during binding or due to water rearrangement that is accompanied with the protein's conformational changes.[6, 249] Thus, $-T\Delta S_{solv}$ and $-T\Delta S_{conf}$ directly reflect changes of the heat capacity in the binding process.

Overall, it was seen that the heat capacity values are positive (expect for ligand 1SDS), resulting in unfavorable solvation entropy values, accompanied by favorable configuration entropic values. The opposite applies for monovalent ligand 1SDS binding to tetramer Con A. With an increasing number of αMan ligands from one to three, the heat capacity further changed by several orders of magnitude, making the solvation entropies even less favorable and the configuration entropies more favorable. A trend was found, in which both entropic terms decreased with an increasing backbone length and ring-size, resulting in relatively reduced configuration and more favorable solvation entropies. However, a clear trend regarding the difference in the cyclic and linear architectures has not been found.

3.6.5. Influence of linear and cyclic architectures on kinetics

As was previously described, kinITC[163-165] was used to obtain kinetic parameters for the ligand-receptor complex formation (Chapter 3.4, 3.5.10 and 3.5.11). Table 16 and 17 show the determined values for the rate constants, k_{on} and k_{off}, and the equilibrium dissociation constant K_d for the

linear and cyclic glycomacromolecules in binding to dimer (Table 16) and tetramer Con A (Table 17).

Table 16. Kinetic data of linear and cyclic glycomacromolecules with different spacers binding to dimer Con A. Measurements were performed at 298.15 K and correspond to the same measurements used for determination of thermodynamic parameters. The rate constants were obtained using the kinITC method.

Ligand	$\overline{k_{on,g}}$[a]	$\overline{k_{off,g}} \cdot 10^{-3}$[b]	$\overline{K_d}$[c]
Monovalent linear (SDS spacer)			
Man(3)-5SDS (**1SDS**)	371 ± 53	$30 \pm 5^*$	$80 \pm 6^*$
Man(4)-7SDS (**1aSDS**)	226 ± 39	$31 \pm 6^*$	$137 \pm 16^*$
Monovalent linear (EDS spacer)			
Man(3)-5 (**1**)	302 ± 97	84 ± 37	278 ± 82
Man(4)-8 (**1a**)	309 ± 89	112 ± 43	361 ± 91
Monovalent cyclic (EDS spacer)			
Man(3)@5 (**1@**)	336 ± 91	133 ± 47	$395 \pm 92^*$
Man(4)@8 (**1a@**)	569 ± 139	122 ± 40	$215 \pm 46^*$
Trivalent linear (SDS spacer)			
Man(1,3,5)-5SDS (**2SDS**)	849 ± 202	66 ± 21	78 ± 16
Man(1,4,7)-7SDS (**2aSDS**)	11134 ± 454	58 ± 32	52 ± 19
Trivalent linear (EDS spacer)			
Man(1,3,5)-5 (**2**)	1235 ± 172	101 ± 16	82 ± 5
Man(1,4,7)-8 (**2a**)	760 ± 192	81 ± 26	107 ± 20
Trivalent cyclic (EDS spacer)			
Man(1,3,5)@5 (**2@**)	1001 ± 137	70 ± 11	70 ± 5
Man(1,4,7)@8 (**2a@**)	1741 ± 305	109 ± 24	63 ± 8

[a] Mean association rate constant $\overline{k_{on,g}}$ is reported in M^{-1} s^{-1}. [b] Mean dissociation rate constant $\overline{k_{off,g}}$ is reported in s^{-1}. Rate constants were determined by fitting the ITC raw data from every heat flow signal, following the relaxation period for every injection of the ligand L (kinITC method, see Chapter 3.4 and Experimental Part). Errors in the rate constants correspond to true uncertainties, following error propagation as described by Butcher *et al.*[164] and in the Experimental Part. [c] Dissociation equilibrium constant $\overline{K_d}$ is reported in μM and was determined from the same ITC experiments used to determine the thermodynamic parameters. Errors in $\overline{K_d}$ refer to the error propagation of thermodynamic parameters as described in the Experimental Part. "*" marks ITC measurements whose $\bar{c}$ − values are outside the traditional range (as described in Chapter 3.4.1). All kinetic quantities refer to best weighted average values from *n* series of measurements (see also Experimental Part). Measurements were performed in acetate buffer pH 5.20 ± 0.02 at 298.15 K, with Con A obtaining its dimer conformation[34, 114, 131, 223].

Table 17. Kinetic data of linear and cyclic glycomacromolecules with different spacers binding to tetramer Con A. Measurements were performed at 298.15 K and correspond to the same measurements used for determination of thermodynamic parameters. The rate constants were obtained using the kinITC method.

Ligand	$\overline{k_{on,g}}$[a]	$\overline{k_{off,g}} \cdot 10^{-3}$[b]	$\overline{K_d}$[c]
Monovalent linear (SDS spacer)			
Man(3)-5SDS (**1SDS**)	125 ± 24	17 ± 4	138 ± 20
Man(4)-7SDS (**1aSDS**)	142 ± 54	21 ± 11	150 ± 54
Monovalent cyclic (SDS spacer)			
Man(3)@5SDS[1] (**1@SDS**)	249 ± 71	37 ± 14	147 ± 38
Monovalent linear (EDS spacer)			
Man(3)-5 (**1**)	223 ± 32	49 ± 8	221 ± 16
Man(4)-8 (**1a**)	206 ± 33	34 ± 6	163 ± 14
Trivalent linear (SDS spacer)			
Man(1,3,5)-5SDS (**2SDS**)	7245 ± 1210	33 ± 6	4.6 ± 0.3
Man(1,4,7)-7SDS (**2aSDS**)	5869 ± 1370	34 ± 9	5.7 ± 0.8
Trivalent cyclic (SDS spacer)			
Man(1,3,5)@5SDS[1] (**2@SDS**)	9852 ± 2087	17 ± 4	1.7 ± 0.2
Trivalent linear (EDS spacer)			
Man(1,3,5)-5 (**2**)	9863 ± 1907	24 ± 6	2.5 ± 0.3
Man(1,4,7)-8 (**2a**)	8148 ± 1406	36 ± 7	4.5 ± 0.5
Trivalent cyclic (EDS spacer)			
Man(1,3,5)@5 (**2@**)	11087 ± 1966	26 ± 5	2.3 ± 0.2
Man(1,4,7)@8 (**2a@**)	8170 ± 1243	29 ± 5	3.6 ± 0.3

[a] Mean association rate constant $\overline{k_{on,g}}$ is reported in M⁻¹ s⁻¹. [b] Mean dissociation rate constant $\overline{k_{off,g}}$ is reported in s⁻¹. Rate constants were determined by fitting the ITC raw data from every heat flow signal, following the relaxation period for every injection of the ligand L (kinITC method, see Chapter 3.4 and Experimental Part). Errors in the rate constants correspond to true uncertainties, following error propagation as described by Butcher *et al.*[164] and in the Experimental Part. [c] Dissociation equilibrium constant $\overline{K_d}$ is reported in µM and was determined from the same ITC experiments used to determine the thermodynamic parameters. Errors in $\overline{K_d}$ refer to the error propagation of thermodynamic parameters as described in the Experimental Part. All $\bar{c}$ − values are inside the traditional range (see Chapter 3.4.1, Experimental Part and Supporting Appendix). For $\bar{c}$ − values, see Table 12 and 13. All kinetic quantities refer to best weighted average values from *n* series of measurements, expect for measurements, which were performed one time (those are highlighted with "1"). Here, the weighted average rate constants refer to weighted average values of all of the heat flow profiles from one measurement (see also Experimental Part). Measurements were performed in LBB pH 7.40 ± 0.01 at 298.15 K, with Con A obtaining its dimer-tetramer equilibrium conformation[131, 223].

The kinetic measurements of linear and cyclic glycomacromolecules should reveal, whether the differences in their structural features translate into a different kinetic behavior. For this purpose, glycomacromolecules were compared in their binding to Con A, regarding the following different structural aspects: (*i*) The overall oligomer architecture and the accompanied change from a linear

to a cyclic architecture, (*ii*) the difference in the backbone length and the ring-size and (*iii*) the difference in the backbone spacer composition, varying in their distance as well as in their chemical composition (SDS *versus* EDS).

Taking a look at the k_{off} values (Figure 48, B) of both dimer (non-dashed) and tetramer Con A (dashed), it can be seen that the k_{off} values for the cyclic and linear glycomacromolecules are in the same range. This indicates that the energy barrier for the off-state is about the same range for all of the linear and cyclic glycomacromolecules. This result suggests that the k_{off} values are irrespective of the oligomer architectures as well as backbone length and ring-size. The k_{off} values of the monovalent compounds are a little higher as compared to those of the trivalent species binding to dimer Con A, thus suggesting that the complex time is prolonged as the valency increases. Although the results show no effect of the backbone composition (SDS *versus* EDS spacer building blocks) for the trivalent species, again the monovalent linear and cyclic compounds carrying SDS building blocks (1SDS and 1@SDS) show decreased k_{off} values, indicating additional contributions, e.g. from potential secondary binding effects. Compared to tetramer Con A, where the binding of different linear and cyclic glycomacromolecules shows little fluctuations in the k_{off} values, their values in binding to dimer Con A are here essentially in the same range.
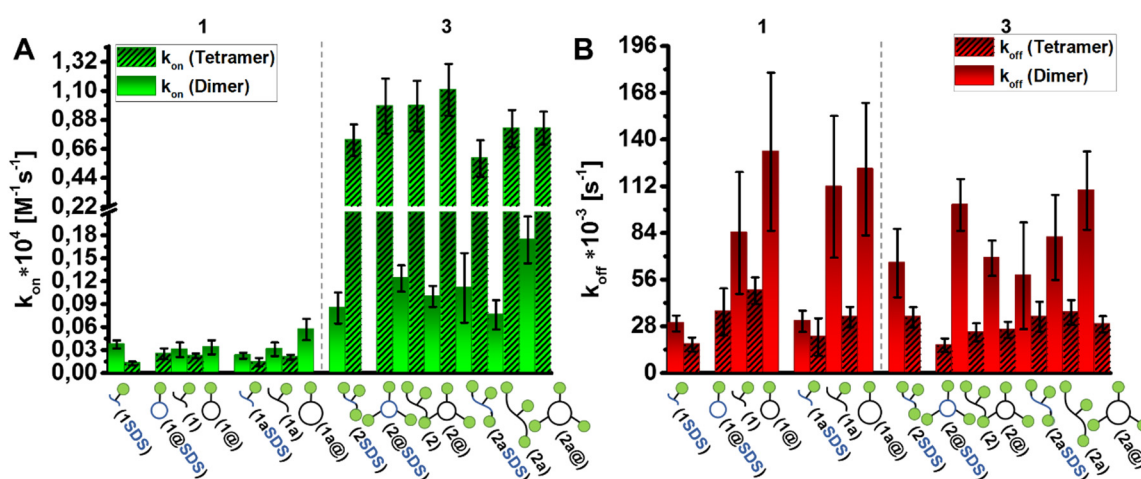

Figure 48. k_{on} **(A) and** k_{off} **(B) values of linear and cyclic glycomacromolecules binding to dimer (non-dashed) and tetramer Con A (dashed).**

Similar trends as for k_{off} were observed for the k_{on} values. Figure 48, A (see also Table 16 and 17) shows that k_{on} values for both, the mono- and the trivalent species are in the same range for binding to either dimer (non-dashed) or tetramer Con A (dashed). Although there are a few fluctuations in the k_{on} values for binding to either one of the Con A conformations, the order of magnitude of the k_{on} values is the same. This result suggests, that the k_{on} values of the investigated structures are not affected by changing their structural features, such as the linear or cyclic architecture, the oligomer length or ring-size or the backbone composition. In this study, an increase in k_{on} is only observed for an increasing valency of the glycomacromolecules. Compared to

the k_{on} values of the linear and cyclic glycomacromolecules binding to dimer Con A, the values for binding to tetramer Con A are significantly enhanced and most likely a result of the additional Con A valency, as has already been discussed in the kinetic subchapter of linear glycomacromolecules (Chapter 3.5.11).

Altogether, the above data suggests the hydrodynamic behavior in solution (in terms of their Brownian motion) between the linear and cyclic architectures to be similar, thus showing no impact on the multivalent kinetics in their binding to Con A.

3.6.6. Transition states of linear and cyclic glycomacromolecules

In order to gain more information on the kinetic processes and specifically the transition state parameters of the cyclic and linear glycomacromolecules binding to tetramer Con A, the on- and off-rate kinetic constants were collected at different temperatures (at 298.15 K, 303.15 K and 308.15 K) as was described in the previous transition state subchapter of linear glycomacromolecules (Chapter 3.5.12, see also Experimental Part).

The transition state parameters for the on- and off-state were determined for representative linear and cyclic glycomacromolecules that account for the following structural features: (*i*) The general difference in linear and cyclic glycomacromolecules, (*ii*) the difference in backbone length and ring-size and (*iii*) the difference in the spacer length and spacer building block composition (SDS *versus* EDS). To only account for a change in the oligomer architecture, the monovalent linear and cyclic species were compared, whereas the trivalent species, altering in the above mentioned structural features, were measured to further take the multivalent effect into consideration. Table 19 lists the described glycomacromolecules binding to tetramer Con A and their transition state parameters $\Delta G^{\ddagger}$, $\Delta H^{\ddagger}$ and $-T\Delta S^{\ddagger}$.[12] Table 18 shows the evolution of the rate constants with the temperature. The different transition states are separated into the on- and off- transition states and their activation free energy $\Delta G^{\ddagger}$, enthalpy $\Delta H^{\ddagger}$ and entropy $-T\Delta S^{\ddagger}$. Thus, these states describe the way as well as the energetic height, which separates the transition state from the unbound glycomacromolecules and Con A and their associated complexes. Figure 49 shows the representative Eyring plots (according to equation 15, see Chapter 3.5.12) that were used for determination of the activation enthalpy $\Delta H^{\ddagger}$, which then together with the Eyring equation (16) (see Chapter 3.5.12) allowed the calculation of the on- and off- activation free energy $\Delta G^{\ddagger}$ and entropy $-T\Delta S^{\ddagger}$ (see Chapter 3.5.12 and Experimental Part).

---

[12]The transition state parameters ($\Delta G^{\ddagger}$, $\Delta H^{\ddagger}$ and $-T\Delta S^{\ddagger}$ for the on- and the off-state) of compounds 1@SDS and 2@SDS have been determined from the evolution of the rate constants (k_{on} and k_{off}) at different temperatures (298.15 K, 303.15 K and 308.15 K) and previously reported by Andreas Ludwig (Heinrich-Heine-Universität Düsseldorf, group of Prof. Dr. Laura Hartmann, Bachelor Thesis, October 2015). In this thesis, all of the above mentioned transition state parameters have been re-assessed using the methods and error calculation described in this thesis. The on- and off-rate constants and their uncertainties presented in the above mentioned Bachelor Thesis have been determined and provided by the author of thesis. Their calculation is reported in this thesis for the first time.

Figure 49. Eyring plots for determination of the activation enthalpy of the linear and cyclic mono- (A) and trivalent compounds (B).

Table 18. Evolution of ITC derived kinetic rate constants of linear and cyclic glycomacromolecules with different spacers measured at different temperatures (298.15 K, 303.15 K, 308.15 K), allowing for determination of the activation Gibbs free binding energy $\Delta G^{\ddagger}_{on/off}$, the transition state enthalpy $\Delta H^{\ddagger}_{on/off}$ and entropy $-T\Delta S^{\ddagger}_{on/off}$ using the Eyring equation (16) and Eyring plot (15), respectively.

Ligand	$\overline{k_{on,g}}$ [a]	$\overline{k_{off,g}} \cdot 10^{-3}$ [b]	$\overline{k_{on,g,dT}}$ [c]	$\overline{k_{off,g,dT}} \cdot 10^{-3}$ [c]
Monovalent linear (SDS spacer)				
Man(3)-5SDS (**1SDS**) 25°C	125 ± 24	17 ± 4	148 ± 21	20 ± 4
Man(3)-5SDS (**1SDS**) 30°C	204 ± 45	49 ± 14	–	–
Man(3)-5SDS (**1SDS**) 35°C	316 ± 116	75 ± 38	–	–
Monovalent cyclic (SDS spacer)				
Man(3)@5SDS[1] (**1@SDS**) 25°C	249 ± 71	37 ± 14	261 ± 54	41 ± 11
Man(3)@5SDS[1] (**1@SDS**) 30°C	277 ± 81	47 ± 18	–	–
Monovalent linear (EDS spacer)				
Man(3)-5 (**1**) 25°C	223 ± 32	49 ± 8	214 ± 18	55 ± 5
Man(3)-5[1] (**1**) 30°C	212 ± 31	57 ± 9	–	–
Man(3)-5[1] (**1**) 35°C	209 ± 30	65 ± 10	–	–
Man(4)-8 (**1a**) 25°C	206 ± 33	34 ± 6	240 ± 21	45 ± 5
Man(4)-8 (**1a**) 30°C	251 ± 37	54 ± 9	–	–
Man(4)-8 (**1a**) 35°C	281 ± 41	75 ± 13	–	–
Trivalent linear (SDS spacer)				
Man(1,3,5)-5SDS (**2SDS**) 25°C	7245 ± 1210	33 ± 6	6621 ± 722	38 ± 5
Man(1,3,5)-5SDS (**2SDS**) 30°C	7238 ± 2163	38 ± 15	–	–
Man(1,3,5)-5SDS (**2SDS**) 35°C	6075 ± 990	50 ± 9	–	–

	$\overline{k_{on,g}}$	$\overline{k_{off,g}}$	$\overline{k_{on,g,dT}}$	$\overline{k_{off,g,dT}}$
Trivalent cyclic (SDS spacer)				
Man(1,3,5)@5SDS[1] (**2@SDS**) 25°C	9852 ± 2087	17 ± 4	11538 ± 1382	23 ± 4
Man(1,3,5)@5SDS[1] (**2@SDS**) 30°C	11737 ± 2357	36 ± 9	–	–
Man(1,3,5)@5SDS[1] (**2@SDS**) 35°C	14630 ± 2966	46 ± 11	–	–
Trivalent linear (EDS spacer)				
Man(1,3,5)-5 (**2**) 25°C	9863 ± 1907	24 ± 6	7296 ± 885	30 ± 4
Man(1,3,5)-5 (**2**) 30°C	7305 ± 1246	37 ± 7	–	–
Man(1,3,5)-5 (**2**) 35°C	5308 ± 1671	60 ± 26	–	–
Man(1,4,7)-8 (**2**) 25°C	8148 ± 1406	36 ± 7	4126 ± 518	42 ± 6
Man(1,4,7)-8 (**2**) 30°C	4419 ± 1355	48 ± 20	–	–
Man(1,4,7)-8 (**2**) 35°C	3304 ± 612	57 ± 13	–	–
Trivalent cyclic (EDS spacer)				
Man(1,3,5)@5 (**2@**) 25°C	11087 ± 1966	26 ± 5	5284 ± 513	34 ± 4
Man(1,3,5)@5[1] (**2@**) 30°C	6163 ± 1037	37 ± 7	–	–
Man(1,3,5)@5 (**2@**) 35°C	4397 ± 619	60 ± 9	–	–
Man(1,4,7)@8 (**2a@**) 25°C	8170 ± 1243	29 ± 5	6112 ± 547	38 ± 4
Man(1,4,7)@8 (**2a@**) 30°C	6784 ± 1056	46 ± 8	–	–
Man(1,4,7)@8 (**2a@**) 35°C	5035 ± 746	73 ± 12	–	–

[a] Mean association rate constant $\overline{k_{on,g}}$ is reported in M^{-1} s^{-1}. [b] Mean dissociation rate constant $\overline{k_{off,g}}$ is reported in s^{-1}. Rate constants were determined by fitting the ITC raw data from every heat flow signal, following the relaxation period for every injection of the ligand L (kinITC method, see Chapter 3.4 and Experimental Part). Errors in the rate constants correspond to true uncertainties, following error propagation as described by Butcher *et al.*[164] and in the Experimental Part. Rate constants were determined at different temperatures (298.15 K, 303.15 K, 308.15 K), allowing for the calculation of the activation enthalpy $\Delta H^{\ddagger}_{on/off}$ from the Eyring plot. [c] Weighted average $\overline{k_{on,g,dT}}$ and $\overline{k_{off,g,dT}}$ values allowed for the determination of the activation free energy $\Delta G^{\ddagger}_{on/off}$ directly from the Eyring equation (16). Their weighted average values were determined from the $\overline{k_{on,g}}$ and $\overline{k_{off,g}}$ values at different temperatures. Errors in the weighted averaged $\overline{k_{on,g,dT}}$ and $\overline{k_{off,g,dT}}$ values correspond to the error of the weighted average as described in the Experimental Part. All $\overline{c}$ − values are inside the traditional range (see Chapter 3.4.1, Experimental Part and Supporting Appendix). For $\overline{c}$ − values, see Table 12 and 13. All kinetic quantities refer to best weighted average values from n series of measurements, expect for measurements, which were performed one time (those are highlighted with "1"). Here, the weighted average rate constants refer to weighted average values of all of the heat flow profiles from one

measurement (see also Experimental Part). Measurements were performed in LBB pH 7.40 $\pm$ 0.01 at 298.15 K with Con A obtaining its dimer-tetramer equilibrium conformation[131, 223].

Table 19. Transition state parameters for the on- and the off-transition state. Representative on- and off-rates were determined at 298.15 K, 303.15 K, 308.15 K. The transition state parameters were then determined from the Eyring plot (15) and the Eyring equation (16) as described above (see also Experimental Part).

Ligand	$\Delta G_{on}^{\ddagger}$ [a]	$\Delta H_{on}^{\ddagger}$ [a]	$-T\Delta S_{on}^{\ddagger}$ [a]	$\Delta G_{off}^{\ddagger}$ [b]	$\Delta H_{off}^{\ddagger}$ [b]	$-T\Delta S_{off}^{\ddagger}$ [b]
Monovalent linear (SDS spacer)						
Man(3)-5SDS (**1SDS**)	+60.6 $\pm$ 0.3	+69 $\pm$ 18	−9 $\pm$ 18	+82.7 $\pm$ 0.5	+125 $\pm$ 27	−42 $\pm$ 26
Monovalent cyclic (SDS spacer)						
Man(3)@5SDS (**1@SDS**)	+59.2 $\pm$ 0.5	+13 $\pm$ 44	+46 $\pm$ 43	+81.0 $\pm$ 0.7	+35 $\pm$ 60	+46 $\pm$ 59
Monovalent linear (EDS spacer)						
Man(3)-5 (**1**)	+59.7 $\pm$ 0.2	−7 $\pm$ 9	+67 $\pm$ 9	+80.2 $\pm$ 0.2	+19 $\pm$ 10	+62 $\pm$ 10
Man(4)-8 (**1a**)	+59.4 $\pm$ 0.2	+21 $\pm$ 10	+38 $\pm$ 10	+80.7 $\pm$ 0.3	+59 $\pm$ 14	+22 $\pm$ 14
Trivalent linear (SDS spacer)						
Man(1,3,5)-5SDS (**2SDS**)	+51.2 $\pm$ 0.3	−16 $\pm$ 12	+67 $\pm$ 12	+81.1 $\pm$ 0.3	+28 $\pm$ 14	+53 $\pm$ 14
Trivalent cyclic (SDS spacer)						
Man(1,3,5)@5SDS (**2@SDS**)	+49.8 $\pm$ 0.3	+28 $\pm$ 14	+22 $\pm$ 13	+82.4 $\pm$ 0.4	+75 $\pm$ 20	+7 $\pm$ 20
Trivalent linear (EDS spacer)						
Man(1,3,5)-5 (**2**)	+51.0 $\pm$ 0.3	−49 $\pm$ 15	+100 $\pm$ 15	+81.7 $\pm$ 0.4	+65 $\pm$ 19	+16 $\pm$ 18
Man(1,4,7)-8 (**2a**)	+52.4 $\pm$ 0.3	−72 $\pm$ 17	+124 $\pm$ 17	+80.9 $\pm$ 0.4	+33 $\pm$ 17	+48 $\pm$ 17
Trivalent cyclic (EDS spacer)						
Man(1,3,5)@5 (**2@**)	+51.2 $\pm$ 0.2	−72 $\pm$ 15	+124 $\pm$ 14	+81.4 $\pm$ 0.3	+63 $\pm$ 15	+19 $\pm$ 15

Man(1,4,7)@8 (**2a@**)	$+51.4 \pm 0.2$	-40 ± 11	$+91 \pm 11$	$+81.1 \pm 0.3$	$+68 \pm 15$	$+13 \pm 15$

[a] Activation Gibbs free binding energy $\Delta G^{\ddagger}_{on/off}$, transition state enthalpy $\Delta H^{\ddagger}_{on/off}$ and entropy $-T\Delta S^{\ddagger}_{on/off}$ are reported in kJ mol^{-1}. Errors in $\Delta G^{\ddagger}_{on/off}$, $\Delta H^{\ddagger}_{on/off}$ and $-T\Delta S^{\ddagger}_{on/off}$ follow error analysis as described in the Experimental Part. Activation Gibbs free binding energy $\Delta G^{\ddagger}_{on/off}$ and transition state entropy $-T\Delta S^{\ddagger}_{on/off}$ are reported for the standard state temperature (298.15 K).

As can be seen from the activation free energy (Table 19), the energetic state for the on-state ranges between $+59 - +61$ kJ mol^{-1} and for the off-state between $+80 - +83$ kJ mol^{-1}. This indicates similar values in the on- and off-state for the monovalent ligands, suggesting the activation free energy to be irrespective of the different structural features of the monovalent compounds. Inspection of the activation free energy for linear and cyclic trivalent compounds binding to tetramer Con A, shows the same trend already observed to the monovalent structures. Their activation free energy values are very similar (Table 19), ranging from $50 - 52$ kJ mol^{-1} and $81 - 83$ kJ mol^{-1} for the on- and the off-state, respectively. This suggest that again the activation free energy barrier for the studied glycomacromolecules is insensitive to changes in the linear and cyclic architectures, the oligomer length and ring-size as well as the spacer length and compositions (SDS *versus* EDS spacer building blocks).

Regarding the activation entropy and enthalpy, the cyclic and linear compounds indeed vary in these energetic barriers (Table 19). The activation enthalpy barrier decreases in the order 2@SDS > 2SDS > 2a@ > 2 > 2a > 2@, while the entropic barrier increases in the reverse order 2@SDS < 2SDS < 2a@ < 2 < 2a < 2@. This means that 2@SDS obtains the highest enthalpic energy barrier accompanied by the lowest entropic energy barrier, while the reverse is true for 2@. Interestingly, all compounds that carry the EDS spacer building blocks in their backbone contain favorable enthalpic contributions for the association state. The dissociation state then simply exhibits the reverse trend, where the enthalpic energy barriers heighten, thereby also lowering the entropic energetic barriers. This result could indicate that for the off-state, both the ligand and protein, regain conformational freedom and thereby result in more favorable entropic terms, while breaking reversible intermolecular bonds then rather results in a raised enthalpic energy barrier that needs to be crossed.

In contrast to those results, the SDS spacer containing glycomacromolecules present an exception, where 2@SDS and 2SDS contain the highest activation enthalpy barrier and the lowest activation entropy barrier. The same is true for the dissociation state, however, here values in the activation enthalpy are more positive and that of the activation entropy clearly less positive. Therefore, no clear trend can be found regarding the enthalpic and entropic energy barrier. Glycomacromolecules based on the SDS spacer building blocks seem to represent exceptions here, thereby also showing the reverse trend compared to the linear and cyclic glycomacromolecules with the EDS building blocks. A further detailed study in future should reveal the influence of different spacer building block compositions, e.g. by including additional methods to characterize ligand-receptor interactions, such as STD-NMR.

Comparing the activation parameter of the mono- and trivalent compounds, it was found that the activation free energy is insensitive to changes in the structural features of the studied linear and cyclic glycomacromolecules. A significant lowering in the energy barrier is only visible as a result of an increasing ligand valency. Different enthalpic and entropic energy barriers indeed may point to a different behavior of the complex during association and dissociation in the transition

states. However, a clear trend regarding the different structural features of the linear and cyclic glycomacromolecules was not seen. Interestingly, linear and cyclic glycomacromolecules that carry SDS spacer building blocks always seem to have the reverse trend, regarding the activation enthalpy and entropy, compared to those of the EDS carrying glycomacromolecules. The origin for this observation is so far not known and would need further evaluation.

4. Conclusion and Outlook

In conclusion, this thesis showed the synthesis of a series of precision glycomacromolecules varying different structural aspects and their multivalent binding to model protein Con A. The different structural features of the glycomacromolecules included: (*i*) The variation in the spacing and linker, as well as the linker composition, (*ii*) the variation in the oligomer architecture that altered from linear to cyclic including (*iii*) the inherent change in the backbone length, ring-size and spacer compositions. SPPoS allowed for the relatively easy alternation of these structural features by simply exchanging spacer, αMan and functional building blocks during the assembly of the oligomers on-resin. Further, a potential tandem reaction for the on-resin macrocyclization of oligo(amido amines) was evaluated, but resulted in unselective *N*-substituted imide formation rather than the synthesis of monocyclic rings.

With the obtained series of linear and cyclic glycomacromolecules, a systematic study of the thermodynamic and kinetic binding parameters, regarding the impact of the mentioned structural features, on the binding behavior with dimer and tetramer Con A was performed. ITC and kinITC were used to investigate both, the thermodynamic and kinetic quantities related to the exchanging structural motifs of the glycomacromolecules.

For the investigated series of glycomacromolecules, this study found that there is an intermolecular binding process and the binding affinity is dictated mainly by the FV, when binding to dimer or tetramer Con A. Further, the binding thermodynamics and kinetics were not altered by (*i*) a different αMan spacing of structures with the same valency or (*ii*) variation of the oligomer architecture from linear to cyclic and the inherent change of the backbone length and ring-size. This is in agreement with previous studies in the literature[18-19, 34, 49, 53, 72, 106, 114] and supported by the theoretical model of Ercolani[50] and Schiaffino[50], which has shown that concentration dependencies outweigh the influence of spacer units[50].

The binding thermodynamics dramatically changed, when the αMan linker or the spacer composition were varied. Two different types of spacer building blocks and three different types of αMan linkers were exchanged and compared for this purpose: (*i*) A long ethylene dioxy ("mini-PEG", EDS) spacer building block and a shorter ethylene diamine building block (SDS); (*ii*) a small ethyl triazole linker, a longer thiol-ether triazole linker and a hydrophobic benzyl triazole linker. With the distinct spacer and linker composition, a significant change in terms of the binding enthalpy and entropy was observed. For the glycomacromolecules that varied in the spacer composition (SDS instead of EDS building block spacing) this, however, only applied to the monovalent linear and cyclic structures binding to dimer Con A and for the trivalent cyclic species binding to tetramer Con A. At this stage, it is believed that the observed changes of the energetic terms result from the spacer's and linker's chemical composition and not from additional ligand-receptor contacts. This was especially seen from monovalent glycomacromolecules, where the single αMan linkers showed an alternation in these energetic terms that was not a result of the FV. This effect can then be

increased in an additive manner *via* their multivalent presentation on the backbone, as was demonstrated in this thesis.

Further, the enthalpic and entropic behavior of glycomacromolecules studied with tetramer in comparison to dimer Con A indicate a sterical hinderance to be operative, that is however compensated by a decrease in the binding free energy. Thus, although the enthalpic and entropic contribution points at the sterical hinderance, there is still an increase in the binding affinity, which is suspected to be a result of an increased statistical chance for binding due to an increasing valency of the protein. To get a more detailed insight into the entropic effects, which varied with the different structural features of the glycomacromolecules, the solvation and configuration entropies were studied. Regarding the different linkers, favorable configuration entropies for compounds carrying the ethyl triazole and thiol-ether triazole linkers were observed, while glycomacromolecules presenting the benzyl triazole linker showed a more favorable solvation entropy. Regarding the changing oligomer architectures from linear to cyclic, as well as the backbone length and ring-size, a continuous reduction was observed in the configuration entropy and increase in the solvation entropy, along with an increasing backbone length and ring-size. Most pronounced was the in- and decrease in the configuration and solvation entropy with an increasing number of αMan ligands, related to a rise in the heat capacity change.

To further evaluate the structural features based on their binding kinetics, the association and dissociation rate constants have been determined for the presented glycomacromolecules and their interactions with dimer and tetramer Con A. Kinetic rate constants were calculated using the recently introduced kinITC method. In this study, it was found that the on- and off- rate constants were insensitive to structural features, such as (*i*) the αMan spacing, (*ii*) cyclic or linear architectures and the inherent (*iii*) increase in backbone length and ring-size. Instead, the k_{on} and k_{off} rate constants significantly changed with the (*i*) αMan valency, (*ii*) the linker composition and (*iii*) the Con A conformation. These different features resulted in accelerated rate constants that (*i*) followed the order of the valency, (*ii*) increased in the order ethyl triazole linker < thiol-ether triazole linker < benzyl triazole linker with respect to the linkers and (*iii*) heightened in the order dimer Con A < tetramer Con A with the protein conformation.

With respect to glycomacromolecules binding to dimer Con A, the following kinetic picture was found. The binding of glycomacromolecules with dimer Con A seems to follow a rebinding mechanism, as it has been proposed by Hunter[107] and Anderson[108] and Weber *et al.*[110]. Fast k_{on} and k_{off} rates are indicative of partially bound states, during glycomacromolecule and protein association. The binding of glycomacromolecules to tetramer Con A seems to follow a binding and sliding mechanism, as proposed by Brewer *et al.*[106]. Taking into account the different structural features, a similar trend was found in the kinetic rate constants as for the binding thermodynamics. The on- and off-rate showed no changes for the different glycomacromolecules with varying αMan density. Glycomacromolecules with different αMan linkers showed a clear change for the association and dissociation rate constants.

Finally, the transition state parameters of the linear and cyclic glycomacromolecules varying in their spacer, linker, backbone length and ring-size have been studied. The transition state parameters of the series of glycomacromolecules binding to tetramer Con A showed that a lowering of the energetic barrier was most likely due to an increase in the valency. Structural features, such as a cyclic architecture and an increasing spacer or backbone length and ring-size, substantially led to very similar free energy barriers. Along with the valency, it was again the linker composition, which significantly lowered the activation free energy barrier in the order ethyl triazole linker > thiol-ether triazole linker > benzyl triazole linker. A clear trend for the enthalpic and entropic energy barriers was not found for all structural features, other than the exchange of αMan linkers.

Although the results presented in this thesis strictly only apply to the here presented class of glycomacromolecules, the observed trends for the thermodynamic and kinetic behavior in dependence of their chemical structure, might also relate to other classes of glycomimetics. Especially the correlation between the thermodynamic and kinetic behavior might lead to new insights into the formation of multivalent carbohydrate-ligand-receptor complexes and potentially allow to design more effective glycopolymer inhibitors or effectors, and their application in medicine and biotechnology based on their kinetic behavior.

Future studies will further extend on the scope of the SPPoS, where glycomacromolecules can be obtained with an even longer spacing and higher molecular weight and therefore even more relate to high molecular weight glycopolymers. The different structural features and their influence on the thermodynamic and kinetic behavior studied in this thesis, can then again be re-evaluated with these polymers. At the moment, studies are ongoing, which extend on the concept of using chemically different linkers and spacers to alter the binding affinity, e.g. by introducing secondary binding motifs in the side- or main-chain of the glycomacromolecule. Different characterization assays, such as STD-NMR and SPR, will then be used to quantify the interactions between such glycomacromolecules and lectin receptors, which will further help to learn about structural aspects of the ligand-receptor complexes and their influence on the thermodynamic and kinetic behavior.

5. Experimental Part

5.1. General materials and methods

Chemicals were purchased from commercial suppliers and used without further purification. Dry solvents of HPLC grade, such as dichloromethane (DCM), tetrahydrofuran (THF), and *N,N'*-dimethylformamide (DMF) were purchased from Sigma/Aldrich and used without further purification. Concanavalin A (Con A) from *Canavalia ensiformis (Jack Bean)* Type IV was purchased from Sigma/Aldrich as lyophilized powder.

All solution-phase reactions (building block and carbohydrate synthesis) were monitored by preparative thin-layer chromatography (TLC) using E. Merck silica gel 60 F254 (0.25 mm thickness). Chromatographic purification of products was performed on Merck Silica Gel 60 (230 – 400 mesh). Reaction progress and chromatographic purification were visualized with UV light and/or by staining with potassium permanganate (potassium permanganate in basic aqueous potassium carbonate/sodium hydroxide solution), ninhydrin (0.2 % ninhydrin in ethanol), Hanessian's stain (4 % ammonium molybdate, 10 % cer(IV) sulfate in 10 % sulfuric acid) and *p*-anisaldehyde (0.5 mL *p*-anisaldehyde in 50 mL glacial acetic acid and 1 mL 97 % sulfuric acid).

All solid phase reactions were performed on 0.025, 0.05 or 0.1 mmol scale (with respect to the resin loading of 0.23 mmol/g, with 109, 217 or 435 mg of a corresponding resin), either by hand-coupling in 5 − 10 mL polypropylene Chromabond columns containing a polypropylene frit and closed at the bottom with a B7 septum, or on a standard peptide synthesizer Activo-P11 from Activotec equipped with an UV detector. Protocols for automated synthesis were written as recommended by Activotec using the supplied software templates for standard Fmoc solid phase synthesis. The solid supports Tentagel S Rink Amide (RAM) and Tentagel S Chlorotrityl (Trt-Cl) resin (both obtaining a resin loading of 0.23 mmol/g) were purchased from Rapp Polymers, the coupling agent benzotriazol-1-yl-oxytripyrrolidinophosphonium hexafluorophosphate (PyBOP) from Novabiochem and protected amino acids (AAs) from Sigma/Aldrich.

Analytical *Reverse-Phase High Performance Liquid Chromatography* (RP-HPLC) measurements were performed on an Agilent 1200 HPLC System at 60°C using an Agilent Eclipse analytical column (C$_{18}$, 4.6 x 150 mm, column 1). Semi-preparative purification was performed at 25°C using a Varian Persuit semi-preparative column (C$_{18}$, 250 x10.0 mm, column 2). The flow rate was 1 mL/min on column 1 and 3 mL/min on column 2 with the following solvent system: 0.1 % trifluoroacetic acid (TFA) in H$_2$O (A) and MeCN (B). Unless otherwise noted, both columns were flushed for 3 min with 100 % B. Then a linear gradient from 95 to 5 % B was used over a time period of 15 min, followed by 5 min flushing with 95 % A before analysis. Conversion of the on-resin macrocyclizations, progress of the building block coupling, as well as determination of the product

purity were monitored by integration of the UV signals at 214 nm with the software ChemStation for LC from Agilent Technologies.

Nuclear Magnetic Resonance (NMR) spectra were recorded at 400, 500 and 600 MHz on a Varian 400-MR, 500-MR or 600-MR spectrometer and on a Bruker Avance III 400 (400 MHz) and 600 (600 MHz) at room temperature. NMR spectra were recorded for both carbon and proton nuclei in dimethyl sulfoxide (DMSO-d_6), methanol (MeOD-d_4) and water (D_2O). Chemical shifts are reported in units of parts per million (ppm), referenced relative to the residual ^1H or ^{13}C peaks of the corresponding solvent, except for D_2O solutions on carbon nuclei, where the ppm scale could not be referenced and 0 ppm was taken as a standard. Proton and carbon signals were assigned using two-dimensional NMR (2D NMR) spectroscopy. The following 2D NMR methods were used: Homonuclear *Correlation Spectroscopy* (COSY), such as $^1H/^1H$ COSY NMR, *Heteronuclear Single Quantum Coherence* (HSQC) NMR, such as $^1H/^{13}C$ HSQC NMR and $^1H/^{15}N$ HSQC NMR, as well as *Heteronuclear Multiple Bond Correlation* (HMBC) NMR, such as $^1H/^{13}C$ HMBC NMR.

Matrix Assisted Laser Desorption Ionization Time of Flight Mass Spectrometry (MALDI-TOF MS) spectra were recorded on a Bruker Autoflex Speed II in Reflector Mode using the following matrices: 2,5-dihydroxybenzoic acid (DHB) and α-cyano-4-hydroxycinnamic acid (CHCA).

High resolution mass spectra were recorded on an Agilent 6210 (*Electrospray Ionization*) ESI-TOF, Agilent Technologies, Santa Clara, CA, USA. The flow rate was 4 µL/min with a spray voltage of 4 kV. The desolvation gas was set to 15 psi (1 bar). All other parameters for the maximal abundance with respect to the corresponding $[M+H]^+$ were optimized.

ESI MS and ESI LC/MS spectra were recorded on an Agilent 6120 Series Quadrupole LC/MS system using an Agilent ZORBAX SB (4.6 x 50 mm, analytical column 3) column as the stationary phase. Measurements were performed either at 25°C or 60°C using the following solvent system: 0.1 % formic acid (FA) in H_2O (A) and MeCN (B). Unless otherwise noted, column 3 was flushed for 10 min with 100 % B. Then a linear gradient from 95 to 5 % B was used over a period of 10 min, followed by 5 min flushing with 95 % A before analysis. The flow rate was 0.4 mL/min with a spray voltage of 4 kV. Data analysis was performed using ChemStation from Agilent Technologies.

Ultraviolet/Visible (UV/Vis) spectra were recorded on an Agilent G1103A 8453 UV-Vis Photometer 190-1100 nm. Quartz cuvettes were used with a layer thickness of 1 cm^{-1}.

5.2. Binding thermodynamics with Con A and cyclic/linear precision glycomacromolecules using isothermal titration calorimetry (ITC)

5.2.1. General ITC experimental procedures: Thermodynamic ITC

ITC measurements were performed on VP-ITC MicroCalorimeter (MicroCal, LLC, USA) with a dead cell and syringe volume of 2.2 mL and 281 µL, respectively. Experiments were either run at 298.15 K, 303.15 K or 308.15 K. Titrations were performed in series of injections ($28 - 29$ aliquots of 10 µL with the first negligible injection of 1 µL, which was deleted from the final data) at 400 s intervals with a constant stirring rate of 417 rpm. All measurements were performed by "normal titration", where the protein is placed in the cell and the macromolecule ligands in the syringe. A fresh solution of both protein and ligand was prepared by dissolving the model protein Con A from *Canavalia ensiformis* (*Jack Bean*) Type IV either in acetate buffer at pH 5.20 ± 0.02 and 25°C (100 mM sodium acetate, 150 or 50 mM sodium chloride (NaCl), with 5 mM or 1 mM manganese chloride ($MnCl_2$) and calcium chloride ($CaCl_2$) aliquots) or HEPES buffered saline at pH 7.40 ± 0.01 and 25°C ("lectin binding buffer" (LBB); 10 mM HEPES, 50 mM NaCl, with 1 mM $MnCl_2$ and $CaCl_2$ aliquots) and a concentration around 5 mg/mL. The exact protein concentration was measured by absorption spectroscopy. The dialyzed buffer was then used to prepare $\sim 0.1 - 6$ mM glycomacromolecule solutions, depending on the glycomacromolecule ligand's affinity for Con A, ranging from mono- to decavalent cyclic/linear glycomacromolecules, with higher affinity of decavalent glycomacromolecules (0.1 mM) for Con A as compared to monovalent (6 mM). The protein concentrations ranged from ~0.056 – 0.132 mM and were prepared according to Wiseman's $c -$ values[224]. Both protein and ligand solutions were degassed at 25°C for 10 min before starting an ITC measurement. Unspecific enthalpic contributions were eliminated from the final data by subtracting the heat of dilution/ligand dilution, previously measured in control experiments. Thermodynamic parameters were then obtained from the remaining data using the least squares non-linear fitting *one set of independent binding sites*. The binding constant K_d, the binding enthalpy ΔH and the binding stoichiometry n were directly obtained and the binding free energy ΔG and binding entropy $-T\Delta S$ computed from the Gibbs-Helmholtz equation (1) (see General Introduction, Chapter 1.2.1). The experiments were designed following the recommendation of Wiseman's $c -$ values ($\sim 1 < c < 1000$). In this work all experiments were performed with $c -$ values ~$0.7 < c < 16670$ (with the lower limit for some of the monovalent glycomacromolecules and with the upper limit representative for one of the decavalent glycomacromolecules binding to the higher affinity tetramer Con A; also see the corresponding tables of the thermodynamic quantities).

5.2.2. General ITC experimental procedures: kinITC

For determination of the association (k_{on}) and dissociation rates (k_{off}) the kinetic ITC (kinITC) method[163-165] was applied, using a least-squares minimized fitting procedure as described in the Supporting Appendix (Chapter 7.1). Application of alternative least-squares fitting procedures to obtain k_{on} and prior deconvolution for the instrumental rate constant k_{ITC} is described in detail by Dumas *et al.*[163], Butcher *et al.*[164] and Yonetani *et al.*[165].

After the deconvolution for the instrumental rate function, each of those raw heat flow signals, following the number of ligand injections, were globally fitted using the least-squares minimization procedure, as was written by Dr. Susanna Röblitz and Dr. Marcus Weber (see Supporting Appendix).[13] The non-linear fitting procedure was written in MATLAB and was then applied to determine individual k_{on} values, following each relaxation period (following each titration point). The non-linear fitting is based on the procedure as was described by Butcher *et al.*[164], but uses another language to compute the measured heat profiles. The concentrations of the ligand, protein and the complex required for the computation of each of the individual k_{on} values within one binding isotherm, were first numerically determined, following the procedures described by Yonetani *et al.*[165]. The final k_{on} value was then calculated as the weighted average value (weighted over the uncertainties) as described by Butcher *et al.*[164], either from one experiment or from a series of experiments.

5.2.3. Error analysis of thermodynamic parameters

Error analysis of thermodynamic parameters was performed to account for random error sources that result from uncertainties in the ligand and protein concentration, in the baseline drift as well as from uncertainties in the fitting procedure when the $c -$ value lie outside the traditional range ($\sim 1 < c < 1000$).[130, 135] Depending on whether repeated experiments or one measurement (*one* or *n* series of measurements) was performed to determine the thermodynamic quantities, slightly different but analogous procedures were used as is described in the following. In the following error propagation, let x be the general variable that defines the thermodynamic values, such as K_d, ΔH and n.

---

[13]The least squares non-linear curve fitting procedure for kinITC has been written by Dr. Susanna Röblitz and Dr. Marcus Weber (Konrad-Zuse-Institut für Informationstechnik, Berlin; see also Supporting Appendix). Every measurement (including experimental design), determination, calculation and evaluation of the rate constants including their uncertainties has been performed by the author of this thesis. The kinITC least squares minimization procedure, required for the determination, calculation and evaluation of the measured ITC data (binding isotherms), has been provided by Dr. Susanna Röblitz and Dr. Marcus Weber. They have written the MATLAB scripts, which then allowed the calculation/determination of the rate constants. These written MATLAB scripts have been applied for the calculation/determination of the kinetic constants by the author of this thesis.

$$\sigma_{x,FE} = \sqrt{\sigma_{x,value}^2 + \Delta x_{c_{L,0}}^2 + \Delta x_{baseline}^2} \tag{18}$$

In the above equation $\sigma_{x,FE}$ presents the final error in a given thermodynamic value, determined from $\sigma_{x,value}$, $\Delta x_{c_{L,0}}$ and $\Delta x_{baseline}$, which correspond to the uncertainty from the fit $\sigma_{x,value} = \sigma_{x,fit}$ or the standard deviation $\sigma_{x,value} = \sigma_{x,SE}$ (either from *one* or n series of measurements), the ligand stock concentration and the baseline drift, respectively. The quantities x that are affected by these error sources are $x = K_d, \Delta H$.

From all of the random error sources, which contribute to the final error $\sigma_{x,FE}$, first the lowest and highest error estimates were determined from a series of experiments. This allowed for the determination of the highest and lowest error barriers, so that the estimation of the random errors, which result from the ligand concentration and the baseline drift ($\Delta x_{c_{L,0}}$ and $\Delta x_{baseline}$), did not had to be performed for every single experiment. The highest possible error barrier/estimate was then used in the error propagation with respect to the single quantities x and their highest limit error sources. The uncertainty in the ligand stock concentration ranged between $\pm 2\% - 4\%$. Since the error in the ligand concentration was not determined for every ligand solution, the highest error estimate of $\pm 4\%$ was used in the error propagation of x. In the ITC experiments reported in thesis, the drift in the baseline ranged between $\pm 2\% - 5\%$. The baseline drift was estimated from the not corrected heat flow values in the beginning and at the end of the experiment. (Before analysis of the binding isotherms with the fitting procedures, the baseline was however always corrected – from blank ligand/buffer titration experiments – yielding a straight baseline.)

For the determination of the final error $\sigma_{x,FE}$ in the binding stoichiometry n, an additional term was considered that contributed to the final error: The uncertainty in the protein concentration $\Delta x_{c_{P,0}}$. From the measurements of the UV standard curves of the Con A concentration, the highest error in estimating the molar extinction coefficient was used. This highest error estimate was about $\pm 10\%$ and was used in all of the binding stoichiometry final error calculations ($\sigma_{x,FE}$ with $x = n$) following equation (19).

$$\sigma_{x,FE} = \sqrt{\sigma_{x,value}^2 + \Delta x_{c_{L,0}}^2 + \Delta x_{baseline}^2 + \Delta x_{c_{P,0}}^2} \tag{19}$$

The error in the binding free energy $\sigma_{\Delta G,FE}$ was then computed from the final error in the dissociation equilibrium constant $\sigma_{K_d,FE}$ using the natural logarithm ($\Delta \ln x = \frac{\Delta x}{x} \approx \sigma_{\ln K_d,FE} = \frac{\sigma_{K_d,FE}}{K_d}$) and the following relationship:

$$\sigma_{\Delta G,FE} = RT * \frac{\sigma_{K_d,FE}}{K_d}. \tag{20}$$

The final error in the binding entropy $\sigma_{-T\Delta S,FE}$ was then obtained using the following equation.

$$\sigma_{-T\Delta S,FE} = \sqrt{\sigma^2_{\Delta H,FE} + \sigma^2_{\Delta G,FE}} \tag{21}$$

To further account for the c − values that were outside the traditional range (exceeding the higher and lower limits of $\sim 1 < c < 1000$), an additional term $\Delta x_{c-value}$ was incorporated into the whole error propagation. The surpass of these limits will directly affect the values in n, K_d and ΔH, since the error in their values is higher due to the associated loss of the c − value precision, which results in poorer fits and representation of these quantities[130, 135]. The error in the fitted values (n, K_d and ΔH) was then typically assumed to be ± 20 %. Thus, the relative error of $\Delta x_{c-value}$ was then incorporated into the error propagation as an additional term that accounts for the loss in the c − value precision (exceeding the lower and higher limits), so that the above equations then become (for $x = K_d$, ΔH):

$$\sigma_{x,FE*} = \sqrt{\sigma^2_{x,value} + \Delta x^2_{c_{L,0}} + \Delta x^2_{baseline} + \Delta x^2_{c-value}} \tag{22}$$

and ($x = n$)

$$\sigma_{x,FE*} = \sqrt{\sigma^2_{x,value} + \Delta x^2_{c_{L,0}} + \Delta x^2_{baseline} + \Delta x^2_{c_{P,0}} + \Delta x^2_{c-value}} \tag{23}$$

The final error in ΔG and $-T\Delta S$, $\sigma_{\Delta G,FE*}$ and $\sigma_{-T\Delta S,FE*}$, was then further calculated using the described relationships from above.

5.2.4. Error analysis in the heat capacity change

Errors in the heat capacity ΔC_p (which allowed for the calculation of the solvation entropy ΔS_{solv}) were determined from the expression:

$$\sigma_{\Delta C_p} = \sqrt{\left(\frac{\sigma_{\Delta T_{1,min}}}{T_{1,min}}\right)^2 + \left(\frac{\sigma_{\Delta T_2}}{T_2}\right)^2 + \left(\frac{\sigma_{\Delta T_{3,max}}}{T_{3,max}}\right)^2 + \left(\frac{\sigma_{\Delta H_{1,min}}}{\Delta H_{1,min}}\right)^2 + \left(\frac{\sigma_{\Delta H_2}}{\Delta H_2}\right)^2 + \left(\frac{\sigma_{\Delta H_{3,max}}}{\Delta H_{3,max}}\right)^2}$$
$$\cdot \Delta C_p. \tag{24}$$

Here, $\sigma_{\Delta T_{1,min}} = \sigma_{\Delta T_2} = \sigma_{\Delta T_{3,max}} = \sigma_{\Delta T} = \sqrt{\left(\Delta T_{1,min}\right)^2 + (\Delta T_2)^2 + \left(\Delta T_{3,max}\right)^2}$, whereas $\Delta T_{1,min} = \Delta T_2 = \Delta T_{3,max} = \Delta T$ were arbitrarily chosen to be $\Delta T = \pm 2$ K. Measurements were performed over three different temperatures $T_{1,min} = 298.15$ K, $T_2 = 303.15$ K and $T_{3,max} = 308.15$ K. The change in heat capacity ΔC_p was calculated using Kirchhoff's law[133], thereby following the evolution of the enthalpy change ($\Delta H_{1,min}$, ΔH_2, $\Delta H_{3,max}$) with these three temperatures. Errors in the enthalpy values $\sigma_{\Delta H_{1,min}}$, $\sigma_{\Delta H_2}$ and $\sigma_{\Delta H_{3,max}}$ were determined following error analysis of thermodynamic parameters, as described in the previous subchapter.

5.2.5. Error analysis and calculation of the weighted average rate constants

Error analysis of kinetic parameters was performed to account for random error sources that result from different uncertainties.[164] Since the here presented least-squares procedure was used to calculate the k_{on} value(s), following every injection of the ligand (L) and thereby the heat flow signals (*ith* injections) in terms of relaxation kinetics, errors in the forward rate constant k_{on} were due to the least-squares fitting procedure and additional arbitrary error sources, resulting from the ITC experimental set-up.[164] These error sources have been described in detail by Butcher *et al.*[164] and for a detailed description the reader is referred to their publication[164].

In the following error propagation, let x be the general variable that defines how the association rate k_{on} was determined. The following nomenclature will be applied to differentiate between individual or weighted average k_{on} values. Individual k_{on} values were obtained for every post-injection heat profile $(x, x(i) = k_{on(i)}, \overline{k_{on(i)}})$, which are calculated to give a final weighted average k_{on} value $(x_g = \overline{k_{on,g(1)}}, \overline{k_{on,g(n)}})$. (The subscript "g" designates the weighted average, and the variable in the bracket "g(1)" or "g(n)" denotes the number of measurements used for the calculation of the weighted average value(s), following either "1" or "n" measurement(s). The subscript "i" presents an individual k_{on} value $(x, x(i) = k_{on(i)}, \overline{k_{on(i)}})$ for every "*ith*" injection, following *one* $(x, x(i) = k_{on(i)})$ or n series $(x, x(i) = \overline{k_{on(i)}})$ of measurements, from which the former overall weighted average k_{on} values were obtained.)

The general error analysis for k_{on} follows the four master equations (25) – (28), as described by Butcher *et al.*[164], allowing for the calculation of a weighted average $x_g = \overline{k_{on,g(1)}}$ (*one* measurement) or $x_g = \overline{k_{on,g(n)}}$ (*n series* of measurements) and its true uncertainty value $\sigma_{x,FE}$.

$$\sigma_{x,fit} = \sqrt{\sigma_{x,LS}^2 + \sigma_{x,a}^2 + \Delta x_{k_{ITC}}^2} \tag{25}$$

$$\sigma_{x,g} = \sqrt{\sum \left[\left(\frac{\partial x_g}{\partial x(i)} \right) \cdot \sigma_{x,fit} \right]^2} = \left(\sum \frac{1}{\sigma_{x,fit}^2} \right)^{-\frac{1}{2}} = \left(\sum g(i) \right)^{-\frac{1}{2}} \tag{26}$$

$$x_g = \frac{\sum x(i) \cdot g(i)}{\sum g(i)} \tag{27}$$

$$\sigma_{x,FE} = \sqrt{\sigma_{x,g}^2 + \Delta x_{K_d}^2 + \Delta x_{c_{P,0}}^2} \tag{28}$$

In equation (25), $\sigma_{x,LS}$ is the standard deviation of the best-fit value, following the least-squares fitting procedure as was written by Dr. Susanna Röblitz and Dr. Marcus Weber (see Supporting Appendix), which uses a 95 % confidence interval, whereas $\sigma_{x,a}$ corresponds either to Δx_{slope} or $\sigma_{x,SE}$. Δx_{slope} was used when the weighted average $x_g = \overline{k_{on,g(1)}}$ value(s) was determined from *one* experiment (one binding isotherm) and its individual $x, x(i) = k_{on(i)}$ values of every heat flow signal.

According to Butcher *et al.*[164], it is a result of the heat flow signal drifting from the baseline during the course of a titration experiment (with $\Delta x_{slope} = \frac{\sigma_{x_{slope}}}{x_{slope}} \cdot x$).[164] $\sigma_{x,SE}$ was used when the weighted average $x_g = \overline{k_{on,g(n)}}$ value(s) was determined from n series of measurements (multiple binding isotherms) and presents the standard deviation of the best mean value $x, x(i) = \overline{k_{on(\iota)}}$ of every heat flow signal over n series of experiments. $\Delta x_{k_{ITC}}$ is the error propagated from the uncertainty in the instrumental rate constant[164], which was determined to be $\sigma_{\overline{k_{ITC}}} = 0.02$ s^{-1}, so that $\Delta x_{k_{ITC}} = \frac{\sigma_{\overline{k_{ITC}}}}{\overline{k_{ITC}}} \cdot x$ with $\overline{k_{ITC}} = 0.08$ s^{-1} (with $x, x(i) = k_{on(i)}, \overline{k_{on(\iota)}}$)

After determination of the error assumed with the fitting $\sigma_{x,fit}$ of the individual k_{on} values from *one* or n series of measurements ($x, x(i) = k_{on(i)}, \overline{k_{on(\iota)}}$)) in equation (25), then the error of the weighted average $\sigma_{x,g}$ was determined according to equation (26). Because every individual k_{on} value ($x, x(i) = k_{on(i)}, \overline{k_{on(\iota)}}$) has a different uncertainty in $\sigma_{x,fit}$, the final weighted average k_{on} value(s) ($x_g = \overline{k_{on,g(1)}}, \overline{k_{on,g(n)}}$) was weighted over the uncertainties in $\sigma_{x,fit}$, according to equation (27). After the weighted average k_{on} value(s) ($x_g = \overline{k_{on,g(1)}}, \overline{k_{on,g(n)}}$) has been recovered, the final error $\sigma_{x,FE}$ was then calculated according to equation (28).

The confidence interval in equation (28) Δx_{K_d} is defined as $\Delta x_{K_d} = \frac{\sigma_{K_d,FE}}{K_d} \cdot x_g$ (with $x_g = \overline{k_{on,g(1)}}$, $\overline{k_{on,g(n)}}$) and presents the uncertainty in the equilibrium dissociation constant K_d, which directly affects the weighted average $x_g = \overline{k_{on,g(1)}}, \overline{k_{on,g(n)}}$ value(s).[164] Here, K_d values correspond either to an individual value K_d or the best-mean value $\overline{K_d}$, following *one* or n series of measurements, with its final errors $\sigma_{K_d,FE}$ or σ_{K_d,FE^*} (depending on the error propagation applied for K_d, see Chapter 5.2.3). Errors in the dissociation equilibrium constant $\frac{\sigma_{K_d,FE}}{K_d}$ ranged relatively between ± 4 % and ± 46 %, following error analysis as described in Chapter 5.2.3 (see also the corresponding tables of thermodynamic and kinetic quantities). An additional arbitrary error source, which may contribute to the final error $\sigma_{x,FE}$ in the $x_g = \overline{k_{on,g(1)}}, \overline{k_{on,g(n)}}$ value(s), is the uncertainty in the determination of the protein concentration[164] $\Delta x_{c_{P,0}}$, which was ± 10 % and determined from the errors in estimating the UV standard curve (see Chapter 5.2.3). The error in estimating the ligand concentration was already included in the final error of the K_d value(s) ($\sigma_{K_d,FE}$ or σ_{K_d,FE^*}, following the error analysis of the thermodynamic parameters as described in Chapter 5.2.3), that contributes to the final error in the $x_g = \overline{k_{on,g(1)}}, \overline{k_{on,g(n)}}$ value(s).

The backward rate constant (k_{off} value(s)) was directly calculated using the general expression (29):

$$k_{off} = k_{on} \cdot K_d \qquad (29)$$

To avoid complicated expressions here, the above variable nomenclature will be omitted, but also holds for the weighted average k_{off} value(s) and its errors. Furthermore, the above variables' nomenclature was used, so that the reader may follow, how to systematically proceed in the error propagation of the corresponding k_{on} value(s) and how to determine the weighted average value(s), which are defined by either *one* or *n series* of measurements. The final error in a resulting k_{off} value was calculated using the general equation (30):

$$\sigma_{k_{off,FE}} = \sqrt{\left(\frac{\sigma_{k_{on,FE}}}{k_{on}}\right)^2 \cdot \left(\frac{\sigma_{K_{d,FE}}}{K_d}\right)^2} \cdot k_{off} \tag{30}$$

All data processing, graphing and analysis procedures were performed using MATLAB and OriginPro9.0 (OriginLab, USA).

5.3. Analysis of the temperature dependence of rate constants using the Eyring equation

For determination of activation parameters according to the Eyring equation, ITC experiments were performed at different temperatures. Subsequent analysis of the heat profiles at the given temperatures, following the here described least-squares minimization procedure (see Supporting Appendix), was then used to recover the rate constants from the heat profiles. Determination of the weighted average k_{on} and k_{off} values and their errors was performed as described in the previous chapter, at 298.15 K, 303.15 K and 308.15 K.

5.3.1. General procedure in the transition state analysis

For determination of the transition state parameters the weighted average on- and off-rate constants $x_g = \overline{k_{on,g(1)}}, \overline{k_{on,g(n)}}, \overline{k_{off,g(1)}}, \overline{k_{off,g(n)}}$ were used, as determined from the procedure, which is described in the last chapter. Before calculation of the activation free energy $\Delta G^{\ddagger} = \Delta G_{on}^{\ddagger}$, $\Delta G_{off}^{\ddagger}$ for the on- and off-transition states using the Eyring equation, the on- and off-rate constants were further weighted averaged over the given temperature range (as every individual on- and off-rate, for each of the three temperatures has a different uncertainty). The over the temperature range weighted averaged on- and off-rate constants $x_{g,dT} = \overline{k_{on,g,dT}}, \overline{k_{off,g,dT}}$ were therefore calculated first, using the following general equations:

$$x_{g,dT} = \frac{\sum x_g(T) \cdot g(T)}{\sum g(T)}, \tag{31}$$

$$\sigma_{xg,dT} = \left(\sum \frac{1}{\sigma_{x,FE}^2}\right)^{-\frac{1}{2}} = \left(\sum g(T)\right)^{-\frac{1}{2}},$$

where $x_g = \overline{k_{on,g(1)}}, \overline{k_{on,g(n)}}, \overline{k_{off,g(1)}}, \overline{k_{off,g(n)}}$ is respectively the determined on- and off-rate constant for one given temperature and $\sigma_{x,FE} = \sigma_{\overline{k_{on,g(1)}}}, \sigma_{\overline{k_{on,g(n)}}}$ or $\sigma_{\overline{k_{off,g(1)}}}, \sigma_{\overline{k_{on,g(n)}}}$ is the final error of the individual weighted average rate constants for one given temperature (as described in the last chapter), whereas $x_{g,dT} = \overline{k_{on,g,dT}}, \overline{k_{off,g,dT}}$ presents the on- and off-rate constant for the given temperature range, with its weighted average error $\sigma_{xg,dT} = \sigma_{\overline{k_{on,g,dT}}}, \sigma_{\overline{k_{off,g,dT}}}$.

Once a weighted average value in the on-/off-rate for the given temperature range was obtained, the on/off-activation free energy $\Delta G^{\ddagger} = \Delta G_{on}^{\ddagger}, \Delta G_{off}^{\ddagger}$ values were calculated according to the Eyring equation (32), with k being either the weighted on- or off-rate constant ($k = x_{g,dT} = \overline{k_{on,g,dT}}$, $\overline{k_{off,g,dT}}$), as determined by equations (31) .

$$\Delta G^{\ddagger} = RT\left[\ln\left(\frac{k_b T}{h}\right) - \ln(k)\right] \tag{32}$$

(Here, $h = 6.626 \cdot 10^{-34}$ J s is Planck's constant and $k_B = 1.3806 \cdot 10^{-23}$ J K^{-1} is the Boltzmann constant.)

Eying plots were then generated from the same weighted averaged individual on- and off-rate constants for one given temperature, with $k = x_g = \overline{k_{on,g(1)}}, \overline{k_{on,g(n)}}, \overline{k_{off,g(1)}}, \overline{k_{off,g(n)}}$ and their final errors $\sigma_{x,FE} = \sigma_{\overline{k_{on,g(1)}}}, \sigma_{\overline{k_{on,g(n)}}}$ or $\sigma_{\overline{k_{off,g(1)}}}, \sigma_{\overline{k_{on,g(n)}}}$, which allowed the calculation of the on-/off-transition state enthalpies $\Delta H^{\ddagger} = \Delta H_{on}^{\ddagger}, \Delta H_{off}^{\ddagger}$ according to:

$$\ln\left(\frac{k}{T}\right) = -\frac{\Delta H^{\ddagger}}{RT} + \frac{\Delta S^{\ddagger}}{R} + \ln\left(\frac{k_B}{h}\right) = -\frac{\Delta H^{\ddagger}}{RT} + \frac{\Delta S^{\ddagger}}{R} + \ln(\alpha). \tag{33}$$

The on-/off-transition state enthalpies $\Delta H^{\ddagger} = \Delta H_{on}^{\ddagger}, \Delta H_{off}^{\ddagger}$ were calculated from the slope ($a = -\frac{\Delta H^{\ddagger}}{R}$) of a plot $\ln\frac{k}{T}$ *versus* the inverse temperature $\frac{1}{T}$. The on-/off-activation entropy $-T\Delta S^{\ddagger} = -T\Delta S_{on}^{\ddagger}, -T\Delta S_{off}^{\ddagger}$ was then determined from the Gibbs-Helmholtz equation (34), instead of using the y-intercept of the Eyring plot (to reduce the error in the activation entropy, since the y-intercept presents a large extrapolation[237]).

$$-T\Delta S^{\ddagger} = \Delta G^{\ddagger} - \Delta H^{\ddagger} \tag{34}$$

Here, $-T\Delta S^{\ddagger} = -T\Delta S_{on}^{\ddagger}, -T\Delta S_{off}^{\ddagger}, \Delta H^{\ddagger} = \Delta H_{on}^{\ddagger}, \Delta H_{off}^{\ddagger}$ and $\Delta G^{\ddagger} = \Delta G_{on}^{\ddagger}, \Delta G_{off}^{\ddagger}$ are representative for the forward and backward processes of the transition state. All Eyring plots of the $k = x_g = \overline{k_{on,g(1)}}$, $\overline{k_{on,g(n)}}, \overline{k_{off,g(1)}}, \overline{k_{off,g(n)}}$ values revealed a linear dependence on temperature.

5.3.2. Error analysis in the transition state parameters

Errors in $\Delta G^{\ddagger}_{on}$, $\Delta G^{\ddagger}_{off}$ were derived from the error of the weighted average $\sigma_{xg,dT} = \sigma_{\overline{k_{on,g,dT}}}$, $\sigma_{\overline{k_{off,g,dT}}}$ in the corresponding on-/off-rate constants as obtained by equations (31) and calculated using equation (35):

$$\sigma_{\Delta G^{\ddagger}_{on;off}} = RT \cdot \frac{\sigma_{xg,dT}}{x_{g,dT}} = RT \cdot \frac{\sigma_{\overline{k_{on,g,dT};k_{off,g,dT}}}}{\overline{k_{on,g,dT}};\overline{k_{off,g,dT}}}. \tag{35}$$

All errors in the activation enthalpy and entropy were propagated as described by equations (36) – (38). Error analysis of the individual rate constants for every single temperature $\sigma_{x,FE} = \sigma_{\overline{k_{on,g(1)}}}$, $\sigma_{\overline{k_{on,g(n)}}}$ or $\sigma_{\overline{k_{off,g(1)}}}$, $\sigma_{\overline{k_{on,g(n)}}}$ was performed as described in the previous chapter by applying equations (28) and (30). These final errors in the association and dissociation rate constants $x_g = \overline{k_{on,g(1)}}$, $\overline{k_{on,g(n)}}$, $\overline{k_{off,g(1)}}$, $\overline{k_{off,g(n)}}$ (rate constants were determined using equations (27) and (29)) were then propagated in the natural logarithm of the Eyring plot (33) using the following expression:

$$\Delta \ln x = \frac{\Delta x}{x} \approx \sigma_{\ln x_g} = \frac{\sigma_{x,FE}}{x_g}. \tag{36}$$

Determination of standard errors in the activation enthalpy $\Delta H^{\ddagger}_{on;off}$ and entropy $-T\Delta S^{\ddagger}_{on;off}$ was performed as described by Girolami *et al.*[238] according to the following equations.

$$\sigma_{\Delta H^{\ddagger}_{on;off}} = \sqrt{\frac{R^2 T^2_{max} T^2_{min}}{\Delta T^2}\left\{\left(\frac{\sigma_T}{T}\right)^2\left[\left(1 + T_{min}\frac{\Delta L}{\Delta T}\right)^2 + \left(1 + T_{max}\frac{\Delta L}{\Delta T}\right)^2\right] + 2\left(\frac{\sigma_{xg,dT}}{x_{g,dT}}\right)^2\right\}} \tag{37}$$

$$\sigma_{\Delta S^{\ddagger}_{on;off}}$$
$$= \sqrt{\frac{R^2}{\Delta T^2}\left\{\left(\frac{\sigma_T}{T}\right)^2\left[T^2_{max}\left(1 + T_{min}\frac{\Delta L}{\Delta T}\right)^2 + T^2_{min}\left(1 + T_{max}\frac{\Delta L}{\Delta T}\right)^2\right] + \left(\frac{\sigma_{xg,dT}}{x_{g,dT}}\right)^2 (T^2_{max} T^2_{min})\right\}} \tag{38}$$

Here, $\Delta T = T_{max} - T_{min}$ (with T_{max} = 308.15 K and T_{min} = 298.15 K) and $\Delta L = \ln x_{g,max} - \ln x_{g,min}$ (with $x_{g,max;min}$ being the corresponding maximum and minimum association and dissociation rate constants $\overline{k_{on,g(1)}}$, $\overline{k_{on,g(n)}}$, $\overline{k_{off,g(1)}}$, $\overline{k_{off,g(n)}}$, according to the maximum and minimum temperatures $T_{max;min}$). $x_{g,dT} = \overline{k_{on,g,dT}}, \overline{k_{off,g,dT}}$ is the respective weighted average on- or off-rate constant determined for the given temperature range according to equations (31), with $\sigma_{xg,dT} = \sigma_{\overline{k_{on,g,dT}}}$, $\sigma_{\overline{k_{off,g,dT}}}$ being their respective weighted average errors. T = 298.15 K is the absolute standard temperature, and σ_T is the error in the temperature (which was empirically estimated to be $\sigma_T = \pm 1$ K), and R = 8.3145 J K^{-1} mol^{-1} is the universal gas constant. The error in the standard state entropy was then calculated according to $-T\Delta S^{\ddagger}_{on;off}$ at 298.15 K:

$$\sigma_{-T\Delta S^{\ddagger}_{on;off}} = -\left(\sigma_{\Delta S^{\ddagger}_{on;off}} \cdot T\right). \tag{39}$$

5.4. Solid phase reactions

5.4.1. General procedures on solid phase

General procedure for oligomer elongation GP 1: All solid phase reactions were performed on 0.025 mmol, 0.05 mmol or 0.1 mmol scale, either by hand-coupling in $5 - 10$ mL polypropylene Chromabond columns with a polypropylene frit closed at the bottom with a B7 septum, or on a standard peptide synthesizer Activo-P11 from Activotec equipped with an UV detector. Protocols for automated synthesis were written as recommended by Activotec, using the supplied software templates for standard Fmoc solid phase synthesis. Before starting the initial coupling, the resin was swollen for 30 min in DCM.

The unprotected EDA-Trt resin or the Fmoc protected Tentagel S RAM resin were used for repetitive building block coupling. The protected oligo(amido amine) resins were prepared using 109 mg, 217 mg or 435 mg of either EDA-Trt or Tentagel S RAM resin (0.23 mmol of NH_2/g of resin) by coupling of a first building block. Depending on the oligomer and peptide composition, either ADS, TDS, EDS, SDS, Fmoc-Lys(Boc)-OH, Fmoc-Lys(Alloc)-OH, Fmoc-Ala-OH, Fmoc-Phe-OH or succinic anhydride were used as building blocks. After each building block coupling, the resin was treated with a 25 % piperidine solution in DMF for 5, 10 and 20 min. The next building block was then added to the growing oligomer chain by step-wise addition, using standard solid phase methods as has been previously described[100, 103, 105].

Each coupling reaction was achieved using a 5-fold excess (0.125, 0.25 or 0.5 mmol) of the corresponding building block (ADS: 64, 127 or 255 mg; TDS: 63, 126 or 253 mg; EDS: 57, 114 or 228 mg; SDS: 49, 96 or 191 mg; Fmoc-Lys(Boc)-OH: 59, 117 or 234 mg; Fmoc-Lys(Alloc)-OH: 57, 113, 226 mg, Fmoc-Ala-OH: 39, 78, 156 mg, Fmoc-Phe-OH: 48, 97, 194 mg), and 4.9 equiv (0.123, 0.245 or 0.49 mmol) PyBOP (64, 128 or 255 mg) in the presence of 10 equiv (0.25, 0.5 or 0.1 mmol) iPr$_2$NEt (43, 85 or 170 µL) in $1 - 2$ mL DMF. The coupling of succinic anhydride (25, 50 or 100 mg) was performed by dissolving a 10-fold excess (0.25, 0.5 or 0.1 mmol) in the presence of 20 equiv (0.5, 1 or 2 mmol) iPr$_2$NEt (87, 175 or 350 µL) in $1 - 2$ mL DMF. The corresponding reagent mixture was directly added to the resin. The suspension was shaken for 1 h. The N^a-Fmoc protecting group was removed by treating the oligomer resin with a 25 % piperidine solution in DMF (1 x 5 min; 1 x 10 min and 1 x 20 min). The peptide resin was washed with DMF (10 x), DCM (5 x) and again with DMF (3 x). Upon complete formation of the protected linear oligo(amido amine), the final N^a-Fmoc protecting group was removed as usual with a 25 % piperidine solution in DMF and acetylated with acetic anhydride for $10 - 20$ min, by treating the resin directly with a fresh

3 − 5 mL of 98 % acetic anhydride solution. All procedures so far were done under argon atmosphere. This general procedure was used to prepare all of the oligo(amido amine) precursors, before addition of either of the different αMan derivatives. The elongation progress and coupling completeness were monitored by UV and the Kaiser test.

General procedure for αMan functionalization *via* CuCAAC GP 2: Functionalization with the three different αMan derivatives was performed as previously described[100, 105], and as will be shortly described in the following. In a typical procedure, to the resin loaded TDS presenting oligo(amido amine), previously washed with DCM, was added an αMan derivative solution in 0.5 − 1 mL DMF, consisting of either 5 equiv (0.25 mmol) *O*-ethyl-2-azido-α-D-mannopyranoside (62 mg), *O*-propyl-3-thio-*S*-ethyl-5-azido-α-D-mannopyranoside (81 mg, "S") or *O*-*p*-benzyl-*p*-ethyl-2-azido-α-D-mannopyranoside (81 mg, "B").[14] Subsequently, a suspension of 20 mol % (10 μmol) $CuSO_4$ (1.6 mg) and sodium ascorbate (2 mg) in 0.5 − 1 mL water and one drop of DMF, was added to the resin and the whole reagent cocktail agitated to yield a homogenous suspension. The reaction was shaken for about 4 h. Then, the glycooligomer resin was washed with a 1 M sodium dithiocarbamate/DMF solution (10 x; scavenger for the copper(I) catalyst), H_2O (10 x), DMF (10 x) and DCM (5 x). The washing process was repeated until the resin and the washing solution decolorized.

(A) General procedure for synthesis of cyclic *N*-substituted imides after generation of the desired backbone on the Tentagel S RAM resin, (B) side-chain-to-tail amide cyclization on the Tentagel S RAM resin *via* step-wise Boc deprotection and subsequent cyclization by coupling or (C) side-chain-to-tail amide cyclization on EDA modified Tentagel S Chloro-Trt resin *via* step-wise Boc deprotection and subsequent cyclization by coupling GP 3. (A) A fresh solution consisting of 20 equiv (0.5, 1 or 2 mmol) of a corresponding trimethylsilyl (TMS) derivative – with either 91, 181, 363 μL TMSOTf or 66, 132, 264 μL TMSBr – and 30 equiv (0.75, 1.5, 3 mmol) *i*Pr$_2$NEt (128, 255, 510 μL) in 2 mL DCM was added to the resin preloaded with a linear oligomer, which contains the Lys-*N*ᵋ-Boc building block as the *C* terminal sequence and succinic acid as the *N* terminal sequence. A fresh solution of the reagent cocktail was prepared every 15 min due to reagents' decomposition. The resin was then treated with the reagent cocktail and the cyclization process allowed to proceed by gentle shaking. After every 5 − 10 min shaking, an aliquot of the suspension was then taken for analysis and quenched, and the conversion was checked after cleavage from solid support according to GP 5 (A) by UV monitoring at 214 nm using RP-HPLC. Therefore, the resin aliquot was filtered and washed with 10 % *i*Pr$_2$NEt in DCM for neutralization and pure DCM, followed by cleavage from the solid support as described in GP 5 (A). After every 15 min the resin was then again treated with a fresh solution of the corresponding TMSX/*i*Pr$_2$NEt mixture in DCM and allowed to react. After another 5 − 10 min shaking, a resin aliquot was again taken for analysis of the reaction

---

[14]   *O*-propyl-3-thio-*S*-ethyl-5-azido-α-D-mannopyranoside   ("S")   and   *O*-*p*-benzyl-*p*-ethyl-2-azido-α-D-mannopyranoside ("B") have been provided by Anne Müller (Christian-Albrechts-Universität Kiel, group of Prof. Dr. Thisbe K. Lindhorst).

progress as described above. The procedure was repeated until the imide cyclization was complete as monitored by RP-HPLC (after a total reaction time of 35 − 45 min).

(B) To compare this protocol to a conventional well-established two-step process, experiments for determining the conversion/cyclization progress were performed using a 3 M phenol/1 M TMSCl solution[203, 209] in 2 mL DCM, freshly prepared. As the Boc deprotection cannot be quantified using the Tentagel S RAM resin due to the acidic cleavage procedure, deprotection had to be quantified by subsequent coupling with PyBOP (cyclization). Therefore, after every 5 – 10 min of Boc deprotection, an resin aliquot was taken and the reaction was quenched as described above, followed by coupling for 20 min with 4.9 equiv PyBOP (0.123 mmol, 64 mg) in the presence of 10 equiv iPr$_2$NEt (0.25 mmol, 44 μL) in 1 mL DMF as described in GP 1. The cyclization progress was then checked by test-cleavage and analysis by RP-HPLC as described above. The procedure was repeated every 5 − 10 min or 30 − 60 min, until the cyclization was complete.

(C) A fresh solution consisting of 33 mL 37 % hydrochloric acid (HCl$_{aq}$, ~12 M) and 67 mL dioxane was prepared (diluted with dioxane to 4 M). 4 mL of the HCl$_{aq}$/dioxane solution were added to the resin, preloaded with a linear oligomer and Lys-N^{ε}-Boc as the C terminal sequence and succinic acid as the N terminal sequence. The observed exotherm was effectively cooled at 0°C with a simple ice-bath (by simply dropping the syringe into ice-water). Boc deprotection was allowed to proceed for 20 min by gentle shaking and slow equilibration first to 4°C and then to RT. Deprotection was quenched by resin filtration, followed by washing with 2 M iPr$_2$NEt in DCM (several times for neutralization, until the gas evolution stopped) and finally with DMF and DCM. The amount/progress of Boc deprotection was checked by RP-HPLC either *after* (*i*) cyclization *via* coupling with 4.9 equiv (0.123, 0.245, 0.49 mmol) PyBOP (64, 128 or 255 mg) and 10 equiv (0.25, 0.5 or 0.1 mmol) iPr$_2$NEt (43, 85 or 170 μL) in 1 − 2 mL for 20 min, as described above and in GP 1 or (*ii*) after acetylation for 10 − 20 min with 3 − 5 mL of a 98 % acetic anhydride solution. (Boc deprotection cannot be quantified *per se* using electrophilically cleavable resins, but only indirectly after additional coupling of the deprotected amine group). Both steps were repeated if cyclization was incomplete (usually in double or triple deprotections).

General procedure for Alloc deprotection of primary N^{ε}- or secondary N^{δ}-Alloc groups (e.g. C terminal Lys side-chain or ADS containing oligomer sequences) GP 4. Alloc deprotection is based on the protocols previously used[99, 142, 184-186, 189, 191-192, 195-196, 199], with few modifications as shortly described in the following. 30 mol % (7.5, 15, 30 μmol) of tetrakis(triphenylphosphine)palladium(0) (Pd^0(PPh$_3$)$_4$) (9, 17, 35 mg) and 10 equiv (0.25, 0.5, 1 mmol) N,N^2-dimethylbarbituric acid (N,N^2-DMBA) (36, 71, 142 mg) were placed into a 15 mL falcon tube, flushed with argon and protected against light. Then, 2 mL of DCM were added to the falcon tube and the catalyst/scavenger dissolved under a gentle argon stream. The resin was immediately treated with the deprotection cocktail and allowed to react for 30 min. After deprotection, the resin was washed several times arbitrarily with several mL of CHCl$_3$, DCM, 1 M iPr$_2$NEt/DMF solution, 1 M dithiocarbamate

solution, DMF and again DCM for resin drying. The washing procedure was repeated until the resin became colorless and the solution was clear. The whole procedure was repeated once or twice for complete deprotection (double or triple deprotection).

General cleavage protocol for the Tentagel S RAM and EDA modified Tentagel S Chloro-Trityl resin GP 5. (A) The resin was treated with a fresh cleavage solution consisting of 95 % trifluoroacetic acid (TFA), 2.5 % triisopropylsilane (*i*Pr₃SiH) and 2.5 % H_2O (1 mL/50 mg resin). The suspension was shaken for 70 min. The cleavage solution was then purged directly into ice-cold diethyl ether (Et_2O) by resin filtration. The precipitate was isolated by centrifugation and washed twice with ice-cold Et_2O. All glycomacromolecules were purified by semi-preparative RP-HPLC (column 2, linear gradient in 30 min with 5 % to 30 % or 5 % to 50 % MeCN (B); see "General materials and methods"). Analytical RP-HPLC was used to check for the glycomacromolecules purity. Finally, the collected fractions were lyophilized overnight, giving the final product and the corresponding yield.

(B) The resin was treated with a fresh cleavage solution consisting of 30 % TFA in DCM and shaken for 30 min. Precipitation, purification and drying were performed as described in **(A)**.

5.5. Characterization data of linear glycomacromolecules with SDS spacer[15]

Compound Man(3)-5SDS (1SDS)

Compound Man(3)-5SDS (1SDS) (25 mg, 21 µmol) was obtained as lyophilized powder according to GP 1, GP 2 and GP 5 (B) in a yield of 42 %. ^1H NMR (600 MHz, D_2O) δ 7.99 (s, 1H), 4.73 – 4.63 (m, 2H), 4.10 (ddd, *J* = 11.1, 7.1, 4.0 Hz, 1H), 3.94 (ddd, *J* = 11.2, 5.4, 3.7 Hz, 1H), 3.86 (dd, *J* = 3.4, 1.8 Hz, 1H), 3.75 (dd, *J* = 12.2, 2.3 Hz, 1H), 3.70 – 3.63 (m, 2H), 3.59 (t, *J* = 9.7 Hz, 1H), 3.53 – 3.42 (m, 6H), 3.41 – 3.23 (m, 20H), 3.14 (t, *J* = 6.0 Hz, 2H), 3.09 – 3.06 (m, 1H), 3.03 (t, *J* = 7.2 Hz, 2H), 2.82 (t, *J* = 7.3 Hz, 2H), 2.61 – 2.41 (m, 20H), 1.97 (s, 3H). 66H out of in total 67H are reported in the ^1H NMR, because the signal for the α-anomeric proton (1H) is hidden behind the HDO signal (as determined by $^1H/^{13}C$ HSQC NMR). MALDI-TOF calcd for $C_{49}H_{85}N_{16}O_{18}^+$ [M+H]⁺, 1185.622 (monoisotopic); found. 1185.630; calcd for $C_{49}H_{84}N_{16}NaO_{18}^+$ [M+Na]⁺, 1207.604 (monoisotopic); found. 1207.610; calcd for $C_{49}H_{84}KN_{16}O_{18}^+$ [M+K]⁺, 1223.578 (monoisotopic); found. 1223.598. RP-HPLC analysis with a linear gradient in 30 min, 5 % to 30 % MeCN (B) at 214 nm, column 1, T_R = 4.7 min, purity > 91 %.

---

[15]Compounds 1SDS, 1aSDS, 2SDS and 2aSDS have been synthesized and characterized (NMR, RP-HPLC and MALDI-TOF) by Hendrik Wöhlk (Heinrich-Heine-Universität Düsseldorf, group of Prof. Dr. Laura Hartmann, Master Thesis, April 2015). In this thesis, the above mentioned compounds have been re-synthesized, and their characterization data (NMR, RP-HPLC and MALDI-TOF) reported and discussed in this thesis corresponds to the re-synthesized compounds and characterization data as re-assessed by the author of this thesis.

Compound Man(4)-7SDS (1aSDS)

Compound Man(4)-7SDS (1aSDS) (40 mg, 27 µmol) was obtained as lyophilized powder according to GP 1, GP 2 and GP 5 (B) in a yield of 54 %. ^{1}H NMR (600 MHz, D$_2$O) δ 7.94 (s, 1H), 4.71 – 4.61 (m, 2H), 4.10 (ddd, J = 11.1, 7.2, 4.0 Hz, 1H), 3.93 (ddd, J = 11.2, 5.4, 3.7 Hz, 1H), 3.86 (dd, J = 3.3, 1.8 Hz, 1H), 3.75 (dd, J = 12.3, 2.4 Hz, 1H), 3.70 – 3.63 (m, 2H), 3.60 (t, J = 9.7 Hz, 1H), 3.54 – 3.42 (m, 6H), 3.42 – 3.23 (m, 28H), 3.15 (t, J = 6.0 Hz, 2H), 3.09 – 2.96 (m, 3H), 2.81 (t, J = 7.3 Hz, 2H), 2.62 – 2.40 (m, 28H), 1.98 (s, 3H). 82H out of in total 83H are reported in the ^{1}H NMR, because the signal for the α-anomeric proton (1H) is hidden behind the HDO signal (as determined by ^{1}H/^{13}C HSQC NMR). MALDI-TOF calcd for C$_{61}$H$_{105}$N$_{20}$O$_{22}^+$ [M+H]$^+$, 1469.771 (monoisotopic); found 1469.796; calcd for C$_{61}$H$_{104}$N$_{20}$NaO$_{22}^+$ [M+Na]$^+$, 1491.753 (monoisotopic); found 1491.793; calcd for C$_{61}$H$_{104}$KN$_{20}$O$_{22}^+$ [M+K]$^+$, 1507.727 (monoisotopic); found 1507.785. RP-HPLC analysis with a linear gradient in 30 min, 5 % to 30 % MeCN (B) at 214 nm, column 1, T$_R$ = 5.9 min, purity > 95 %.

Compound Man(1,3,5)-5SDS (2SDS)

Compound Man(1,3,5)-5SDS (2SDS) (49 mg, 25 µmol) was obtained as lyophilized powder according to GP 1, GP 2 and GP 5 (B) in a yield of 51 %. ^{1}H NMR (600 MHz, D$_2$O) δ 7.97 – 7.89 (m, 3H), 4.72 – 4.58 (m, 6H), 4.14 – 4.05 (m, 3H), 3.97 – 3.89 (m, 3H), 3.86 (dd, J = 3.3, 1.7 Hz, 3H), 3.78 – 3.70 (m, 3H), 3.70 – 3.63 (m, 6H), 3.60 (t, J = 9.7 Hz, 3H), 3.54 – 3.41 (m, 14H), 3.41 – 3.35 (m, 6H), 3.35 – 3.30 (m, 6H), 3.28 (s, 8H), 3.15 (t, J = 5.9 Hz, 2H), 3.09 – 3.03 (m, 3H), 3.03 – 2.96 (m, 6H), 2.86 – 2.75 (m, 6H), 2.61 – 2.39 (m, 20H), 1.94 + 1.93 (two s, 3H, due to 1:1 mixture of rotamers). 104H out of in total 107H are reported in the ^{1}H NMR, because the signal for the α-anomeric protons (3H) is hidden behind the HDO signal (as determined by ^{1}H/^{13}C HSQC NMR). MALDI-TOF calcd for C$_{79}$H$_{133}$N$_{24}$O$_{32}^+$ [M+H]$^+$, 1929.951 (monoisotopic); found. 1929.987; calcd for C$_{79}$H$_{132}$N$_{24}$NaO$_{32}^+$ [M+Na]$^+$, 1951.933 (monoisotopic); found. 1952.007; calcd for C$_{79}$H$_{132}$KN$_{24}$O$_{32}^+$ [M+K]$^+$, 1967.907 (monoisotopic); found. 1967.999. RP-HPLC analysis with a linear gradient in 30 min, 5 % to 30 % MeCN (B) at 214 nm, column 1, T$_R$ = 6.8min, purity > 96 %.

Compound Man(1,4,7)-7SDS (2aSDS)

Compound Man(1,4,7)-7SDS (2aSDS) (35 mg, 16 µmol) was obtained as lyophilized powder according to GP 1, GP 2 and GP 5 (B) in a yield of 32 %. ^{1}H NMR (600 MHz, D$_2$O) δ 8.03 – 7.89 (m, 3H), 4.72 – 4.60 (m, 6H), 4.15 – 4.04 (m, 3H), 3.97 – 3.89 (m, 3H), 3.89 – 3.82 (m, 3H), 3.77 – 3.70 (m, 3H), 3.70 – 3.63 (m, 6H), 3.60 (t, J = 9.7 Hz, 3H), 3.53 – 3.40 (m, 14H), 3.40 – 3.31 (m, 12H), 3.28 (s, 16H), 3.14 (t, J = 5.9 Hz, 2H), 3.11 – 3.05 (m, 3H), 3.04 – 2.97 (m, 6H), 2.81 (t, J = 7.3 Hz, 6H), 2.58 – 2.39 (m, 28H), 1.94 + 1.93 (two s, 3H, due to 1:1 mixture of rotamers). 120H out of in total 123H are reported in the ^{1}H NMR, because the signal for the α-anomeric protons (3H) is hidden behind the HDO signal (as determined by ^{1}H/^{13}C HSQC NMR). MALDI-TOF calcd for C$_{91}$H$_{153}$N$_{28}$O$_{36}^+$ [M+H]$^+$, 2214.100 (monoisotopic); found. 2214.175; calcd for C$_{91}$H$_{152}$N$_{28}$NaO$_{36}^+$

[M+Na]+, 2236.082 (monoisotopic); found. 2236.199; calcd for $C_{91}H_{152}KN_{28}O_{36}^+$ [M+K]+, 2252.056 (monoisotopic); found. 2252.165. RP-HPLC analysis with a linear gradient in 30 min, 5 % to 30 % MeCN (B) at 214 nm, column 1, T_R = 7.8 min, purity > 95 %.

5.6. Characterization data of linear glycomacromolecules with EDS spacer

Compound Man(3)-5 (1)

Compound Man(3)-5 (1) (60 mg, 39 µmol) was obtained as lyophilized oil according to GP 1, GP 2 and GP 5 (B) in a yield of 78 %. ^{1}H NMR (600 MHz, D$_2$O) δ 7.93 (s, 1H), 4.70 – 4.62 (m, 2H), 4.10 (ddd, J = 11.0, 7.2, 3.9 Hz, 1H), 3.93 (ddd, J = 11.1, 5.3, 3.7 Hz, 1H), 3.86 (dd, J = 3.3, 1.8 Hz, 1H), 3.75 (dd, J = 12.2, 2.4 Hz, 1H), 3.72 – 3.66 (m, 17H), 3.65 – 3.58 (m, 17H), 3.57 – 3.44 (m, 7H), 3.43 – 3.28 (m, 20H), 3.15 (t, J = 5.9 Hz, 2H), 3.08 – 3.04 (m, 1H), 3.02 (t, J = 7.2 Hz, 2H), 2.81 (t, J = 7.3 Hz, 2H), 2.65 – 2.40 (m, 20H), 2.00 (s, 3H). 98H out of in total 99H are reported in the ^{1}H NMR, because the signal for the α-anomeric proton (1H) is hidden behind the HDO signal (as determined by ^{1}H/^{13}C HSQC NMR). MALDI-TOF calcd for $C_{65}H_{117}N_{16}O_{26}^+$ [M+H]+, 1537.832 (monoisotopic); found. 1537.663; calcd for $C_{65}H_{116}N_{16}NaO_{26}^+$ [M+Na]+, 1559.814 (monoisotopic); found. 1559.656; calcd for $C_{65}H_{116}KN_{16}O_{26}^+$ [M+K]+, 1575.788 (monoisotopic); found. 1575.632. RP-HPLC analysis with a linear gradient in 30 min, 5 % to 95 % MeCN (B) at 214 nm, column 1, T_R = 7.7 min, purity > 98 %.

Compound Man(4)-8 (1a)

Compound Man(4)-8 (1a) (60 mg, 27 µmol) was obtained as lyophilized oil according to GP 1, GP 2 and GP 5 (B) in a yield of 54 %. ^{1}H NMR (600 MHz, D$_2$O) δ 8.01 (s, 1H), 4.74 – 4.63 (m, 2H), 4.11 (ddd, J = 11.0, 7.1, 4.0 Hz, 1H), 3.94 (dt, J = 11.2, 4.1 Hz, 1H), 3.86 (dd, J = 3.4, 1.7 Hz, 1H), 3.75 (dd, J = 12.3, 2.3 Hz, 1H), 3.73 – 3.65 (m, 30H), 3.64 – 3.53 (m, 29H), 3.53 – 3.43 (m, 7H), 3.38 (t, J = 5.5 Hz, 31H), 3.14 (t, J = 5.9 Hz, 2H), 3.11 – 3.07 (m, 1H), 3.04 (t, J = 7.3 Hz, 2H), 2.82 (t, J = 7.2 Hz, 2H), 2.65 – 2.38 (m, 32H), 2.00 (s, 3H). 146H out of in total 147H are reported in the ^{1}H NMR, because the signal for the α-anomeric proton (1H) is hidden behind the HDO signal (as determined by ^{1}H/^{13}C HSQC NMR). MALDI-TOF calcd for $C_{95}H_{171}N_{22}O_{38}^+$ [M+H]+, 2228.212 (monoisotopic); found. 2228.014; calcd for $C_{95}H_{170}N_{22}NaO_{38}^+$ [M+Na]+, 2250.194 (monoisotopic); found. 2250.008; calcd for $C_{95}H_{170}KN_{22}O_{38}^+$ [M+K]+, 2266.168 (monoisotopic); found. 2265.990. LC/MS ESI calcd for $C_{95}H_{173}N_{22}O_{38}^{3+}$ [M+3H]3+, 743.7; found. 743.6; calcd for $C_{95}H_{174}N_{22}O_{38}^{4+}$ [M+4H]4+, 558.1; found. 558.0; calcd for $C_{95}H_{175}N_{22}O_{38}^{5+}$ [M+5H]5+, 446.6; found. 446.6. RP-HPLC analysis with a linear gradient in 30 min, 5 % to 30 % MeCN (B) at 214 nm, column 1, T_R = 15.9 min, purity > 95 %.

Compound Man(1,5)-5 (2)

Compound Man(1,5)-5 (2) (36 mg, 20 µmol) was obtained as lyophilized oil according to GP 1, GP 2 and GP 5 (B) in a yield of 40 %. ^{1}H NMR (500 MHz, D$_2$O) δ 7.99 (s, 2H), 4.25 – 4.09 (m, 2H), 4.08 – 3.97 (m, 2H), 3.94 (dd, J = 3.3, 1.8 Hz, 2H), 3.87 – 3.61 (m, 32H), 3.61 – 3.53 (m, 9H), 3.52 – 3.30 (m, 21H), 3.23 (t, J = 6.0 Hz, 2H), 3.20 – 3.13 (m, 2H), 3.09 (t, J = 7.2 Hz, 4H), 2.88 (t, J = 7.3 Hz, 4H), 2.74 – 2.43 (m, 20H), 2.02 + 2.01 (two s, 3H, due to 1:1 mixture of rotamers). 105H out of in total 111H are reported in the ^{1}H NMR, because the signals for α-anomeric protons (2H) and the CH$_2$ group protons (4H) next to the triazole ring (O−CH$_2$−CH_2−NCHN−) are hidden behind the HDO signal (as determined by ^{1}H/^{13}C HSQC NMR). MALDI-TOF calcd for C$_{76}$H$_{133}$N$_{20}$O$_{31}$$^+$ [M+H]$^+$, 1821.945 (monoisotopic); found. 1821.972; calcd for C$_{76}$H$_{132}$N$_{20}$NaO$_{31}$$^+$ [M+Na]$^+$, 1843.927 (monoisotopic); found. 1843.973; calcd for C$_{76}$H$_{132}$KN$_{20}$O$_{31}$$^+$ [M+K]$^+$, 1859.900 (monoisotopic); found. 1859,923. HRMS (TOF MS ESI) calcd for C$_{76}$H$_{135}$N$_{20}$O$_{31}$$^{3+}$ [M+3H]$^{3+}$, 607.9862 (monoisotopic); found. 607.9869; calcd for C$_{76}$H$_{136}$N$_{20}$O$_{31}$$^{4+}$ [M+4H]$^{4+}$, 456.2415 (monoisotopic); found. 456.2426. LC/MS ESI calcd for C$_{76}$H$_{134}$N$_{20}$O$_{31}$$^{2+}$ [M+2H]$^{2+}$, 911.9; found. 911.8; calcd for C$_{76}$H$_{135}$N$_{20}$O$_{31}$$^{3+}$ [M+3H]$^{3+}$, 608.0; found. 608.2; calcd for C$_{76}$H$_{136}$N$_{20}$O$_{31}$$^{4+}$ [M+4H]$^{4+}$, 456.24; found. 456.25. RP-HPLC analysis with a linear gradient in 30 min, 5 % to 30 % MeCN (B) at 214 nm, column 1, T$_R$ = 10.3 min, purity > 95 %.

Compound Man(1,6)-6 (2a)

Compound Man(1,6)-6 (2a) (60 mg, 29 µmol) was obtained as lyophilized oil according to GP 1, GP 2 and GP 5 (B) in a yield of 58 %. ^{1}H NMR (600 MHz, D$_2$O) δ 8.02 – 7.89 (m, 2H), 4.74 – 4.59 (m, 4H), 4.15 – 4.05 (m, 2H), 3.99 – 3.89 (m, 2H), 3.86 (dd, J = 3.4, 1.7 Hz, 2H), 3.79 – 3.71 (m, 2H), 3.71 – 3.64 (m, 19H), 3.64 – 3.54 (m, 18H), 3.54 – 3.42 (m, 11H), 3.42 – 3.36 (m, 19H), 3.35 – 3.27 (m, 5H), 3.22 – 2.95 (m, 8H), 2.91 – 2.72 (m, 4H), 2.64 – 2.35 (m, 24H), 1.94 + 1.93 (two s, 3H, due to 1:1 mixture of rotamers). 125H out of in total 127H are reported in the ^{1}H NMR, because the signal for α-anomeric protons (2H) is hidden behind the HDO signal (as determined by ^{1}H/^{13}C HSQC NMR). MALDI-TOF calcd for C$_{86}$H$_{151}$N$_{22}$O$_{35}$$^+$ [M+H]$^+$, 2052.071 (monoisotopic); found. 2052.110; calcd for C$_{86}$H$_{150}$N$_{22}$NaO$_{35}$$^+$ [M+Na]$^+$, 2074.053 (monoisotopic); found. 2074.110; calcd for C$_{86}$H$_{150}$KN$_{22}$O$_{35}$$^+$ [M+K]$^+$, 2090.027 (monoisotopic); found. 2090.071. HRMS (TOF MS ESI) calcd for C$_{86}$H$_{153}$N$_{22}$O$_{35}$$^{3+}$ [M+3H]$^{3+}$, 684.6951 (monoisotopic); found. 684.6951. LC/MS ESI calcd for C$_{86}$H$_{152}$N$_{22}$O$_{35}$$^{2+}$ [M+2H]$^{2+}$, 1026.5; found. 1026.8; calcd for C$_{86}$H$_{153}$N$_{22}$O$_{35}$$^{3+}$ [M+3H]$^{3+}$, 684.7; found 685.0; calcd for C$_{86}$H$_{154}$N$_{22}$O$_{35}$$^{4+}$ [M+4H]$^{4+}$, 513.8; found. 514.0; calcd for C$_{86}$H$_{155}$N$_{22}$O$_{35}$$^{5+}$ [M+5H]$^{5+}$, 411.2; found. 411.2. RP-HPLC analysis with a linear gradient in 30 min, 5 % to 30 % MeCN (B) at 214 nm, column 1, T$_R$ = 12.3 min, purity > 94 %.

Compound Man(1,9)-9 (2b)

Compound Man(1,9)-9 (2b) (70 mg, 26 µmol) was obtained as lyophilized oil according to GP 1, GP 2 and GP 5 (B) in a yield of 51 %. ^{1}H NMR (600 MHz, D$_2$O) δ 8.02 – 7.94 (m, 2H), 4.71 – 4.64

(m, 4H), 4.14 – 4.05 (m, 2H), 3.97 – 3.89 (m, 2H), 3.86 (dd, J = 3.3, 1.8 Hz, 2H), 3.77 – 3.72 (m, 2H), 3.72 – 3.63 (m, 30H), 3.63 – 3.52 (m, 29H), 3.52 – 3.43 (m, 13H), 3.42 – 3.35 (m, 29H), 3.35 – 3.29 (m, 6H), 3.14 (t, J = 6.0 Hz, 3H), 3.10 – 3.05 (m, 2H), 3.05 – 3.00 (m, 4H), 2.87 – 2.76 (m, 4H), 2.64 – 2.37 (m, 36H), 1.94 + 1.93 (two s, 3H, due to 1:1 mixture of rotamers). 173H out of in total 175H are reported in the ^{1}H NMR, because the signal for the α-anomeric protons (2H) is hidden behind the HDO signal (as determined by ^{1}H/^{13}C HSQC NMR). MALDI-TOF calcd for $C_{116}H_{205}N_{28}O_{47}^+$ [M+H]$^+$, 2742.451 (monoisotopic); found. 2742.466; $C_{116}H_{204}N_{28}NaO_{47}^+$ [M+Na]$^+$, 2764.433 (monoisotopic); found 2764.461; $C_{116}H_{204}KN_{28}O_{47}^+$ [M+K]$^+$, 2780.407 (monoisotopic); found 2780.439. HRMS (TOF MS ESI) calcd for $C_{116}H_{208}N_{28}O_{47}^{4+}$ [M+4H]$^{4+}$, 686.6190 (monoisotopic); found. 686.6199; calcd for $C_{116}H_{209}N_{28}O_{47}^{5+}$ [M+5H]$^{5+}$, 549.4966 (monoisotopic); found. 549.4979. LC/MS ESI calcd for $C_{116}H_{206}N_{28}O_{47}^{2+}$ [M+2H]$^{2+}$, 1371.7; found. 1371.9; calcd for $C_{116}H_{207}N_{28}O_{47}^{3+}$ [M+3H]$^{3+}$, 915.2; found. 915.1; calcd for $C_{116}H_{208}N_{28}O_{47}^{4+}$ [M+4H]$^{4+}$, 686.6; found. 686.6, calcd for $C_{116}H_{209}N_{28}O_{47}^{5+}$ [M+5H]$^{5+}$, 549.5 (monoisotopic); found. 549.5 calcd for $C_{116}H_{210}N_{28}O_{47}^{6+}$ [M+6H]$^{6+}$, 458.1; found. 458.0. RP-HPLC analysis with a linear gradient in 30 min, 5 % to 30 % MeCN (B) at 214 nm, column 1, T$_R$ = 16.6 min, purity > 92 %.

Compound Man(all)-3 (3)

Compound Man(all)-3 (3) (44 mg, 27 µmol) was obtained as lyophilized powder according to GP 1, GP 2 and GP 5 (B) in a yield of 53 %. ^{1}H NMR (600 MHz, D$_2$O) δ 8.02 (s, 3H), 4.74 – 4.61 (m, 6H), 4.17 – 4.05 (m, 3H), 4.00 – 3.89 (m, 3H), 3.85 (dd, J = 3.2, 1.7 Hz, 3H), 3.80 – 3.70 (m, 3H), 3.70 – 3.62 (m, 6H), 3.62 – 3.56 (m, 3H), 3.55 – 3.41 (m, 14H), 3.41 – 3.26 (m, 12H), 3.13 (t, J = 5.9 Hz, 2H), 3.11 – 2.94 (m, 9H), 2.90 – 2.73 (m, 6H), 2.59 – 2.36 (m, 12H), 1.92 + 1.92 (two s, 3H, due to 1:1 mixture of rotamers). 88H out of in total 91H are reported in the ^{1}H NMR, because the signal for the α-anomeric protons (3H) is hidden behind the HDO signal (as determined by ^{1}H/^{13}C HSQC NMR). MALDI-TOF calcd for $C_{67}H_{113}N_{20}O_{28}^+$ [M+H]$^+$, 1645.803 (monoisotopic); found. 1645.916; calcd for $C_{67}H_{112}N_{20}NaO_{28}^+$ [M+Na]$^+$, 1667.785 (monoisotopic); found. 1667.928; calcd for $C_{67}H_{112}KN_{20}O_{28}^+$ [M+K]$^+$, 1683.759 (monoisotopic); found. 1683.899. HRMS (TOF MS ESI) calcd for $C_{67}H_{113}N_{20}O_{28}^+$ [M+H]$^+$, 1645.8028 (monoisotopic); found. 1645.8026; calcd for $C_{67}H_{112}N_{20}NaO_{28}^+$ [M+Na]$^+$, 1667.7847 (monoisotopic); found. 1667.7839; calcd for $C_{67}H_{112}KN_{20}O_{28}^+$ [M+K]$^+$, 1683.7587 (monoisotopic); found. 1683.7577; calcd for $C_{67}H_{114}N_{20}O_{28}^{2+}$ [M+2H]$^{2+}$, 823.4050 (monoisotopic); found. 823.4062; calcd for $C_{67}H_{113}N_{20}NaO_{28}^{2+}$ [M+H+Na]$^{2+}$, 834.3960 (monoisotopic); found. 834.3967; calcd for $C_{67}H_{113}KN_{20}O_{28}^{2+}$ [M+H+K]$^{2+}$, 842.3830 (monoisotopic); found. 842.3817. RP-HPLC analysis with a linear gradient in 30 min, 5 % to 30 % MeCN (B) at 214 nm, column 1, T$_R$ = 6.0 min, purity > 95 %.

Compound Man(1,3,5)-5 (3a, 2)

Compound Man(1,3,5)-5 (3a, 2) (54 mg, 27 µmol) was obtained as lyophilized oil according to GP 1, GP 2 and GP 5 (B) in a yield of 51 %. ^{1}H NMR (600 MHz, D$_2$O) δ 8.05 – 7.96 (m, 3H), 4.75 – 4.61 (m, 6H), 4.15 – 4.06 (m, 3H), 3.97 – 3.90 (m, 3H), 3.85 (dd, J = 3.3, 1.7 Hz, 3H),

3.77 – 3.72 (m, 3H), 3.70 – 3.63 (m, 14H), 3.63 – 3.53 (m, 11H), 3.53 – 3.42 (m, 14H), 3.41 – 3.25 (m, 20H), 3.14 (t, $J = 6.0$ Hz, 2H), 3.12 – 3.07 (m, 3H), 3.06 – 2.99 (m, 6H), 2.88 – 2.76 (m, 6H), 2.63 – 2.38 (m, 20H), 1.93 + 1.92 (two s, 3H, due to 1:1 mixture of rotamers). 120H out of in total 123H are reported in the ^{1}H NMR, because the signal for the α-anomeric protons (3H) is hidden behind the HDO signal (as determined by ^{1}H/^{13}C HSQC NMR). MALDI-TOF calcd for $C_{87}H_{149}N_{24}O_{36}^+$ [M+H]$^+$, 2106.056 (monoisotopic); found. 2105.905; calcd for $C_{87}H_{148}N_{24}NaO_{36}^+$ [M+Na]$^+$, 2128.038 (monoisotopic); found. 2127.910; calcd for $C_{87}H_{148}KN_{24}O_{36}^+$ [M+K]$^+$, 2144.012 (monoisotopic); found. 2143.888. RP-HPLC analysis with a linear gradient in 30 min, 5 % to 95 % MeCN (B) at 214 nm, column 1, T$_R$ = 7.2 min, purity > 97 %.

Compound Man(1,6,7)-7 (3b)

Compound Man(1,6,7)-7 (3b) (64 mg, 25 µmol) was obtained as lyophilized oil according to GP 1, GP 2 and GP 5 (B) in a yield of 50 %. ^{1}H NMR (600 MHz, D$_2$O) δ 8.09 – 7.99 (m, 3H), 4.76 – 4.63 (m, 6H), 4.17 – 4.04 (m, 3H), 3.93 (ddd, $J = 11.2, 5.5, 3.7$ Hz, 3H), 3.85 (dd, $J = 3.4, 1.7$ Hz, 3H), 3.78 – 3.71 (m, 3H), 3.70 – 3.51 (m, 43H), 3.50 – 3.41 (m, 14H), 3.41 – 3.27 (m, 28H), 3.19 – 2.97 (m, 10H), 2.82 (t, $J = 7.2$ Hz, 5H), 2.59 – 2.38 (m, 28H), 1.92 + 1.92 (two s, 3H, due to 1:1 mixture of rotamers). 152H out of in total 155H are reported in the ^{1}H NMR, because the signal for the α-anomeric protons (3H) is hidden behind the HDO signal (as determined by ^{1}H/^{13}C HSQC NMR). Not all peaks included due to low signal intensity. MALDI-TOF calcd for $C_{108}H_{186}N_{27}O_{44}^+$ [M+H]$^+$, 2565.315 (monoisotopic); found. 2566.399; calcd for $C_{108}H_{185}N_{27}NaO_{44}^+$ [M+Na]$^+$, 2587.297 (monoisotopic); found. 2588.395; calcd for $C_{108}H_{185}KN_{27}O_{44}^+$ [M+K]$^+$, 2603.271 (monoisotopic); found. 2604.405. HRMS (TOF MS ESI) calcd for $C_{108}H_{188}N_{27}O_{44}^{3+}$ [M+3H]$^{3+}$, 856.1107 (monoisotopic); found. 856.1085; calcd for $C_{108}H_{189}N_{27}O_{44}^{4+}$ [M+4H]$^{4+}$, 642.3348 (monoisotopic); found. 642.3342; calcd for $C_{108}H_{190}N_{27}O_{44}^{5+}$ [M+5H]$^{5+}$, 514.0693 (monoisotopic); found. 514.2705. LC/MS ESI calcd for $C_{108}H_{187}N_{27}O_{44}^{2+}$ [M+2H]$^{2+}$, 1283.66; found. 1283.95; calcd for $C_{108}H_{188}N_{27}O_{44}^{3+}$ [M+3H]$^{3+}$, 856.11; found. 856.45; calcd for $C_{108}H_{189}N_{27}O_{44}^{4+}$ [M+4H]$^{4+}$, 642.3; found. 642.6, calcd for $C_{108}H_{190}N_{27}O_{44}^{5+}$ [M+5H]$^{5+}$, 514.1; found 514.2. RP-HPLC analysis with a linear gradient in 10 min, 5 % to 95 % MeCN (B) at 214 nm, column 3, T$_R$ = 3.3 min, purity > 96 %.

Compound Man(1,4,7)-8 (3c, 2a)

Compound Man(1,4,7)-8 (3c, 2a) (49 mg, 18 µmol) was obtained as lyophilized oil according to GP 1, GP 2 and GP 5 (B) in a yield of 35 %. ^{1}H NMR (600 MHz, D$_2$O) δ 8.05 – 7.91 (m, 3H), 4.72 – 4.63 (m, 6H), 4.16 – 4.05 (m, 3H), 3.93 (ddd, $J = 10.9, 6.4, 3.6$ Hz, 3H), 3.86 (dd, $J = 3.3, 1.8$ Hz, 3H), 3.79 – 3.72 (m, 4H), 3.72 – 3.53 (m, 48H), 3.52 – 3.42 (m, 15H), 3.42 – 3.25 (m, 31H), 3.14 (t, $J = 6.0$ Hz, 2H), 3.11 – 3.05 (m, 3H), 3.05 – 2.96 (m, 6H), 2.89 – 2.75 (m, 6H), 2.62 – 2.39 (m, 32H), 1.99 (s, 3H). 168H out of in total 171H are reported in the ^{1}H NMR, because the signal for the α-anomeric protons (3H) is hidden behind the HDO signal (as determined by ^{1}H/^{13}C HSQC NMR). MALDI-TOF calcd for $C_{117}H_{203}N_{30}O_{48}^+$ [M+H]$^+$, 2796.436 (monoisotopic); found. 2796.278; calcd for $C_{117}H_{202}N_{30}NaO_{48}^+$ [M+Na]$^+$, 2818.418 (monoisotopic); found. 2818.235;

calcd for $C_{117}H_{202}KN_{30}O_{48}^+$ [M+K]$^+$, 2834.392 (monoisotopic); found. 2834.221. HRMS (TOF MS ESI) calcd for $C_{117}H_{204}N_{30}O_{48}^{2+}$ [M+2H]$^{2+}$, 1399.2233 (monoisotopic); found. 1399.2362; calcd for $C_{117}H_{205}N_{30}O_{48}^{3+}$ [M+3H]$^{3+}$, 933.1513 (monoisotopic); found. 933.1632; calcd for $C_{117}H_{206}N_{30}O_{48}^{4+}$ [M+4H]$^{4+}$, 700.1153 (monoisotopic); found. 700.1241. RP-HPLC analysis with a linear gradient in 30 min, 5 % to 30 % MeCN (B) at 214 nm, column 1, T_R = 14.8 min, purity > 92 %.

Compound Man(all)-5 (4)

Compound Man(all)-5 (4) (56 mg, 42µmol) was obtained as lyophilized powder according to GP 1, GP 2 and GP 5 (B) in a yield of 42 %. ^{1}H NMR (600 MHz, D$_2$O) δ 7.90 (s, 5H), 4.69 – 4.59 (m, 10H), 4.14 – 4.04 (m, 5H), 3.97 – 3.89 (m, 5H), 3.89 – 3.82 (m, 5H), 3.74 (dd, J = 12.3, 2.4 Hz, 5H), 3.71 – 3.53 (m, 16H), 3.53 – 3.42 (m, 21H), 3.42 – 3.27 (m, 20H), 3.15 (t, J = 5.9 Hz, 2H), 3.11 – 2.94 (m, 15H), 2.88 – 2.72 (m, 10H), 2.59 – 2.38 (m, 20H), 1.94 + 1.93 (two s, 3H, due to 1:1 mixture of rotamers). 142H out of in total 147H are reported in the ^{1}H NMR, because the signal for the α-anomeric protons (5H) is hidden behind the HDO signal (as determined by ^{1}H/^{13}C HSQC NMR). MALDI-TOF calcd for $C_{109}H_{181}N_{32}O_{46}^+$ [M+H]$^+$, 2674.280 (monoisotopic); found. 2674.510; calcd for $C_{109}H_{180}N_{32}NaO_{46}^+$ [M+Na]$^+$, 2696.262 (monoisotopic); found. 2696.476; calcd for $C_{109}H_{180}KN_{32}O_{46}^+$ [M+K]$^+$, 2712.236 (monoisotopic); found. 2712.467. HRMS (TOF ESI MS) calcd for $C_{109}H_{182}N_{32}O_{46}^{2+}$ [M+2H]$^{2+}$, 1338.1454 (monoisotopic); found. 1338.1441; calcd for $C_{109}H_{181}N_{32}NaO_{46}^{2+}$ [M+H+Na]$^{2+}$, 1349.1364 (monoisotopic); found. 1349.1347; calcd for $C_{109}H_{181}KN_{32}O_{46}^{2+}$ [M+H+K]$^{2+}$, 1357.1234 (monoisotopic); found. 1357.1196; calcd for $C_{109}H_{180}N_{32}Na_2O_{46}^{2+}$ [M+2Na]$^{2+}$, 1360.1274 (monoisotopic); found. 1360.1260; calcd for $C_{109}H_{183}N_{32}O_{46}^{3+}$ [M+3H]$^{3+}$, 892.4327 (monoisotopic); found. 892.4327; calcd for $C_{109}H_{182}N_{32}NaO_{46}^{3+}$ [M+2H+Na]$^{3+}$, 899.7600 (monoisotopic); found. 899.7586; calcd for $C_{109}H_{182}KN_{32}O_{46}^{3+}$ [M+2H+K]$^{3+}$, 905.0847 (monoisotopic); found. 905.0830; calcd for $C_{109}H_{181}N_{32}Na_2O_{46}^{3+}$ [M+H+2Na]$^{3+}$, 907.0873 (monoisotopic); found. 907.0867. RP-HPLC analysis with a linear gradient in 10 min, 5 % to 95 % MeCN (B) at 214 nm, column 1, T_R = 4.6min, purity > 96 %.

Compound Man(1,3,5,7,9)-9 (4a)

Compound Man(1,3,5,7,9)-9 (4a) (59 mg, 16 µmol) was obtained as lyophilized oil according to GP 1, GP 2 and GP 5 (B) in a yield of 33 %. ^{1}H NMR (600 MHz, D$_2$O) δ 7.96 (s, 5H), 4.75 – 4.58 (m, 10H), 4.15 – 4.06 (m, 5H), 3.98 – 3.7H), 3.53 – 3.43 (m, 22H), 3.43 – 3.24 (m, 36H), 3.14 (t, J = 5.8 Hz, 2H), 3.11 – 2.96 (m, 15H), 2.89 – 2.74 (m, 10H), 2.62 – 2.37 (m, 36H), 1.94 + 1.93 (two s, 3H, due to 1:1 mixture of rotamers). 206H out of in total 211H are reported in the ^{1}H NMR, because the signal for the α-anomeric protons (5H) is hidden behind the HDO signal (as determined by ^{1}H/^{13}C HSQC NMR). MALDI-TOF calcd for $C_{149}H_{253}N_{40}O_{62}^+$ [M+H]$^+$, 3594.787 (monoisotopic); found. 3595.084; calcd for $C_{149}H_{252}N_{40}NaO_{62}^+$ [M+Na]$^+$, 3616.769 (monoisotopic); found. 3616.947; calcd for $C_{149}H_{252}KN_{40}O_{62}^+$ [M+K]$^+$, 3632.743 (monoisotopic); found. 3632.952. HRMS (TOF MS ESI) calcd for $C_{149}H_{254}N_{40}O_{62}^{2+}$ [M+2H]$^{2+}$, 1798.3987 (monoisotopic); found. 1798.3956; calcd for $C_{149}H_{253}N_{40}NaO_{62}^{2+}$ [M+H+Na]$^{2+}$, 1809.3897 (monoisotopic); found. 1809.8858; calcd for

$C_{149}H_{255}N_{40}O_{62}{}^{3+}$ [M+3H]$^{3+}$, 1199.2683 (monoisotopic); found. 1199.2675; calcd for $C_{149}H_{254}N_{40}NaO_{62}{}^{3+}$ [M+2H+Na]$^{3+}$, 1206.5956 (monoisotopic); found. 1206.2603; calcd for $C_{149}H_{256}N_{40}O_{62}{}^{4+}$ [M+4H]$^{4+}$, 899.7030 (monoisotopic); found. 899.7021; calcd for $C_{149}H_{255}N_{40}NaO_{62}{}^{4+}$ [M+3H+Na]$^{4+}$, 905.1985 (monoisotopic); found. 905.4472. LC/MS ESI calcd for $C_{149}H_{255}N_{40}O_{62}{}^{3+}$ [M+3H]$^{3+}$, 1199.3; found. 1199.4; calcd for $C_{149}H_{256}N_{40}O_{62}{}^{4+}$ [M+4H]$^{4+}$, 899.7; found. 899.8; calcd for $C_{149}H_{257}N_{40}O_{62}{}^{5+}$ [M+5H]$^{5+}$, 720.0; found. 720.0; calcd for $C_{149}H_{258}N_{40}O_{62}{}^{6+}$ [M+6H]$^{6+}$, 600.1; found. 600.2. RP-HPLC analysis with a linear gradient in 10 min, 5 % to 95 % MeCN (B) at 214 nm, column 3, T_R = 4.1 min, purity > 96 %.

Compound Man(1,4,7,10,13)-13 (4b)

Compound Man(1,4,7,10,13)-13 (4b) (100 mg, 22 µmol) was obtained as lyophilized oil according to GP 1, GP 2 and GP 5 (B) in a yield of 44 %. ^{1}H NMR (600 MHz, D$_2$O) δ 7.90 (s, 5H), 4.72 – 4.56 (m, 10H), 4.09 (ddd, J = 11.1, 7.2, 4.0 Hz, 5H), 3.92 (ddd, J = 11.0, 5.4, 4.0 Hz, 5H), 3.86 (dd, J = 3.2, 1.7 Hz, 5H), 3.80 – 3.57 (m, 82H), 3.57 – 3.44 (m, 24H), 3.44 – 3.24 (m, 52H), 3.15 (t, J = 5.9 Hz, 3H), 3.10 – 2.92 (m, 14H), 2.80 (t, J = 7.4 Hz, 10H), 2.60 – 2.43 (m, 52H), 1.94 + 1.93 (two s, 3H, due to 1:1 mixture of rotamers). 270H out of in total 275H are reported in the ^{1}H NMR, because the signal for the α-anomeric protons (5H) is hidden behind the HDO signal (as determined by ^{1}H/^{13}C HSQC NMR). MALDI-TOF calcd for $C_{189}H_{326}N_{48}O_{78}{}^{+}$ [M+H]$^+$, 4516.301 (monoisotopic); found. 4516.030; calcd for $C_{189}H_{325}N_{48}NaO_{78}{}^{+}$ [M+Na]$^+$, 4538.283 (monoisotopic); found. 4537.860; calcd for $C_{189}H_{325}KN_{48}O_{78}{}^{+}$ [M+K]$^+$, 4554.257 (monoisotopic); found. 4553.836. HRMS (TOF MS ESI) calcd for $C_{189}H_{330}N_{48}O_{78}{}^{5+}$ [M+5H]$^{5+}$, 904.2668 (monoisotopic); found. 904.2649. LC/MS ESI calcd for $C_{189}H_{329}N_{48}O_{78}{}^{4+}$ [M+4H]$^{4+}$, 1130.3; found. 1129.8; calcd for $C_{189}H_{330}N_{48}O_{78}{}^{5+}$ [M+5H]$^{5+}$, 904.47; found. 904.25; calcd for $C_{189}H_{33}N_{48}O_{78}{}^{6+}$ [M+6H]$^{6+}$, 753.9; found 753.7; calcd for $C_{189}H_{332}N_{48}O_{78}{}^{7+}$ [M+7H]$^{7+}$, 646.3; found. 646.1; calcd for $C_{189}H_{333}N_{48}O_{78}{}^{8+}$ [M+8H]$^{8+}$, 565.7; found 565.6. RP-HPLC analysis with a linear gradient in 30 min, 5 % to 30 % MeCN (B) at 214 nm, column 1, T_R = 17.9 min, purity > 90 %.

Compound Man(all)-10 (5)

Compound Man(all)-10 (5) (127 mg, 24 µmol) was obtained as lyophilized oil according to GP 1, GP 2 and GP 5 (B) in a yield of 48 %. ^{1}H NMR (600 MHz, D$_2$O) δ 7.88 (s, 10H), 4.68 – 4.57 (m, 20H), 4.12 – 4.04 (m, 10H), 3.95 – 3.89 (m, 10H), 3.86 (dd, J = 3.3, 1.7 Hz, 10H), 3.74 (dd, J = 12.2, 2.3 Hz, 10H), 3.71 – 3.57 (m, 30H), 3.56 – 3.42 (m, 40H), 3.42 – 3.22 (m, 41H), 3.15 (t, J = 5.9 Hz, 3H), 3.08 – 2.91 (m, 30H), 2.86 – 2.70 (m, 20H), 2.58 – 2.34 (m, 40H), 1.94 + 1.92 (two s, 3H, due to 1:1 mixture of rotamers). 277H out of in total 287H are reported in the ^{1}H NMR, because the signal for the α-anomeric protons (10H) is hidden behind the HDO signal (as determined by ^{1}H/^{13}C HSQC NMR). MALDI-TOF calcd for $C_{214}H_{351}N_{62}O_{91}{}^{+}$ [M+H]$^+$, 5245.474 (monoisotopic); found. 5245.453; calcd for $C_{214}H_{350}N_{62}NaO_{91}{}^{+}$ [M+Na]$^+$, 5267.456 (monoisotopic); found. 5267.948; calcd for $C_{214}H_{350}KN_{62}O_{91}{}^{+}$ [M+K]$^+$, 5283.430 (monoisotopic); found. 5283.248. HRMS (TOF MS ESI) calcd for $C_{214}H_{353}N_{62}O_{91}{}^{3+}$ [M+3H]$^{3+}$, 1749.8317 (monoisotopic); found. 1750.1647; calcd for

$C_{214}H_{354}N_{62}O_{91}{}^{4+}$ [M+4H]$^{4+}$, 1312.6256 (monoisotopic); found. 1312.8753; calcd for $C_{214}H_{355}N_{62}O_{91}{}^{5+}$ [M+5H]$^{5+}$, 1050.3019 (monoisotopic); found. 1050.5007; calcd for $C_{214}H_{356}N_{62}O_{91}{}^{6+}$ [M+6H]$^{6+}$, 875.4195 (monoisotopic); found. 875.4193. RP-HPLC analysis with a linear gradient in 10 min, 5 % to 95 % MeCN (B) at 214 nm, column 1, T_R = 5.1 min, purity > 94 %.

5.7. Characterization data of linear glycomacromolecules with EDS spacer and thiol-ether triazole linker on mannoside

Compound Man(3)S-5 (1S)

Compound Man(3)S-5 (1S) (15 mg, 10 µmol) was obtained as lyophilized oil according to GP 1, GP 2 and GP 5 (B) in a yield of 19 %. ^{1}H NMR (600 MHz, D$_2$O) δ 8.04 (s, 1H), 4.83 (d, J = 1.9 Hz, 1H), 4.67 (t, J = 6.3 Hz, 2H), 3.91 (dd, J = 3.4, 1.7 Hz, 1H), 3.86 (dd, J = 12.2, 2.1 Hz, 1H), 3.78 – 3.73 (m, 3H), 3.70 – 3.65 (m, 16H), 3.63 – 3.58 (m, 16H), 3.56 – 3.52 (m, 2H), 3.49 (t, J = 5.9 Hz, 3H), 3.47 – 3.41 (m, 4H), 3.41 – 3.25 (m, 20H), 3.13 (t, J = 5.9 Hz, 2H), 3.09 (t, J = 6.4 Hz, 2H), 3.06 (t, J = 7.0 Hz, 2H), 2.82 (t, J = 6.9 Hz, 2H), 2.61 – 2.43 (m, 22H), 1.99 (s, 3H), 1.90 – 1.78 (m, 2H). MALDI-TOF calcd for $C_{68}H_{123}N_{16}O_{26}S^+$ [M+H]$^+$, 1611.852 (monoisotopic); found. 1611.947 (monoisotopic); calcd for $C_{68}H_{122}N_{16}NaO_{26}S^+$ [M+Na]$^+$, 1633.833 (monoisotopic); found. 1633.950; calcd for $C_{68}H_{122}KN_{16}O_{26}S^+$ [M+K]$^+$, 1649.807 (monoisotopic); found. 1649.949. RP-HPLC analysis with a linear gradient in 30 min, 5 % to 50 % MeCN (B) at 214 nm, column 2, T_R = 14.7 min, purity > 95 %.

Compound Man(4)S-8 (1aS)

Compound Man(4)S-8 (1aS) (16 mg, 7 µmol) was obtained as lyophilized oil according to GP 1, GP 2 and GP 5 (B) in a yield of 14 %. ^{1}H NMR (600 MHz, D$_2$O) δ 7.96 – 7.88 (m, 1H), 4.84 (s, 1H), 4.66 – 4.61 (m, 2H), 3.92 (dt, J = 3.0, 1.5 Hz, 1H), 3.87 (dd, J = 12.2, 2.1 Hz, 1H), 3.81 – 3.73 (m, 3H), 3.73 – 3.66 (m, 28H), 3.64 – 3.58 (m, 28H), 3.57 – 3.53 (m, 2H), 3.52 – 3.50 (m, 3H), 3.47 – 3.44 (m, 4H), 3.43 – 3.26 (m, 32H), 3.15 (t, J = 6.0 Hz, 2H), 3.10 – 3.07 (m, 2H), 3.05 – 3.01 (m, 2H), 2.80 (t, J = 7.1 Hz, 2H), 2.61 – 2.42 (m, 34H), 2.00 (s, 3H), 1.89 – 1.79 (m, 2H). MALDI-TOF calcd for $C_{98}H_{177}N_{22}O_{38}S^+$ [M+H]$^+$, 2302.231 (monoisotopic); found. 2302.392; calcd for $C_{98}H_{176}N_{22}NaO_{38}S^+$ [M+Na]$^+$, 2324.213 (monoisotopic); found. 2324.397; calcd for $C_{98}H_{176}KN_{22}O_{38}S^+$ [M+K]$^+$, 2340.187 (monoisotopic); found. 2340.383. RP-HPLC analysis with a linear gradient in 30 min, 5 % to 50 % MeCN (B) at 214 nm, column 2, T_R = 15.9 min, purity > 95 %.

Compound Man(1,5)S-5 (2S)

Compound Man(1,5)S-5 (2S) (14 mg, 7 µmol) was obtained as lyophilized oil according to GP 1, GP 2 and GP 5 (B) in a yield of 14 %. ^{1}H NMR (600 MHz, D$_2$O) δ 7.97 (dd, J = 12.4, 4.0 Hz, 2H), 4.83 (d, J = 1.8 Hz, 2H), 4.65 (q, J = 6.1 Hz, 4H), 3.92 (dd, J = 3.5, 1.7 Hz, 2H), 3.87 (dd, J = 12.2,

2.2 Hz, 2H), 3.81 – 3.72 (m, 6H), 3.72 – 3.65 (m, 13H), 3.65 – 3.59 (m, 14H), 3.59 – 3.52 (m, 3H), 3.52 – 3.48 (m, 3H), 3.45 (q, J = 6.1 Hz, 8H), 3.42 – 3.29 (m, 19H), 3.14 (t, J = 6.0 Hz, 2H), 3.12 – 3.07 (m, 4H), 3.07 – 2.99 (m, 4H), 2.88 – 2.75 (m, 4H), 2.64 – 2.40 (m, 24H), 1.94 + 1.93 (two s, 3H, due to 1:1 mixture of rotamers), 1.92 – 1.76 (m, 4H). MALDI-TOF calcd for $C_{82}H_{145}N_{20}O_{31}S_2^+$ [M+H]$^+$, 1969.983 (monoisotopic); found. 1970.141; calcd for $C_{82}H_{144}N_{20}NaO_{31}S_2^+$ [M+Na]$^+$, 1991.965 (monoisotopic); found. 1992.119; calcd for $C_{82}H_{144}KN_{20}O_{31}S_2^+$ [M+K]$^+$, 2007.938 (monoisotopic); found. 2008.125. RP-HPLC analysis with a linear gradient in 30 min, 5 % to 50 % MeCN (B) at 214 nm, column 2, T_R = 15.3 min, purity > 95 %.

Compound Man(1,6)S-6 (2aS)

Compound Man(1,6)S-6 (2aS) (15 mg, 7 µmol) was obtained as lyophilized oil according to GP 1, GP 2 and GP 5 (B) in a yield of 14 %. ^{1}H NMR (600 MHz, D$_2$O) δ 7.89 (s, 2H), 4.84 (s, 2H), 4.66 – 4.59 (m, 4H), 3.97 – 3.91 (m, 2H), 3.90 – 3.84 (m, 2H), 3.82 – 3.73 (m, 6H), 3.73 – 3.66 (m, 17H), 3.66 – 3.58 (m, 19H), 3.58 – 3.53 (m, 2H), 3.53 – 3.45 (m, 3H), 3.45 – 3.43 (m, 8H), 3.42 – 3.37 (m, 16H), 3.36 – 3.27 (m, 7H), 3.15 (t, J = 6.0 Hz, 2H), 3.08 (t, J = 6.3 Hz, 4H), 3.03 (t, J = 7.2 Hz, 4H), 2.89 – 2.75 (m, 4H), 2.63 – 2.40 (m, 28H), 1.95 + 1.93 (two s, 3H, due to 1:1 mixture of rotamers), 1.91 – 1.75 (m, 4H). MALDI-TOF calcd for $C_{92}H_{163}N_{22}O_{35}S_2^+$ [M+H]$^+$, 2200.109 (monoisotopic); found. 2200.245; calcd for $C_{92}H_{162}N_{22}NaO_{35}S_2^+$ [M+Na]$^+$, 2222.091 (monoisotopic); found. 2222.264; calcd for $C_{92}H_{162}KN_{22}O_{35}S_2^+$ [M+K]$^+$, 2238.065 (monoisotopic); found. 2238.214. RP-HPLC analysis with a linear gradient in 30 min, 5 % to 50 % MeCN (B) at 214 nm, column 1, T_R = 11.0 min, purity > 93 %.

Compound Man(1,9)S-9 (2bS)

Compound Man(1,9)S-9 (2bS) (14 mg, 5 µmol) was obtained as lyophilized oil according to GP 1, GP 2 and GP 5 (B) in a yield of 10 %. ^{1}H NMR (600 MHz, D$_2$O) δ 7.94 – 7.91 (m, 2H), 4.84 (d, J = 1.8 Hz, 2H), 4.65 – 4.62 (m, 4H), 3.92 (dd, J = 3.4, 1.7 Hz, 2H), 3.87 (dd, J = 12.2, 2.2 Hz, 2H), 3.80 – 3.74 (m, 7H), 3.71 – 3.65 (m, 27H), 3.64 – 3.59 (m, 27H), 3.55 (dt, J = 10.0, 5.8 Hz, 3H), 3.51 – 3.49 (m, 6H), 3.48 – 3.43 (m, 9H), 3.42 – 3.35 (m, 27H), 3.35 – 3.30 (m, 6H), 3.15 (t, J = 5.9 Hz, 4H), 3.11 – 3.06 (m, 4H), 3.05 – 3.01 (m, 4H), 2.84 – 2.77 (m, 4H), 2.62 – 2.41 (m, 40H), 1.94 + 1.93 (two s, 3H, due to 1:1 mixture of rotamers), 1.89 – 1.78 (m, 4H). MALDI-TOF calcd for $C_{122}H_{217}N_{28}O_{47}S_2^+$ [M+H]$^+$, 2890.489 (monoisotopic); found. 2890.649; calcd for $C_{122}H_{216}N_{28}NaO_{47}S_2^+$ [M+Na]$^+$, 2912.471 (monoisotopic); found. 2912.651; calcd for $C_{122}H_{216}KN_{28}O_{47}S_2^+$ [M+K]$^+$, 2928.445 (monoisotopic); found. 2928.616. LC/MS ESI calcd for $C_{122}H_{219}N_{28}O_{47}S_2^{3+}$ [M+3H]$^{3+}$, 964.5; found. 964.6; calcd for $C_{122}H_{220}N_{28}O_{47}S_2^{4+}$ [M+4H]$^{4+}$, 964.5; found. 964.6;. calcd for $C_{122}H_{221}N_{28}O_{47}S_2^{5+}$ [M+5H]$^{5+}$, 579.1; found. 579.2; calcd for $C_{122}H_{222}N_{28}O_{47}S_2^{6+}$ [M+6H]$^{6+}$, 482.8; found. 482.8. RP-HPLC analysis with a linear gradient in 10 min, 5 % to 95 % MeCN (B) at 214 nm, column 3, T_R = 4.0 min, purity > 95 %

Compound Man(all)S-3 (3S)

Compound Man(all)S-3 (3S) (29 mg, 16 µmol) was obtained as lyophilized oil according to GP 1, GP 2 and GP 5 (B) in a yield of 31 %. ^{1}H NMR (600 MHz, D$_2$O) δ 7.88 (d, J = 2.2 Hz, 3H), 4.83 (s, 3H), 4.63 – 4.60 (m, 6H), 3.92 (dd, J = 3.7, 1.7 Hz, 3H), 3.87 (dd, J = 12.2, 2.2 Hz, 3H), 3.81 – 3.73 (m, 9H), 3.66 (t, J = 9.6 Hz, 3H), 3.62 – 3.59 (m, 3H), 3.58 – 3.48 (m, 6H), 3.45 – 3.42 (m, 11H), 3.40 – 3.27 (m, 12H), 3.15 (t, J = 5.9 Hz, 2H), 3.08 – 3.05 (m, 6H), 3.03 – 2.99 (m, 6H), 2.87 – 2.71 (m, 6H), 2.60 – 2.39 (m, 18H), 1.94 + 1.92 (two s, 3H, due to 1:1 mixture of rotamers), 1.87 – 1.78 (m, 6H). MALDI-TOF calcd for C$_{76}$H$_{131}$N$_{20}$O$_{28}$S$_3^+$ [M+H]$^+$, 1867.860 (monoisotopic); found. 1868.007; calcd for C$_{76}$H$_{130}$N$_{20}$NaO$_{28}$S$_3^+$ [M+Na]$^+$, 1889.842 (monoisotopic); found. 1889.994. LC/MS ESI calcd for C$_{76}$H$_{132}$N$_{20}$O$_{28}$S$_3^{2+}$ [M+2H]$^{2+}$, 934.4; found. 934.6; calcd for C$_{76}$H$_{133}$N$_{20}$O$_{28}$S$_3^{3+}$ [M+3H]$^{3+}$, 623.3; found. 623.6. RP-HPLC analysis with a linear gradient in 10 min, 5 % to 95 % MeCN (B) at 214 nm, column 3, T$_R$ = 4.4 min, purity > 93 %.

Compound Man(1,3,5)S-5 (3aS)

Compound Man(1,3,5)S-5 (3aS) (22 mg, 9 µmol) was obtained as lyophilized oil according GP 1, GP 2 and GP 5 (B) in a yield of 15 %. ^{1}H NMR (600 MHz, D$_2$O) δ 7.89 (s, 3H), 4.85 – 4.83 (m, 3H), 4.71 – 4.53 (m, 6H), 3.93 (dd, J = 3.5, 1.7 Hz, 3H), 3.87 (dd, J = 12.2, 2.2 Hz, 3H), 3.84 – 3.72 (m, 8H), 3.72 – 3.58 (m, 21H), 3.58 – 3.48 (m, 8H), 3.48 – 3.43 (m, 9H), 3.43 – 3.24 (m, 21H), 3.15 (t, J = 5.9 Hz, 3H), 3.12 – 2.90 (m, 12H), 2.88 – 2.72 (m, 6H), 2.60 – 2.40 (m, 26H), 1.94 + 1.93 (two s, 3H, due to 1:1 mixture of rotamers), 1.90 – 1.76 (m, 6H). MALDI-TOF calcd for C$_{96}$H$_{167}$N$_{24}$O$_{36}$S$_3^+$ [M+H]$^+$, 2328.114 (monoisotopic); found. 2327.976; calcd for C$_{96}$H$_{166}$N$_{24}$NaO$_{36}$S$_3^+$ [M+Na]$^+$, 2350.096 (monoisotopic); found. 2349.971; calcd for C$_{96}$H$_{166}$KN$_{24}$O$_{36}$S$_3^+$ [M+K]$^+$, 2366.070 (monoisotopic); found. 2365.946. LC/MS ESI calcd for C$_{96}$H$_{168}$N$_{24}$O$_{36}$S$_3^{2+}$ [M+2H]$^{2+}$, 1165.06; found. 1164.85; calcd for C$_{96}$H$_{169}$N$_{24}$O$_{36}$S$_3^{3+}$ [M+3H]$^{3+}$, 777.0; found. 777.0; calcd for C$_{96}$H$_{170}$N$_{24}$O$_{36}$S$_3^{4+}$ [M+4H]$^{4+}$, 583.0; found. 583.0. RP-HPLC analysis with a linear gradient in 10 min, 5 % to 95 % MeCN (B) at 214 nm, column 3, T$_R$ = 3.8 min, purity > 91 %.

Compound Man(1,6,7)S-7 (3bS)

Compound Man(1,6,7)S-7 (3bS) (10 mg, 3 µmol) was obtained as lyophilized oil according to GP 1, GP 2 and GP 5 (B) in a yield of 7 %. ^{1}H NMR (600 MHz, D$_2$O) δ 7.92 (bs, 3H), 4.84 (bs, 3H), 4.70 – 4.56 (m, 6H), 3.96 – 3.90 (m, 3H), 3.90 – 3.84 (m, 3H), 3.82 – 3.72 (m, 9H), 3.71 – 3.65 (m, 18H), 3.65 – 3.58 (m, 19H), 3.58 – 3.52 (m, 3H), 3.52 – 3.49 (m, 3H), 3.48 – 3.42 (m, 12H), 3.38 (t, J = 5.5 Hz, 16H), 3.37 – 3.30 (m, 11H), 3.15 (t, J = 6.0 Hz, 3H), 3.12 – 3.06 (m, 6H), 3.06 – 2.99 (m, 6H), 2.89 – 2.72 (m, 6H), 2.64 – 2.37 (m, 34H), 1.94 + 1.92 (two s, 3H, due to 1:1 mixture of rotamers), 1.91 – 1.64 (m, 6H). MALDI-TOF calcd for C$_{116}$H$_{203}$N$_{28}$O$_{44}$S$_3^+$ [M+H]$^+$, 2788.367 (monoisotopic); found. 2788.533; calcd for C$_{116}$H$_{202}$N$_{28}$NaO$_{44}$S$_3^+$ [M+Na]$^+$, 2810.349 (monoisotopic); found. 2810.535; calcd for C$_{116}$H$_{202}$KN$_{28}$O$_{44}$S$_3^+$ [M+K]$^+$, 2826.323 (monoisotopic); found. 2826.504.

RP-HPLC analysis with a linear gradient in 30 min, 5 % to 50 % MeCN (B) at 214 nm, column 2, T_R = 16.1 min, purity > 95 %.

Compound Man(1,4,7)S-8 (3cS)

Compound Man(1,4,7)S-8 (3cS) (16 mg, 5 µmol) was obtained as lyophilized oil according to GP 1, GP 2 and GP 5 (B) in a yield of 10 %. ^{1}H NMR (600 MHz, D_2O) δ 7.96 – 7.84 (m, 3H), 4.84 (s, 3H), 4.73 – 4.53 (m, 6H), 3.93 (dd, J = 3.4, 1.8 Hz, 3H), 3.91 – 3.84 (m, 3H), 3.84 – 3.72 (m, 9H), 3.72 – 3.58 (m, 43H), 3.58 – 3.24 (m, 51H), 3.15 (t, J = 6.2 Hz, 3H), 3.13 – 2.90 (m, 12H), 2.80 (t, J = 7.1 Hz, 6H), 2.62 – 2.40 (m, 38H), 2.00 (s, 3H), 1.93 – 1.75 (m, 6H). MALDI-TOF calcd for $C_{126}H_{221}N_{30}O_{48}S_3^+$ [M+H]$^+$, 3018.494 (monoisotopic); found. 3018.280; calcd for $C_{126}H_{220}N_{30}NaO_{48}S_3^+$ [M+Na]$^+$, 3040.476 (monoisotopic); found. 3040.278.; calcd for $C_{126}H_{220}KN_{30}O_{48}S_3^+$ [M+K]$^+$, 3056.450 (monoisotopic); found. 3056.252. RP-HPLC analysis with a linear gradient in 30 min, 5 % to 30 % MeCN (B) at 214 nm, column 1, T_R = 18.0 min, purity > 95 %.

Compound Man(all)S-5 (4S)

Compound Man(all)S-5 (4S) (44 mg, 14 µmol) was obtained as lyophilized oil according to GP 1, GP 2 and GP 5 (B) in a yield of 29 %. ^{1}H NMR (500 MHz, D_2O) δ 8.02 (bs, 5H), 4.91 (s, 5H), 4.74 – 4.68 (m, 10H), 4.00 (dd, J = 3.5, 1.8 Hz, 5H), 3.94 (dd, J = 12.3, 2.3 Hz, 5H), 3.88 – 3.80 (m, 13H), 3.79 – 3.65 (m, 10H), 3.65 – 3.56 (m, 9H), 3.56 – 3.47 (m, 19H), 3.46 – 3.32 (m, 20H), 3.31 – 3.04 (m, 23H), 3.04 – 2.74 (m, 10H), 2.71 – 2.43 (m, 30H), 2.02 + 2.00 (two s, 3H, due to 1:1 mixture of rotamers), 1.99 – 1.81 (m, 10H). MALDI-TOF calcd for $C_{124}H_{211}N_{32}O_{46}S_5^+$ [M+H]$^+$, 3044.376 (monoisotopic); found. 3044.634; calcd for $C_{124}H_{210}N_{32}NaO_{46}S_5^+$ [M+Na]$^+$, 3066.358 (monoisotopic); found. 3066.617; calcd for $C_{124}H_{210}KN_{32}O_{46}S_5^+$ [M+K]$^+$, 3082.332 (monoisotopic); found. 3082.587. RP-HPLC analysis with a linear gradient in 30 min, 5 % to 50 % MeCN (B) at 214 nm, column 2, T_R = 15.7 min, purity > 95 %.

Compound Man(1,3,5,7,9)S-9 (4aS)

Compound Man(1,3,5,7,9)S-9 (4aS) (28 mg, 7 µmol) was obtained as lyophilized oil according to GP 1, GP 2 and GP 5 (B) in a yield of 14 %. ^{1}H NMR (600 MHz, D_2O) δ 7.89 (s, 5H), 4.82 (s, 5H), 4.65 – 4.59 (m, 10H), 3.96 – 3.91 (m, 5H), 3.90 – 3.85 (m, 5H), 3.82 – 3.74 (m, 13H), 3.73 – 3.58 (m, 41H), 3.58 – 3.29 (m, 65H), 3.15 (t, J = 5.9 Hz, 3H), 3.13 – 2.91 (m, 20H), 2.86 – 2.73 (m, 10H), 2.63 – 2.40 (m, 46H), 1.95 + 1.93 (two s, 3H, due to 1:1 mixture of rotamers), 1.92 – 1.73 (m, 10H). MALDI-TOF calcd for $C_{164}H_{283}N_{40}O_{62}S_5^+$ [M+H]$^+$, 3964.883 (monoisotopic); found. 3965.168; calcd for $C_{164}H_{282}N_{40}NaO_{62}S_5^+$ [M+Na]$^+$, 3986.864 (monoisotopic); found. 3987.064. RP-HPLC analysis with a linear gradient in 30 min, 5 % to 50 % MeCN (B) at 214 nm, column 2, T_R = 16.7 min, purity > 95 %.

Compound Man(all)S-10 (5S)

Compound Man(all)S-10 (5S) (75 mg, 13 µmol) was obtained as lyophilized oil according to GP 1, GP 2 and GP 5 (B) in a yield of 25 %. ^{1}H NMR (600 MHz, D$_2$O) δ 7.88 (s, 10H), 4.83 (s, 10H), 4.69 – 4.52 (m, 20H), 3.92 (dd, J = 3.5, 1.8 Hz, 10H), 3.91 – 3.82 (m, 10H), 3.82 – 3.71 (m, 25H), 3.66 (t, J = 9.7 Hz, 10H), 3.63 – 3.58 (m, 9H), 3.58 – 3.24 (m, 97H), 3.24 – 2.89 (m, 43H), 2.88 – 2.67 (m, 20H), 2.58 – 2.40 (m, 60H), 1.94 + 1.92 (two s, 3H, due to 1:1 mixture of rotamers), 1.90 – 1.64 (m, 20H). LC/MS ESI calcd for C$_{244}$H$_{414}$N$_{62}$O$_{91}$S$_{10}$$^{4+}$ [M+4H]$^{4+}$, 1497.7; found. 1497.6; calcd for C$_{244}$H$_{415}$N$_{62}$O$_{91}$S$_{10}$$^{5+}$ [M+5H]$^{5+}$, 1198.3; found. 1198.4; calcd for C$_{244}$H$_{416}$N$_{62}$O$_{91}$S$_{10}$$^{6+}$ [M+6H]$^{6+}$, 998.8; found. 999.0; calcd for C$_{244}$H$_{417}$N$_{62}$O$_{91}$S$_{10}$$^{7+}$ [M+7H]$^{7+}$, 856.2; found 856.2; calcd for C$_{244}$H$_{418}$N$_{62}$O$_{91}$S$_{10}$$^{8+}$ [M+8H]$^{8+}$, 749.3; found 749.3. RP-HPLC analysis with a linear gradient in 30 min, 5 % to 50 % MeCN (B) at 214 nm, column 2, T$_R$ = 16.7 min, purity > 95 %.

5.8. Characterization data of linear glycomacromolecules with EDS spacer and benzyl triazole linker on mannoside

Compound Man(3)B-5 (1B)

Compound Man(3)B-5 (1B) (19 mg, 12 µmol) was obtained as lyophilized powder according to GP 1, GP 2 and GP 5 (B) in a yield of 24 %. ^{1}H NMR (500 MHz, D$_2$O) δ 7.67 (s, 1H), 7.13 (s, 4H), 5.64 (s, 1H), 4.75 (s, 2H), 4.22 (d, J = 3.1 Hz, 1H), 4.10 (dd, J = 9.4, 3.4 Hz, 1H), 3.87 – 3.80 (m, 3H), 3.79 – 3.73 (m, 16H), 3.72 – 3.66 (m, 16H), 3.59 (t, J = 6.0 Hz, 3H), 3.54 – 3.43 (m, 20H), 3.40 (q, J = 5.7 Hz, 4H), 3.24 (q, J = 5.5 Hz, 4H), 3.01 (t, J = 7.1 Hz, 2H), 2.79 (t, J = 7.1 Hz, 2H), 2.69 – 2.50 (m, 20H), 2.08 (s, 3H). MALDI-TOF calcd for C$_{71}$H$_{121}$N$_{16}$O$_{26}$$^+$ [M+H]$^+$, 1613.864 (monoisotopic); found. 1613.944; calcd for C$_{71}$H$_{120}$N$_{16}$NaO$_{26}$$^+$ [M+Na]$^+$, 1635.846 (monoisotopic); found. 1635.933; calcd for C$_{71}$H$_{120}$KN$_{16}$O$_{26}$$^+$ [M+K]$^+$, 1651.820 (monoisotopic); found. 1651.914. RP-HPLC analysis with a linear gradient in 30 min, 5 % to 50 % MeCN (B) at 214 nm, column 2, T$_R$ = 15.3 min, purity > 95 %.

Compound Man(4)B-8 (1aB)

Compound Man(4)B-8 (1aB) (23 mg, 10 µmol) was obtained as lyophilized powder according to GP 1, GP 2 and GP 5 (B) in a yield of 20 %. ^{1}H NMR (500 MHz, D$_2$O) δ 7.67 (s, 1H), 7.13 (s, 4H), 5.64 (s, 1H), 4.22 (d, J = 3.1 Hz, 1H), 4.10 (dd, J = 9.4, 3.5 Hz, 1H), 3.86 – 3.81 (m, 4H), 3.79 – 3.73 (m, 27H), 3.72 – 3.67 (m, 27H), 3.59 (t, J = 6.0 Hz, 6H), 3.52 – 3.43 (m, 30H), 3.42 – 3.38 (m, 4H), 3.26 – 3.21 (m, 4H), 3.01 (t, J = 7.2 Hz, 2H), 2.79 (t, J = 7.1 Hz, 2H), 2.74 – 2.45 (m, 32H), 2.08 (s, 3H). 149H out of in total 151H are reported in the ^{1}H NMR, because the signal for the CH$_2$ group protons (2H) next to the triazole ring (O−CH$_2$−CH_2−NCHN−) is hidden behind the HDO signal (as determined by ^{1}H/^{13}C HSQC NMR). MALDI-TOF calcd for C$_{101}$H$_{175}$N$_{22}$O$_{38}$$^+$ [M+H]$^+$, 2304.244 (monoisotopic); found. 2304.404; calcd for C$_{101}$H$_{174}$N$_{22}$NaO$_{38}$$^+$ [M+Na]$^+$, 2326.226 (monoisotopic);

found. 2326.385; calcd for $C_{101}H_{174}KN_{22}O_{38}^+$ [M+K]$^+$, 2342.200 (monoisotopic); found. 2342.410. RP-HPLC analysis with a linear gradient in 30 min, 5 % to 50 % MeCN (B) at 214 nm, column 2, T_R = 16.2 min, purity > 95 %.

Compound Man(1,5)B-5 (2B)

Compound Man(1,5)B-5 (2B) (16 mg, 8 µmol) was obtained as lyophilized powder according to GP 1, GP 2 and GP 5 (B) in a yield of 17 %. ^{1}H NMR (500 MHz, D$_2$O) δ 7.72 – 7.63 (m, 2H), 7.12 (s, 8H), 5.63 (d, J = 1.8 Hz, 2H), 4.73 – 4.70 (m, 4H), 4.22 (dd, J = 3.5, 1.9 Hz, 2H), 4.09 (dd, J = 9.4, 3.5 Hz, 2H), 3.90 – 3.77 (m, 8H), 3.76 – 3.71 (m, 12H), 3.71 – 3.62 (m, 12H), 3.57 (td, J = 5.9, 3.2 Hz, 3H), 3.54 – 3.42 (m, 19H), 3.42 – 3.36 (m, 8H), 3.23 (q, J = 6.1, 5.7 Hz, 6H), 3.01 (t, J = 7.1 Hz, 4H), 2.85 – 2.74 (m, 4H), 2.69 – 2.44 (m, 20H), 2.02 + 2.00 (two s, 3H, due to 1:1 mixture of rotamers). MALDI-TOF calcd for $C_{88}H_{141}N_{20}O_{31}^+$ [M+H]$^+$, 1974.007 (monoisotopic); found. 1974.137; calcd for $C_{88}H_{140}N_{20}NaO_{31}^+$ [M+Na]$^+$, 1995.989 (monoisotopic); found. 1996.136.; calcd for $C_{88}H_{140}KN_{20}O_{31}^+$ [M+K]$^+$, 2011.963 (monoisotopic); found. 2012.128. RP-HPLC analysis with a linear gradient in 30 min, 5 % to 50 % MeCN (B) at 214 nm, column 2, T_R = 16.1 min, purity > 95 %.

Compound Man(1,6)B-6 (2aB)

Compound Man(1,6)B-6 (2aB) (21 mg, 9 µmol) was obtained as lyophilized powder according to GP 1, GP 2 and GP 5 (B) in a yield of 19 %. ^{1}H NMR (500 MHz, D$_2$O) δ 7.74 – 7.65 (m, 2H), 7.12 (s, 8H), 5.63 (d, J = 1.9 Hz, 2H), 4.74 – 4.72 (m, 4H), 4.22 (dd, J = 3.5, 1.9 Hz, 2H), 4.09 (dd, J = 9.4, 3.4 Hz, 2H), 3.88 – 3.81 (m, 5H), 3.81 – 3.71 (m, 18H), 3.71 – 3.59 (m, 17H), 3.57 (td, J = 5.9, 3.1 Hz, 3H), 3.55 – 3.42 (m, 23H), 3.42 – 3.36 (m, 8H), 3.23 (q, J = 6.7 Hz, 6H), 3.02 (t, J = 7.1 Hz, 4H), 2.85 – 2.74 (m, 4H), 2.68 – 2.45 (m, 24H), 2.02 + 2.00 (two s, 3H, due to 1:1 mixture of rotamers). MALDI-TOF calcd for $C_{98}H_{159}N_{22}O_{35}^+$ [M+H]$^+$, 2204.134 (monoisotopic); found. 2204.259; calcd for $C_{98}H_{158}N_{22}NaO_{35}^+$ [M+Na]$^+$, 2226.116 (monoisotopic); found. 2226.266; calcd for $C_{98}H_{158}KN_{22}O_{35}^+$ [M+K]$^+$, 2242.090 (monoisotopic); found. 2242.261. RP-HPLC analysis with a linear gradient in 30 min, 5 % to 50 % MeCN (B) at 214 nm, column 2, T_R = 16.4 min, purity > 95 %.

Compound Man(1,9)B-9 (2bB)

Compound Man(1,9)B-9 (2bB) (25 mg, 9 µmol) was obtained as lyophilized powder according to GP 1, GP 2 and GP 5 (B) in a yield of 17 %. ^{1}H NMR (500 MHz, D$_2$O) δ 7.66 (s, 2H), 7.12 (s, 8H), 5.63 (s, 2H), 4.72 – 4.70 (m, 4H), 4.22 (dt, J = 3.6, 1.8 Hz, 2H), 4.09 (dd, J = 9.5, 3.4 Hz, 2H), 3.86 – 3.80 (m, 7H), 3.79 – 3.72 (m, 26H), 3.72 – 3.62 (m, 26H), 3.57 (td, J = 5.8, 3.1 Hz, 7H), 3.53 – 3.35 (m, 43H), 3.25 – 3.21 (m, 7H), 3.00 (t, J = 7.2 Hz, 4H), 2.78 (t, J = 7.1 Hz, 4H), 2.72 – 2.40 (m, 36H), 2.01 + 2.00 (two s, 3H, due to 1:1 mixture of rotamers). MALDI-TOF calcd for $C_{128}H_{213}N_{28}O_{47}^+$ [M+H]$^+$, 2894.514 (monoisotopic); found. 2894.544; calcd for $C_{128}H_{212}N_{28}NaO_{47}^+$ [M+Na]$^+$, 2916.496 (monoisotopic); found. 2916.524. RP-HPLC analysis with a linear gradient in 30 min, 5 % to 50 % MeCN (B) at 214 nm, column 2, T_R = 17.3 min, purity > 95 %.

Compound Man(all)B-3 (3B)

Compound Man(all)B-3 (3B) (35 mg, 18 µmol) was obtained as lyophilized powder according to GP 1, GP 2 and GP 5 (B) in a yield of 37 %. ^{1}H NMR (600 MHz, D_2O) δ 7.66 – 7.52 (m, 3H), 7.08 – 6.89 (m, 12H), 5.57 – 5.44 (m, 3H), 4.67 – 4.49 (m, 6H), 4.18 – 4.06 (m, 3H), 4.06 – 3.93 (m, 3H), 3.85 – 3.56 (m, 12H), 3.56 – 3.45 (m, 3H), 3.44 – 3.35 (m, 12H), 3.35 – 3.22 (m, 12H), 3.21 – 3.00 (m, 8H), 3.00 – 2.79 (m, 6H), 2.79 – 2.59 (m, 5H), 2.59 – 2.32 (m, 12H), 1.92 + 1.91 (two s, 3H, due to 1:1 mixture of rotamers). MALDI-TOF calcd for $C_{85}H_{125}N_{20}O_{28}^+$ [M+H]$^+$, 1873.897 (monoisotopic); found. 1874.020; calcd for $C_{85}H_{124}N_{20}NaO_{28}^+$ [M+Na]$^+$, 1895.879 (monoisotopic); found. 1896.012; calcd for $C_{85}H_{124}KN_{20}O_{28}^+$ [M+K]$^+$, 1911.853 (monoisotopic); found. 1912.038. RP-HPLC analysis with a linear gradient in 30 min, 5 % to 50 % MeCN (B) at 214 nm, column 2, T_R = 16.2 min, purity > 95 %.

Compound Man(1,3,5)B-5 (3aB)

Compound Man(1,3,5)B-5 (3aB) (33 mg, 14 µmol) was obtained as lyophilized powder according to GP 1, GP 2 and GP 5 (B) in a yield of 28 %. ^{1}H NMR (600 MHz, D_2O) δ 7.72 – 7.53 (m, 3H), 7.15 – 6.87 (m, 12H), 5.58 – 5.48 (m, 3H), 4.67 – 4.56 (m, 6H), 4.16 – 4.09 (m, 3H), 4.00 (dt, J = 9.6, 2.9 Hz, 3H), 3.80 – 3.70 (m, 9H), 3.70 – 3.65 (m, 3H), 3.65 – 3.61 (m, 8H), 3.61 – 3.54 (m, 8H), 3.54 – 3.46 (m, 3H), 3.46 – 3.37 (m, 12H), 3.37 – 3.24 (m, 19H), 3.21 – 3.06 (m, 8H), 2.92 (t, J = 7.5 Hz, 6H), 2.78 – 3.63 (m, 6H), 2.60 – 2.37 (m, 20H), 1.93 + 1.91 (two s, 3H, due to 1:1 mixture of rotamers). MALDI-TOF calcd for $C_{105}H_{161}N_{24}O_{36}^+$ [M+H]$^+$, 2334.151 (monoisotopic); found. 2334.299; calcd for $C_{105}H_{160}N_{24}NaO_{36}^+$ [M+Na]$^+$, 2356.132 (monoisotopic); found. 2356.291; calcd for $C_{105}H_{160}KN_{24}O_{36}^+$ [M+K]$^+$, 2372.106 (monoisotopic); found. 2372.288. RP-HPLC analysis with a linear gradient in 30 min, 5 % to 50 % MeCN (B) at 214 nm, column 2, T_R = 16.4 min, purity > 95 %.

Compound Man(1,6,7)B-7 (3bB)

Compound Man(1,6,7)B-7 (3bB) (45 mg, 16 µmol) was obtained as lyophilized powder according to GP 1, GP 2 and GP 5 (B) in a yield of 32 %. ^{1}H NMR (500 MHz, D_2O) δ 7.89 – 7.54 (m, 3H), 7.37 – 6.78 (m, 12H), 5.69 – 5.52 (m, 3H), 4.73 – 4.66 (m, 6H), 4.20 (ddd, J = 10.7, 3.3, 1.6 Hz, 3H), 4.13 – 4.02 (m, 3H), 3.88 – 3.78 (m, 9H), 3.78 – 3.62 (m, 36H), 3.62 – 3.54 (m, 5H), 3.53 – 3.42 (m, 27H), 3.42 – 3.30 (t, J = 7.3 Hz, 11H), 3.30 – 3.12 (m, 7H), 3.11 – 2.88 (m, 5H), 2.87 – 2.70 (m, 6H), 2.70 – 2.42 (m, 28H), 2.01 + 1.99 (two s, 3H, due to 1:1 mixture of rotamers). MALDI-TOF calcd for $C_{125}H_{197}N_{28}O_{44}^+$ [M+H]$^+$, 2794.404 (monoisotopic); found. 2794.513; calcd for $C_{125}H_{196}N_{28}NaO_{44}^+$ [M+Na]$^+$, 2816.386 (monoisotopic); found. 2816.502; calcd for $C_{125}H_{196}KN_{28}O_{44}^+$ [M+K]$^+$, 2832.360 (monoisotopic); found. 2832.487. RP-HPLC analysis with a linear gradient in 30 min, 5 % to 50 % MeCN (B) at 214 nm, column 2, T_R = 17.1 min, purity > 95 %.

Compound Man(1,4,7)B-8 (3cB)

Compound Man(1,4,7)B-8 (3cB) (34 mg, 11 µmol) was obtained as lyophilized powder according to GP 1, GP 2 and GP 5 (B) in a yield of 23 %. ^{1}H NMR (500 MHz, D$_2$O) δ 7.73 – 7.60 (m, 3H), 7.19 – 7.02 (m, 12H), 5.67 – 5.56 (m, 3H), 4.72 – 4.69 (m, 6H), 4.26 – 4.15 (m, 3H), 4.12 – 4.04 (m, 3H), 3.91 – 3.76 (m, 11H), 3.76 – 3.71 (m, 19H), 3.70 – 3.62 (m, 20H), 3.57 (td, J = 6.0, 3.3 Hz, 4H), 3.52 – 3.45 (m, 12H), 3.46 – 3.31 (m, 32H), 3.22 (q, J = 5.4, 4.6 Hz, 8H), 3.01 (t, J = 7.3 Hz, 6H), 2.79 (t, J = 7.0 Hz, 6H), 2.67 – 2.45 (m, 32H), 2.06 (s, 3H). MALDI-TOF calcd for C$_{135}$H$_{215}$N$_{30}$O$_{48}^+$ [M+H]$^+$, 3024.531 (monoisotopic); found. 3024.702; calcd for C$_{135}$H$_{214}$N$_{30}$NaO$_{48}^+$ [M+Na]$^+$, 3046.512 (monoisotopic); found. 3046.686; calcd for C$_{135}$H$_{214}$KN$_{30}$O$_{48}^+$ [M+K]$^+$, 3062.486 (monoisotopic); found. 3062.641. RP-HPLC analysis with a linear gradient in 30 min, 5 % to 50 % MeCN (B) at 214 nm, column 2, T$_R$ = 17.3 min, purity > 95 %.

Compound Man(all)B-5 (4B)

Compound Man(all)B-5 (4B) (61 mg, 20 µmol) was obtained as lyophilized powder according to GP 1, GP 2 and GP 5 (B) in a yield of 40 %. ^{1}H NMR (500 MHz, D$_2$O) δ 7.77 – 7.58 (m, 5H), 7.23 – 6.82 (m, 20H), 5.65 – 5.47 (m, 5H), 4.70 – 4.56 (m, 10H), 4.29 – 4.12 (m, 5H), 4.11 – 3.94 (m, 5H), 3.88 – 3.68 (m, 19H), 3.62 – 3.30 (m, 43H), 3.26 – 3.08 (m, 12H), 3.07 – 2.85 (m, 10H), 2.83 – 2.65 (m, 10H), 2.61 – 2.42 (m, 20H), 1.99 + 1.98 (two s, 3H, due to 1:1 mixture of rotamers). MALDI-TOF calcd for C$_{139}$H$_{201}$N$_{32}$O$_{46}^+$ [M+H]$^+$, 3054.437 (monoisotopic); found. 3054.550; calcd for C$_{139}$H$_{200}$N$_{32}$NaO$_{46}^+$ [M+Na]$^+$, 3076.419 (monoisotopic); found. 3076.531; calcd for C$_{139}$H$_{200}$KN$_{32}$O$_{46}^+$ [M+K]$^+$, 3092.393 (monoisotopic); found. 3092.526. RP-HPLC analysis with a linear gradient in 30 min, 5 % to 50 % MeCN (B) at 214 nm, column 2, T$_R$ = 17.2 min, purity > 95 %.

Compound Man(1,3,5,7,9)B-9 (4aB)

Compound Man(1,3,5,7,9)B-9 (4aB) (47 mg, 12 µmol) was obtained as lyophilized powder according to GP 1, GP 2 and GP 5 (B) in a yield of 24 %. ^{1}H NMR (600 MHz, D$_2$O) δ 7.68 – 7.49 (m, 5H), 7.24 – 6.75 (m, 20H), 5.51 (d, J = 9.5 Hz, 5H), 4.65 – 4.52 (m, 10H), 4.16 – 4.07 (m, 5H), 4.04 – 3.96 (m, 5H), 3.85 – 3.70 (m, 15H), 3.70 – 3.55 (m, 35H), 3.55 – 3.47 (m, 7H), 3.47 – 3.20 (m, 53H), 3.19 – 3.09 (m, 12H), 2.99 – 2.83 (m, 10H), 2.76 – 2.64 (m, 10H), 2.59 – 2.39 (m, 36H), 1.93 + 1.91 (two s, 3H, due to 1:1 mixture of rotamers). MALDI-TOF calcd for C$_{179}$H$_{273}$N$_{40}$O$_{62}^+$ [M+H]$^+$, 3974.944 (monoisotopic); found. 3975.038; calcd for C$_{179}$H$_{272}$N$_{40}$NaO$_{62}^+$ [M+Na]$^+$, 3996.926 (monoisotopic); found. 3997.046; calcd for C$_{179}$H$_{272}$KN$_{40}$O$_{62}^+$ [M+K]$^+$, 4012.900 (monoisotopic); found. 4013.058. RP-HPLC analysis with a linear gradient in 30 min, 5 % to 50 % MeCN (B) at 214 nm, column 2, T$_R$ = 17.8 min, purity > 95 %.

Compound Man(all)B-10 (5B)

Compound Man(all)B-10 (5B) (74 mg, 12 µmol) was obtained as lyophilized powder according to GP 1, GP 2 and GP 5 (B) in a yield of 25 %. ^{1}H NMR (600 MHz, D$_2$O) δ 7.57 (s, 10H), 7.15 – 6.71

(m, 40H), 5.54 – 5.38 (m, 10H), 4.60 – 4.44 (m, 20H), 4.12 – 4.03 (m, 10H), 4.02 – 3.92 (m, 10H), 3.81 – 3.67 (m, 27H), 3.67 – 3.56 (m, 11H), 3.56 – 3.45 (m, 9H), 3.45 – 3.17 (m, 74H), 3.17 – 3.11 (m, 4H), 3.11 – 2.96 (m, 19H), 2.96 – 2.78 (m, 20H), 2.75 – 2.59 (m, 20H), 2.53 – 2.35 (m, 40H), 1.91 + 1.89 (two s, 3H, due to 1:1 mixture of rotamers). LC/MS ESI calcd for $C_{274}H_{394}N_{62}O_{91}{}^{4+}$ $[M+4H]^{4+}$, 1502.70; found. 1502.85; calcd for $C_{274}H_{395}N_{62}O_{91}{}^{5+}$ $[M+5H]^{5+}$, 1202.4; found. 1202.4; calcd for $C_{274}H_{396}N_{62}O_{91}{}^{6+}$ $[M+6H]^{6+}$, 1002.1; found. 1002.2; calcd for $C_{274}H_{397}N_{62}O_{91}{}^{7+}$ $[M+7H]^{7+}$, 859.1; found 859.6; calcd for $C_{274}H_{398}N_{62}O_{91}{}^{8+}$ $[M+8H]^{8+}$, 751.9; found 751.8. RP-HPLC analysis with a linear gradient in 30 min, 5 % to 50 % MeCN (B) at 214 nm, column 2, T_R = 18.2 min, purity > 95 %.

5.9. Characterization data of cyclic glycomacromolecules with SDS spacer[16]

Compound Man(3)@5SDS (1@SDS)

Compound Man(3)@5SDS (1@SDS) (2.7 mg, 2 µmol) was obtained as lyophilized powder according to GP 1, GP 3 (C), GP 2 and GP 5 (B) in a yield of 4 %. ^{1}H NMR (600 MHz, D_2O) δ 7.88 (s, 1H), 4.69 – 4.59 (m, 2H), 4.22 (dd, J = 9.5, 4.8 Hz, 1H), 4.12 – 4.04 (m, 1H), 3.96 – 3.89 (m, 1H), 3.86 (dd, J = 3.4, 1.8 Hz, 1H), 3.74 (dd, J = 12.2, 2.3 Hz, 1H), 3.70 – 3.63 (m, 2H), 3.63 – 3.50 (m, 4H), 3.50 – 3.38 (m, 5H), 3.38 – 3.21 (m, 18H), 3.21 – 3.08 (m, 4H), 3.06 – 2.95 (m, 3H), 2.80 (t, J = 7.2 Hz, 2H), 2.72 – 2.30 (m, 24H), 1.87 – 1.78 (m, 1H), 1.73 – 1.66 (m, 1H), 1.56 – 1.44 (m, 2H), 1.44 – 1.37 (m, 1H), 1.37 – 1.28 (m, 1H). 76H out of in total 77H are reported in the ^{1}H NMR, because the signal for the α-anomeric proton (1H) is hidden behind the HDO signal (as determined by ^{1}H/^{13}C HSQC NMR). MALDI-TOF calcd for $C_{57}H_{97}N_{18}O_{20}{}^+$ $[M+H]^+$, 1353.713 (monoisotopic); found. 1353.729; calcd for $C_{57}H_{96}N_{18}NaO_{20}{}^+$ $[M+Na]^+$, 1375.695 (monoisotopic); found. 1375.714; calcd for $C_{57}H_{96}KN_{18}O_{20}{}^+$ $[M+K]^+$, 1391.669 (monoisotopic); found. 1391.723. RP-HPLC analysis with a linear gradient in 10 min, 5 % to 95 % MeCN (B) at 214 nm, column 1, T_R = 3.7 min, purity > 88 %.

Compound Man(1,3,5)@5SDS (2@SDS)

Compound Man(1,3,5)@5SDS (2@SDS) (3.5 mg, 2 µmol) was obtained as lyophilized powder according to GP 1, GP 3 (C), GP 2 and GP 5 (B) in a yield of 3 %. ^{1}H NMR (600 MHz, D_2O) δ 8.19 – 7.84 (m, 3H), 4.29 (dd, J = 9.2, 4.9 Hz, 1H), 4.18 (ddd, J = 11.1, 7.2, 4.2 Hz, 3H), 4.09 – 3.97 (m, 3H), 3.94 (dd, J = 3.3, 1.8 Hz, 3H), 3.83 (dd, J = 12.6, 2.2 Hz, 3H), 3.78 – 3.64 (m, 9H), 3.64 – 3.47 (m, 15H), 3.47 – 3.38 (m, 11H), 3.36 (s, 8H), 3.23 (q, J = 6.9, 6.3 Hz, 4H), 3.19 – 3.13 (m, 3H), 3.10 (t, J = 7.3 Hz, 6H), 2.89 (t, J = 7.3 Hz, 6H), 2.73 – 2.42 (m, 24H), 1.97 – 1.83 (m, 1H), 1.83 – 1.69 (m, 1H), 1.66 – 1.52 (m, 2H), 1.51 – 1.33 (m, 2H). 108H out of in total 117H are reported

---

[16] 1@SDS and 2@SDS were synthesized and characterized (NMR, RP-HPLC and MALDI-TOF) by Andreas Ludwig (Heinrich-Heine-Universität Düsseldorf, group of Prof. Dr. Laura Hartmann, Bachelor Thesis, October 2015). In this thesis, the characterization data of the above mentioned compounds (NMR) has been re-assessed by the author of this thesis.

in the ^{1}H NMR, because the signals for α-anomeric protons (3H) and the CH_2 group protons (6H) next to the triazole ring (O−CH_2−CH_2−NCHN−) are hidden behind the HDO signal (as determined by ^{1}H/^{13}C HSQC NMR). MALDI-TOF calcd for $C_{87}H_{145}N_{26}O_{34}{}^+$ [M+H]$^+$, 2098.042 (monoisotopic); found. 2098.018; calcd for $C_{87}H_{144}N_{26}NaO_{34}{}^+$ [M+Na]$^+$, 2120.024 (monoisotopic); found. 2120.013; calcd for $C_{87}H_{144}KN_{26}O_{34}{}^+$ [M+K]$^+$, 2135.998 (monoisotopic); found. 2135.962. RP-HPLC analysis with a linear gradient in 10 min, 5 % to 95 % MeCN (B) at 214 nm, column 1, T$_R$ = 4.0 min, purity > 93 %.

5.10. Characterization data of cyclic glycomacromolecules with linear and cyclic precursors and EDS spacer

Compound P1

Compound P1 was obtained as lyophilized oil according to GP 1 and GP 5 (B) on analytical scale. MALDI-TOF calcd for $C_{65}H_{117}N_{15}O_{23}{}^+$ [M+H]$^+$, 1474.836 (monoisotopic); found. 1474.741; calcd for $C_{65}H_{115}N_{15}NaO_{23}{}^+$ [M+Na]$^+$, 1512.792 (monoisotopic); found. 1512.713; calcd for $C_{65}H_{115}KN_{15}O_{23}{}^+$ [M+K]$^+$, 1496.818 (monoisotopic); found. 1496.774. HRMS (TOF MS ESI) calcd for $C_{65}H_{116}N_{15}O_{23}{}^+$ [M+H]$^+$, 1474.8363 (monoisotopic); found. 1474.8421; calcd for $C_{65}H_{115}N_{15}NaO_{23}{}^+$ [M+Na]$^+$, 1496.8182 (monoisotopic); found. 1496.8193; calcd for $C_{65}H_{115}KN_{15}O_{23}{}^+$ [M+K]$^+$, 1512.7922 (monoisotopic); found. 1512.7873. RP-HPLC analysis with a linear gradient in 30 min, 5 % to 95 % MeCN (B) at 214 nm, column 1, T$_R$ = 7.4 min, purity > 96 %.

Compound P1@

Compound P1@ was obtained as lyophilized oil according to GP 1, GP 3 (C) and GP 5 (B) on analytical scale. MALDI-TOF calcd for $C_{65}H_{114}N_{15}O_{22}{}^+$ [M+H]$^+$, 1456.826 (monoisotopic); found. 1456.763; calcd for $C_{65}H_{113}N_{15}NaO_{22}{}^+$ [M+Na]$^+$, 1478.808 (monoisotopic); found. 1478.791; calcd for $C_{65}H_{113}KN_{15}O_{22}{}^+$ [M+K]$^+$, 1494.782 (monoisotopic); found. 1494.764. HRMS (TOF MS ESI) calcd for $C_{65}H_{114}N_{15}O_{22}{}^+$ [M+H]$^+$, 1456.8257 (monoisotopic); found. 1456.8486; calcd for $C_{65}H_{113}N_{15}NaO_{22}{}^+$ [M+Na]$^+$, 1478.8077 (monoisotopic); found. 1478.8305; calcd for $C_{65}H_{115}N_{15}O_{22}{}^{2+}$ [M+2H]$^{2+}$, 728.9165 (monoisotopic); found. 728.9317; calcd for $C_{65}H_{114}N_{15}NaO_{22}{}^{2+}$ [M+H+Na]$^{2+}$, 739.9075 (monoisotopic); found. 739.9225; calcd for $C_{65}H_{114}KN_{15}O_{22}{}^{2+}$ [M+H+K]$^{2+}$, 747.8944 (monoisotopic); found. 747.9052. RP-HPLC analysis with a linear gradient in 30 min, 5 % to 95 % MeCN (B) at 214 nm, column 1, T$_R$ = 9.2 min, purity > 93 %.

Compound Man(3)@5 (1@)

Compound Man(3)@5 (1@) (18 mg, 11 μmol) was obtained as lyophilized oil according to GP 1, GP 3 (C), GP 2 and GP 5 (B) in a yield of 21 %. ^{1}H NMR (600 MHz, D$_2$O) δ 7.90 (s, 1H), 4.68 − 4.60 (m, 2H), 4.22 (dd, J = 9.6, 4.8 Hz, 1H), 4.09 (ddd, J = 11.1, 7.2, 4.0 Hz, 1H), 3.93 (ddd, J = 11.1, 5.3,

3.7 Hz, 1H), 3.86 (dd, J = 3.3, 1.8 Hz, 1H), 3.81 – 3.74 (m, 1H), 3.74 – 3.66 (m, 17H), 3.66 – 3.60 (m, 17H), 3.59 – 3.43 (m, 8H), 3.42 – 3.36 (m, 17H), 3.34 (t, J = 6.0 Hz, 2H), 3.22 – 3.11 (m, 4H), 3.08 – 2.96 (m, 3H), 2.81 (t, J = 7.3 Hz, 2H), 2.68 – 2.40 (m, 24H), 1.89 – 1.78 (m, , 1H), 1.74 – 1.67 (m, 1H), 1.57 – 1.46 (m, 2H), 1.46 – 1.38 (m, 1H), 1.38 – 1.29 (m, 1H). 108H out of in total 109H are reported in the ^{1}H NMR, because the signal for the α-anomeric proton (1H) is hidden behind the HDO signal (as determined by ^{1}H/^{13}C HSQC NMR). MALDI-TOF calcd for $C_{73}H_{129}N_{18}O_{28}^+$ [M+H]$^+$, 1705.922 (monoisotopic); found. 1705.921; calcd for $C_{73}H_{128}N_{18}NaO_{28}^+$ [M+Na]$^+$, 1727.904 (monoisotopic); found. 1727.910; calcd for $C_{73}H_{128}KN_{18}O_{28}^+$ [M+K]$^+$, 1743.878 (monoisotopic); found. 1743.940. HRMS (TOF MS ESI) calcd for $C_{73}H_{129}N_{18}O_{28}^+$ [M+H]$^+$, 1705.9218 (monoisotopic); found. 1705.9266; calcd for $C_{73}H_{130}N_{18}O_{28}^{2+}$ [M+2H]$^{2+}$, 853.4646 (monoisotopic); found. 853.4693; calcd for $C_{73}H_{129}N_{18}NaO_{28}^{2+}$ [M+H+Na]$^{2+}$, 864.4555 (monoisotopic); found. 864.4582; calcd for $C_{73}H_{129}KN_{18}O_{28}^{2+}$ [M+H+K]$^{2+}$, 872.4425 (monoisotopic); found. 872.4434. RP-HPLC analysis with a linear gradient in 10 min, 5 % to 30 % MeCN (B) at 214 nm, column 1, T_R = 13.3 min, purity > 95 %.

Compound P1a

Compound P1a was obtained as lyophilized oil according to GP 1 and GP 5 (B) on analytical scale. MALDI-TOF calcd for $C_{95}H_{170}N_{21}O_{35}^+$ [M+H]$^+$, 2165.216 (monoisotopic); found. 2165.151; calcd for $C_{95}H_{169}N_{21}NaO_{35}^+$ [M+Na]$^+$, 2187.198 (monoisotopic); found. 2187.148; calcd for $C_{95}H_{169}KN_{21}O_{35}^+$ [M+K]$^+$, 2203.172 (monoisotopic); found. 2203.095. HRMS (TOF MS ESI) calcd for $C_{95}H_{171}N_{21}O_{35}^{2+}$ [M+2H]$^{2+}$, 1083.6135 (monoisotopic); found. 1083.6164; calcd for $C_{95}H_{170}N_{21}NaO_{35}^{2+}$ [M+H+Na]$^{2+}$, 1094.6044 (monoisotopic); found. 1094.6065. RP-HPLC analysis with a linear gradient in 30 min, 5 % to 95 % MeCN (B) at 214 nm, column 1, T_R = 9.0 min, purity > 91 %.

Compound P1a@

Compound P1a@ was obtained as lyophilized oil according to GP 1, GP 3 (C) and GP 5 (B) on analytical scale. MALDI-TOF calcd for $C_{95}H_{168}N_{21}O_{34}^+$ [M+H]$^+$, 2147.206 (monoisotopic); found. 2147.242; calcd for $C_{95}H_{167}N_{21}NaO_{34}^+$ [M+Na]$^+$, 2169.188 (monoisotopic); found. 2169.242; calcd for $C_{95}H_{167}KN_{21}O_{34}^+$ [M+K]$^+$, 2185.162 (monoisotopic); found. 2185.218. HRMS (TOF MS ESI) calcd for $C_{95}H_{168}N_{21}O_{34}^+$ [M+H]$^+$, 2147.2057 (monoisotopic); found. 2147.2344; calcd for $C_{95}H_{167}N_{21}NaO_{34}^+$ [M+Na]$^+$, 2169.1877 (monoisotopic); found. 2170.2165; calcd for $C_{95}H_{167}KN_{21}O_{34}^+$ [M+K]$^+$, 2185.1616 (monoisotopic); found. 2186.1934; calcd for $C_{95}H_{168}N_{21}NaO_{34}^{2+}$ [M+H+Na]$^{2+}$, 1085.5991 (monoisotopic); found. 1085.6163; calcd for $C_{95}H_{168}KN_{21}O_{34}^{2+}$ [M+H+K]$^{2+}$, 1093.5861 (monoisotopic); found. 1093.6035; calcd for $C_{95}H_{167}N_{21}Na_2O_{34}^{2+}$ [M+2Na]$^{2+}$, 1096.5901 (monoisotopic); found. 1096.6078; calcd for $C_{95}H_{167}KN_{21}NaO_{34}^{2+}$ [M+Na+K]$^{2+}$, 1104.5771 (monoisotopic); found. 1104.5915; calcd for $C_{95}H_{169}N_{21}NaO_{34}^{3+}$ [M+2H+Na]$^{3+}$, 724.0685 (monoisotopic); found. 724.0805; calcd for $C_{95}H_{169}KN_{21}O_{34}^{3+}$ [M+2H+K]$^{3+}$, 729.3932 (monoisotopic); found. 729.4052; calcd for $C_{95}H_{168}N_{21}Na_2O_{34}^{3+}$ [M+H+2Na]$^{3+}$, 731.3958 (monoisotopic); found. 731.4115; calcd for $C_{95}H_{168}KN_{21}NaO_{34}^{3+}$ [M+H+Na+K]$^{3+}$, 736.7205 (monoisotopic); found. 736.7342; calcd for $C_{95}H_{167}N_{21}Na_3O_{34}^{3+}$ [M+3Na]$^{3+}$, 738.7231 (monoisotopic); found. 738.7373; calcd for

$C_{95}H_{168}K_2N_{21}O_{34}{}^{3+}$ [M+H+2K]$^{3+}$, 742.0451 (monoisotopic); found. 742.0578; calcd for $C_{95}H_{167}KN_{21}Na_2O_{34}{}^{3+}$ [M+2Na+K]$^{3+}$, 744.0478 (monoisotopic); found. 744.0620. RP. RP-HPLC analysis with a linear gradient in 30 min, 5 % to 95 % MeCN (B) at 214 nm, column 1, T$_R$ = 12.3 min, purity > 97 %.

Compound Man(4)@8 (1a@)

Compound Man(4)@8 (1a@) (23 mg, 10 µmol) was obtained as lyophilized oil according to GP 1, GP 3 (C), GP 2 and GP 5 (B) in a yield of 19 %. ^{1}H NMR (600 MHz, D$_2$O) δ 7.89 (s, 1H), 4.69 – 4.59 (m, 2H), 4.22 (dd, J = 9.4, 5.0 Hz, 1H), 4.09 (ddd, J = 11.1, 7.3, 4.0 Hz, 1H), 3.92 (dt, J = 11.1, 4.2 Hz, 1H), 3.86 (dd, J = 3.4, 1.7 Hz, 1H), 3.74 (dd, J = 12.2, 2.4 Hz, 1H), 3.71 – 3.58 (m, 59H), 3.58 – 3.42 (m, 7H), 3.42 – 3.28 (m, 32H), 3.21 – 3.12 (m, 4H), 3.07 – 2.96 (m, 3H), 2.80 (t, J = 7.4 Hz, 2H), 2.62 – 2.40 (m, 35H), 1.90 – 1.78 (m, 1H), 1.78 – 1.63 (m, 1H), 1.58 – 1.45 (m, 2H), 1.45 – 1.37 (m, 1H), 1.37 – 1.28 (m, 1H). 156H out of in total 157H are reported in the ^{1}H NMR, because the signal for the α-anomeric proton (1H) is hidden behind the HDO signal (as determined by ^{1}H/^{13}C HSQC NMR). MALDI-TOF calcd for $C_{103}H_{183}N_{24}O_{40}{}^+$ [M+H]$^+$, 2396.302 (monoisotopic); found. 2396.276; calcd for $C_{103}H_{182}N_{24}NaO_{40}{}^+$ [M+Na]$^+$, 2418.284 (monoisotopic); found. 2418.292; calcd for $C_{103}H_{182}KN_{24}O_{40}{}^+$ [M+K]$^+$, 2434.258 (monoisotopic); found. 2434.232. LC/MS ESI calcd for $C_{103}H_{184}N_{24}O_{40}{}^{2+}$ [M+2H]$^{2+}$ 1199.16; found. 1199.15; calcd for $C_{103}H_{185}N_{24}O_{40}{}^{3+}$ [M+3H]$^{3+}$ 799.8; found. 799.7; calcd for $C_{103}H_{186}N_{24}O_{40}{}^{4+}$ [M+4H]$^{4+}$ 600.1; found. 600.0. RP-HPLC analysis with a linear gradient in 30 min, 5 % to 30 % MeCN (B) at 214 nm, column 1, T$_R$ = 18.4 min, purity > 95 %.

Compound P2

Compound P2 was obtained as lyophilized oil according to GP 1 and GP 5 (B) on analytical scale. MALDI-TOF calcd for $C_{71}H_{118}N_{17}O_{21}{}^+$ [M+H]$^+$, 1544.868 (monoisotopic); found. 1544.839; calcd for $C_{71}H_{117}N_{17}NaO_{21}{}^+$ [M+Na]$^+$, 1566.850 (monoisotopic); found. 1566.803; calcd for $C_{71}H_{117}KN_{17}O_{21}{}^+$ [M+K]$^+$, 1582.824 (monoisotopic); found. 1582.790. HRMS (TOF MS ESI) calcd for $C_{101}H_{173}N_{23}O_{33}{}^{2+}$ [M+2H]$^{2+}$, 1118.6294 (monoisotopic); found. 1118.6285; calcd for $C_{101}H_{172}N_{23}NaO_{33}{}^{2+}$ [M+H+Na]$^{2+}$, 1129.6294 (monoisotopic); found. 1129.6180; calcd for $C_{101}H_{172}KN_{23}NaO_{33}{}^{3+}$ [M+H+Na+K]$^{3+}$, 766.0680 (monoisotopic); found. 766.4026; calcd for $C_{101}H_{171}N_{23}Na_3O_{33}{}^{3+}$ [M+3Na]$^{3+}$, 768.0707 (monoisotopic); found. 768.07690; calcd for $C_{101}H_{171}KN_{23}Na_2O_{33}{}^{3+}$ [M+2Na+K]$^{3+}$, 773.3953 (monoisotopic); found. 773.3921. RP-HPLC analysis with a linear gradient in 30 min, 5 % to 95 % MeCN (B) at 214 nm, column 1, T$_R$ = 7.3 min, purity > 90 %.

Compound P2@

Compound P2@ was obtained as lyophilized oil according to GP 1, GP 3 (C) and GP 5 (B) on analytical scale. MALDI-TOF calcd for $C_{71}H_{116}N_{17}O_{20}{}^+$ [M+H]$^+$, 1526.858 (monoisotopic); found. 1544.869; calcd for $C_{71}H_{115}N_{17}NaO_{20}{}^+$ [M+Na]$^+$, 1548.840 (monoisotopic); found. 1548.863; calcd for $C_{71}H_{115}KN_{17}O_{20}{}^+$ [M+K]$^+$, 1564.814 (monoisotopic); found. 1564.837. HRMS (TOF MS ESI) calcd for $C_{101}H_{170}N_{23}NaO_{32}{}^{2+}$ [M+H+Na]$^{2+}$, 1120.6151 (monoisotopic); found. 1120.6210; calcd for

$C_{101}H_{170}KN_{23}O_{32}^{2+}$ [M+H+K]$^{2+}$, 1128.6021 (monoisotopic); found. 1128.6080; calcd for $C_{101}H_{169}N_{23}Na_2O_{32}^{2+}$ [M+2Na]$^{2+}$, 1131.6061 (monoisotopic); found. 1131.6137. RP-HPLC analysis with a linear gradient in 30 min, 5 % to 95 % MeCN (B) at 214 nm, column 1, T_R = 9.1 min, purity > 98 %.

Compound Man(1,3,5)@5 (2@)

Compound Man(1,3,5)@5 (2@) (22 mg, 10 µmol) was obtained as lyophilized oil according to GP 1, GP 3 (C), GP 2 and GP 5 (B) in a yield of 19 %. ^{1}H NMR (600 MHz, D$_2$O) δ 7.89 (s, 3H), 4.72 – 4.56 (m, 6H), 4.25 – 4.15 (m, 1H), 4.09 (ddd, J = 11.1, 7.2, 4.0 Hz, 3H), 3.92 (ddd, J = 11.0, 5.4, 3.8 Hz, 3H), 3.86 (dd, J = 3.4, 1.7 Hz, 3H), 3.74 (dd, J = 12.2, 2.3 Hz, 3H), 3.71 – 3.64 (m, 13H), 3.63 – 3.57 (m, 11H), 3.57 – 3.41 (m, 14H), 3.42 – 3.22 (m, 21H), 3.22 – 3.10 (m, 4H), 3.09 – 2.93 (m, 9H), 2.80 (t, J = 7.4 Hz, 6H), 2.62 – 2.37 (m, 24H), 1.88 – 1.78 (m, 1H), 1.75 – 1.63 (m, 1H), 1.54 – 1.44 (m, 2H), 1.44 – 1.35 (m, 1H), 1.35 – 1.26 (m, 1H). 130H out of in total 133H are reported in the ^{1}H NMR, because the signal for the α-anomeric protons (3H) is hidden behind the HDO signal (as determined by ^{1}H/^{13}C HSQC NMR). MALDI-TOF calcd for $C_{95}H_{161}N_{26}O_{38}^+$ [M+H]$^+$, 2274.147 (monoisotopic); found. 2274.103; calcd for $C_{95}H_{160}N_{26}NaO_{38}^+$ [M+Na]$^+$, 2296.128 (monoisotopic); found. 2296.100; calcd for $C_{95}H_{160}KN_{26}O_{38}^+$ [M+K]$^+$, 2312.102 (monoisotopic); found. 2312.085. HRMS (TOF MS ESI) calcd for $C_{95}H_{161}KN_{26}O_{38}^{2+}$ [M+H+K]$^{2+}$, 1157.0562 (monoisotopic); found. 1157.0490; calcd for $C_{95}H_{160}N_{26}Na_2O_{38}^{2+}$ [M+2Na]$^{2+}$, 1160.0602 (monoisotopic); found. 1160.0590; calcd for $C_{95}H_{160}KN_{26}NaO_{38}^{2+}$ [M+Na+K]$^{2+}$, 1168.0472 (monoisotopic); found. 1168.0427. RP-HPLC analysis with a linear gradient in 30 min, 5 % to 30 % MeCN (B) at 214 nm, column 1, T_R = 11.1 min, purity > 95 %.

Compound P2a

Compound P2a was obtained as lyophilized oil according to GP 1 and GP 5 (B) on analytical scale. MALDI-TOF calcd for $C_{101}H_{172}N_{23}O_{33}^+$ [M+H]$^+$, 2235.248 (monoisotopic); found. 2235.163; calcd for $C_{101}H_{171}N_{23}NaO_{33}^+$ [M+Na]$^+$, 2257.230 (monoisotopic); found. 2257.225; calcd for $C_{101}H_{171}KN_{23}O_{33}^+$ [M+K]$^+$, 2273.204 (monoisotopic); found. 2273.301. LC/MS ESI calcd for $C_{101}H_{174}N_{23}O_{33}^{3+}$ [M+3H]$^{3+}$, 746.09; found. 746.24; calcd for $C_{101}H_{175}N_{23}O_{33}^{4+}$ [M+4H]$^{4+}$, 559.82; found. 559.93; calcd for $C_{101}H_{176}N_{23}O_{33}^{5+}$ [M+5H]$^{5+}$, 448.06; found. 448.18. RP-HPLC analysis with a linear gradient in 30 min, 5 % to 95 % MeCN (B) at 214 nm, column 1, T_R = 8.4 min, purity > 96 %.

Compound P2a@

Compound P2a@ was obtained as lyophilized oil according to GP 1, GP 3 (C) and GP 5 (B) on analytical scale. MALDI-TOF calcd for $C_{101}H_{170}N_{23}O_{32}^+$ [M+H]$^+$, 2217.238 (monoisotopic); found. 2217.315; calcd for $C_{101}H_{169}N_{23}NaO_{32}^+$ [M+Na]$^+$, 2239.220 (monoisotopic); found. 2239.289; calcd for $C_{101}H_{169}KN_{23}O_{32}^+$ [M+K]$^+$, 2255.194 (monoisotopic); found. 2255.234. LC/MS ESI calcd for $C_{101}H_{171}N_{23}O_{32}^{2+}$ [M+2H]$^{2+}$, 1109.12; found. 1109.38; calcd for $C_{101}H_{174}N_{23}O_{33}^{3+}$ [M+3H]$^{3+}$, 740.09;

found. 740.04; calcd for $C_{101}H_{173}N_{23}O_{32}{}^{4+}$ [M+4H]$^{4+}$, 555.32; found. 555.41; calcd for $C_{101}H_{174}N_{23}O_{32}{}^{5+}$ [M+5H]$^{5+}$, 444.45; found. 444.53. RP-HPLC analysis with a linear gradient in 30 min, 5 % to 95 % MeCN (B) at 214 nm, column 1, T_R = 11.2 min, purity > 98 %.

Compound Man(1,4,7)@8 (2a@)

Compound Man(1,4,7)@8 (2a@) (12 mg, 5 µmol) was obtained as lyophilized oil according to GP 1, GP 3 (C), GP 2 and GP 5 (B) in a yield of 11 %. ^{1}H NMR (600 MHz, D$_2$O) δ 7.87 (t, J = 9.5 Hz, 3H), 4.66 – 4.61 (m, 6H), 4.23 – 4.19 (m, 1H), 4.08 (ddd, J = 11.0, 7.2, 4.0 Hz, 3H), 3.95 – 3.90 (m, 3H), 3.88 – 3.83 (m, 3H), 3.78 – 3.57 (m, 52H), 3.57 – 3.44 (m, 12H), 3.44 – 3.30 (m, 34H), 3.22 – 3.11 (m, 4H), 3.07 – 2.94 (m, 9H), 2.87 – 2.38 (m, 42H), 1.88 – 1.75 (m, 1H), 1.75 – 1.65 (m, 1H), 1.56 – 1.46 (m, 2H), 1.46 – 1.37 (m, 1H), 1.37 – 1.37 (m, 1H). 178H out of in total 181H are reported in the ^{1}H NMR, because the signal for the α-anomeric protons (3H) is hidden behind the HDO signal (as determined by ^{1}H/^{13}C HSQC NMR). MALDI-TOF calcd for $C_{125}H_{215}N_{32}O_{50}{}^+$ [M+H]$^+$, 2964.526 (monoisotopic); found. 2964.504; calcd for $C_{125}H_{214}N_{32}NaO_{50}{}^+$ [M+Na]$^+$, 2986.508 (monoisotopic); found. 2986.489. RP-HPLC analysis with a linear gradient in 30 min, 5 % to 30 % MeCN (B) at 214 nm, column 1, T_R = 15.9 min, purity > 95 %.

5.11. Characterization data of cyclic glycomacromolecules with EDS spacer and thiol-ether triazole linker on mannoside

Compound Man(3)S@5 (1@S)

Compound Man(3)S@5 (1@S) (21 mg, 12 µmol) was obtained as lyophilized oil according to GP 1, GP 3 (C), GP 2 and GP 5 (B) in a yield of 24 %. ^{1}H NMR (600 MHz, D$_2$O) δ 7.89 (s, 1H), 4.84 (s, 1H), 4.62 (t, J = 6.3 Hz, 2H), 4.22 (dd, J = 9.5, 4.9 Hz, 1H), 3.93 (dd, J = 3.5, 1.7 Hz, 1H), 3.88 (dd, J = 12.3, 2.2 Hz, 1H), 3.84 – 3.74 (m, 4H), 3.73 – 3.59 (m, 34H), 3.59 – 3.50 (m, 3H), 3.50 – 3.44 (m, 4H), 3.44 – 3.26 (m, 19H), 3.23 – 3.13 (m, 4H), 3.08 (t, J = 6.3 Hz, 2H), 3.03 (t, J = 7.1 Hz, 2H), 2.80 (t, J = 7.2 Hz, 2H), 2.71 – 2.35 (m, 26H), 1.94 – 1.76 (m, 3H), 1.76 – 1.66 (m, 1H), 1.59 – 1.46 (m, 2H), 1.45 – 1.38 (m, 1H), 1.37 – 1.28 (m, 1H). MALDI-TOF calcd for $C_{76}H_{135}N_{18}O_{28}S^+$ [M+H]$^+$, 1779.941 (monoisotopic); found. 1780.186; calcd for $C_{76}H_{134}N_{18}NaO_{28}S^+$ [M+Na]$^+$, 1801.923 (monoisotopic); found. 1802.164. RP-HPLC analysis with a linear gradient in 30 min, 5 % to 30 % MeCN (B) at 214 nm, column 1, T_R = 15.0 min, purity > 95 %.

Compound Man(1,3,5)S@5 (2@S)

Compound Man(1,3,5)S@5 (2@S) (18 mg, 7 µmol) was obtained as lyophilized oil according to GP 1, GP 3 (C), GP 2 and GP 5 (B) in a yield of 14 %. ^{1}H NMR (600 MHz, D$_2$O) δ 7.88 (s, 3H), 4.84 (s, 3H), 4.61 (t, J = 6.1 Hz, 6H), 4.21 (dd, J = 9.5, 4.7 Hz, 1H), 3.97 – 3.90 (m, 3H), 3.87 (dd, J = 12.2, 2.3 Hz, 3H), 3.82 – 3.71 (m, 9H), 3.71 – 3.64 (m, 11H), 3.64 – 3.59 (m, 10H), 3.59 – 3.50 (m, 6H),

3.50 – 3.42 (m, 12H), 3.42 – 3.27 (m, 20H), 3.18 – 3.12 (m, 4H), 3.12 – 2.94 (m, 12H), 2.79 (t, J = 7.2 Hz, 6H), 2.68 – 2.35 (m, 30H), 1.94 – 1.73 (m, 7H), 1.72 – 1.66 (m, 1H), 1.53 – 1.45 (m, 2H), 1.42 – 1.36 (m, 1H), 1.34 – 1.26 (m, 1H). MALDI-TOF calcd for $C_{104}H_{179}N_{26}O_{38}S_3^+$ [M+H]$^+$, 2496.204 (monoisotopic); found. 2496.356; calcd for $C_{104}H_{178}N_{26}NaO_{38}S_3^+$ [M+Na]$^+$, 2518.186 (monoisotopic); found. 2518.354; calcd for $C_{104}H_{178}KN_{26}O_{38}S_3^+$ [M+K]$^+$, 2534.159 (monoisotopic); found. 2534.349. RP-HPLC analysis with a linear gradient in 30 min, 5 % to 30 % MeCN (B) at 214 nm, column 1, T_R = 16.0 min, purity > 89 %.

5.12. Characterization data of cyclic glycomacromolecules with EDS spacer and benzyl triazole linker on mannoside

Compound Man(3)B@5 (1@B)

Compound Man(3)B@5 (1@B) (12 mg, 7 μmol) was obtained as lyophilized powder according to GP 1, GP 3 (C), GP 2 and GP 5 (B) in a yield of 27 %. ^{1}H NMR (400 MHz, D$_2$O) δ 7.60 (s, 1H), 7.02 (s, 4H), 5.53 (d, J = 1.6 Hz, 1H), 4.62 (t, J = 6.2 Hz, 2H), 4.19 (dd, J = 9.3, 4.8 Hz, 1H), 4.12 (s, 1H), 3.99 (dd, J = 9.3, 3.2 Hz, 1H), 3.93 – 3.48 (m, 38H), 3.48 – 3.20 (m, 24H), 3.18 – 3.09 (m, 6H), 2.92 (t, J = 6.8 Hz, 2H), 2.69 (t, J = 6.8 Hz, 2H), 2.63 – 2.33 (m, 24H), 1.85 – 1.75 (m, 1H), 1.71 – 1.63 (dd, J = 9.3, 4.7 Hz, 1H), 1.53 – 1.44 (m, 2H), 1.40 – 1.29 (m, 2H). MALDI-TOF calcd for $C_{79}H_{133}N_{18}O_{28}^+$ [M+H]$^+$, 1781.953 (monoisotopic); found. 1782.061; calcd for $C_{79}H_{132}N_{18}NaO_{28}^+$ [M+Na]$^+$, 1803.935 (monoisotopic); found. 1803.107. HRMS (TOF MS ESI) calcd for $C_{79}H_{133}N_{18}NaO_{28}^{2+}$ [M+H+Na]$^{2+}$, 902.4712 (monoisotopic); found. 902.4687; calcd for $C_{79}H_{133}KN_{18}O_{28}^{2+}$ [M+H+K]$^{2+}$, 910.4581 (monoisotopic); found. 910.4531; calcd for $C_{79}H_{132}KN_{18}NaO_{28}^{2+}$ [M+Na+K]$^{2+}$, 921.4491 (monoisotopic); found. 921.9684. RP-HPLC analysis with a linear gradient in 30 min, 5 % to 30 % MeCN (B) at 214 nm, column 1, T_R = 16.2 min, purity > 91 %.

Compound Man(1,3,5)B@5 (2@B)

Compound Man(1,3,5)B@5 (2@B) (14 mg, 6 μmol) was obtained as lyophilized powder according to GP 1, GP 3 (C), GP 2 and GP 5 (B) in a yield of 22 %. ^{1}H NMR (400 MHz, D$_2$O) δ 7.59 (s, 3H), 6.97 (s, 12H), 5.49 (s, 3H), 4.64 – 4.50 (m, 6H), 4.16 (dd, J = 9.0, 4.3 Hz, 1H), 4.09 (dd, J = 3.3, 1.8 Hz, 3H), 3.97 (dd, J = 9.4, 3.4 Hz, 3H), 3.90 – 3.68 (m, 10H), 3.68 – 3.57 (m, 11H), 3.57 – 3.51 (m, 8H), 3.51 – 3.44 (m, 3H), 3.44 – 2.97 (m, 40H), 2.89 (t, J = 6.4 Hz, 6H), 2.67 (t, J = 6.9 Hz, 6H), 2.60 – 2.24 (m, 24H), 1.79 – 1.73 (m, 1H), 1.66 – 1.60 (m, 1H), 1.46 – 1.39 (m, 2H), 1.34 – 1.25 (m, 2H). MALDI-TOF calcd for $C_{113}H_{173}N_{26}O_{38}^+$ [M+H]$^+$, 2502.240 (monoisotopic); found. 2502.421; calcd for $C_{113}H_{172}N_{26}NaO_{38}^+$ [M+Na]$^+$, 2524.222 (monoisotopic); found. 2524.413; calcd for $C_{113}H_{172}KN_{26}O_{38}^+$ [M+K]$^+$, 2540.196 (monoisotopic); found. 2540.394. HRMS (TOF MS ESI) calcd for $C_{113}H_{174}N_{26}O_{38}^{2+}$ [M+2H]$^{2+}$, 1252.1253 (monoisotopic); found. 1252.1216; calcd for $C_{113}H_{173}N_{26}NaO_{38}^{2+}$ [M+H+Na]$^{2+}$, 1263.1162 (monoisotopic); found. 1263.1115; calcd for

$C_{113}H_{173}KN_{26}O_{38}^{2+}$ [M+H+K]$^{2+}$, 1271.1032 (monoisotopic); found. 1271.0953; calcd for $C_{113}H_{172}N_{26}Na_2O_{38}^{2+}$ [M+2Na]$^{2+}$, 1274.1072 (monoisotopic); found. 1274.1030. RP-HPLC analysis with a linear gradient in 30 min, 5 % to 30 % MeCN (B) at 214 nm, column 1, T_R = 18.2 min, purity > 95 %.

5.13. Characterization data of compounds 6-12, 6a-12a (bi-12a) & 6b-10b

Compound 6

Compound 6 was obtained as lyophilized oil according to GP 1 and GP 5 (A) on analytical scale. ^{1}H NMR (400 MHz, D$_2$O) δ 5.98 (ddt, J = 17.3, 10.6, 5.3 Hz, 1H), 5.43 – 5.16 (m, 2H), 4.60 (dt, J = 5.4, 1.5 Hz, 1H), 4.25 (dt, J = 8.9, 3.3 Hz, 2H), 3.60 – 3.22 (m, 8H), 3.01 (t, J = 7.5 Hz, 2H), 2.76 – 2.43 (m, 8H), 1.94 – 1.81 (m, 1H), 1.81 – 1.58 (m, 3H), 1.58 – 1.36 (m, 2H). ^{1}H NMR (600 MHz, DMSO-d_6) δ 12.18 (bs, 1H), 8.18 – 8.05 (m, 1H), 8.05 – 7.92 (m, 1H), 7.91 – 7.63 (m, 3H), 7.31 (s, 1H), 6.99 (s, 1H), 6.05 – 5.78 (m, 1H), 5.45 – 5.06 (m, 2H), 4.64 – 4.40 (m, 2H), 4.24 – 3.99 (m, 1H), 3.29 – 3.10 (m, 4H), 3.06 – 2.85 (m, 2H), 2.76 (bs, 2H), 2.47 – 2.18 (m, 6H), 1.79 – 1.62 (m, 1H), 1.61 – 1.42 (m, 3H), 1.41 – 1.18 (m, 2H). 34H out of in total 38H are reported in the ^{1}H NMR, because the signal for the CH$_2$ triamine group (-OC-NH-CH_2-CH$_2$-NH-, 4H) is hidden behind the HDO signal, whereas protons of the CH$_2$ succinic acid group (-OC-CH_2-CH$_2$-CO-, 2H) are hidden behind the DMSO-d_5 signal (as determined by ^{1}H/^{1}H COSY NMR). HRMS (TOF MS ESI) calcd for $C_{22}H_{39}N_6O_8^+$ [M+H]$^+$, 515.2824 (monoisotopic); found. 515.2828. RP-HPLC analysis with a linear gradient in 30 min, 5 % to 50 % MeCN (B) at 214 nm, column 1, T_R = 4.0 min, purity > 91 %.

Compound 6a

Compound 6a (9.7 mg, 19 µmol) was obtained as lyophilized oil according to GP 1, GP 3 (A) and GP 5 (A) in a yield of 76 % after direct cleavage from solid support. Yield after purification was 17 % (2.1 mg, 4.2 µmol). ^{1}H NMR (400 MHz, D$_2$O) δ 6.07 – 5.83 (m, 1H), 5.46 – 5.15 (m, 2H), 4.64 – 4.45 (m, 2H), 4.33 – 4.17 (m, 1H), 3.70 (t, J = 5.5 Hz, 2H), 3.62 – 3.25 (m, 6H), 3.02 (t, J = 7.8 Hz, 2H), 2.76 (d, J = 9.6 Hz, 4H), 2.66 – 2.42 (m, 4H), 1.95 – 1.82 (m, 1H), 1.81 – 1.61 (m, 3H), 1.60 – 1.33 (m, 2H). ^{1}H NMR (600 MHz, DMSO-d_6) δ 8.16 – 7.88 (m, 1H), 7.66 (bs, 2H), 7.32 (s, 1H), 6.99 (s, 1H), 5.99 – 5.79 (m, 1H), 5.30 (dd, J = 33.9, 17.3 Hz, 1H), 5.19 (t, J = 11.9 Hz, 1H), 4.58 – 4.40 (m, 2H), 4.18 – 4.04 (m, 1H), 3.51 (t, J = 5.9 Hz, 2H), 3.26 – 3.10 (m, 4H), 2.84 – 2.69 (m, 2H), 2.66 – 2.54 (m, 4H), 2.44 – 2.21 (m, 4H), 1.78 – 1.62 (m, 1H), 1.61 – 1.40 (m, 3H), 1.40 – 1.19 (m, 2H). 33H out of in total 36H are reported in the ^{1}H NMR, because the signal for the CH$_2$ triamine group (-OC-NH-CH_2-CH$_2$-NH-, 2H) is hidden behind the HDO signal and the two -NH- protons at 8.16 – 7.88 ppm yield only an integral of 1 (as determined by ^{1}H/^{1}H COSY NMR; integrals of exchangeable protons are unprecise). HRMS (TOF MS ESI) calcd for $C_{22}H_{36}N_6NaO_7^+$

[M+Na]$^+$ 519.2528 (monoisotopic), found. 519.2528. RP-HPLC analysis with a linear gradient in 30 min, 5 % to 50 % MeCN (B) at 214 nm, column 1, T$_R$ = 4.7 min, purity > 92 %.

Compound 6b

Compound 6b (5.6 mg, 13 μmol) was obtained as lyophilized oil according to GP 1, GP 3 (A), GP 4 and GP 5 (A) in a yield of 53 % after direct cleavage from solid support. Yield after purification was 12 % (1.2 mg, 2.9 μmol). ^{1}H NMR (400 MHz, D$_2$O) δ 4.24 (dd, J = 8.9, 5.4 Hz, 1H), 3.94 – 3.81 (m, 2H), 3.54 (t, J = 5.7 Hz, 2H), 3.32 (t, J = 5.8 Hz, 2H), 3.23 (t, J = 5.7 Hz, 2H), 3.02 (t, J = 7.6 Hz, 2H), 2.83 (s, 4H), 2.72 – 2.50 (m, 4H), 1.95 – 1.81 (m, 1H), 1.80 – 1.60 (m, 3H), 1.60 – 1.36 (m, 2H). ^{1}H NMR (600 MHz, DMSO-d_6) δ 8.23 – 8.06 (m, 1H), 8.00 (d, J = 7.9 Hz, 1H), 7.79 (bs, 2H), 7.31 (s, 1H), 7.00 (s, 1H), 4.21 – 4.00 (m, 1H), 3.77 – 3.56 (m, 2H), 3.11 (t, J = 6.0 Hz, 2H), 2.99 (t, J = 6.2 Hz, 2H), 2.75 (td, J = 7.7, 2.5 Hz, 2H), 2.70 – 2.56 (m, 4H), 2.48 – 2.20 (m, 4H), 1.77 – 1.62 (m, 1H), 1.62 – 1.40 (m, 3H), 1.40 – 1.15 (m, 2H). 29H out of in total 32H are reported in the ^{1}H NMR, because the signal for the CH$_2$ triamine group (-OC-NH-CH_2-CH$_2$-NH-, 2H) is hidden behind the HDO signal and the -NH- protons (between 8.23 – 8.06 ppm and 8.00 ppm) yield only an integral of 2 although it is supposed to be 3 -NH- protons (as determined by ^{1}H/^{1}H COSY NMR; integrals of exchangeable protons are unprecise). HRMS (TOF MS ESI) calcd for C$_{18}$H$_{32}$N$_6$NaO$_5$$^+$ [M+Na]$^+$, 435.2326 (monoisotopic); found. 435.2324. RP-HPLC analysis with a linear gradient in 30 min, 5 % to 50 % MeCN (B) at 214 nm, column 1, T$_R$ = 1.9 min, purity > 95 %

Compound 7

Compound **7** was obtained as lyophilized oil according to GP 1 and GP 5 (A) on analytical scale. ^{1}H NMR (600 MHz, D$_2$O) δ 5.99 (ddt, J = 16.3, 10.6, 5.3 Hz, 2H), 5.34 (dd, J = 17.1, 2.2 Hz, 2H), 5.30 – 5.20 (m, 2H), 4.60 (d, J = 5.3 Hz, 4H), 4.30 – 4.22 (m, 1H), 3.72 – 3.16 (m, 16H), 3.07 – 2.96 (m, 2H), 2.74 – 2.30 (m, 12H), 1.92 – 1.84 (m, 1H), 1.79 – 1.66 (m, 3H), 1.53 – 1.42 (m, 2H). HRMS (TOF MS ESI) calcd for C$_{34}$H$_{58}$N$_9$NaO$_{12}$$^+$ [M+H]$^+$ 784.4199 (monoisotopic), found. 784.4202; calcd for C$_{34}$H$_{59}$N$_9$NaO$_{12}$$^+$ [M+2H]$^{2+}$ 392.7136 (monoisotopic), found. 392.7139. RP-HPLC analysis with a linear gradient in 30 min, 5 % to 50 % MeCN (B) at 214 nm, column 1, T$_R$ = 8.2 min, purity > 87 %.

Compound 7a

Compound 7a (13 mg, 17 μmol) was obtained as lyophilized oil according to GP 1, GP 3 (A) and GP 5 (A) in a yield of 67 % after direct cleavage from solid support. Yield after purification was 14 % (2.6 mg, 3.4 μmol). ^{1}H NMR (400 MHz, D$_2$O) δ 6.16 – 5.82 (m, 2H), 5.46 – 5.14 (m, 4H), 4.62 – 4.50 (m, 4H), 4.25 (dd, J = 9.1, 5.2 Hz, 1H), 3.70 (t, J = 5.6 Hz, 2H), 3.65 – 3.20 (m, 14H), 3.01 (t, J = 7.6 Hz, 2H), 2.76 (d, J = 9.6 Hz, 4H), 2.68 – 2.34 (m, 8H), 1.96 – 1.81 (m, 1H), 1.81 – 1.62 (m, 3H), 1.61 – 1.35 (m, 2H). HRMS (TOF MS ESI) calcd for C$_{34}$H$_{57}$N$_9$O$_{11}$$^{2+}$ [M+2H]$^{2+}$, 383.7083 (monoisotopic); found. 383.7082. RP-HPLC analysis with a linear gradient in 30 min, 5 % to 50 % MeCN (B) at 214 nm, column 1, T$_R$ = 9.3 min, purity > 92 %.

Compound 7b

Compound 7b (10 mg, 16 µmol) was obtained as lyophilized oil according to GP 1, GP 3 (A), GP 4 and GP 5 (A) in a yield of 65 % after direct cleavage from solid support. Yield after purification was 11 % (1.7 mg, 2.8 µmol). ^{1}H NMR (400 MHz, D$_2$O) δ 4.23 (dd, J = 8.8, 5.4 Hz, 1H), 3.88 (t, J = 5.7 Hz, 2H), 3.61 – 3.47 (m, 6H), 3.36 – 3.29 (m, 2H), 3.29 – 3.17 (m, 6H), 3.01 (t, J = 7.6 Hz, 2H), 2.84 (s, 4H), 2.70 – 2.49 (m, 8H), 2.12 – 1.61 (m, 4H), 1.61 – 1.32 (m, 2H). HRMS (TOF MS ESI) calcd for C$_{26}$H$_{49}$N$_9$O$_7$$^{2+}$ [M+2H]$^{2+}$, 299.6872 (monoisotopic); found. 299.6873. RP-HPLC analysis with a linear gradient in 30 min, 5 % to 50 % MeCN (B) at 214 nm, column 1, T$_R$ = 1.9 min, purity > 95 %.

Compound 8

Compound 8 was obtained as lyophilized oil according to GP 1 and GP 5 (A) on analytical scale. ^{1}H NMR (400 MHz, D$_2$O) δ 5.98 (ddt, J = 16.2, 10.6, 5.3 Hz, 3H), 5.44 – 5.15 (m, 6H), 4.60 (dd, J = 5.5, 1.8 Hz, 6H), 4.25 (dd, J = 9.1, 5.1 Hz, 1H), 3.74 – 3.11 (m, 24H), 3.01 (t, J = 7.6 Hz, 2H), 2.77 – 2.35 (m, 16H), 1.94 – 1.83 (m, 1H), 1.80 – 1.65 (m, 3H), 1.54 – 1.41 (m, 2H). HRMS (TOF MS ESI) calcd for. C$_{46}$H$_{78}$N$_{12}$O$_{16}$$^{2+}$ [M+2H]$^{2+}$, 527.2824 (monoisotopic); found. 527.2824. RP-HPLC analysis with a linear gradient in 30 min, 5 % to 50 % MeCN (B) at 214 nm, column 1, T$_R$ = 11.1 min, purity > 88 %.

Compound 8a

Compound 8a (19.8 mg, 19 µmol) was obtained as lyophilized oil according to GP 1, GP 3 (A) and GP 5 (A) in a yield of 75 % after direct cleavage from solid support. Yield after purification was 15 % (3.8 mg, 3.6 µmol). ^{1}H NMR (400 MHz, D$_2$O) δ 5.98 (ddt, J = 16.4, 10.7, 5.3 Hz, 3H), 5.47 – 5.16 (m, 6H), 4.71 – 4.42 (m, 6H), 4.25 (dd, J = 9.1, 5.1 Hz, 1H), 3.90 – 3.15 (m, 24H), 3.01 (t, J = 7.6 Hz, 2H), 2.93 – 2.30 (m, 16H), 1.91 – 1.82 (m, 1H), 1.81 – 1.62 (m, 3H), 1.55 – 1.40 (m, 2H). HRMS (TOF MS ESI) calcd for. C$_{46}$H$_{76}$N$_{12}$O$_{15}$$^{2+}$ [M+2H]$^{2+}$, 518.2771 (monoisotopic); found. 518.2777. RP-HPLC analysis with a linear gradient in 30 min, 5 % to 50 % MeCN (B) at 214 nm, column 1, T$_R$ = 12.0 min, purity > 87 %.

Compound 8b

Compound 8b (14.7 mg, 18 µmol) was obtained as lyophilized oil according to GP 1, GP 3 (A), GP 4 and GP 5 (A) in a yield of 74 % after direct cleavage from solid support. Yield after purification was 13 % (2.6 mg, 3.3 µmol). ^{1}H NMR (400 MHz, D$_2$O) δ 4.23 (dd, J = 8.7, 5.4 Hz, 1H), 3.88 (t, J = 5.7 Hz, 2H), 3.72 – 3.45 (m, 10H), 3.32 (t, J = 5.8 Hz, 3H), 3.30 – 3.10 (m, 9H), 3.01 (t, J = 7.7 Hz, 2H), 2.84 (s, 4H), 2.78 – 2.40 (m, 12H), 1.92 – 1.81 (m, 1H), 1.81 – 1.61 (m, 3H), 1.58 – 1.36 (m, 2H). HRMS (TOF MS ESI) calcd for. C$_{34}$H$_{64}$N$_{12}$O$_9$$^+$ [M+2H]$^{2+}$, 392.2454

(monoisotopic); found. 392.2457. RP-HPLC analysis with a linear gradient in 30 min, 5 % to 50 % MeCN (B) at 214 nm, column 1, T_R = 1.8 min, purity > 95 %.

Compound 9

Compound 9 was obtained as lyophilized oil according to GP 1 and GP 5 (A) on analytical scale. ^{1}H NMR (400 MHz, D$_2$O) δ 6.11 – 5.84 (m, 4H), 5.50 – 5.13 (m, 8H), 4.71 – 4.45 (m, 8H), 4.25 (dd, J = 9.1, 5.1 Hz, 1H), 3.81 – 3.10 (m, 32H), 3.01 (t, J = 7.6 Hz, 2H), 2.83 – 2.28 (m, 20H), 1.92 – 1.83 (m, 1H), 1.77 – 1.65 (m, 3H), 1.54 – 1.44 (m, 2H). HRMS (TOF MS ESI) calcd for. $C_{58}H_{97}N_{15}O_{20}^{2+}$ [M+2H]$^{2+}$, 661.8512 (monoisotopic); found. 661.8512. RP-HPLC analysis with a linear gradient in 30 min, 5 % to 50 % MeCN (B) at 214 nm, column 1, T_R = 13.1 min, purity > 86 %.

Compound 9a

Compound 9a (24.8 mg, 19 µmol) was obtained as lyophilized oil according to GP 1, GP 3 (A) and GP 5 (A) in a yield of 75 % after direct cleavage from solid support. Yield after purification was 13 % (4.2 mg, 3.3 µmol). ^{1}H NMR (400 MHz, D$_2$O) δ 6.20 – 5.76 (m, 4H), 5.65 – 4.98 (m, 8H), 4.69 – 4.41 (m, 8H), 4.25 (dd, J = 9.1, 5.1 Hz, 1H), 3.85 – 3.18 (m, 32H), 3.01 (t, J = 7.6 Hz, 2H), 2.76 (d, J = 9.5 Hz, 4H), 2.70 – 2.29 (m, 16H), 1.94 – 1.81 (m, 1H), 1.81 – 1.60 (m, 3H), 1.59 – 1.37 (m, 2H). HRMS (TOF MS ESI) calcd for $C_{58}H_{95}N_{15}O_{19}^{2+}$ [M+2H]$^{2+}$, 652.8459 (monoisotopic); found 652.8457. RP-HPLC analysis with a linear gradient in 30 min, 5 % to 50 % MeCN (B) at 214 nm, column 1, T_R = 14.0 min, purity > 91 %.

Compound 9b

Compound 9b (18.3 mg, 19 µmol) was obtained as lyophilized oil according to GP 1, GP 3 (A), GP 4 and GP 5 (A) in a yield of 75 % after direct cleavage from solid support. Yield after purification was 13 % (3.2 mg, 3.3 µmol). ^{1}H NMR (400 MHz, D$_2$O) δ 4.23 (dd, J = 8.8, 5.4 Hz, 1H), 3.88 (t, J = 5.7 Hz, 2H), 3.72 – 3.43 (m, 14H), 3.32 (t, J = 5.8 Hz, 3H), 3.30 – 3.09 (m, 13H), 3.01 (t, J = 7.7 Hz, 2H), 2.84 (s, 4H), 2.76 – 2.42 (m, 16H), 1.93 – 1.81 (m, 1H), 1.81 – 1.63 (m, 3H), 1.57 – 1.39 (m, 2H). HRMS (TOF MS ESI) calcd for $C_{42}H_{79}N_{15}O_{11}^{2+}$ [M+2H]$^{2+}$, 484.8036 (monoisotopic); found. 484.8035. RP-HPLC analysis with a linear gradient in 30 min, 5 % to 50 % MeCN (B) at 214 nm, column 1, T_R = 1.8 min, purity > 96 %.

Compound 10

Compound 10 was obtained as lyophilized oil according to GP 1 and GP 5 (A) on analytical scale. ^{1}H NMR (600 MHz, D$_2$O) δ 6.11 – 5.86 (m, 5H), 5.49 – 5.10 (m, 10H), 4.72 – 4.47 (m, 10H), 4.26 (dt, J = 9.8, 3.3 Hz, 1H), 3.74 – 3.14 (m, 40H), 3.02 (t, J = 7.6 Hz, 2H), 2.75 – 2.36 (m, 24H), 1.90 – 1.84 (m, 1H), 1.77 – 1.67 (m, 3H), 1.53 – 1.44 (m, 2H). HRMS (TOF MS ESI) calcd for $C_{70}H_{116}N_{18}O_{24}^{2+}$ [M+2H]$^{2+}$, 796.4199 (monoisotopic); found. 796.4191. RP-HPLC analysis with a linear gradient in 30 min, 5 % to 50 % MeCN (B) at 214 nm, column 1, T_R = 14.6 min, purity > 85 %.

Compound 10a

Compound 10a (28.4 mg, 18 µmol) was obtained as lyophilized oil according to GP 1, GP 3 (A) and GP 5 (A) in a yield of 72 % after direct cleavage from solid support. Yield after purification was 12 % (4.8 mg, 3 µmol). ^{1}H NMR (400 MHz, D$_2$O) δ 5.98 (ddt, J = 16.4, 10.6, 5.3 Hz, 5H), 5.56 − 5.03 (m, 10H), 4.71 − 4.44 (m, 10H), 4.25 (dd, J = 9.1, 5.1 Hz, 1H), 3.78 − 3.63 (m, 2H), 3.63 − 3.24 (m, 38H), 3.01 (t, J = 7.6 Hz, 2H), 2.76 (d, J = 9.6 Hz, 4H), 2.69 − 2.32 (m, 20H), 1.94 − 1.82 (m, 1H), 1.81 − 1.62 (m, 3H), 1.60 − 1.36 (m, 2H). HRMS (TOF MS ESI) calcd for $C_{70}H_{114}N_{18}O_{23}{}^{2+}$ [M+2H]$^{2+}$, 787.4147 (monoisotopic); found. 787.4153. RP-HPLC analysis with a linear gradient in 30 min, 5 % to 50 % MeCN (B) at 214 nm, column 1, T_R = 15.5 min, purity > 95 %.

Compound 10b

Compound 10b (20 mg, 17 µmol) was obtained as lyophilized oil according to GP 1, GP 3 (A), GP 4 and GP 5 (A) in a yield of 69 % after direct cleavage from solid support. Yield after purification was 11 % (3.2 mg, 2.8µmol). ^{1}H NMR (400 MHz, D$_2$O) δ 4.22 (dd, J = 8.8, 5.4 Hz, 1H), 3.87 (t, J = 5.7 Hz, 2H), 3.75 − 3.42 (m, 18H), 3.32 (t, J = 5.8 Hz, 3H), 3.29 − 3.07 (m, 17H), 3.01 (t, J = 7.7 Hz, 2H), 2.83 (s, 4H), 2.76 − 2.37 (m, 20H), 1.90 − 1.80 (m, 1H), 1.79 − 1.64 (m, 3H), 1.54 − 1.41 (m, 2H). HRMS (TOF MS ESI) calcd for $C_{50}H_{94}N_{18}O_{13}{}^{2+}$ [M+2H]$^{2+}$, 577.3618 (monoisotopic); found. 577.3617. RP-HPLC analysis with a linear gradient in 30 min, 5 % to 30 % MeCN (B) at 214 nm, column 1, T_R = 4.3 min, purity > 96 %.

Compound 11, peptide sequence Suc-Phe-Ala-Lys

Compound 11 was obtained as lyophilized powder according to GP 1 and GP 5 (A) on analytical scale. LC/MS ESI calcd for $C_{22}H_{34}N_5O_6{}^+$ [M+H]$^+$, 464.25; found. 464.29. RP-HPLC analysis with a linear gradient in 60 min, 5 % to 25 % MeCN (B) at 214 nm, column 1, T_R = 4.8 min, purity > 84 %.

Compound 11a, peptide sequence cyclo-imide-Suc-Phe-Ala-Lys

Compound 11a was obtained as lyophilized powder according to GP 1, GP 3 (A) and GP 5 (A) on analytical scale. HRMS (TOF MS ESI) calcd for $C_{22}H_{32}N_5O_5{}^+$ [M+H]$^+$, 446.2398 (monoisotopic); found. 446.2397. RP-HPLC analysis with a linear gradient in 60 min, 5 % to 25 % MeCN (B) at 214 nm, column 1, T_R = 7.7 min.

Compound 12, peptide sequence Suc-Phe-Phe-Ala-Lys[17]

Compound 12 was obtained as lyophilized powder according to GP 1 and GP 5 (A) on analytical scale. ^{1}H NMR (600 MHz, DMSO-d_6) δ 12.16 (bs, 1H), 8.10 (d, J = 6.9 Hz, 1H), 7.99 (d, J = 7.8 Hz,

---

[17]Linear tetrapeptide 12 has been synthesized and characterized (NMR, RP-HPLC and MALDI-TOF) by Genesha Olgar (Heinrich-Heine-Universität Düsseldorf, group of Prof. Dr. Laura Hartmann, Bachelor Thesis, November 2015).

1H), 7.93 (d, J = 8.2 Hz, 1H), 7.88 (d, J = 7.9 Hz, 1H), 7.72 (bs, 3H), 7.39 – 7.14 (m, 10H), 7.09 (d, J = 33.5 Hz, 2H), 4.51 (td, J = 8.5, 5.0 Hz, 1H), 4.39 (ddd, J = 9.7, 8.0, 4.5 Hz, 1H), 4.24 – 4.10 (m, 2H), 3.08 (dd, J = 14.0, 5.0 Hz, 1H), 2.95 (dd, J = 14.1, 4.5 Hz, 1H), 2.86 (dd, J = 14.0, 9.0 Hz, 1H), 2.81 – 2.68 (m, 3H), 2.49 – 2.26 (m, 4H), 1.76 – 1.63 (m, 1H), 1.63 – 1.43 (m, 3H), 1.41 – 1.20 (m, 2H), 1.09 (d, J = 7.1 Hz, 3H). 43H instead of total 42H are reported in the ^{1}H NMR, because the integration of the amine protons was not reliable (-NH_2, 3H instead of 2H). Signal allocation was performed using ^{1}H/^{1}H COSY, ^{1}H/^{1}H ROESY, ^{1}H/^{13}C HMBC and ^{1}H/^{15}N HSQC NMR. HRMS (TOF MS ESI) calcd for $C_{31}H_{43}N_6O_7^+$ [M+H]$^+$, 611.3188 (monoisotopic); found. 611.3188. RP-HPLC analysis with a linear gradient in 10 min, 5 % to 95 % MeCN (B) at 214 nm, column 1, T$_R$ = 5.1 min, purity > 94 %.

Compound 12a and bi-12a, peptide sequence cyclo-imide-Suc-Phe-Phe-Ala-Lys[18]

Compound 12a and bi-12a was obtained as lyophilized powder according to GP 1, GP 3 (A) and GP 5 (A) on analytical scale. ^{1}H NMR (600 MHz, DMSO-d_6) δ 8.08 (d, J = 7.8 Hz, 1H), 8.02 (d, J = 7.8 Hz, 1H), 7.92 (d, J = 8.2 Hz, 1H), 7.69 (bs, 3H), 7.37 – 7.11 (m, 11H), 7.07 (s, 1H), 4.48 (td, J = 8.5, 4.9 Hz, 1H), 4.42 (q, J = 7.2 Hz, 1H), 4.36 (ddd, J = 9.8, 7.7, 4.7 Hz, 1H), 4.16 (td, J = 8.4, 5.1 Hz, 1H), 3.06 (dd, J = 14.0, 4.9 Hz, 1H), 2.96 – 2.82 (m, 2H), 2.82 – 2.67 (m, 3H), 2.66 – 2.51 (m, 4H), 1.77 – 1.61 (m, 1H), 1.61 – 1.43 (m, 3H), 1.41 – 1.15 (m, 5H). 41H instead of total 40H are reported in the ^{1}H NMR, because the integration of the amine protons was not reliable (-NH_2, 3H instead of 2H). Signal allocation was performed using ^{1}H/^{1}H COSY, ^{1}H/^{1}H ROESY, ^{1}H/^{13}C HMBC and ^{1}H/^{15}N HSQC NMR. HRMS (TOF MS ESI) calcd for $C_{31}H_{41}N_6O_6^+$ [M+H]$^+$, 593.3082 (monoisotopic); found. 593.3082 (7a); calcd for $C_{62}H_{82}N_{12}O_{12}^{2+}$ [M+2H]$^{2+}$, 593.3082 (monoisotopic); found. 593.3082 (bi-7a). MALDI-TOF calcd for $C_{62}H_{81}N_{12}O_{12}^+$ [M+H]$^+$, 1185.609 (monoisotopic); found. 1186.799 (bi-7a). LC/MS ESI calcd for $C_{31}H_{41}N_6O_6^+$ [M+H]$^+$, 593.31; found. 593.25 (7a). RP-HPLC analysis with a linear gradient in 10 min, 5 % to 95 % MeCN (B) at 214 nm, column 3, T$_R$ = 4.1 min, purity > 95 %.

Compound 12a', peptide sequence cyclo-amide-Suc-Phe-Phe-Ala-Lys

Compound 12a' was obtained as lyophilized powder according to GP 1, GP 3 (B) and GP 5 (A) on analytical scale. HRMS (TOF MS ESI) calcd for $C_{31}H_{41}N_6O_6^+$ [M+H]$^+$, 593.3082 (monoisotopic); found. 593.3087. LC/MS ESI calcd for $C_{31}H_{41}N_6O_6^+$ [M+H]$^+$, 593.31; found. 593.35; (ByPr 594.2). RP-HPLC analysis with a linear gradient in 10 min, 5 % to 95 % MeCN (B) at 214 nm, column 3, T$_R$ = 5.4; 5.6 min, purity > 82 %.

---

[18]Mono- and bi-cyclic tetrapeptides 12a and bi-12a have been synthesized and characterized (NMR, RP-HPLC and MALDI-TOF) by Genesha Olgar (Heinrich-Heine-Universität Düsseldorf, group of Prof. Dr. Laura Hartmann, Bachelor Thesis, November 2015). In this thesis, the characterization data of the mentioned linear tetrapeptide and cyclic tetrapeptides have been re-assessed by the author of this thesis. Analysis and evaluation of the in this thesis presented 2D ^{1}H/^{1}H COSY NMR and 2D ^{1}H/^{15}N HSQC NMR spectra of the mentioned linear tetrapeptide and cyclic tetrapeptides has exclusively been performed by the author of this thesis and has not been presented previously.

6. References

[1]   H. Lis, N. Sharon, *Chem. Rev.* **1998**, *98*, 637-674.

[2]   K. Drickamer, M. E. Taylor, *Annual Review of Cell Biology* **1993**, *9*, 237-264.

[3]   A. Varki, *Glycobiology* **1993**, *3*, 97-130.

[4]   T. K. Lindhorst, *Host-Guest Chemistry* **2002**, *218*, 201-235.

[5]   B. T. Houseman, M. Mrksich, *Host-Guest Chemistry* **2002**, *218*, 1-44.

[6]   M. Ambrosi, N. R. Cameron, B. G. Davis, *Org. Biomol. Chem.* **2005**, *3*, 1593-1608.

[7]   R. D. Cummings, *Molecular Biosystems* **2009**, *5*, 1087-1104.

[8]   H. J. Gabius, H. C. Siebert, S. Andre, J. Jimenez-Barbero, H. Rudiger, *Chembiochem* **2004**, *5*, 740-764.

[9]   J. E. Hudak, C. R. Bertozzi, *Chem. Biol.* **2014**, *21*, 16-37.

[10]   X. Q. Zeng, C. A. S. Andrade, M. D. L. Oliveira, X. L. Sun, *Analytical and Bioanalytical Chemistry* **2012**, *402*, 3161-3176.

[11]   Y. C. Lee, R. T. Lee, *Accounts of Chemical Research* **1995**, *28*, 321-327.

[12]   L. L. Kiessling, N. L. Pohl, *Chem. Biol.* **1996**, *3*, 71-77.

[13]   R. Roy, *Curr. Opin. Struct. Biol.* **1996**, *6*, 692-702.

[14]   N. K. Sauter, M. D. Bednarski, B. A. Wurzburg, J. E. Hanson, G. M. Whitesides, J. J. Skehel, D. C. Wiley, *Biochemistry* **1989**, *28*, 8388-8396.

[15]   D. R. Davies, S. Sheriff, E. A. Padlan, *J. Biol. Chem.* **1988**, *263*, 10541-10544.

[16]   D. R. Davies, H. Metzger, *Annual Review of Immunology* **1983**, *1*, 87-117.

[17]   M. Mammen, S. K. Choi, G. M. Whitesides, *Angew. Chem.-Int. Edit.* **1998**, *37*, 2755-2794.

6. References

[18]   T. K. Dam, C. F. Brewer, *Biochemistry* **2008**, *47*, 8470-8476.

[19]   C. F. Brewer, M. C. Miceli, L. G. Baum, *Curr. Opin. Struct. Biol.* **2002**, *12*, 616-623.

[20]   K. H. Mortell, R. V. Weatherman, L. L. Kiessling, *J. Am. Chem. Soc.* **1996**, *118*, 2297-2298.

[21]   K. H. Mortell, M. Gingras, L. L. Kiessling, *J. Am. Chem. Soc.* **1994**, *116*, 12053-12054.

[22]   P. R. Crocker, T. Feizi, *Curr. Opin. Struct. Biol.* **1996**, *6*, 679-691.

[23]   R. Liang, L. Yan, J. Loebach, M. Ge, Y. Uozumi, K. Sekanina, N. Horan, J. Gildersleeve, C. Thompson, A. Smith, K. Biswas, W. C. Still, D. Kahne, *Science* **1996**, *274*, 1520-1522.

[24]   L. L. Kiessling, J. E. Gestwicki, L. E. Strong, *Current Opinion in Chemical Biology* **2000**, *4*, 696-703.

[25]   J. J. Lundquist, E. J. Toone, *Chem. Rev.* **2002**, *102*, 555-578.

[26]   C. Fasting, C. A. Schalley, M. Weber, O. Seitz, S. Hecht, B. Koksch, J. Dernedde, C. Graf, E. W. Knapp, R. Haag, *Angew. Chem.-Int. Edit.* **2012**, *51*, 10472-10498.

[27]   A. Spaltenstein, G. M. Whitesides, *J. Am. Chem. Soc.* **1991**, *113*, 686-687.

[28]   W. J. Lees, A. Spaltenstein, J. E. Kingerywood, G. M. Whitesides, *J. Med. Chem.* **1994**, *37*, 3419-3433.

[29]   T. J. Boltje, T. Buskas, G. J. Boons, *Nat. Chem.* **2009**, *1*, 611-622.

[30]   J. L. Zhu, J. D. Warren, S. J. Danishefsky, *Expert Review of Vaccines* **2009**, *8*, 1399-1413.

[31]   I. Papp, J. Dernedde, S. Enders, R. Haag, *Chem. Commun.* **2008**, 5851-5853.

[32]   C. R. Becer, *Macromol. Rapid Commun.* **2012**, *33*, 742-752.

[33]   J. E. Gestwicki, C. W. Cairo, L. E. Strong, K. A. Oetjen, L. L. Kiessling, *J. Am. Chem. Soc.* **2002**, *124*, 14922-14933.

[34]   T. K. Dam, R. Roy, S. K. Das, S. Oscarson, C. F. Brewer, *J. Biol. Chem.* **2000**, *275*, 14223-14230.

[35]   M. Reynolds, S. Perez, *Comptes Rendus Chimie* **2011**, *14*, 74-95.

[36]   D. Schwefel, C. Maierhofer, J. G. Beck, S. Seeberger, K. Diederichs, H. M. Moller, W. Welte, V. Wittmann, *J. Am. Chem. Soc.* **2010**, *132*, 8704-8719.

[37]   J. J. Lundquist, S. D. Debenham, E. J. Toone, *J. Org. Chem.* **2000**, *65*, 8245-8250.

[38]   J. B. Corbell, J. J. Lundquist, E. J. Toone, *Tetrahedron-Asymmetry* **2000**, *11*, 95-111.

[39]   D. A. Mann, M. Kanai, D. J. Maly, L. L. Kiessling, *J. Am. Chem. Soc.* **1998**, *120*, 10575-10582.

[40]   M. Kanai, K. H. Mortell, L. L. Kiessling, *J. Am. Chem. Soc.* **1997**, *119*, 9931-9932.

[41]   T. K. Lindhorst, M. Dubber, U. Krallmann-Wenzel, S. Ehlers, *European Journal of Organic Chemistry* **2000**, 2027-2034.

[42]   J. L. Jimenez Blanco, C. Ortiz Mellet, J. M. Garcia Fernandez, *Chem. Soc. Rev.* **2013**, *42*, 4518-4531.

[43]   E. K. Woller, E. D. Walter, J. R. Morgan, D. J. Singel, M. J. Cloninger, *J. Am. Chem. Soc.* **2003**, *125*, 8820-8826.

[44]   E. K. Woller, M. J. Cloninger, *Org. Lett.* **2002**, *4*, 7-10.

[45]   S. L. Mangold, M. J. Cloninger, *Org. Biomol. Chem.* **2006**, *4*, 2458-2465.

[46]   J. D. Reuter, A. Myc, M. M. Hayes, Z. H. Gan, R. Roy, D. J. Qin, R. Yin, L. T. Piehler, R. Esfand, D. A. Tomalia, J. R. Baker, *Bioconjugate Chem.* **1999**, *10*, 271-278.

[47]   D. Appelhans, B. Klajnert-Maculewicz, A. Janaszewska, J. Lazniewska, B. Voit, *Chem. Soc. Rev.* **2015**, *44*, 3968-3996.

[48]   N. Parera Pera, H. M. Branderhorst, R. Kooij, C. Maierhofer, M. van der Kaaden, R. M. J. Liskamp, V. Wittmann, R. Ruijtenbeek, R. J. Pieters, *Chembiochem : a European journal of chemical biology* **2010**, *11*, 1896-1904.

[49]   T. K. Dam, C. F. Brewer, *Chem. Rev.* **2002**, *102*, 387-429.

6. References

[50]   G. Ercolani, L. Schiaffino, *Angew. Chem.-Int. Edit.* **2011**, *50*, 1762-1768.

[51]   H. X. Zhou, M. K. Gilson, *Chem. Rev.* **2009**, *109*, 4092-4107.

[52]   R. S. Kane, *Langmuir* **2010**, *26*, 8636-8640.

[53]   T. K. Dam, R. Roy, D. Page, C. F. Brewer, *Biochemistry* **2002**, *41*, 1351-1358.

[54]   M. Gomez-Garcia, J. M. Benito, R. Gutierrez-Gallego, A. Maestre, C. Ortiz Mellet, J. M. Garcia Fernandez, J. L. Jimenez Blanco, *Org. Biomol. Chem.* **2010**, *8*, 1849-1860.

[55]   C. R. Becer, M. I. Gibson, J. Geng, R. Ilyas, R. Wallis, D. A. Mitchell, D. M. Haddleton, *J. Am. Chem. Soc.* **2010**, *132*, 15130-15132.

[56]   C. W. Cairo, J. E. Gestwicki, M. Kanai, L. L. Kiessling, *J. Am. Chem. Soc.* **2002**, *124*, 1615-1619.

[57]   X.-L. Meng, Y. Fang, L.-S. Wan, X.-J. Huang, Z.-K. Xu, *Langmuir* **2012**, *28*, 13616-13623.

[58]   H. Park, R. R. Rosencrantz, L. Elling, A. Boeker, *Macromol. Rapid Commun.* **2015**, *36*, 45-54.

[59]   V. Ladmiral, E. Melia, D. M. Haddleton, *Eur. Polym. J.* **2004**, *40*, 431-449.

[60]   N. Horan, L. Yan, H. Isobe, G. M. Whitesides, D. Kahne, *Proceedings of the National Academy of Sciences of the United States of America* **1999**, *96*, 11782-11786.

[61]   G. Maheshwari, G. Brown, D. A. Lauffenburger, A. Wells, L. G. Griffith, *Journal of Cell Science* **2000**, *113*, 1677-1686.

[62]   M. J. Krantz, N. A. Holtzman, C. P. Stowell, Y. C. Lee, *Biochemistry* **1976**, *15*, 3963-3968.

[63]   J. R. Allen, C. R. Harris, S. J. Danishefsky, *J. Am. Chem. Soc.* **2001**, *123*, 1890-1897.

[64]   S. Cecioni, J. P. Praly, S. E. Matthews, M. Wimmerova, A. Imberty, S. Vidal, *Chem.-Eur. J.* **2012**, *18*, 6250-6263.

[65]   J. E. Gestwicki, L. L. Kiessling, *Nature* **2002**, *415*, 81-84.

[66]   J. R. Cochran, L. J. Stern, *Chem. Biol.* **2000**, *7*, 683-696.

[67]   R. Roy, D. Page, S. F. Perez, V. V. Bencomo, *Glycoconjugate Journal* **1998**, *15*, 251-263.

[68]   R. E. Bruehl, F. Dasgupta, T. R. Katsumoto, J. H. Tan, C. R. Bertozzi, W. Spevak, D. J. Ahn, S. D. Rosen, J. O. Nagy, *Biochemistry* **2001**, *40*, 5964-5974.

[69]   V. Kudryashov, P. W. Glunz, L. J. Williams, S. Hintermann, S. J. Danishefsky, K. O. Lloyd, *Proceedings of the National Academy of Sciences of the United States of America* **2001**, *98*, 3264-3269.

[70]   J. A. Reddy, D. Dean, M. D. Kennedy, P. S. Low, *Journal of Pharmaceutical Sciences* **1999**, *88*, 1112-1118.

[71]   R. R. Rosencrantz, V. H. Nguyen, H. Park, C. Schulte, A. Boker, U. Schnakenberg, L. Elling, *Analytical and Bioanalytical Chemistry* **2016**, *408*, 5633-5640.

[72]   R. S. Loka, M. S. McConnell, H. M. Nguyen, *Biomacromolecules* **2015**, *16*, 4013-4021.

[73]   E. K. Fan, Z. S. Zhang, W. E. Minke, Z. Hou, C. Verlinde, W. G. J. Hol, *J. Am. Chem. Soc.* **2000**, *122*, 2663-2664.

[74]   M. Toyoshima, T. Oura, T. Fukuda, E. Matsumoto, Y. Miura, *Polymer Journal* **2010**, *42*, 172-178.

[75]   Y. Chen, M. S. Lord, A. Piloni, M. H. Stenzel, *Macromolecules* **2015**, *48*, 346-357.

[76]   C. Diehl, H. Schlaad, *Polimery* **2013**, *58*, 650-653.

[77]   M. N. Matrosovich, L. V. Mochalova, V. P. Marinina, N. E. Byramova, N. V. Bovin, *Febs Letters* **1990**, *272*, 209-212.

[78]   C. Maierhofer, K. Rohmer, V. Wittmann, *Bioorg. Med. Chem.* **2007**, *15*, 7661-7676.

[79]   V. Wittmann, S. Seeberger, *Angew. Chem.-Int. Edit.* **2000**, *39*, 4348-4352.

[80]   V. Wittmann, *Current Opinion in Chemical Biology* **2013**, *17*, 982-989.

[81]   R. T. Lee, Y. C. Lee, *Bioconjugate Chem.* **1997**, *8*, 762-765.

[82]   Y. C. Lee, R. T. Lee, K. Rice, Y. Ichikawa, T. C. Wong, *Pure and Applied Chemistry* **1991**, *63*, 499-506.

[83]   J. M. Lord, D. C. Smith, L. M. Roberts, *Cellular Microbiology* **1999**, *1*, 85-91.

[84]   P. I. Kitov, J. M. Sadowska, G. Mulvey, G. D. Armstrong, H. Ling, N. S. Pannu, R. J. Read, D. R. Bundle, *Nature* **2000**, *403*, 669-672.

[85]   S. Andre, P. J. C. Ortega, M. A. Perez, R. Roy, H. J. Gabius, *Glycobiology* **1999**, *9*, 1253-1261.

[86]   S. K. Choi, M. Mammen, G. M. Whitesides, *Chem. Biol.* **1996**, *3*, 97-104.

[87]   M. Mammen, G. Dahmann, G. M. Whitesides, *J. Med. Chem.* **1995**, *38*, 4179-4190.

[88]   G. B. Sigal, M. Mammen, G. Dahmann, G. M. Whitesides, *J. Am. Chem. Soc.* **1996**, *118*, 3789-3800.

[89]   M. Mammen, K. Helmerson, R. Kishore, S. K. Choi, W. D. Phillips, G. M. Whitesides, *Chem. Biol.* **1996**, *3*, 757-763.

[90]   G. Yilmaz, C. R. Becer, *Eur. Polym. J.* **2013**, *49*, 3046-3051.

[91]   S. Slavin, J. Burns, D. M. Haddleton, C. R. Becer, *Eur. Polym. J.* **2011**, *47*, 435-446.

[92]   J. Dernedde, I. Papp, S. Enders, S. Wedepohl, F. Paulus, R. Haag, *J. Carbohydr. Chem.* **2011**, *30*, 347-360.

[93]   M. Ambrosi, N. R. Cameron, B. G. Davis, S. Stolnik, *Org. Biomol. Chem.* **2005**, *3*, 1476-1480.

[94]   L. Hartmann, *Macromol. Chem. Phys.* **2011**, *212*, 8-13.

[95]   L. Hartmann, H. G. Borner, *Adv. Mater.* **2009**, *21*, 3425-3431.

[96]   S. Mosca, F. Wojcik, L. Hartmann, *Macromol. Rapid Commun.* **2011**, *32*, 197-202.

[97]   L. Hartmann, S. Haefele, R. Peschka-Suess, M. Antonietti, H. G. Borner, *Chem.-Eur. J.* **2008**, *14*, 2025-2033.

[98]   L. Hartmann, E. Krause, M. Antonietti, H. G. Borner, *Biomacromolecules* **2006**, *7*, 1239-1244.

[99]   F. Wojcik, S. Mosca, L. Hartmann, *J. Org. Chem.* **2012**, *77*, 4226-4234.

[100]   D. Ponader, S. Igde, M. Wehle, K. Marker, M. Santer, D. Bleger, L. Hartmann, *Beilstein J. Org. Chem.* **2014**, *10*, 1603-1612.

[101]   F. Wojcik, S. Lel, A. G. O'Brien, P. H. Seeberger, L. Hartmann, *Beilstein J. Org. Chem.* **2013**, *9*, 2395-2403.

[102]   F. Wojcik, A. G. O'Brien, S. Gotze, P. H. Seeberger, L. Hartmann, *Chem.-Eur. J.* **2013**, *19*, 3090-3098.

[103]   D. Ponader, P. Maffre, J. Aretz, D. Pussak, N. M. Ninnemann, S. Schmidt, P. H. Seeberger, C. Rademacher, G. U. Nienhaus, L. Hartmann, *J. Am. Chem. Soc.* **2014**, *136*, 2008-2016.

[104]   D. Ponader, D. Pussak, M. Glanz, S. Schmidt, F. Wojcik, L. Hartmann, *Abstr. Pap. Am. Chem. Soc.* **2013**, *245*, 1.

[105]   D. Ponader, F. Wojcik, F. Beceren-Braun, J. Dernedde, L. Hartmann, *Biomacromolecules* **2012**, *13*, 1845-1852.

[106]   T. K. Dam, T. A. Gerken, C. F. Brewer, *Biochemistry* **2009**, *48*, 3822-3827.

[107]   C. A. Hunter, S. Tomas, *Chem. Biol.* **2003**, *10*, 1023-1032.

[108]   C. A. Hunter, H. L. Anderson, *Angew. Chem.-Int. Edit.* **2009**, *48*, 7488-7499.

[109]   E. J. Toone, *Curr. Opin. Struct. Biol.* **1994**, *4*, 719-728.

[110]   M. Weber, A. Bujotzek, R. Haag, *Journal of Chemical Physics* **2012**, *137*, 054111.

[111]   E. T. Mack, P. W. Snyder, R. Perez-Castillejos, G. M. Whitesides, *J. Am. Chem. Soc.* **2011**, *133*, 11701-11715.

[112]   J. S. Graham, R. C. Johnson, J. F. Marko, *Nucleic Acids Research* **2011**, *39*, 2249-2259.

[113]   C. E. Sing, M. O. de la Cruz, J. F. Marko, *Nucleic Acids Research* **2014**, *42*, 3783-3791.

[114]   T. K. Dam, R. Roy, D. Page, C. F. Brewer, *Biochemistry* **2002**, *41*, 1359-1363.

[115]   W. B. Turnbull, B. L. Precious, S. W. Homans, *J. Am. Chem. Soc.* **2004**, *126*, 1047-1054.

[116]   B. A. Williams, M. C. Chervenak, E. J. Toone, *J. Biol. Chem.* **1992**, *267*, 22907-22911.

[117]   G. Vauquelin, S. J. Charlton, *British Journal of Pharmacology* **2013**, *168*, 1771-1785.

[118]   P. Braun, B. Nagele, V. Wittmann, M. Drescher, *Angew. Chem.-Int. Edit.* **2011**, *50*, 8428-8431.

[119]   J. H. Rao, L. Yan, J. Lahiri, G. M. Whitesides, R. M. Weis, H. S. Warren, *Chem. Biol.* **1999**, *6*, 353-359.

[120]   J. H. Rao, J. Lahiri, L. Isaacs, R. M. Weis, G. M. Whitesides, *Science* **1998**, *280*, 708-711.

[121]   A. Cooper, *Current Opinion in Chemical Biology* **1999**, *3*, 557-563.

[122]   J. Huskens, A. Mulder, T. Auletta, C. A. Nijhuis, M. J. W. Ludden, D. N. Reinhoudt, *J. Am. Chem. Soc.* **2004**, *126*, 6784-6797.

[123]   M. K. Gilson, J. A. Given, B. L. Bush, J. A. McCammon, *Biophys. J.* **1997**, *72*, 1047-1069.

[124]   T. W. Mak, M. E. Saunders, in *The Immune Response: Basic and Clinical Principles*, 1 ed., Academic Press, Burlington, **2006**, pp. 147-177.

[125]   R. H. Kramer, J. W. Karpen, *Nature* **1998**, *395*, 710-713.

[126]   L. L. Kiessling, J. C. Grim, *Chem. Soc. Rev.* **2013**, *42*, 4476-4491.

[127]   F. Wojcik, D. Ponader, S. Mosca, L. Hartmann, in *Sequence-Controlled Polymers: Synthesis, Self-Assembly, and Properties, Vol. 1170*, American Chemical Society, **2014**, pp. 85-101.

[128]   J. F. Lutz, M. Ouchi, D. R. Liu, M. Sawamoto, *Science* **2013**, *341*, 1238149.

[129]   M. W. Freyer, E. A. Lewis, in *Biophysical Tools for Biologists: Vol 1 in Vitro Techniques, Vol. 84* (Eds.: J. J. Correia, H. W. Detrich), **2008**, pp. 79-113.

[130]   J. D. Chodera, D. L. Mobley, *Annual Review of Biophysics, Vol 42* **2013**, *42*, 121-142.

[131]   R. V. Weatherman, K. I. Mortell, M. Chervenak, L. L. Kiessling, E. J. Toone, *Biochemistry* **1996**, *35*, 3619-3624.

[132]   M. C. Chervenak, E. J. Toone, *Biochemistry* **1995**, *34*, 5685-5695.

[133]   M. C. Chervenak, E. J. Toone, *J. Am. Chem. Soc.* **1994**, *116*, 10533-10539.

[134]   M. C. Chervenak, E. J. Toone, *Biochemistry* **1995**, *34*, 7966-7966.

[135]   J. Tellinghuisen, J. D. Chodera, *Anal. Biochem.* **2011**, *414*, 297-299.

[136]   J. D. Dunitz, *Chem. Biol.* **1995**, *2*, 709-712.

[137]   D. M. Ford, *J. Am. Chem. Soc.* **2005**, *127*, 16167-16170.

[138]   A. Cornish-Bowden, *Journal of Biosciences* **2002**, *27*, 121-126.

[139]   U. Ryde, *MedChemComm* **2014**, *5*, 1324-1336.

[140]   R. B. Merrifield, *J. Am. Chem. Soc.* **1963**, *85*, 2149-2154.

[141]   I. Coin, M. Beyermann, M. Bienert, *Nature Protocols* **2007**, *2*, 3247-3256.

[142]   P. Grieco, P. M. Gitu, V. J. Hruby, *J. Pept. Res.* **2001**, *57*, 250-256.

[143]   J. Chatterjee, B. Laufer, H. Kessler, *Nature Protocols* **2012**, *7*, 432-444.

[144]   Y. C. Tang, H. B. Xie, G. L. Tian, Y. H. Ye, *J. Pept. Res.* **2002**, *60*, 95-103.

[145]   X. Elduque, E. Pedroso, A. Grandas, *Org. Lett.* **2013**, *15*, 2038-2041.

[146]   C. Rosenbaum, H. Waldmann, *Tetrahedron Lett.* **2001**, *42*, 5677-5680.

[147]   M. C. Alcaro, G. Sabatino, J. Uziel, M. Chelli, M. Ginanneschi, P. Rovero, A. M. Papini, *J. Pept. Sci.* **2004**, *10*, 218-228.

[148]   C. J. White, A. K. Yudin, *Nat. Chem.* **2011**, *3*, 509-524.

[149]   S. J. Danishefsky, K. F. McClure, J. T. Randolph, R. B. Ruggeri, *Science* **1993**, *260*, 1307-1309.

[150]   R. Verduyn, P. A. M. Vanderklein, M. Douwes, G. A. Vandermarel, J. H. Vanboom, *Recl. Trav. Chim. Pays-Bas-J. Roy. Neth. Chem. Soc.* **1993**, *112*, 464-466.

[151]   M. Schuster, P. Wang, J. C. Paulson, C. H. Wong, *J. Am. Chem. Soc.* **1994**, *116*, 1135-1136.

[152]   S. L. Beaucage, R. P. Iyer, *Tetrahedron* **1992**, *48*, 2223-2311.

[153]   W. Bannwarth, *Helvetica Chimica Acta* **1988**, *71*, 1517-1527.

[154]   O. J. Plante, E. R. Palmacci, P. H. Seeberger, *Science* **2001**, *291*, 1523-1527.

[155]   P. H. Seeberger, *Chem. Soc. Rev.* **2008**, *37*, 19-28.

[156]   H. Paulsen, T. Bielfeldt, S. Peters, M. Meldal, K. Bock, *Liebigs Annalen Der Chemie* **1994**, 369-379.

[157]   A. S. Culf, R. J. Ouellette, *Molecules* **2010**, *15*, 5282-5335.

[158]   J. S. Fruchtel, G. Jung, *Angew. Chem.-Int. Edit.* **1996**, *35*, 17-42.

[159]   L. Raibaut, N. Ollivier, O. Melnyk, *Chem. Soc. Rev.* **2012**, *41*, 7001-7015.

[160]   Y. C. Lee, in *Neoglycoconjugates: Preparation and Applications* (Eds.: Y. C. Lee, R. T. Lee), Academic Press, London, **1994**, p. 3.

[161]   D. Schaffert, N. Badgujar, E. Wagner, *Org. Lett.* **2011**, *13*, 1586-1589.

[162]   D. Altschuh, H. Bjorkelund, J. Strandgard, L. Choulier, M. Malmqvist, K. Andersson, *Biochemical and Biophysical Research Communications* **2012**, *428*, 74-79.

[163]   D. Burnouf, E. Ennifar, S. Guedich, B. Puffer, G. Hoffmann, G. Bec, F. Disdier, M. Baltzinger, P. Dumas, *J. Am. Chem. Soc.* **2012**, *134*, 559-565.

[164]   K. A. Vander Meulen, S. E. Butcher, *Nucleic acids research* **2012**, *40*, 2140-2151.

[165]   T. Egawa, A. Tsuneshige, M. Suematsu, T. Yonetani, *Analytical Chemistry* **2007**, *79*, 2972-2978.

[166]   E. Valeur, M. Bradley, *Chem. Soc. Rev.* **2009**, *38*, 606-631.

[167]   J. Fastrez, *Journal of Physical Chemistry* **1989**, *93*, 2635-2642.

[168]   J. A. Kaitz, C. E. Diesendruck, J. S. Moore, *Macromolecules* **2014**, *47*, 3603-3607.

[169]   M. Schulz, S. Tanner, H. Barqawi, W. H. Binder, *Journal of Polymer Science Part a-Polymer Chemistry* **2010**, *48*, 671-680.

[170]   Z. E. Perlman, J. E. Bock, J. R. Peterson, R. S. Lokey, *Bioorg. Med. Chem. Lett.* **2005**, *15*, 5329-5334.

[171]   A. Thakkar, T. B. Trinh, D. H. Pei, *ACS Comb. Sci.* **2013**, *15*, 120-129.

[172]   J. S. McMurray, C. A. Lewis, N. U. Obeyesekere, *Peptide Res.* **1994**, *7*, 195-206.

[173]   S. Mazur, P. Jayalekshmy, *J. Am. Chem. Soc.* **1979**, *101*, 677-683.

[174]   L. T. Scott, J. Rebek, L. Ovsyanko, C. L. Sims, *J. Am. Chem. Soc.* **1977**, *99*, 625-626.

[175]   A. A. Aimetti, R. K. Shoemaker, C. C. Lin, K. S. Anseth, *Chem. Commun.* **2010**, *46*, 4061-4063.

[176]   T. M. Postma, F. Albericio, *Org. Lett.* **2014**, *16*, 1772-1775.

[177]   A. Ganesan, *Methods Enzymol.* **2003**, *369*, 415-434.

[178]   B. H. Lee, F. E. Dutton, D. P. Thompson, E. M. Thomas, *Bioorg. Med. Chem. Lett.* **2002**, *12*, 353-356.

[179]   C. Neagoie, V. Krchnak, *ACS Comb. Sci.* **2012**, *14*, 399-402.

[180]   L. H. Jensen, A. Renodon-Corniere, I. Wessel, S. W. Langer, B. Sokilde, E. V. Carstensen, M. Sehested, P. B. Jensen, *Mol. Pharmacol.* **2002**, *61*, 1235-1243.

[181] B. Q. Shen, K. Y. Xu, L. N. Liu, H. Raab, S. Bhakta, M. Kenrick, K. L. Parsons-Reponte, J. Tien, S. F. Yu, E. Mai, D. W. Li, J. Tibbitts, J. Baudys, O. M. Saadi, S. J. Scales, P. J. McDonald, P. E. Hass, C. Eigenbrot, T. Nguyen, W. A. Solis, R. N. Fuji, K. M. Flagella, D. Patel, S. D. Spencer, L. A. Khawlil, A. Ebens, W. L. Wong, R. Vandlen, S. Kaur, M. X. Sliwkowski, R. H. Scheller, P. Polakis, J. R. Junutula, *Nat. Biotechnol.* **2012**, *30*, 184-189.

[182] D. Pussak, D. Ponader, S. Mosca, S. V. Ruiz, L. Hartmann, S. Schmidt, *Angew. Chem.-Int. Edit.* **2013**, *52*, 6084-6087.

[183] A. V. Mayorov, M. Y. Cai, E. S. Palmer, Z. H. Liu, J. P. Cain, J. Vagner, D. Trivedi, V. J. Hruby, *Peptides* **2010**, *31*, 1894-1905.

[184] A. Isidro-Llobet, M. Alvarez, F. Albericio, *Chem. Rev.* **2009**, *109*, 2455-2504.

[185] C. M. Stevens, R. Watanabe, *J. Am. Chem. Soc.* **1950**, *72*, 725-727.

[186] J. Tsuji, *Tetrahedron* **1986**, *42*, 4361-4401.

[187] B. M. Trost, D. L. VanVranken, *Chem. Rev.* **1996**, *96*, 395-422.

[188] F. Guibe, *Tetrahedron* **1997**, *53*, 13509-13556.

[189] F. Guibe, *Tetrahedron* **1998**, *54*, 2967-3042.

[190] H. Kunz, C. Unverzagt, *Angew. Chem.-Int. Edit.* **1984**, *23*, 436-437.

[191] N. Thieriet, P. Gomez-Martinez, F. Guibe, *Tetrahedron Lett.* **1999**, *40*, 2505-2508.

[192] P. Gomez-Martinez, M. Dessolin, F. Guibe, F. Albericio, *Journal of the Chemical Society-Perkin Transactions 1* **1999**, 2871-2874.

[193] R. Deziel, *Tetrahedron Lett.* **1987**, *28*, 4371-4372.

[194] M. Honda, H. Morita, I. Nagakura, *J. Org. Chem.* **1997**, *62*, 8932-8936.

[195] N. Thieriet, J. Alsina, E. Giralt, F. Guibe, F. Albericio, *Tetrahedron Lett.* **1997**, *38*, 7275-7278.

6. References

[196]   E. C. Roos, P. Bernabe, H. Hiemstra, W. N. Speckamp, B. Kaptein, W. H. J. Boesten, *J. Org. Chem.* **1995**, *60*, 1733-1740.

[197]   H. Kunz, H. Waldmann, *Angew. Chem.-Int. Edit.* **1984**, *23*, 71-72.

[198]   H. Kunz, J. Marz, *Angew. Chem.-Int. Edit.* **1988**, *27*, 1375-1377.

[199]   J. P. Genet, E. Blart, M. Savignac, S. Lemeune, S. Lemaireaudoire, J. M. Bernard, *Synlett* **1993**, 680-682.

[200]   V. Lejeune, J. Martinez, F. Cavelier, *Tetrahedron Lett.* **2003**, *44*, 4757-4759.

[201]   H. S. Trivedi, M. Anson, P. G. Steel, J. Worley, *Synlett* **2001**, 1932-1934.

[202]   N. S. Freeman, C. Gilon, *Synlett* **2009**, 2097-2100.

[203]   E. Kaiser, J. P. Tam, T. M. Kubiak, R. B. Merrifield, *Tetrahedron Lett.* **1988**, *29*, 303-306.

[204]   K. M. Sivanandaiah, V. V. Sureshbabu, S. C. Shankaramma, *Int. J. Pept. Protein Res.* **1995**, *45*, 377-379.

[205]   K. M. Sivanandaiah, V. V. S. Babu, B. P. Gangadhar, *Tetrahedron Lett.* **1996**, *37*, 5989-5990.

[206]   K. D. James, A. D. Ellington, *Tetrahedron Lett.* **1998**, *39*, 175-178.

[207]   J. M. Stewart, D. W. Woolley, *Nature* **1965**, *206*, 619-620.

[208]   R. A. Houghten, M. K. Bray, S. T. Degraw, C. J. Kirby, *Int. J. Pept. Protein Res.* **1986**, *27*, 673-678.

[209]   E. Kaiser, F. Picart, T. Kubiak, J. P. Tam, R. B. Merrifield, *J. Org. Chem.* **1993**, *58*, 5167-5175.

[210]   C. Ressler, H. Ratzkin, *J. Org. Chem.* **1961**, *26*, 3356-3360.

[211]   D. V. Kashelikar, C. Ressler, *J. Am. Chem. Soc.* **1964**, *86*, 2467-2473.

[212]   H. Gausepohl, M. Kraft, R. W. Frank, *Int. J. Pept. Protein Res.* **1989**, *34*, 287-294.

6. References

[213]   F. Albericio, R. Chinchilla, D. J. Dodsworth, C. Najera, *Organic Preparations and Procedures International* **2001**, *33*, 205-303.

[214]   S. Y. Han, Y. A. Kim, *Tetrahedron* **2004**, *60*, 2447-2467.

[215]   L. T. L. Wong, Ph.D. thesis, McGill University **March 1971**.

[216]   A. J. Zhang, D. H. Russell, J. P. Zhu, K. Burgess, *Tetrahedron Lett.* **1998**, *39*, 7439-7442.

[217]   W. Wu, Z. Zhang, L. S. Liebeskind, *J. Am. Chem. Soc.* **2011**, *133*, 14256-14259.

[218]   P. Stathopoulos, S. Papas, V. Tsikaris, *J. Pept. Sci.* **2006**, *12*, 227-232.

[219]   V. Krchnak, Z. Flegelova, J. Vagner, *Int. J. Pept. Protein Res.* **1993**, *42*, 450-454.

[220]   J. P. Tam, M. W. Riemen, R. B. Merrifield, *Peptide Res.* **1988**, *1*, 6-18.

[221]   E. Nicolas, E. Pedroso, E. Giralt, *Tetrahedron Lett.* **1989**, *30*, 497-500.

[222]   S. Kostidis, P. Stathopoulos, N. I. Chondrogiannis, C. Sakarellos, V. Tsikaris, *Tetrahedron Lett.* **2003**, *44*, 8673-8676.

[223]   R. A. Bryce, I. H. Hillier, J. H. Naismith, *Biophys. J.* **2001**, *81*, 1373-1388.

[224]   T. Wiseman, S. Williston, J. F. Brandts, L. N. Lin, *Anal. Biochem.* **1989**, *179*, 131-137.

[225]   D. K. Mandal, L. Bhattacharyya, S. H. Koenig, R. D. Brown, S. Oscarson, C. F. Brewer, *Biochemistry* **1994**, *33*, 1157-1162.

[226]   W. B. Turnbull, in *GE Healthcare Life Sciences protocol.* (Ed.: G. H. L. S. protocol.), School of Chemistry and Astbury Centre for Structural Molecular Biology, University of Leeds, Leeds LS2 9JT UK, **2005**, pp. 1-11.

[227]   L. Wadso, X. Li, *Journal of Chemical Education* **2008**, *85*, 112-116.

[228]   K. Yu, A. L. Creagh, C. A. Haynes, J. N. Kizhakkedathu, *Analytical Chemistry* **2013**, *85*, 7786-7793.

[229]   M. Hartmann, T. K. Lindhorst, *European Journal of Organic Chemistry* **2011**, 3583-3609.

[230]   Fessele C., T. K. Lindhorst, *Biology* **2013**, *2*, 1135-1149.

[231]   R. D. Poretz, I. J. Goldstein, *Biochemical Pharmacology* **1971**, *20*, 2727-2739.

[232]   W. Kauzmann, *Advances in Protein Chemistry* **1959**, *14*, 1-63.

[233]   K. P. Murphy, D. Xie, K. C. Garcia, L. M. Amzel, E. Freire, *Proteins-Structure Function and Genetics* **1993**, *15*, 113-120.

[234]   A. Parsaeian, M. O. de la Cruz, J. F. Marko, *Physical Review E* **2013**, *88*, 040703.

[235]   A. C. Pan, D. W. Borhani, R. O. Dror, D. E. Shaw, *Drug Discovery Today* **2013**, *18*, 667-673.

[236]   K. J. Laidler, M. C. King, *Journal of Physical Chemistry* **1983**, *87*, 2657-2664.

[237]   G. Lente, I. Fabian, A. J. Poe, *New Journal of Chemistry* **2005**, *29*, 759-760.

[238]   P. M. Morse, M. D. Spencer, S. R. Wilson, G. S. Girolami, *Organometallics* **1994**, *13*, 1646-1655.

[239]   D. H. Williams, E. Stephens, D. P. O'Brien, M. Zhou, *Angew. Chem.-Int. Edit.* **2004**, *43*, 6596-6616.

[240]   T. Yamamoto, Y. Tezuka, *Soft Matter* **2015**, *11*, 7458-7468.

[241]   D. Richter, S. Goossen, A. Wischnewski, *Soft Matter* **2015**, *11*, 8535-8549.

[242]   H. R. Kricheldorf, *Journal of Polymer Science Part a-Polymer Chemistry* **2010**, *48*, 251-284.

[243]   Z. F. Jia, M. J. Monteiro, *Journal of Polymer Science Part a-Polymer Chemistry* **2012**, *50*, 2085-2097.

[244]   C. D. Roland, H. Li, K. A. Abboud, K. B. Wagener, A. S. Veige, *Nat. Chem.* **2016**, *8*, 791-796.

[245]   K. W. Hsiao, C. M. Schroeder, C. E. Sing, *Macromolecules* **2016**, *49*, 1961-1971.

[246]   T. McLeish, *Science* **2002**, *297*, 2005-2006.

[247]   S. P. Obukhov, M. Rubinstein, T. Duke, *Physical Review Letters* **1994**, *73*, 1263-1266.

[248]   M. E. Cates, J. M. Deutsch, *Journal De Physique* **1986**, *47*, 2121-2128.

[249]   J. M. Sturtevant, *Proceedings of the National Academy of Sciences of the United States of America* **1977**, *74*, 2236-2240.

[250]   P. Deuflhard, *Newton Methods for Nonlinear Problems: Affine Invariance and Adaptive Algorithms*, Springer Berlin Heidelberg, **2005**.

[251]   A. Hohmann, P. Deuflhard, *Numerical Analysis in Modern Scientific Computing: An Introduction*, Springer New York, **2003**.

[252]   P. Deuflhard, W. Sautter, *Linear Algebra and Its Applications* **1980**, *29*, 91-111.

[253]   P. Deuflhard, S. Röblitz, *A Guide to Numerical Modelling in Systems Biology, Vol. 12*, 1 ed., Springer International Publishing, Switzerland, **2015**.

7. Supporting Appendix

7.1. Numerical determination of binding kinetics

This MATLAB script and the procedure how to apply the least-squares fitting procedure was written by Dr. Susanna Röblitz and Dr. Marcus Weber. It is included in this thesis in order to understand, how the kinetic constants were determined and is essential for the kinetic method that was used in this thesis. The use of this method is based on procedures that are described in this Supporting Appendix subchapter.

We consider the general, possibly multivalent, reaction scheme:

$$s_L \cdot L + s_P \cdot P \xrightleftharpoons[k_{off}]{k_{on}} s_{LP} \cdot LP \tag{A1}$$
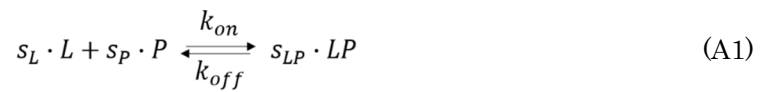
where s_L, s_P, s_{LP} denote the stoichiometric coefficients. The change of concentrations over time is described by the following system of ordinary differential equations (ODEs):

$$c_L'(t) = -k_{on} \cdot s_L \cdot c_L^{s_L} \cdot c_P^{s_P} + k_{off} \cdot s_L \cdot c_{LP}^{s_{LP}}, \quad c_L(0) = c_{L,0},$$

$$c_P'(t) = -k_{on} \cdot s_P \cdot c_L^{s_L} \cdot c_P^{s_P} + k_{off} \cdot s_P \cdot c_{LP}^{s_{LP}}, \quad c_P(0) = c_{P,0}, \tag{A2}$$

$$c_{LP}'(t) = +k_{on} \cdot s_{LP} \cdot c_L^{s_L} \cdot c_P^{s_P} - k_{off} \cdot s_{LP} \cdot c_{LP}^{s_{LP}}, \quad c_{LP}(0) = c_{LP,0},$$

where c_L, c_P, c_{LP} denote the time-dependent concentrations with initial values $c_{L,0}$, $c_{P,0}$, $c_{LP,0}$, and c' is the corresponding time derivative. Given the time-dependent concentration $c_{LP}(t)$, the amount of heat produced, e.g. the thermal power $P(t)$, is given by:

$$P(t) = -\Delta H V_0 c_{LP}'(t) = -\Delta H V_0 \cdot \left(k_{on} \cdot s_{LP} \cdot c_L^{s_L}(t) \cdot c_P^{s_P}(t) - k_{off} \cdot s_{LP} \cdot c_{LP}^{s_{LP}}(t) \right). \tag{A3}$$

In this model scheme, k_{on} and $\Delta H V_0$ are unknown model parameters, whereas the stoichiometric coefficients and the initial concentrations are given. The value for k_{off} is computed as:

$$k_{off} = K_d \cdot k_{on}, \tag{A4}$$

whereby an estimate for K_d is provided by the ITC kinetic analysis tool. The task now is to estimate the parameters k_{on} and $\Delta H V_0$ in such a way, that the simulated amount of heat $P(t)$ agrees with the measured values.

For this purpose, we briefly describe the mathematical techniques that we use for parameter estimation. Since in the experiments multiple injections are applied, we considered here the case of multiple experiments by using the index $i = 1, \dots, \text{nexp}$ for the injection number.

In mathematical short-hand notation, the system of differential equations (A2) can be formally written as:

$$\begin{cases} (y^i)'(t, \mathbf{p}^i) = f(t, y^i, \mathbf{p}^i), & t \geq 0 \\ y^i(0, \mathbf{p}^i) = y_0^i, \end{cases} \tag{A5}$$

where $\mathbf{p}^i$ is the vector of parameters in experiment i, and the right-hand side f depends on both the states, $y^i \in \mathbb{R}^n$, and the parameter vector, $\mathbf{p}^i \in \mathbb{R}^q$. The initial condition vector y_0^i has the same dimension as the state vector y^i. The model (A2) can be written in the form of equation (A6), where:

$$y^i(t, \mathbf{p}^i) = \left(c_L^i(t, \mathbf{p}^i), c_P^i(t, \mathbf{p}^i), c_{LP}^i(t, \mathbf{p}^i) \right) \in \mathbb{R}^3 \tag{A6}$$

and

$$\mathbf{p}^i = \left(k_{on}^i, \Delta HV_0^i \right) \in \mathbb{R}^2. \tag{A7}$$

Assume in each experiment i there are given m experimental measurement time-points $\tau_1, \dots, \tau_m$, and corresponding data values $z_j^i \in \mathbb{R}^n$, $j = 1, \dots, m$, associated with corresponding measurement tolerances $\delta z_j^i \in \mathbb{R}^n$. In our case, we have $m = 40$. For ease of presentation, these tolerances are assumed to be positive, but the algorithm to be described is also able to tackle strictly zero tolerances (indicating equality constraints); details are omitted here, but can be found, e.g. in the book[250]. For each new injection, the time is reset to $t = 0$ such that the measurement time points are the same for each experiment, e.g. independent of i.

Parameter identification consists of solving the least-squares minimization problem:

$$g(\mathbf{p}) = \frac{1}{m \cdot \text{nexp}} \sum_{i=1}^{\text{nexp}} \sum_{j=1}^{m} \left\| \left(D_j^i \right)^{-1} \cdot \left(y^i(\tau_j, \mathbf{p}^i) - z_j^i \right) \right\|_2^2 \to \min_{\mathbf{p}} \tag{A8}$$

with diagonal weighting

$$D_j^i := diag \left(\left(\delta z_j^i \right)_1, \dots, \left(\delta z_j^i \right)_n \right) \in \mathbb{R}^{n \times n} \quad j = 1, \dots, m \quad i = 1, \dots, \text{nexp}. \tag{A9}$$

That means we want to minimize the relative deviation of model and data at the measurement time points τ_j. Here, the component to be optimized is the vector:

$$\mathbf{p} = (\mathbf{p}^1, \dots, \mathbf{p}^{\text{nexp}}) \in \mathbb{R}^{q \cdot \text{nexp}}, \tag{A10}$$

which is the overall vector of unknown parameter values formed by concatenating all experiment specific parameter vectors $\mathbf{p}^i$. In our numerical computations, we assumed the measurement error

to be equal throughout all injections and all measurement time points. Hence, the matrices D_j^i can be factored out in (A8) or considered to be the identity.

In short-hand notation, the minimization problem (A8) can be written as:

$$g(\mathbf{p}) \coloneqq F(\mathbf{p})^T \cdot F(\mathbf{p})^T \to \min_{\mathbf{p}}, \tag{A11}$$

where $F(\mathbf{p}) = F_1(\mathbf{p}), \dots, F_m(\mathbf{p})$ is the residual vector of length $N = m \cdot n \cdot \text{nexp}$ with entries defined by:

$$F(\mathbf{p}) = \begin{bmatrix} (D_1^1)^{-1} \cdot (y^1(\tau_1, \mathbf{p}^1) - z_1^1) \\ \vdots \\ (D_m^1)^{-1} \cdot (y^1(\tau_m, \mathbf{p}^1) - z_m^1) \\ (D_1^2)^{-1} \cdot (y^2(\tau_1, \mathbf{p}^2) - z_1^2) \\ \vdots \\ (D_m^{\text{nexp}})^{-1} \cdot (y^{\text{nexp}}(\tau_m, \mathbf{p}^{\text{nexp}}) - z_m^{\text{nexp}}) \end{bmatrix}. \tag{A12}$$

$F \colon \mathbb{R}^{q \cdot \text{nexp}} \to \mathbb{R}^n$ is a non-linear mapping and structured as a stacked vector. If not all components of a measurement z_j^i are given, the number N is accordingly smaller, $N < m \cdot n \cdot \text{nexp}$. The above problem (A11), which is highly nonlinear in $\mathbf{p}$, can be solved by affine covariant Gauss-Newton iteration[250], where each iteration step k requires the solution of a linear least-squares problem:

$$\|J(\mathbf{p}^k) \cdot \Delta\mathbf{p}^k + F(\mathbf{p}^k)\|_2 \to \min_{\mathbf{p}^k}, \tag{A13}$$

$$\mathbf{p}^{k+1} = \mathbf{p}^k + \Delta\mathbf{p}^k, \tag{A14}$$

where $J(\mathbf{p}^k) = F'(\mathbf{p}^k) \in \mathbb{R}^{N \times q}$ denotes the Jacobian matrix. Its elements contain the *sensitivities*:

$$s_{ij}(t) = \frac{\partial y_i(t)}{\partial p_i}. \tag{A15}$$

An analysis of the matrix $J(\mathbf{p})$ gives some hints, whether the current combination of model and data will allow an identification of a given parameter. Parameters with very small sensitivity have nearly no influence on the solution at the measurement time-points and therefore cannot be estimated. In this case the entries of the corresponding column in $J(\mathbf{p})$ are almost zero. Furthermore, some of the parameters might be linearly dependent, which leads to nearly identical columns in $J(\mathbf{p})$. In both cases the matrix $J(\mathbf{p})$ will be singular or, from a numerical point of view, "nearly" singular. In order to reveal such properties, the linear least-squares problem (A13) is solved by QR factorization with column pivoting[251]. By a suitable permutation of the columns of the matrix $J(\mathbf{p})$, the diagonal elements of the upper triangular matrix R can be ordered in the form:

$$|r_{11}| \geq |r_{22}| \geq \cdots \geq |r_{qq}| \geq 0. \tag{A16}$$

As a measure of the term "nearly singular", the sub-condition of parameter $\mathbf{p}_j$ is defined by:

$$sc_j = \frac{|r_{11}|}{|r_{jj}|}. \tag{A17}$$

Thus, the permutation of matrix columns corresponds to a new ordering of parameters according to increasing sub-condition. The sub-condition indicates whether a parameter can be estimated from the given data or not. Only those parameters can be estimated for which:

$$sc_j \leq 1/\varepsilon, \tag{A18}$$

where ε is the relative precision of the Jacobian $J(\mathbf{p})$[252]. Herein, the Jacobian has been computed with a finite difference scheme, resulting in a precision of $\sqrt{\varepsilon_{\text{TOL}}}$, whereby $\varepsilon_{\text{TOL}} = 10^{-8}$ is the relative error tolerance of the numerical integrator for solving the ODE system (A2). For details, the reader is referred to[253]. Thus, we set $\varepsilon = 10^{-4}$ throughout the numerical computations in this study. In fact, during the identification process it turned out that all unknown parameters in our model were identifiably from the given measurement data.

At the final iterate, the matrix R from the QR-factorization of the Jacobian $F'(\mathbf{p}^k)$ is the basis for a statistical analysis of the linear least-squares estimate. The matrix $\sigma^2 (R^T R)^{-1}$ represents the variance-covariance matrix, whereby σ is the standard deviation of the residual vector $F(\mathbf{p}^k)$. From this matrix, correlation coefficients and confidence intervals (95 %-probability level using the F-distribution) for the final parameter estimates are derived.

The iterative scheme (A13) can be generalized to the so-called global Gauss-Newton method by introducing the following damping factors λ_k:

$$\mathbf{p}^{k+1} = \mathbf{p}^k + \lambda_k \Delta \mathbf{p}^k, \qquad 0 < \lambda_k \leq 1 \tag{A19}$$

The step length λ_k is computed successively in each iteration by an adaptive trust-region method[250]. This method for solving a non-linear least squares problem is implemented in the software code NLSCON[19], which has been used for all the computations.

7.2. Multivalent binding kinetics of precision glycomacromolecules: Some basic support for understanding the kinITC

In this subchapter, shortly the evolution of the rate constants of an ITC experiment is highlighted. It is essential to this kinITC method to understand how the rate constants behave during the measurements. Their evolution during the experiment will directly affect the final rate values obtained from the weighted average of all of the individual rate constants that are representative for one titration period. The below described evolution of the rate constants is

---

[19] available from http://www.zib.de/weimann/NewtonLib/index.html

strictly based on the observations and assumptions already been made and formulated by Yonetani *et al.*[165] and should only shortly illustrate the behavior of the rate constants during an ITC experiment, representative for the study described in this thesis.

Representative evolution of rate of association (k_{on}) and dissociation (k_{off}) is shown in Figure A1. The rate constants, the equilibrium concentration of the complex ($c_{LP,eq}$) as well as the concentration of free protein P (Con A) and ligand L ($c_{L,eq} + c_{P,eq}$) are plotted against the number of successive ligand injections (i), with $i = 28$. The forward and backward rates, the increasing free P and L ($c_{L,eq} + c_{P,eq}$), and the increasing P·L concentrations ($c_{LP,eq}$) were calculated from the least-squares fitting procedure as described in the previous subchapter 7.1 and following the procedure of Yonetani *et al.*[165]. These quantities were then plotted against the number of injections in Figure A1 to illustrate their evolution during an ITC experiment. As we are dealing with low(er) affinity complexes as illustrated in Figure A1, higher concentrations of P and L are required to reach representative c − values. All uncertainties were determined by the theory of error propagation, thereby applying the procedure as described by Butcher *et al.*[164] and in Chapter 5.2.5.

As is visible from Figure A1 the overall macroscopic rate of association (k_{on}) strongly depends on the concentration of both free L and P ($c_{L,eq} + c_{P,eq}$) and the complex P·L ($c_{LP,eq}$), which continuously change during the course of each injection of L. The more L and P molecules there are, the more likely they are to meet each other and associate. While the total number of L and P molecules bound to each other increase steadily with the L concentration, the forward rate decreases steadily, with successive injection of L and increasing saturation of P. This downward concave behavior of k_{on} during titration of the ligand strongly depends on the concentration of both free L and P ($c_{L,eq} + c_{P,eq}$), and also on the complex concentration ($c_{LP,eq}$), while both $c_{LP,eq}$ and $c_{L,eq} + c_{P,eq}$ depend on the equilibrium dissociation constant K_d and thus on the overall binding affinity. Such a behavior of k_{on} results from the fact that in early steps of the titration there is less complex. Then during successive injection of L, the concentration of the new complex steadily increases, thereby decreasing the concentration of free L and P. As a result k_{on} decreases and approaches a minimum value, while the concentration of free L and P ($c_{L,eq} + c_{P,eq}$) approach a maximum value in their upward concave behavior. Here, the initial on-rate will be higher than the following, leading to a steady decrease of the latter. In this scenario, the sum of free L and P concentration ($c_{L,eq} + c_{P,eq}$) will increase immediately and will remain greater throughout the experiment as compared to the concentration of the complex.[165]

If the binding process (and distortion of equilibrium) is initiated by titration of L at the beginning of the experiment, then the rate of association will dominate the binding process and the dissociation rate will be greater in the beginning (faster process) because there would be little P·L complex. As more complexes form, however, the association rate k_{on} begins to decrease and so does the dissociation rate k_{off} (lower rate of dissociation, increasing complex life time). Thus, the resulting values during titration are the footprints of the concentration range/window of the complex and the free P and L concentrations formed during titration.
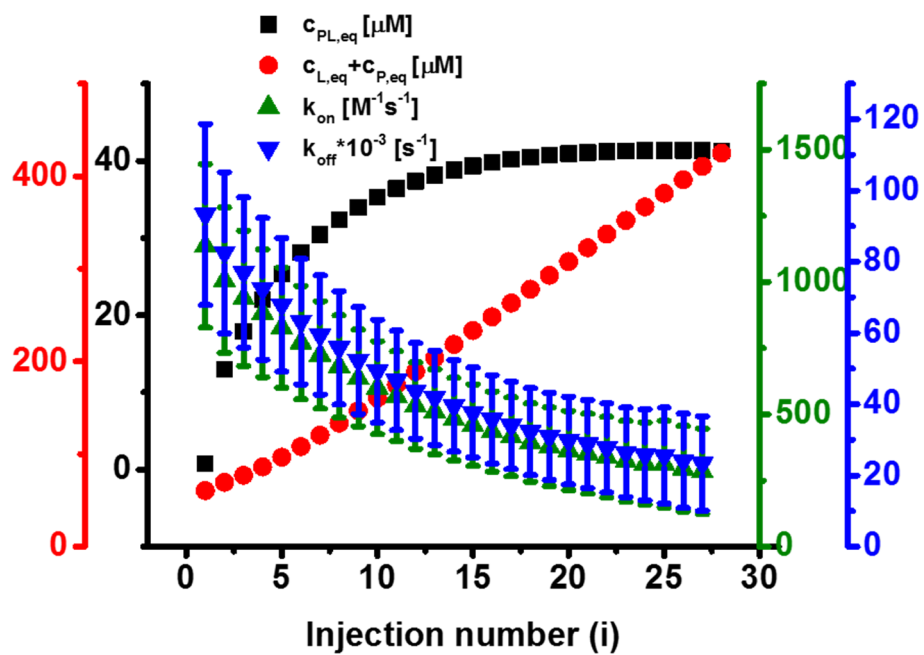
Figure A1. Evolution of the on- and off-rates, as well as the equilibrium complex ($c_{LP,eq}$) and free protein and ligand concentration ($c_{L,eq} + c_{P,eq}$) plotted *versus* the number of injections during the titration experiment.

## 7.3. Supporting 2 D NMR spectra of linear glycomacromolecules

¹H/¹³C HSQC of compound **Man(all)-3 (3)**
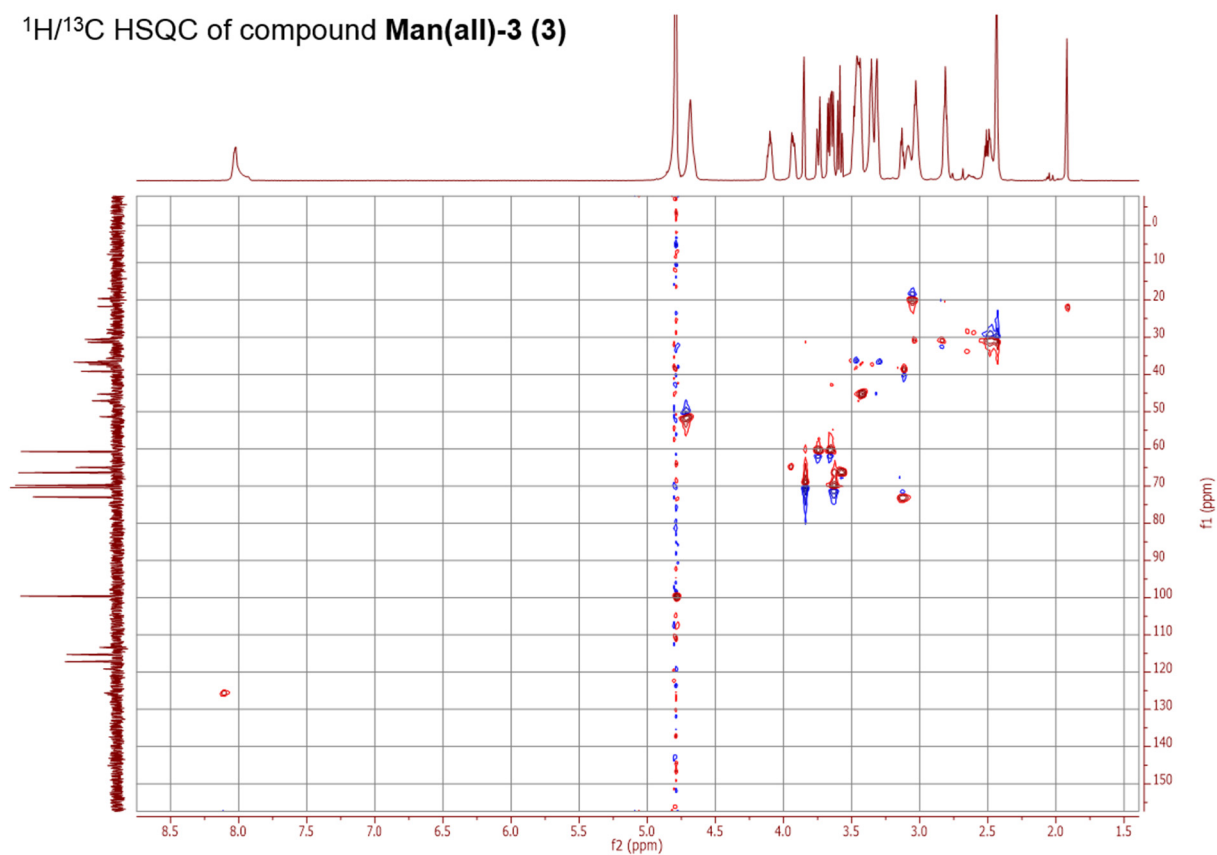
¹H/¹³C HSQC of compound **Man(1,4,7)-8 (3c)**
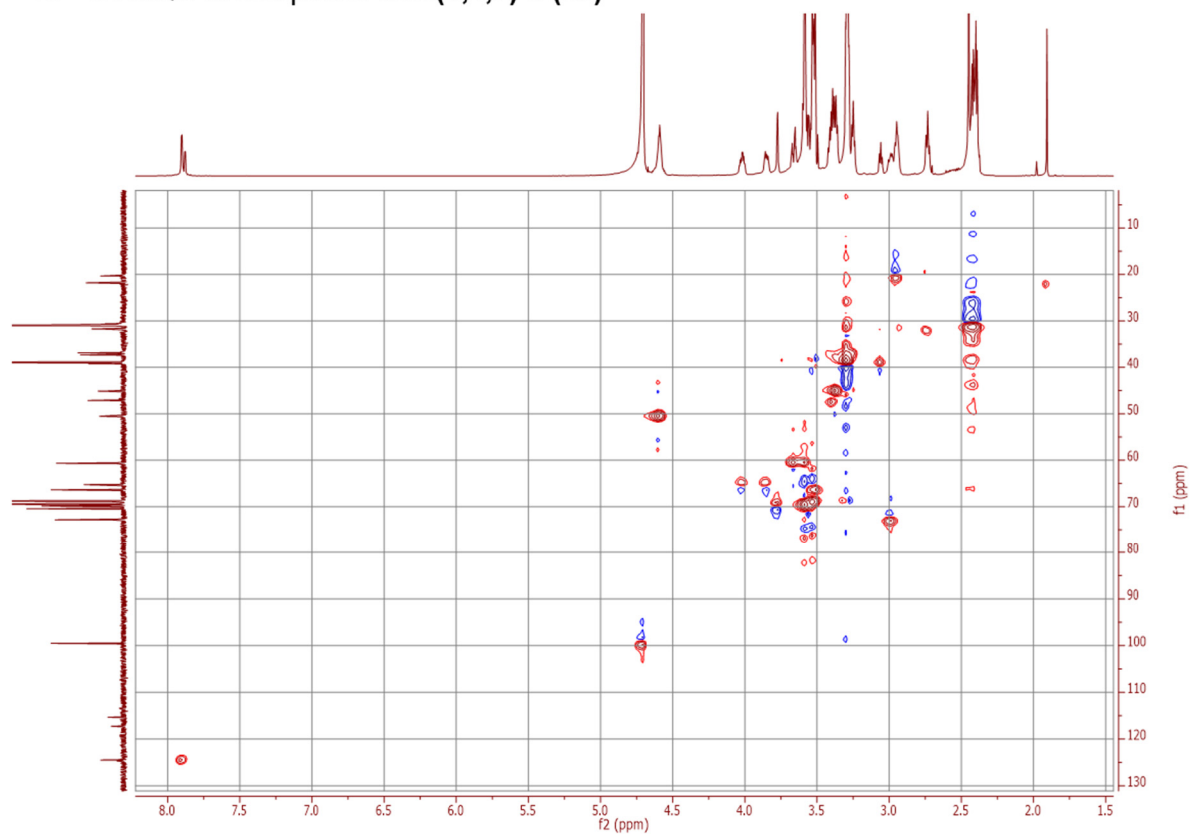
¹H/¹³C HSQC of compound **Man(all)S-3 (3S)**
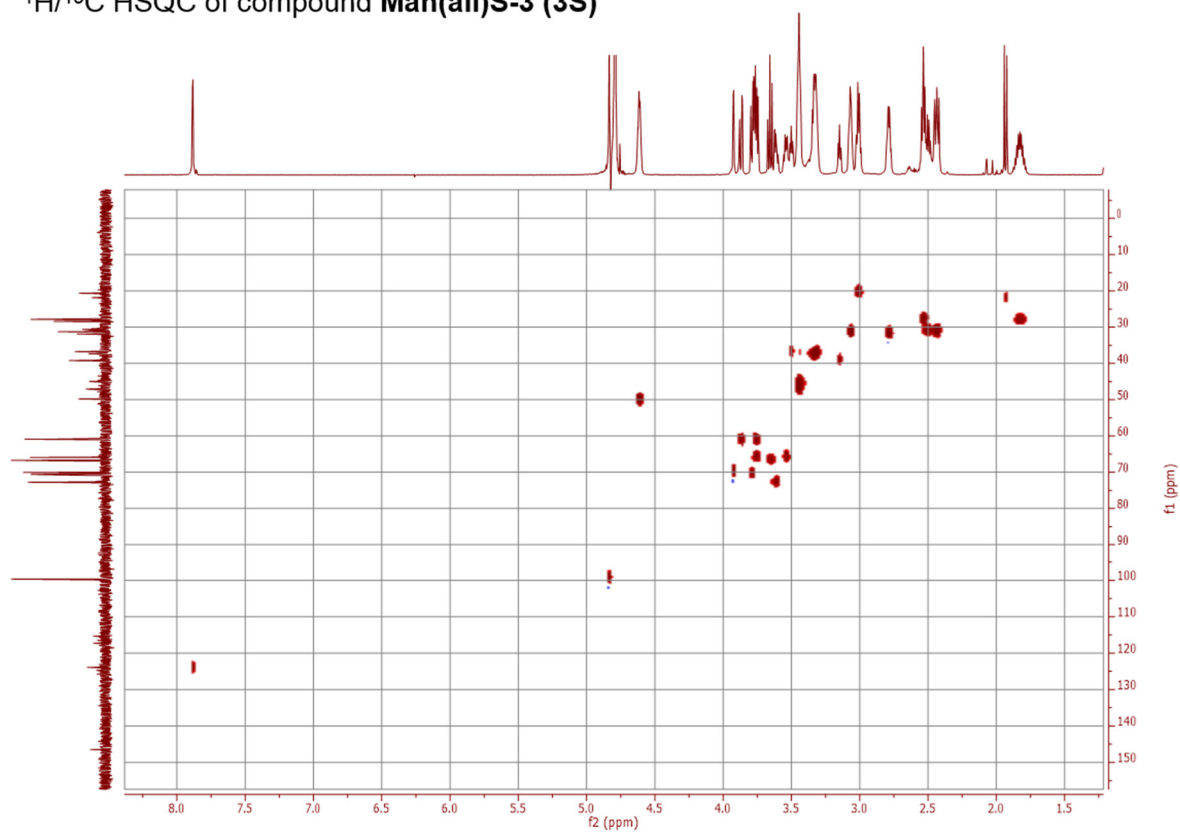
¹H/¹³C HSQC of compound **Man(all)B-3 (3B)**
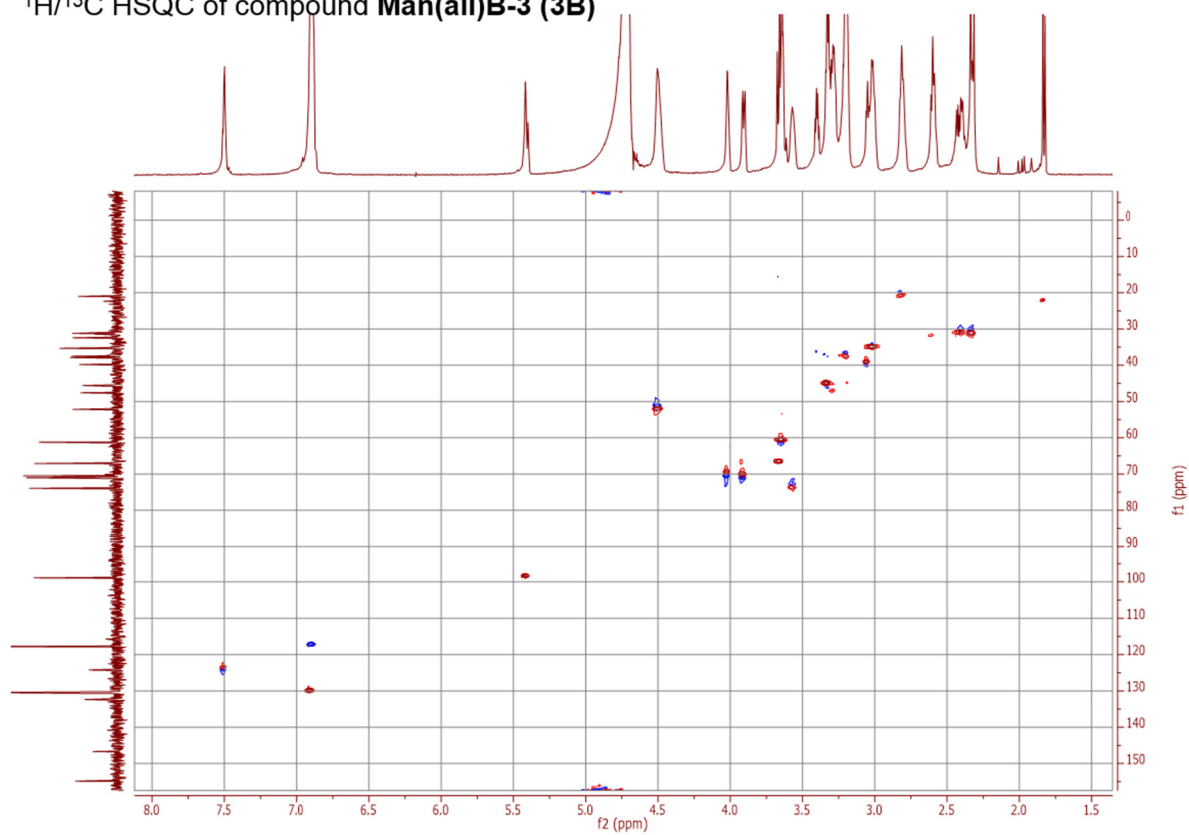
7.4. Supporting 1D ^{1}H NMR spectra and MALDI-TOF spectrum of compounds 6 and 6a confirming PEG miscleavage

^{1}H NMR (600 MHz) in D$_2$O of compound **6** after
semi-preparative purification on RP-HPLC (column **2**)

PEG impurities
from Tentagel S RAM resin

Crude ^{1}H NMR (400 MHz) in MeOD of compound **6**
after direct cleavage from solid support: PEG
impurities observed due to miscleavage.
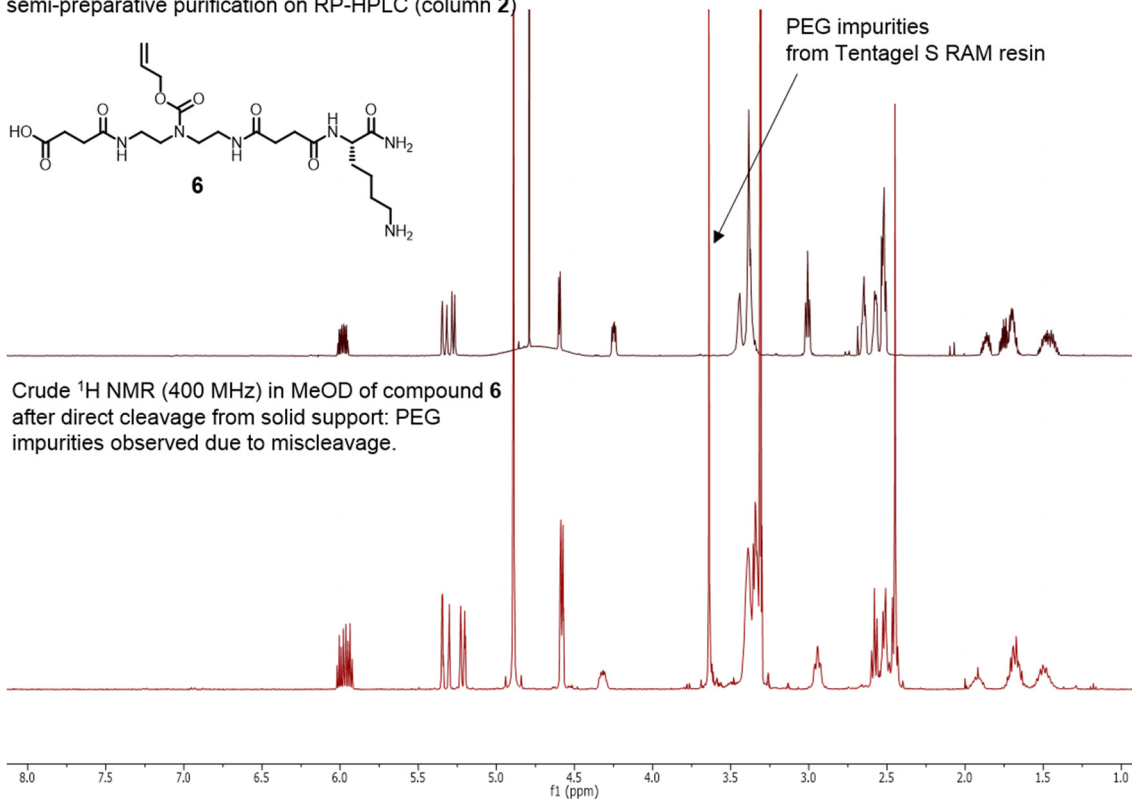
^{1}H NMR (600 MHz) in D$_2$O of compound **6a** after
semi-preparative purification on RP-HPLC (column **2**)

PEG impurities
from Tentagel S RAM resin

Crude ^{1}H NMR (400 MHz) in MeOD of compound **6a**
after 35 min conversion (reagent: TMSBr/ iPr$_2$NEt)
and direct cleavage from solid support: PEG impurities
observed due to miscleavage.
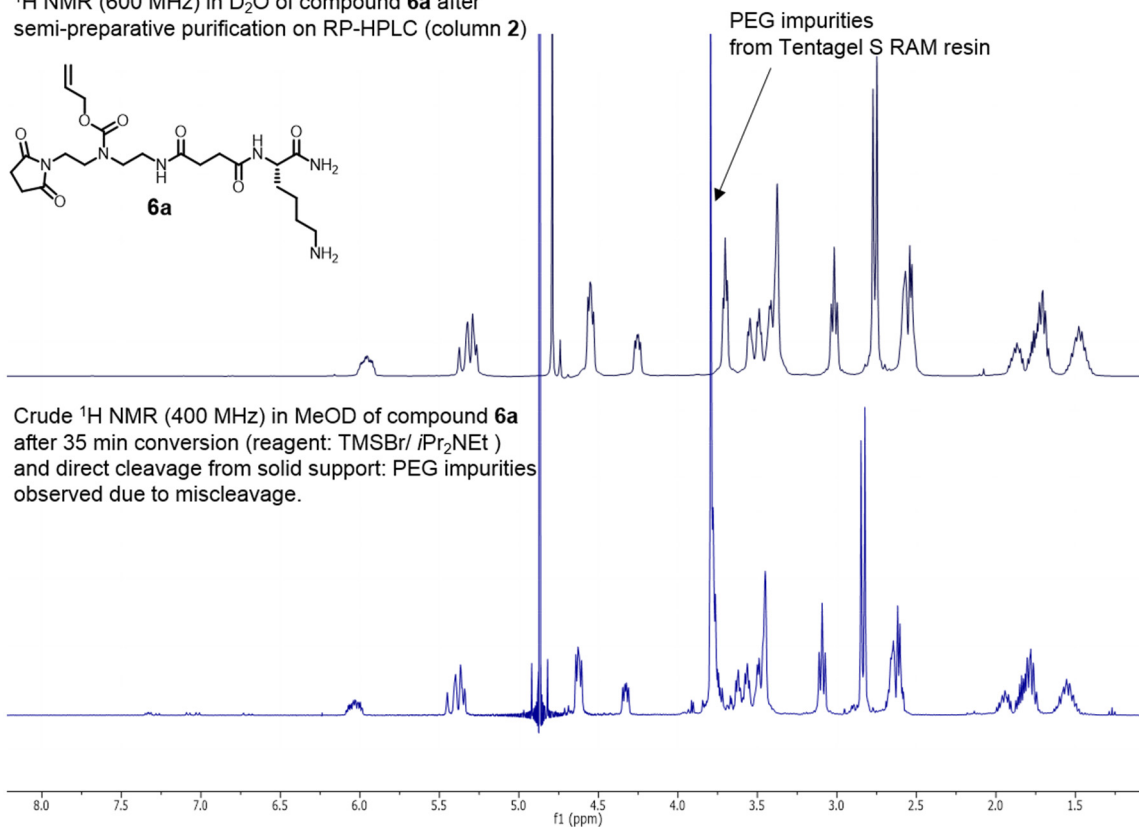
MALDI-TOF (positive mode): Conversion **6** to **6a**.
Reagent: TMSBr/ *i*Pr$_2$NEt, 35 min. Range: 2000 to 6000 m/z → mass distribution observed; PEG impurities observed due to miscleavage on Tentagel S RAM.
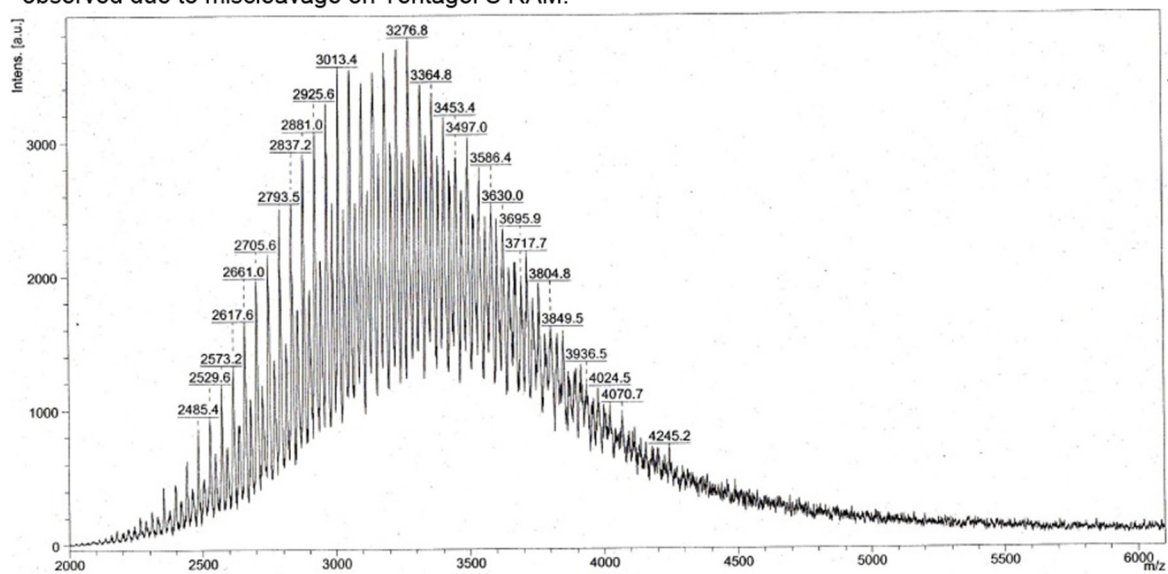
7.5. Supporting temperature dependent 1D ¹H NMR spectra confirming 1:1 rotamers mixture

¹H NMR (D₂O) of compound **Man(1,3,5)-5SDS* (SDS*)**: at 20°C, 25°C, 40°C, 60°C, 80°C (top to bottom)

Amide derivative* of Man(1,3,5)-5SDS (**2SDS**)

Acetyl protons and azide protons fall into one signal, which confirms presence of 1:1 mixture of rotational isomers (rotamers)
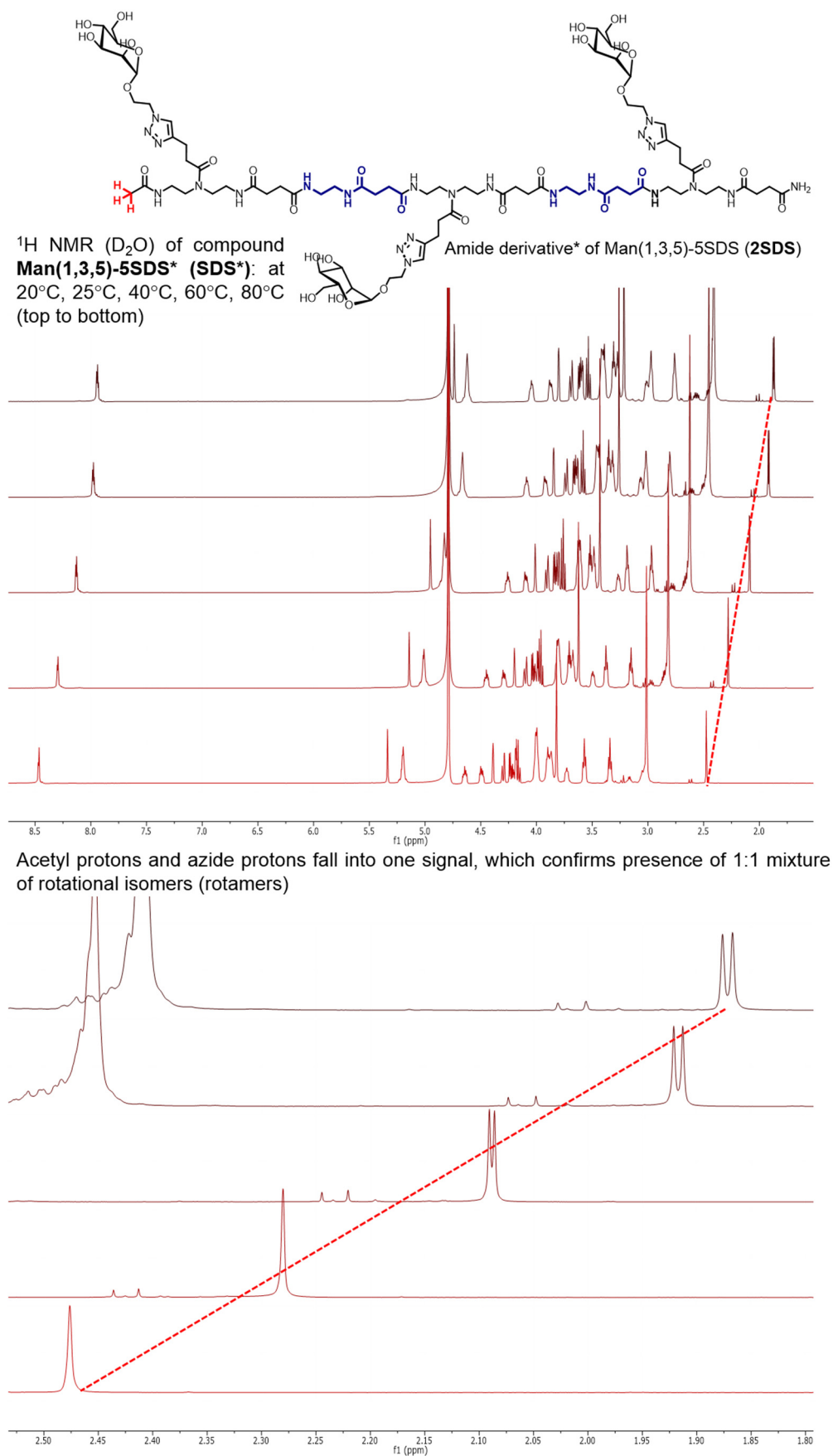
7.6. Supporting tables for calculation of the transition state enthalpies

Table A1. Determination of the activation enthalpies $\Delta H^{\ddagger}_{on;off}$ using the Eyring plot (15) from the slopes $a_{on;off}$ of the corresponding $\overline{k_{on,g(1,n)}}$ and $\overline{k_{off,g(1,n)}}$ values for the given temperature range (298.15 K, 303.15 K, 308.15 K) of linear glycomacromolecules with different linkers binding to tetramer Con A.

Ligand	$a_{on} = -\Delta H^{\ddagger}_{on}/R$ [a]	$\Delta H^{\ddagger}_{on} = -(a_{on} \cdot R) \cdot 10^{-3}$ [b]	R^2_{on} [c]	$a_{off} = -\Delta H^{\ddagger}_{off}/R$ [a]	$\Delta H^{\ddagger}_{off} = -(a_{off} \cdot R) \cdot 10^{-3}$ [b]	R^2_{off} [c]
Monovalent (ethyl triazole linker)						
Man(3)-5 (**1**)	+895	-7 ± 9	0.9	-2225	$+19 \pm 10$	1
Monovalent (thiol-ether triazole linker)						
Man(3)S-5 (**1S**)	+13865	-115 ± 24	1	+6895	-57 ± 21	1
Monovalent (benzyl triazole linker)						
Man(3)B-5 (**1B**)	-122	$+1 \pm 10$	1	-4886	$+41 \pm 13$	1
Trivalent (ethyl triazole linker)						
Man(1,3,5)-5 (**3a**)	+5927	-49 ± 15	1	-7863	$+65 \pm 19$	1
Trivalent (thiol-ether triazole linker)						
Man(1,3,5)S-5[1] (**3aS**)	+6534	-54 ± 21	0.9	+2400	-20 ± 25	0.9
Trivalent (benzyl triazole linker)						
Man(1,3,5)B-5 (**3aB**)	+6498	-54 ± 20	1	+4613	-38 ± 24	0.9

[a] $a_{on;off}$ are the on-/off-slopes determined from the Eyring plot (15), following the evolution of the on-/off-rate constants ($\overline{k_{on,g(1,n)}}$ and $\overline{k_{off,g(1,n)}}$) with temperature (linear regression analysis). Errors of the slopes are not reported, since the errors in the on-/off-transition state enthalpy values $\Delta H^{\ddagger}_{on;off}$ were determined, following the error propagation as described by Girolami *et al.*[238] and in Chapter 5.3.2. [b] Enthalpy values $\Delta H^{\ddagger}_{on;off}$ were determined from the on-/off-slopes $a_{on;off}$ and are reported in kJ mol^{-1}. [c] The squared correlation coefficient $R^2_{on;off}$ reports on the quality of the fit, following the linear regression analysis.

Table A2. Determination of the activation enthalpies $\Delta H^{\ddagger}_{on;off}$ using the Eyring plot (15) from the slopes $a_{on;off}$ of the corresponding $\overline{k_{on,g(1,n)}}$ and $\overline{k_{off,g(1,n)}}$ values for the given temperature range (298.15 K, 303.15 K, 308.15 K) of linear and cyclic glycomacromolecules with different spacers binding to tetramer Con A.

Ligand	$a_{on} = -\Delta H^{\ddagger}_{on}/R$ [a]	$\Delta H^{\ddagger}_{on} = -(a_{on} \cdot R) \cdot 10^{-3}$ [b]	R^2_{on} [c]	$a_{off} = -\Delta H^{\ddagger}_{off}/R$ [a]	$\Delta H^{\ddagger}_{off} = -(a_{off} \cdot R) \cdot 10^{-3}$ [b]	R^2_{off} [c]
Monovalent linear (SDS spacer)						
Man(3)-5SDS (**1SDS**)	-8345	$+69 \pm 18$	1	-15045	$+125 \pm 27$	0.9
Monovalent cyclic (SDS spacer)						
Man(3)@5SDS (**1@SDS**)	-1591	$+13 \pm 44$	1	-4241	$+35 \pm 60$	1
Monovalent linear (EDS spacer)						
Man(3)-5 (**1**)	$+895$	-7 ± 9	0.9	-2225	$+19 \pm 10$	1
Man(4)-8 (**1a**)	-2556	$+21 \pm 10$	0.9	-7068	$+59 \pm 14$	1
Trivalent linear (SDS spacer)						
Man(1,3,5)-5SDS (**2SDS**)	1924	-16 ± 12	1	-3380	$+28 \pm 14$	0.8
Trivalent cyclic (SDS spacer)						
Man(1,3,5)@5SDS (**2@SDS**)	-3334	$+28 \pm 14$	1	-9056	$+75 \pm 20$	0.8
Trivalent linear (EDS spacer)						
Man(1,3,5)-5 (**2**)	$+5927$	-49 ± 15	1	-7863	$+65 \pm 19$	1
Man(1,4,7)-8 (**2a**)	8630	-72 ± 17	1	-3919	$+33 \pm 17$	1
Trivalent cyclic (EDS spacer)						
Man(1,3,5)@5 (**2@**)	8660	-72 ± 15	1	-7511	$+63 \pm 15$	1
Man(1,4,7)@8 (**2a@**)	4755	-40 ± 11	1	-8187	$+68 \pm 15$	1

[a] $a_{on;off}$ are the on-/off-slopes determined from the Eyring plot (15), following the evolution of the on-/off-rate constants ($\overline{k_{on,g(1,n)}}$ and $\overline{k_{off,g(1,n)}}$) with temperature (linear regression analysis). Errors of the slopes are not reported, since the errors in the on-/off-transition state enthalpy values $\Delta H^{\ddagger}_{on;off}$ were determined, following the error

propagation as described by Girolami *et al.*[238] and in Chapter 5.3.2. [b] Enthalpy values $\Delta H^{\ddagger}_{on;off}$ were determined from the on-/off-slopes $a_{on;off}$ and are reported in kJ mol^{-1}. [c] The squared correlation coefficient $R^2_{on;off}$ reports on the quality of the fit, following the linear regression analysis.

8. Collaborator Contributions to this Thesis

Some parts of the presented results in this thesis have been achieved together with three collaborators and three graduate students. In the following, the contributions of the three collaborators and graduate students on this thesis are listed. Every contribution including a collaborator is listed once and has been assigned by a footnote both, in Chapters 3 and 5, e.g. for the synthesis of a molecule or performance of an experiment. If not stated otherwise, all other contributions have been exclusively performed by the author of this thesis. All glycomacromolecule and peptide structures were designed by the author of this thesis, all experimental procedures (ITC and kinITC) were established by the author of this thesis.

Chapter 3, Part 1: Synthesis of Precision Glycomacromolecules:

- *Anne Müller (Ph.D. student, Christian-Albrechts-Universität Kiel, group of Prof. Dr. Thisbe K. Lindhorst):*

O-propyl-3-thio-S-ethyl-5-azido-α-D-mannopyranoside ("S") and O-p-benzyl-p-ethyl-2-azido-α-D-mannopyranoside ("B") have been provided by Anne Müller (Christian-Albrechts-Universität Kiel, group of Prof. Dr. Thisbe K. Lindhorst).

- *Hendrik Wöhlk (Master student, Heinrich-Heine-Universität Düsseldorf, group of Prof. Dr. Laura Hartmann):*

Compounds 1SDS, 1aSDS, 2SDS and 2aSDS have been synthesized and characterized (NMR, RP-HPLC and MALDI-TOF) by Hendrik Wöhlk (Heinrich-Heine-Universität Düsseldorf, group of Prof. Dr. Laura Hartmann, Master Thesis, April 2015).

  Author of this thesis:

In this thesis, the above mentioned compounds have been re-synthesized, and their characterization data (NMR, RP-HPLC and MALDI-TOF) reported and discussed in this thesis corresponds to the re-synthesized compounds and characterization data as re-assessed by the author of this thesis.

- *Andreas Ludwig (Bachelor student, Heinrich-Heine-Universität, group of Prof. Dr. Laura Hartmann):*

1@SDS and 2@SDS were synthesized and characterized (NMR, RP-HPLC and MALDI-TOF) by Andreas Ludwig (Heinrich-Heine-Universität Düsseldorf, group of Prof. Dr. Laura Hartmann, Bachelor Thesis, October 2015).

  Author of this thesis:

In this thesis, the characterization data of the above mentioned compounds (NMR) has been re-assessed by the author of this thesis.

- *Genesha Olgar (Bachelor student, Heinrich-Heine-Universität, group of Prof. Dr. Laura Hartmann):*

Linear tetrapeptide 12 and mono- and bi-cyclic tetrapeptides 12a and bi-12a have been synthesized and characterized (NMR, RP-HPLC and MALDI-TOF) by Genesha Olgar (Heinrich-

Heine-Universität Düsseldorf, group of Prof. Dr. Laura Hartmann, Bachelor Thesis, November 2015).

Author of this thesis:

In this thesis, the characterization data of the mentioned linear tetrapeptide and cyclic tetrapeptides have been re-assessed by the author of this thesis. Analysis and evaluation of the in this thesis presented 2D ^{1}H/^{1}H COSY NMR and 2D ^{1}H/^{15}N HSQC NMR spectra of the mentioned linear tetrapeptide and cyclic tetrapeptides has exclusively been performed by the author of this thesis and has not been presented previously.

Chapter 3, Part 2: Thermodynamic and Kinetic Parameters of Precision Glycomacromolecules Binding to Con A:

- *Dr. Susanna Röblitz (Research Scientist, Konrad-Zuse-Institut für Informationstechnik, Berlin, group of Dr. Marcus Weber):*

The least squares non-linear curve fitting procedure for kinITC has been written by Dr. Susanna Röblitz and Dr. Marcus Weber (Konrad-Zuse-Institut für Informationstechnik, Berlin; see also Supporting Appendix).

Author of this thesis:

Every measurement (including experimental design), determination, calculation and evaluation of the rate constants including their uncertainties has been performed by the author of this thesis. The kinITC least squares minimization procedure, required for the determination, calculation and evaluation of the measured ITC data (binding isotherms), has been provided by Dr. Susanna Röblitz and Dr. Marcus Weber. They have written the MATLAB scripts, which then allowed the calculation/determination of the rate constants. These written MATLAB scripts have been applied for the calculation/determination of the kinetic constants by the author of this thesis.

- *Hendrik Wöhlk (Master student, Heinrich-Heine-Universität Düsseldorf, group of Prof. Dr. Laura Hartmann):*

ITC measurements of compounds 1SDS, 1aSDS, 2SDS and 2aSDS at 298.15 K have been performed by Hendrik Wöhlk (Heinrich-Heine-Universität Düsseldorf, group of Prof. Dr. Laura Hartmann, Master Thesis, April 2015).

Author of this thesis:

In this thesis, the here listed thermodynamic quantities have been re-assessed using the methods and error calculation described in this thesis. Kinetic evaluation of the same binding isotherms has completely and exclusively been performed by the author of this thesis. Their rate constants including their uncertainties are presented in this thesis for the first time.

ITC measurements of the compounds 1SDS and 2SDS at 303.15 K and 308.15 K as well as the evaluation, determination and calculation of all of their in this thesis presented thermodynamic quantities have exclusively been performed by the author of this thesis. Kinetic evaluation of the same binding isotherms has exclusively been performed by the author of this thesis. Their rate constants including their uncertainties are presented in this thesis for the first time.

- *Andreas Ludwig (Bachelor student, Heinrich-Heine-Universität, group of Prof. Dr. Laura Hartmann):*

ITC measurements of compounds 1@SDS and 2@SDS at different temperatures (298.15 K, 303.15 K and 308.15 K) have been performed by Andreas Ludwig (Heinrich-Heine-Universität Düsseldorf, group of Prof. Dr. Laura Hartmann, Bachelor Thesis, October 2015).

The transition state parameters ($\Delta G^{\ddagger}$, $\Delta H^{\ddagger}$ and $-T\Delta S^{\ddagger}$ for the on- and the off-state) of compounds 1@SDS and 2@SDS have been determined from the evolution of the rate constants (k_{on} and k_{off}) at different temperatures (298.15 K, 303.15 K and 308.15 K) and previously reported by Andreas Ludwig (Heinrich-Heine-Universität Düsseldorf, group of Prof. Dr. Laura Hartmann, Bachelor Thesis, October 2015).

Author of this thesis:

In this thesis, the thermodynamic and kinetic quantities previously reported by Andreas Ludwig have been re-assessed using the methods and error calculation described in this thesis.

Determination and evaluation of the entropic terms $\Delta S_{trans+rot} \cdot FV$ for the above mentioned compounds is reported for the first time in this thesis.

In this thesis, all of the above mentioned transition state parameters have been re-assessed using the methods and error calculation described in this thesis. The on- and off-rate constants and their uncertainties presented in the above mentioned Bachelor Thesis have been determined and provided by the author of thesis. Their calculation is reported in this thesis for the first time.

9. Acknowledgements

First, I would like to thank my supervisor and mentor Prof. Dr. Laura Hartmann for this interesting and challenging topic, her countless ideas and her steady motivation, helping me to successfully move my thesis forward. I am very grateful to her guidance that helped me in all the time of research and writing of my thesis, while granting me the freedom to develop my own ideas. I am also very thankful to Prof. Dr. Peter H. Seeberger for the opportunity to work in a very stimulating and challenging department during the first half of my Ph.D. Thesis.

Besides my first supervisor, I am very grateful to my second supervisor Prof. Dr. Christoph A. Schalley for agreeing to review my thesis and for his support during my Bachelor Thesis.

My sincere thanks goes to Prof. Dr. Nicole Snyder and senior scientist Dr. Monir Tabatabai, for their insightful comments, their review of my Experimental Part, and not only for always taking the time to discuss scientific issues with me, but most importantly for their encouragement, which intended me to widen my research also from different perspectives. Further, I would like to thank our lab technician Stephanie Scheelen and our precious secretary Michaela Kitza for their support in the lab and the office, always providing us with enough material to work with and most importantly for their friendship outside the lab.

I also would like sincerely to thank my graduate students, Hendrik Wöhlk, Genesha Olgar and Andreas Ludwig on their contributions to my thesis, and especially my research collaborators, Dr. Susanna Röblitz, Dr. Marcus Weber and Anne Müller. Dear Susanna and Marcus, most of the presented results would have not been possible without our collaboration. I sincerely thank you for your collaboration, giving me the opportunity to collect a lot of data by applying your written MATLAB scripts.

Further, I am very pleased to have worked together with the Hartmann and the Ritter group. Due to the people in these groups, it was a lot of fun to work day after day.

I thank my fellow labmates and friends, past and present, Dr. Felix Wojcik, Dr. Simone Mosca, Dr. Daniela Ponader, Dr. Daniel Pussak, Nina M. Mujkic-Ninnemann, Christoph Gerke, Fawad Jacobi, Dr. Melanie Lievenbrück, Judita Brittner and Dr. Olga Majatska for our stimulating discussions, for sleepless nights before deadlines, and most importantly for the fun we have had during the last years. Especially, I want to thank my precious former labmate Nina M. Mujkic-Ninnemann, for a lot of fun in the lab and during our countless coffee breaks that has brought me so much more laughter lines. We started with a lablove that has turned into a friendship.

I would like to thank two of my dearest and nearest friends to me, Juliane Latzke and Aileen Gregory. Hopefully, our sincere friendship will continue until the end of our days. Thank you for your support during my Ph.D. Thesis. It must have been exhausting to listen to the countless issues related to my thesis. Thank you for keeping me motivated.

Last but not least, I would like to thank my precious family: my parents, my parents-in-law, my sisters-in-law, my husband and my son, for supporting me spiritually throughout my thesis and my life in general. Especially without my parents and my husband, I would have not been able to perform all of my studies. Thank you for that.